FINAL REPORT

Integrated Field-Scale, Lab-Scale, and Modeling Studies for Improving Our Ability to Assess the Groundwater to Indoor Air Pathway at Chlorinated Solvent-Impacted Groundwater Sites

SERDP Project ER-1686

JULY 2016

Paul C. Johnson, Ph.D.
Chase Holton, Ph.D.
Yuanming Guo, Ph.D.
Paul Dahlen, Ph.D.
Hong Luo, Ph.D.
Arizona State University

Kyle Gorder
Erik Dettenmaier, Ph.D.
Hill Air Force Base

Robert E. Hinchee, Ph.D.
Integrated Science & Technology

SERDP
DOD ▪ EPA ▪ DOE

REPORT DOCUMENTATION PAGE

Form Approved
OMB No. 0704-0188

1. REPORT DATE *(DD-MM-YYYY)*	2. REPORT TYPE	3. DATES COVERED *(From - To)*
01/07/2016	Final Report	09/29/2009 - 12/30/2014

4. TITLE AND SUBTITLE

Integrated Field-Scale, Lab-Scale, and Modeling Studies for Improving the Ability to Assess the Groundwater to Indoor Air Pathway at Chlorinated Solvent-Impacted Groundwater Sites

5a. CONTRACT NUMBER
W912HQ-09-C-0052

5b. GRANT NUMBER

5c. PROGRAM ELEMENT NUMBER

6. AUTHOR(S)
Paul C. Johnson, Ph.D. - Chase Holton, Ph.D. - Yuanming Guo, Ph.D. - Paul Dahlen, Ph.D. - Hong Luo, Ph.D. - Arizona State University

Kyle Gorder, Erik Dettenmaier, Ph.D. - Hill Air Force Base
Robert E. Hinchee, Ph.D. - Integrated Science & Technology

5d. PROJECT NUMBER
ER-1686

5e. TASK NUMBER

5f. WORK UNIT NUMBER

7. PERFORMING ORGANIZATION NAME(S) AND ADDRESS(ES)
Arizona State University
1001 S McAllister
Tempe, AZ 85287

8. PERFORMING ORGANIZATION REPORT NUMBER

9. SPONSORING/MONITORING AGENCY NAME(S) AND ADDRESS(ES)
Strategic Environmental Research and Development Program Office
4800 Mark Center Drive
Suite 17D03
Alexandria, VA 22350-3605

10. SPONSOR/MONITOR'S ACRONYM(S)
SERDP

11. SPONSOR/MONITOR'S REPORT NUMBER(S)

12. DISTRIBUTION/AVAILABILITY STATEMENT
Approved for public release; distribution is unlimited.

13. SUPPLEMENTARY NOTES
N/A

14. ABSTRACT

This study focused on improving our ability to confidently assess the groundwater to indoor air vapor intrusion (VI) pathway at chlorinated solvent-impacted groundwater plume sites. Federal, state, and local agency guidance has evolved toward multiple-lines-of-evidence-based approaches that involve indoor air, sub-slab soil gas, deeper soil gas, groundwater, and soil sampling in combination with empirical analysis and screening-level modeling. Of these, indoor air data tend to be most heavily weighted in decision-making.

15. SUBJECT TERMS

Indoor air vapor intrusion (VI), ground water, chlorinated solvents, indoor air data, trichloroethylene (TCE), screening-level modeling.

16. SECURITY CLASSIFICATION OF:			17. LIMITATION OF ABSTRACT	18. NUMBER OF PAGES	19a. NAME OF RESPONSIBLE PERSON
a. REPORT	b. ABSTRACT	c. THIS PAGE			Paul C. Johnson
					19b. TELEPHONE NUMBER *(Include area code)*
Unclassified	Unclassified	UU	UL	247	480-965-9115

ABSTRACT

This study focused on improving our ability to confidently assess the groundwater to indoor air vapor intrusion (VI) pathway at chlorinated solvent-impacted groundwater plume sites. Federal, state, and local agency guidance has evolved toward multiple-lines-of-evidence-based approaches that involve indoor air, sub-slab soil gas, deeper soil gas, groundwater, and soil sampling in combination with empirical analysis and screening-level modeling. Of these, indoor air data tend to be most heavily weighted in decision-making.

Prior to this study, it was recognized that there could be temporal variability in pathway assessment data, but little was known about this topic. This project focused on collecting the first high-frequency and long-term data set at a VI site, with the hope that it would be useful for advancing our understanding of temporal variability and determining how it should be accounted for in designing sampling plans and interpreting data.

This project was primarily conducted at a house overlying a dilute chlorinated hydrocarbon groundwater plume. The house was outfitted with sensors and automated systems to facilitate monitoring of indoor air and ambient and building conditions as well as groundwater and soil gas. Monitoring was conducted under both natural and controlled building conditions, and both chlorinated hydrocarbons and radon were quantified in indoor air and soil gas.

Sampling was conducted under natural conditions for about 2.5 years. During that time trichloroethylene (TCE) concentrations in groundwater were relatively constant (10 – 50 μg/L-H_2O) while indoor air concentrations varied by three orders of magnitude (<0.01 to 10 ppb_v). Two recurring behaviors were observed with the indoor air data. The temporal behavior prevalent in fall, winter, and spring involved time-varying impacts intermixed with sporadic periods of inactivity. In summer, VI activity was more dormant, having long periods of inactivity combined with sporadic VI impacts. Subsurface concentrations were less temporally variable than indoor air and the variability increased in moving from the source to indoor air.

Indoor air data were used to predict the likely outcomes of three sampling plans representative of conventional practice. The analysis showed a significant potential for poor characterization of long-term mean concentrations and exposures (both false negative and false positive outcomes) and a need for further investigation into the robustness of VI assessment paradigms. It also suggested the need for other long-term high-frequency indoor air data sets to better understand the range of behaviors that might be observed at other sites.

In contrast to indoor air concentrations under natural conditions, the long-term (9 month) controlled pressure method (CPM) test results were relatively constant with time across all seasons, indoor air concentrations were similar to the maximum values measured under natural conditions, and false-negative results were not obtained. This suggests that CPM tests might reliably detect VI occurrence and worst-case impacts regardless of day or time of year of the CPM test. The results also showed that CPM testing might reveal alternative VI pathways not detectable through routine monitoring under natural conditions.

It was also observed during this study that indoor air sources can create subsurface soil gas plumes, and that these can persist for weeks following removal of the indoor source. This is of note because some regulatory guidance allows for VI pathway assessment within days of indoor source identification and removal. If that happens, and the soil gas plume created by the indoor source persists, then the VI pathway assessment data might lead to false-positive conclusions concerning the potential for VI impacts.

Field, laboratory, and modeling studies were also conducted to improve the understanding of the impact of groundwater table elevation changes on vapor emissions from dissolved groundwater sources. The results suggested long-term average emission increases due to groundwater table elevation changes are likely to be less than two times for most site conditions. The practical implication is that groundwater table elevation movement should not be considered a major factor in VI pathway assessment plan design at dissolved plume sites, unless the groundwater table is shallow and elevation fluctuations are frequent.

Table of Contents

List of Tables

List of Figures

List of Acronyms

1,2-DCA	-	1,2-dichloroethane
1,1-DCE	-	1,1- dichloroethene
AFB	-	Air Force Base
ASU	-	Arizona State University
BS	-	Below slab
cis-DCE	-	cis-1,2-dichloroethene
DELCD	-	Dry electrolytic conductivity detector
CHC	-	Chlorinated hydrocarbon
CPM	-	Controlled pressure method
DoD	-	Department of Defense
ECD	-	Electron capture detector
h	-	hour
HVAC	-	Heating, ventilation and air conditioning
GC	-	Gas chromatography
GW	-	Groundwater
MDL	-	Method detection limit
MLE	-	Multiple-lines-of-evidence
MS	-	Mass spectroscopy
NAPL	-	Non-aqueous phase liquid
PCE	-	Tetrachloroethylene
PDD	-	Pulse discharge detector
ppb_v	-	Parts per billion in volume
SF_6	-	Sulfur hexafluoride
SIM	-	Selective-ion monitoring
SS	-	Sub-slab
TCE	-	Trichloroethylene
USEPA	-	United States Environmental Protection Agency
VI	-	Vapor intrusion
VOA	-	Volatile organic analysis

Key Words

Alternative VI pathway
Controlled pressure method
CPM
Indoor VI sources
Spatial variability
Temporal variability
Vapor intrusion
VI
VI pathway assessment

1 OBJECTIVE

The SERDP Statement-of-Need ERSON-09-03 sought fundamental and applied research leading to improved assessment of the groundwater to indoor air exposure pathway at chlorinated solvent-impacted groundwater plume sites. It reflected an increasing awareness of the vapor intrusion (VI) pathway and its significance at Department of Defense (DoD) sites. This pathway is now the risk and clean-up driver at many dissolved chlorinated solvent groundwater plume sites, especially for those sites where groundwater plumes have migrated beneath buildings or to areas where future development is planned.

Guidance for assessing this exposure pathway is variable across federal, state, and local levels; however, most documents reflect the evolution of federal guidance toward multiple-lines-of-evidence (MLE)-based approaches. These call for indoor air and subsurface samples (sub-slab soil gas, deeper soil gas, groundwater, and soil), and allow for screening-level modeling and empirical assessment (e.g., USEPA, 2002; ITRC, 2007; USEPA, 2015). MLE data interpretation and decision-making have become more heavily weighted toward indoor air data. The emphasis on indoor air concentrations reflects a sense of security in using exposure point measurements as well as a desire to not have to resolve conflicting lines-of-evidence, questions about modeling reliability, and a limited peer-reviewed experience base to rely upon.

Opinions vary as to how much data are needed for decision-making. Decisions may be made based on a few sampling events, or multi-year periodic sampling maybe required. It has been recognized that there could be temporal variability in pathway assessment data (Luo, 2009), but guidance is not clear on how it should be accounted for in designing sampling plans and interpreting data.

Consistent with ERSON-09-03, the overall objectives of this project were to gain a better understanding of the utility and limitations of the current VI pathway assessment approaches, and to identify pathway assessment options that could lead to greater cost effectiveness and increased confidence in VI pathway assessment decisions.

The unique feature of this project was the use of a house overlying a dilute chlorinated solvent groundwater plume as a laboratory; it was outfitted with sensors and monitoring systems to facilitate the first-ever collection of a long-term high-frequency indoor air, ambient conditions, and building conditions data set in combination with periodic synoptic snapshots of groundwater and soil gas concentrations. Data were collected under both natural and controlled conditions. In addition, lab studies and simulation analyses were conducted to look specifically at relationships between groundwater elevation changes and vapor emissions from groundwater, and to complement the results from an analysis using the field study data.

2 BACKGROUND

In 2002, the United States Environmental Protection Agency (USEPA, 2002) issued draft guidance for assessing the subsurface vapor intrusion-to-indoor (VI) air pathway. That guidance acknowledged the potential for contaminant vapors originating from impacted soils and groundwater to migrate to buildings. It also provided a sequence of steps to follow when assessing the significance of the VI pathway under current conditions. Its development was stimulated in part by the detection of unacceptable indoor air concentrations attributed to subsurface contamination at a few well-studied and well-publicized sites – all of which involved residences overlying chlorinated solvent-impacted groundwater plumes (e.g., Johnson et al., 2002; EnviroGroup, 2008; NYSDOH, 2008; USEPA, 2012a).

Sites associated with chlorinated solvent-impacted groundwater plumes are challenging because their dissolved groundwater plumes vary widely in size; at one site the plume may be small enough that only a few buildings are at risk and at another site it may be large enough that the VI pathway assessment is needed for an entire neighborhood where assessment of all buildings is impracticable. Groundwater-related VI impacts to indoor air quality have been documented in some buildings overlying groundwater with concentrations as low as about 10 $\mu g/L\text{-}H_2O$. In addition, our ability to anticipate where impacts should and should not occur is not well-developed. For example, while it is rational to expect that the greatest indoor air impacts should be found in buildings overlying the highest groundwater concentrations at larger sites, this pattern is not always observed.

The peer-reviewed VI knowledge base originated with studies focused on naturally occurring radon intrusion (e.g., Nazaroff et al., 1985; Loureiro, 1987; Robinson and Sextro, 1995; Riley et al., 1996) and later included chemical vapors emanating from impacted soil and groundwater (e.g., Johnson et al., 1991; Little et al., 1992; Hodgson et al., 1992; Hers et al., 2003; Abreu and Johnson, 2005, 2006). These established the foundation for features of the common pathway conceptualization shown in Figure 2.1 for dissolved groundwater sources. In brief, chemicals partition from impacted groundwater into soil gas and diffuse upward toward the foundation and ground surface. As the chemical vapors approach the building foundation, they are carried with soil gas flow into the building through gaps/penetrations in the foundation (e.g., plumbing, sumps, expansion joints). This advective soil gas flow (estimated to be about 1 – 10 L/min) results from building under-pressurization of about 1- 10 Pa relative to the atmosphere. Under-pressurization is caused by wind blowing against the building, indoor-outdoor temperature differences, and heating/cooling systems. The chemical vapors entering the building are diluted as they mix with the indoor air, and then eventually are carried to outdoor air with the building air exchange (about 10 – 20 building volume changes per day). The resulting indoor air concentrations and sub-foundation soil gas profiles reflect the combination of all of these transport processes acting in concert.

Screening-level models (Johnson and Ettinger, 1991; Sanders and Stern, 1994; Ferguson et al., 1995; Johnson et al., 1999; Hers et al., 2002, 2003) and more sophisticated numerical codes (Garbesi et al., 1989; Loureiro et al., 1990; Robinson and Sextro, 1997; Abreu and Johnson, 2005 and 2006; Yao et al., 2011) have been developed to describe the processes discussed above

and to anticipate relationships between system properties (e.g., soil type, foundation characteristics, building under-pressurization, etc.) and indoor air concentrations.

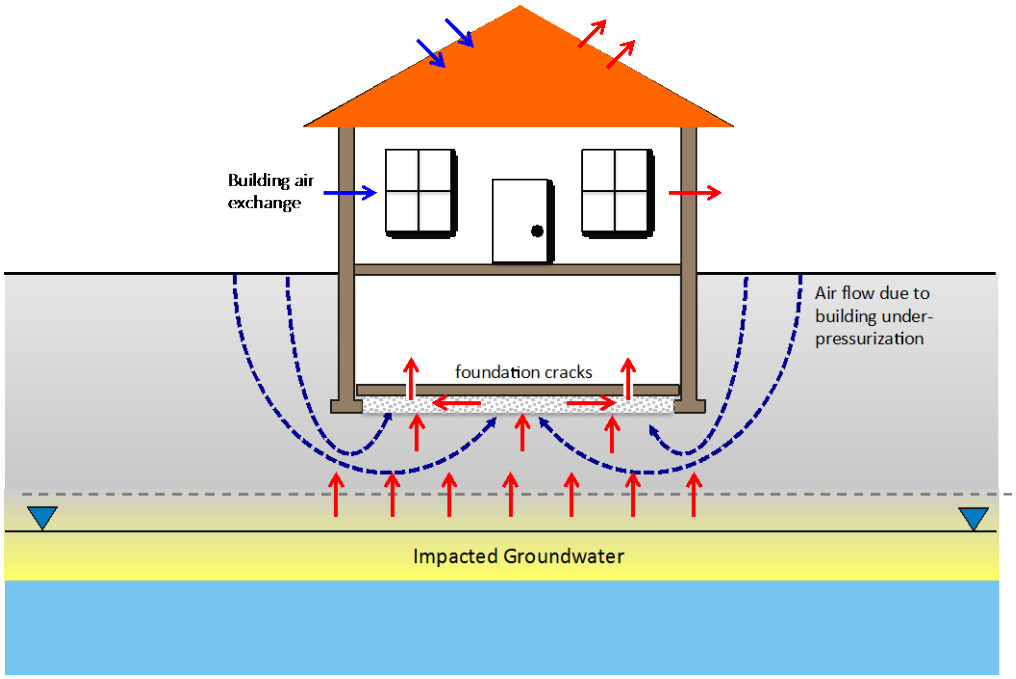

Figure 2.1. Common mechanistic conceptualization of the groundwater-to-indoor air pathway.

With respect to chlorinated hydrocarbon (CHC)-impacted groundwater sites, theoretical analyses suggest that the significance of the pathway should be influenced primarily by groundwater concentration, physical characteristics of the soil (e.g., air permeability, moisture, porosity, capillary rise height), and geometry (i.e., the distance from groundwater to the building foundation and position of the building relative to the vapor source). Foundation characteristics (e.g., geometry, depth, cracks and openings), building air exchange rate, and indoor-outdoor pressure fluctuations (driven by wind, ventilation, barometric pressure changes, etc.) are anticipated to have a lesser effect (Johnson, 2005).

Parallel attempts to empirically determine relationships between groundwater concentrations, indoor air impacts, and site-specific properties have been conducted. The compiled data have been used to develop groundwater attenuation factors (indoor concentration/predicted soil gas concentration in equilibrium with groundwater), but the empirical analyses have not led to any clear correlations with site-specific factors. That may reflect a combination of variable data quality, limited data quantity, and the fact that most of the data come from a few larger chlorinated solvent-impacted groundwater plume sites (Hers et al., 2006; USEPA, 2012a).

In the absence of confidence in the ability to anticipate VI behavior, regulatory guidance emphasizes measurement as summarized in Table 2.1. While variable across the federal, state,

and local levels, guidance has converged to a multiple-lines-of-evidence-based paradigm that involves combinations of indoor air, sub-slab soil gas, deeper soil gas, groundwater, and soil sampling in addition to screening-level modeling. In practice, heavy weighting is given to indoor air data from sparse data sets (e.g., USEPA, 2015; California Department of Toxic Substances Control, 2011). It is recognized that there could be temporal variability in pathway assessment data, but guidance is not clear on how it should be accounted for in designing sampling plans and interpreting data.

Table 2.1. Typical components of VI pathway assessment guidance.

Pathway Assessment Step	Brief Description	Other Comments
Collect site data: multiple-lines-of-evidence (MLE) pathway assessment sampling	Generally involves 24-h indoor air sample, and short-duration sub-slab soil gas, deep soil gas, and/or groundwater samples; typically the temporal frequency and spatial density of samples is very low (e.g., a few sampling events and sampling locations)	For sites involving multiple buildings, it is not clear how to efficiently and confidently assess the pathway without having to address each building individually. Temporal variability, factors affecting it, and how to account for it in VI pathway assessment plans are not known.
Estimate indoor air impacts	Use of the MLE data in combination with generic empirically-derived attenuation factors or screening-level models	Vapor intrusion impacts have been detected in buildings thought not to lie over the groundwater plume at some well-publicized sites and maximum indoor air impacts do not always correlate with maximum source zone concentrations.
Decision – Is VI pathway complete or incomplete, or are more data and analyses needed?	Data reviewed for adequacy and then projected indoor concentration impacts are compared against values in look-up tables.	When MLE data sets contain conflicting results indoor air data are weighted most heavily. Temporal variability, factors affecting it, and how to account for it in VI pathway decision-making are not known. (The VI pathway is “complete” if estimated indoor air impacts exceed target health-based thresholds)

Thus there is a need to better understand the utility and limitations of the current VI pathway assessment approach and to identify new paradigms that could lead to greater cost effectiveness and increased confidence in VI pathway assessment decisions.

At the onset of this project, it was hypothesized that:

- In the absence of new research, pathway assessment guidance would continue to emphasize point-in-time and point-in-space multiple-lines-of-evidence data collection, combined with conservative data interpretation and decision-making. Such an approach would lead to costly pathway assessment without any increase in confidence and might also lead to erroneous decision-making.

- There was opportunity for new knowledge to impact pathway assessment guidance development; however, in the near-term, it was likely that any revised guidance would retain aspects of the current point-in-time and point-in-space multiple-lines-of-evidence approach. For example, indoor air data would likely continue to be weighted most heavily, users would want to continue to use conventional dissolved groundwater plume characterization data from their site assessments, and USEPA would want to continue use of its sub-slab soil gas sampling guidance.

- It was important, therefore, to understand the temporal and spatial variability in these measurements and the factors that affect that variability. That knowledge is critical in order to appropriately design sampling plans (sampling frequency, location, etc.) and to be able to appropriately interpret and weight the data during pathway assessment. It was also possible that, in increasing our understanding, use of some of the current multiple-lines-of-evidence might be discontinued.

- The temporal indoor air signatures associated with indoor and subsurface vapor sources were likely to be different; if that was true, then that information could be used to discern indoor air contributions from these two sources.

- The apparent lack of correlation between dissolved groundwater, soil gas, and indoor air concentrations observed at some chlorinated solvent-impacted sites was likely the result of using wells with broad screen intervals. Better correlation would likely be achieved by discrete groundwater sampling at the top of the saturated zone.

- The pathway assessment paradigm of the future would de-emphasize the point-in-time and point-in-space multiple-lines-of-evidence data collection of the present, and would instead emphasize characterization of vapor flux and use of longer-term integrated concentration monitoring.

Based on these considerations, the studies in this project were initially designed to focus on a few key topics that would address issues believed to be critical to the development of new guidance that would be both cost effective and lead to higher-levels of confidence in the pathway assessment. They included:

- <u>Temporal variability of indoor air concentrations:</u> As long as regulatory guidance requires indoor air quality monitoring for homes overlying chlorinated solvent groundwater plumes, a solid technical basis for selecting sampling frequency and duration is needed.

- Spatial and temporal variability in sub-slab and near-foundation soil gas: As long as regulatory guidance encourages sub-slab soil gas monitoring, a solid technical basis for selecting sampling frequency and duration and spatial density is needed; in addition, there is debate on the desirability and efficacy of sub-slab soil gas sampling.

- Indoor chemical sources: Indoor chemical vapor sources can confound the pathway assessment. An inventory of common household items that can contribute to chlorinated solvent vapors would be useful as well as guidance for differentiating contributions from groundwater plumes and indoor chemical sources. This inventory was provided by Dettenmaier (2010) and is shown in Appendix C.

- Investigation of alternate assessment monitoring approaches: Current assessment focuses on concentration measurements and the extrapolation of that data to long-term indoor air concentrations. There has been ongoing debate concerning data requirements; for example, some would prefer not to do intrusive indoor air and sub-slab sampling unless other data suggest it is warranted. There is also on-going debate concerning the extrapolation of groundwater, soil gas, and sub-slab soil gas concentrations to indoor air concentrations. Examples of alternate approaches that would involve less extrapolation are: a) the determination of vapor flux from groundwater (e.g., from soil gas profiles and measured in situ diffusion coefficients) and b) indoor air quality measured under controlled building depressurization conditions.

- Changes with time in vapor emissions from chlorinated solvent groundwater plumes: A better understanding of the dynamics of vapor emission rates under changing groundwater conditions is needed in order to more intelligently design sampling plans. Groundwater plumes are dynamic systems; groundwater table elevations, moisture infiltration rates, and moisture profiles change with time. These may cause temporal changes in the vapor emission rate from groundwater; however, the magnitude and frequency of vapor emission rate fluctuations have yet to be studied in great detail.

3 MATERIALS AND METHODS

3.1 GENERAL METHODOLOGY/APPROACH

Table 3.1 below summarizes the focused research topics identified above and an overview of how they were addressed in this study. The research approaches are discussed in more detail below.

Table 3.1. Key research topics and brief overview of how they were addressed in this study.

Key Research Topic	Research Approach
Temporal variability of indoor air concentrations	*Field study utilizing a house overlying a groundwater plume.* Continuous, long-term, high-frequency collection/analysis of indoor air samples under natural conditions.
Spatial and temporal variability in subsurface concentrations	*Field study utilizing a house overlying a groundwater plume.* Periodic snapshots and continuous collection/analysis of soil gas and sub-slab soil gas samples under both natural conditions.
Indoor chemical sources	*Literature and field study utilizing a house overlying a groundwater plume.* List of chemicals known to suspected of containing TCE or chlorinated solvents compiled. Use of tracer gas release indoors to simulate indoor contaminant source and its ability to generate a subsurface soil gas plume.
Investigation of alternate assessment monitoring approaches	*Field study utilizing a house overlying a groundwater plume.* Collection of indoor air samples and building exchange rates during long-term controlled pressurization method (CPM) test, and comparison with data collected under natural conditions.
Changes with time in vapor emissions from chlorinated solvent groundwater plumes	*Field study utilizing a house overlying a groundwater plume.* Collection of indoor air samples and building exchange rates during long-term controlled pressurization method (CPM) test. L*ab-scale physical model study*. Study of changes in vapor emissions in response to changes in groundwater level for two soil types. *Numeric modeling study*. Sensitivity analysis of various factors that may affect CHC transport with fluctuating water table.

3.1.1 **Field study utilizing a house overlying a groundwater plume**

A unique element of this study was the purchase a house overlying a dissolved chlorinated hydrocarbon (CHC) groundwater plume and the outfitting of it for use as a field laboratory. The study house, shown in Figure 3.1, overlies the OU-8 dissolved chlorinated solvent groundwater plume near Hill Air Force Base, UT. Located north of Salt Lake City, Hill AFB has been in operation since 1934. Historic waste management practices resulted in a number of CHC groundwater plumes that migrated off site and beneath residential neighborhoods. Trichloroethylene (TCE) is the primary groundwater contaminant in these off-site plumes and

1,2-dichloroethane (1,2-DCA), 1,1- dichloroethene (1,1-DCE), *cis*-1,2-dichloroethene (*cis*-DCE), and tetrachloroethylene (PCE) are also present in some areas.

Figure 3.1. Field study house

The study house is a two-story, split-level building built into a slope with a 2.5 m elevation drop from the back to front yard. There is a living space and attached garage on the lower level. This house was selected because it was for sale, it had a history of occasional CHC detections in indoor air prior to installation and operation of a sub-slab depressurization/mitigation system, and indoor CHC levels increased during a short-term mitigation system shut-down test prior to its purchase.

Multi-level soil gas and groundwater sampling points were installed inside through the foundation and outside of the building as shown in Figure 3.2, which provides both and aerial and cross-sectional view of the general layout of the monitoring network. Specific depths and locations of sampling points were selected to best match site conditions and to reasonably delineate the vapor distribution beneath the slab. Soil gas sampling depths were referenced to the sub-slab level of the house.

Table 3.2 summarizes key site measurements, duration of study for given measurements, analytical equipment methods, sampling media and location, frequency, and data QA/QC. These included:

- Outdoor conditions: barometric pressure, wind speed/direction, temperature, precipitation, and CHC, radon, Sulfur hexafluoride (SF_6) concentrations in ambient air.

- Indoor conditions: temperature, HVAC operation, differential pressures relative to outdoor air and soil gas, indoor air CHC, radon, and SF_6 tracer gas concentrations.

- Subsurface conditions: temperature, soil moisture, differential pressures relative to indoor or outdoor air, in situ diffusion coefficients, air permeability tests, CHC, radon, and SF_6 tracer gas concentrations.

3.1.2 **Lab Studies: two-dimensional physical model experiments**

Laboratory-scale physical model experiments were conducted to study relationships between groundwater table fluctuations, soil type, and groundwater emission rates. They were conducted in the two-dimensional tanks shown schematically in Figure 3.3. These were designed to allow simultaneous measurement of groundwater and soil gas concentration distributions, water level, and emission rate. Groundwater level fluctuations could be driven by vertical or lateral water introduction and/or flow from the tanks. Water level fluctuations of approximately 1 ft were created and emission rates were determined by measuring the effluent sweep gas flow rate and concentration. Table 3.3 outlines tank operations and measurements and Table 3.4 summarizes the properties of chemicals used in these experiments.

	Outdoor Sampling Locations					Indoor Sampling Locations							Outdoor Sampling Locations				
	**GW1	**GW2	A	B	F	1	2	3	4	5	6	7	C	D	**GW3	E	**GW4
***Depth relative to Subslab (ft)																	
+11	*GS - 10.3'	*GS - 10.7'															
+10																	
+9																	
+8																	
+7			*GS-6.2'														
+6				*GS-6.0'													
+5					"GS-5.0'												
+4													*GS-3.7'				
+3																	
+2																	
+1														*GS-1.0'	*GS-1.0'		
0 - Subslab			1,2,3,4,6	1,2,3,4,6	1,2,3,4,6	1,2,3,4,5	1,2,3,4	1,2,3,4	1,2,3,4	1,2,3,4	1,2,3,4	1,2,3,4	1,2,3,4,5,6	---		*GS-0.6'	*GS-0.6'
-1																1,2,3,4,6	
-2																	
-3			1,2,3,4,6	1,2,3,4,6	1,2,3,4,6	1,2,3,4,5,6	1,2,3,4,6	1,2,3,4,6	1,2,3,4,6	1,2,3,4,6	1,2,3,4,6		1,2,3,4,5,6	1,2,3,4,6		1,2,3,4,6	
-4	7	7															
-5																	
-6			---	---	6	6,5	1,2,4	1,2,4	1,2,4	1,2,4	1,2,4		1,2,3,4,5,6	1,2,3,4,6		1,2,3,4,6	
-7																	
-8																	
-9			---	---	---	7,5	7	7	7	7	7		5	---		---	
-10																	7
-11															8		
-12			---	---	---	5							5	---		---	
-13																	
-14																	
-15																	
-16																	
-17																	
-18																	
-19																	
-20																	
-21	7	7													8		7
-22																	
-23																	
-24																	
-25																	
-26																	
-27																	
-28																	
-29																	
-30	7	7													8		7
-31																	

***Depth relative to Subslab (ft)

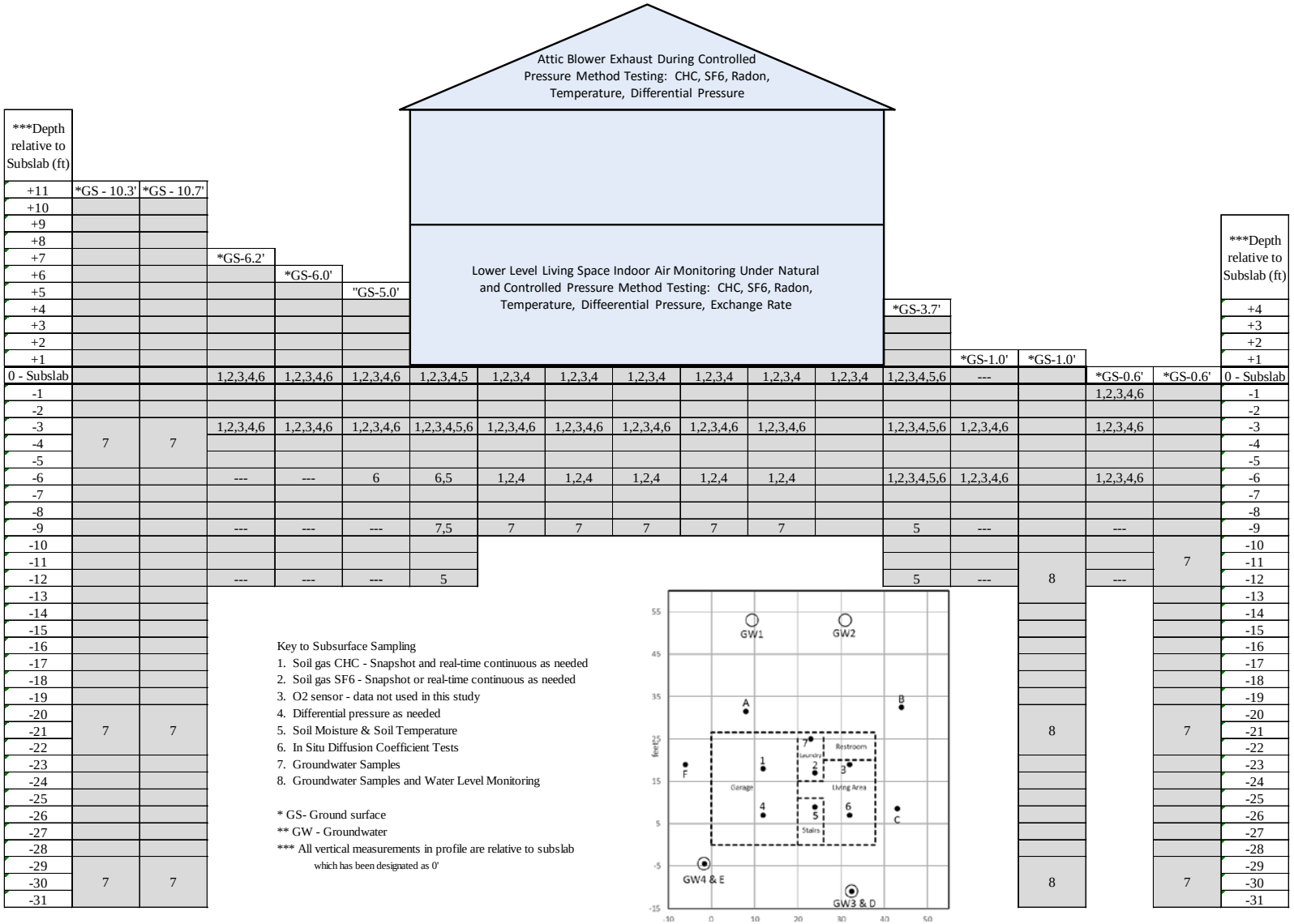

Figure 3.2. Aerial and cross-sectional views illustrating the discrete depth monitoring network.

Table 3.2. Summary of key on-site measurements, including duration and frequency, analytical methods, and data QA/QC.

Key Site Measurement	Data Collection Period	Analytical Equipment, Methods, and Frequency	Sampling Media and Location	Data QA/QC
Differential pressures: soil gas relative to indoor air pressure	August 2010 - December 2014	Pace Scientific Differential P300 pressure sensors connected to data loggers; readings on 2-minute intervals	All sub-slab depths if not otherwise being used for soil gas sampling. Also, other locations as desired	Sensor readings referenced to a zero differential pressure reading every day
Soil temperature	August 2010 - December 2014	Type J thermocouples connected to data loggers; readings on 2-minute intervals	Depth discrete monitoring adjacent to locations 1 and C	Review for reasonable values
Soil moisture	August 2010 - December 2014	Decagon 10HS soil moisture sensors connected to data loggers; readings on 2-minute intervals	Depth discrete monitoring adjacent to locations 1 and C	Moisture readings compared with soil moisture measurements from soil cores
Soil gas O_2 concentration	August 2010 - December 2014	Figaro KE-50 Oxygen sensor connected to data loggers; readings on 2-minute intervals	All soil gas locations at sub-slab, 3 ft below slab (BS), and 6 ft BS depths	Calibrated to known O_2 sample prior to installation
Indoor air, outdoor air, and HVAC temperature	December 2010 - December 2014	Type J thermocouples connected to data loggers; readings on 2-minute intervals	Indoor, garage, outdoor, AC duct, attic	Review for reasonable values

Key Site Measurement	Data Collection Period	Analytical Equipment, Methods, and Frequency	Sampling Media and Location	Data QA/QC
Outdoor temperature, wind speed/direction, barometric pressure, precipitation, humidity	August 2010 - December 2014	Nova Lynx weather station with data logger; readings every 10 minutes	Site meteorological conditions	Data checked against local government weather records
Chlorinated compound concentrations	GCMS/Thermal Desorption: November 2010 – December 2014	Samples collected on thermal desorption tubes using SRI data system and two 20-stream gas samplers, followed by desorption and analysis by Markes Unity thermal desorber and GC-MS at ASU lab; 4-hour time-averaged indoor air sampling	Indoor air in living room downstairs, outdoor air sampling along north property line away from house	Standard QA/QC procedures including blanks, duplicates, calibrations, and internal standards
Chlorinated compound concentrations	February 2010 – February 2013	Collected and analyzed using portable HAPSITE GC-MS unit provided by Hill Air Force Base; discrete (1-minute) samples collected every 2 hours	Indoor air beneath stairwell downstairs; adjacent to living room	Standard QA/QC procedures including blanks, duplicates, and calibrations
Chlorinated compound concentrations	February 2011 – December 2014	Sample collected/analyzed using SRI 10-stream gas-sampler onto thermal desorption trap followed by desorption and analysis using on-site GC-TO-14-ECD; sampling every 5 hours or less from each location	Indoor air in living room downstairs, outdoor sample from backyard away from house, and selected soil gas locations	Standard QA/QC procedures including calibrations

Key Site Measurement	Data Collection Period	Analytical Equipment, Methods, and Frequency	Sampling Media and Location	Data QA/QC
SF_6 concentrations (note: SF_6 is released indoors continuously at 5 ml/min)	February 2011 – December 2014	Sample collected/analyzed using SRI 10-stream gas-sampler and analyzed by GC-PDD; sampling every 2 hours or less from each location	Indoor air in living room downstairs, outdoor sample from backyard away from house, and selected soil gas locations	A reference standard is run every 10^{th} sample run, approximately every 5 hours
Radon concentrations	February 2011 – December 2014	Collected and analyzed on site using Durridge Rad-7 radon detector; 2-hour time-averaged indoor air samples	Indoor air in living room downstairs	Instrument calibrated at the factory every 12 months
Groundwater elevation	November 2010 – December 2014	In situ Solinst Level-Logger transducers; height of water above transducer recorded every 12 hours	GW3 at three depth discrete intervals	Data review for reasonableness
In-situ effective diffusion coefficients	Aug 2011 Feb 2012 Apr 2012 May 2012 Aug 2012	Helium detector using Johnson et al (1998) push-pull method	All available soil gas sampling points	Helium detector calibrated, and duplicates and replicates run

Key Site Measurement	Data Collection Period	Analytical Equipment, Methods, and Frequency	Sampling Media and Location	Data QA/QC
Synoptic concentration "snapshots": • SF_6, radon, and CHCs in soil gas • CHCs in groundwater • Depth to groundwater	2010 - Aug, Nov, Dec 2011 - Jan, Feb, Mar, May, Jul, Aug, Sep, Nov, Dec 2012 – Jan, Feb, Apr, May, Aug, Nov, Dec 2013 – Feb, May, Jul, Aug, Oct 2014 – Jan, Mar, Jun, Dec SF_6 started Dec 2010 Radon started Feb 2011	Soil gas samples collected in tedlar bags using lung-sampler, then analyzed using GC-TO-14-DELCD or GC-DELCD and GC-PDD; groundwater samples collected and preserved with HCl in 40-ml VOA bottles and transported back to ASU lab for analysis using GC-DELCD; depth-to-water determined using Solinst water level sounder; soil gas radon collected and analyzed using Durridge Rad-7 radon detector; snapshot events occurred every month for first two years and then tapered to every three months toward the end of the sampling period in December 2014	All available soil gas and groundwater locations	Standard QA/QC procedures using blanks, duplicates, replicates, trip blanks, and calibration samples.

a)

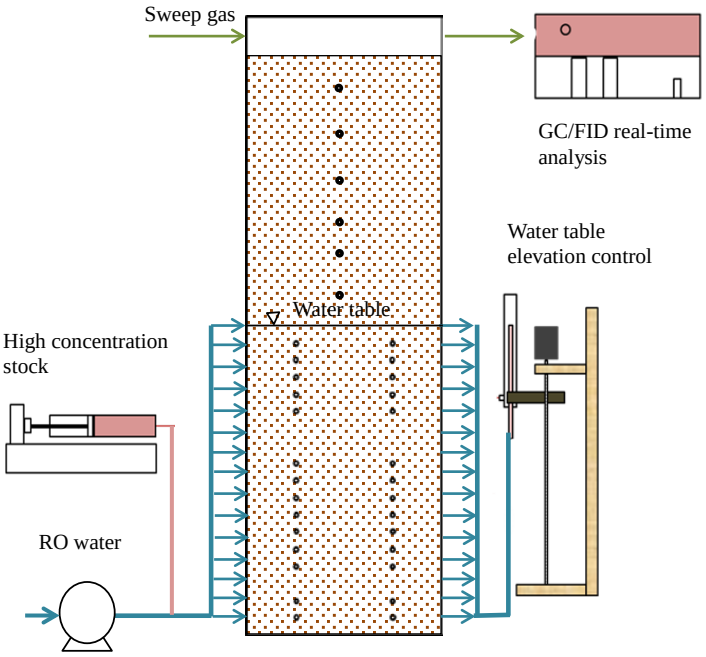

b)

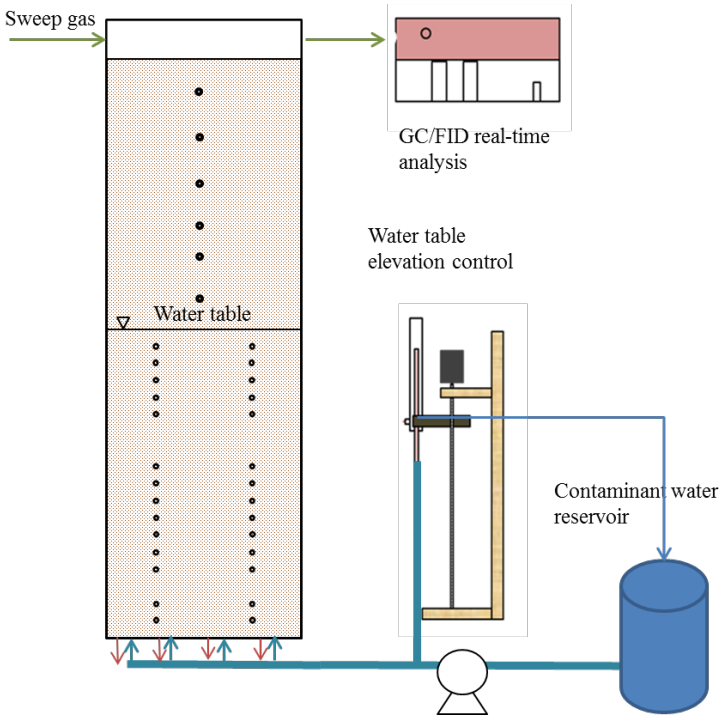

Figure 3.3. Schematic of lab-scale physical models with water level fluctuations controlled by a) horizontal flow and b) vertical flow.

Table 3.3. Lab-scale experimental conditions and measurements.

Test	Operation Condition							Measurements			
	GW fluctuation range [m]	GW Flow	Initial water table elevation [m]	Final water table elevation [m]	GW velocity rate [m/d]	Water table change rate [cm/d]	Feed water concentrations [mg/L]	Sweep gas CHC concentration	Temperature and relative humidity in/out of sweep gas	GW contaminant profile	Real-time soil moisture content
Water table drop	0.3	horizontal	0.9	0.6	0.3	9.2	2.6 for 1,2-DCA, 2.1 for TCE and 1.2 for PCE	Yes	No	Yes	Yes
Water table rise	0.3	horizontal	0.6	0.9	0.3	10		Yes	No	Yes	Yes
Water table fluctuation	0.3	horizontal	0.9	0.9	0.3	10	1.7 for 1,2-DCA, 1.6 for TCE and 0.9 for PCE	Yes	No	Yes	Yes
Water table fluctuation	0.3	horizontal	0.9	0.9	0.3	5	1.8 for 1,2-DCA, 1.7 for TCE and 1.0 for PCE	Yes	Yes	Yes	Yes
Water table fluctuation	0.3	no net flow into the tank	0.9	0.9	0	5	Initial concentrations were 1.1 for 1,2-DCA, 0.9 for TCE and 0.5 for PCE.	Yes	Yes	Yes	Yes

Table 3.4. Chemical properties for TCE, PCE, and 1,2-DCA

	Unit	TCE	PCE	1,2- DCA
Dimensionless Henry's Law Constant (25 ℃)	-	0.42	0.75	0.04
Organic carbon water partition coefficient K_{ow}	cm^3-H_2O/g-OC	166	155	17.4
Diffusion Coefficient in Water (25 ℃)	cm^2/s	9.1×10^{-6}	8.2×10^{-6}	9.9×10^{-6}
Diffusion Coefficient in Air (25 ℃)	cm^2/s	7.9×10^{-2}	7.2×10^{-2}	1.0×10^{-1}
Solubility (25 ℃)	mg/L-H_2O	1.1×10^{3}	2.0×10^{2}	8.5×10^{3}

*: values from USEPA (2000)

3.1.3 **Modeling Analysis**

Simulations were conducted to understand the effect of soil and chemical properties and water table fluctuation patterns (magnitude and frequency) on emission rate changes. For simplicity, the conceptual model used for this modeling investigation was the one-dimensional soil column shown in Figure 3.4 below. Water table fluctuations were created by changing the lower water pressure boundary condition in the modeling domain. Contaminant transport included volatilization from the water phase, migration through the soil matrix, and emission to clean air at the modeling domain upper boundary.

HYDRUS-1D version 4.16 (Simunek, 2013) was used to perform simulations; it is public domain software and includes the one-dimensional finite element model HYDRUS for simulation of water, heat, and solute movement in variably water-saturated media. Only water and solute flow were considered in this study; the system was isothermal without hysteresis in saturation-capillary pressure profiles.

A constant pressure head was assigned at the upper boundary and a time-varying pressure head was assigned at the lower boundary. For solute transport, a 0.5 cm stagnant upper boundary layer thickness was selected, as it was recommended in HYDRUS-1 D (Simunek, 2013) when both water and gas phases are present at the soil surface. The vapor emission from the soil to the atmosphere is calculated based on the difference in gas concentrations above (atmosphere) and below (soil gas) this layer. The atmosphere concentration at the upper boundary of this stagnant layer was held at zero. A constant concentration was held at the lower model boundary for source below water table condition as shown in Figure 3.4. This modeling tool was validated by using the groundwater table fluctuation lab experiment results with water recharging/depleting from the lower boundary of the tank. Detailed validation simulation information can be found in Appendix A.6.

Based on field and lab observations, soil properties, chemical properties, and water table fluctuation patterns may affect vapor emissions from groundwater to the soil surface. A sensitivity analysis was performed for these parameters with the dissolved concentration source strength being 1 mg/L.

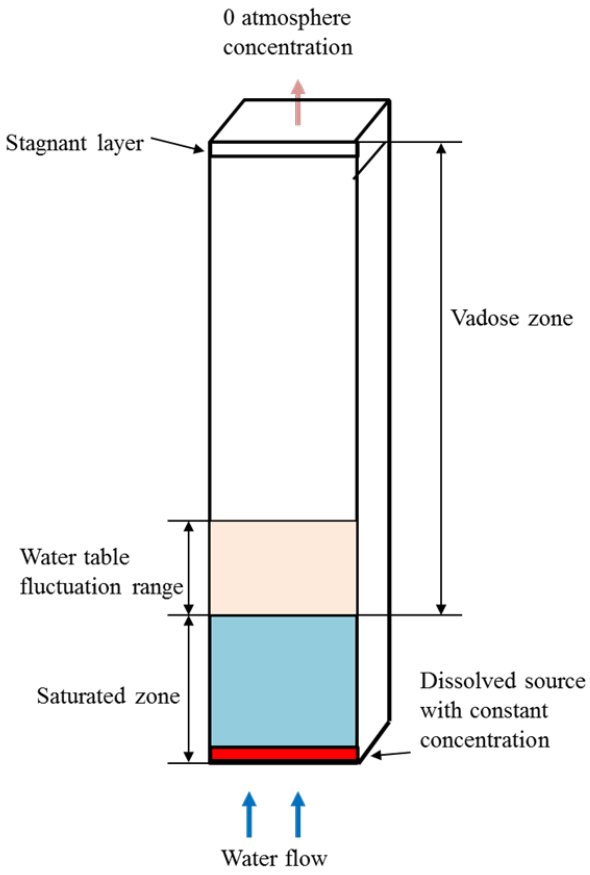

Figure 3.4. Conceptual models for simulation boundary condition.

Two source zone conditions were simulated, one was a dissolved source located 50 cm below the initial water table, and the other was a dissolved source located 200 cm below the initial water table elevation. Both might be representative of regions where non-aqueous phase liquid (NAPL) source zones are submerged at or near the initial CHC spills.

Simulations for each scenario were conducted using the concentration distributions from fixed/non-moving water table conditions as the starting point for time-varying head condition simulations. The emission for the fixed water table elevation at $z_{initial} + L/2$ (E_{static}) was calculated to normalize time-varying simulation emissions, since the bottom pressure head followed: $Head(bot) = L[sin(2\pi t/P - \pi/2)+1] + z_{initial}$. For example, Figure 3.5 illustrates the TCE emissions normalized to E_{static} during the transition process from a static water table (65 cm above lower boundary) to 30 cm monthly oscillation with a 50 cm initial vadose zone thickness and 50 cm source depth below the initial water table level. Maximum and minimum emission rates were obtained after t = 250 d, when the system reached dynamic steady state.

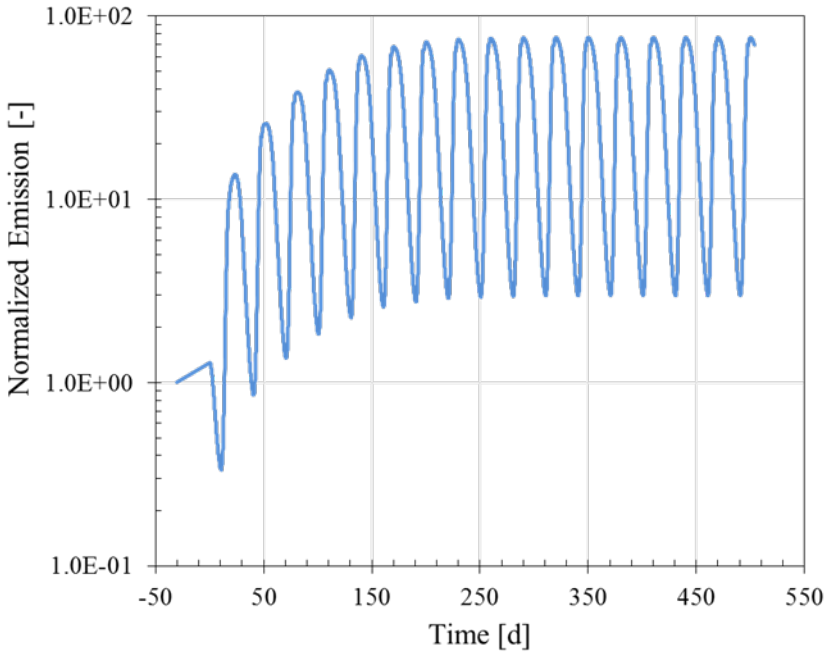

Figure 3.5. Normalized TCE emissions during the transition from static water table conditions to dynamic steady state for a source located 50 cm below the initial water table, 30 monthly water table oscillations, and 50 cm depth to the initial water table.

The reference scenario simulation involved a constant TCE concentration source, 150 cm vadose zone thickness above the initial water table elevation, and 30 cm monthly water table fluctuations. Changes in inputs about this reference scenario were then evaluated with a focus on the following: (1) water table fluctuation pattern, (2) vadose zone thickness, (3) soil type, and (4) chemical properties.

Water table fluctuations were created by applying a sine-wave time-variable pressure head condition at the lower boundary ($Head(bot) = L[sin(2\pi t/P - \pi/2)+1] + z_{initial}$). Annual, monthly and daily water table variations of 30 cm were simulated, as well as monthly fluctuations ranging from 1 cm to 100 cm.

Soil capillary properties usually reflect soil hydraulic conductivity, and higher hydraulic conductivity soils commonly have smaller capillary fringe heights. Simulations were conducted using three types of soil: coarse sand, sand, and loam, with capillary fringe heights ranging from less than 5 cm to more than 200 cm, and their K_s values varied over 100X. Soil properties for sand and loam were obtained from values built-in HYDRUS 1-D. Soil properties for coarse sand were selected to match the silica sand tank steady-state saturation profiles. The soil saturation vs. elevation curves for these soil types are presented in Figure 3.6.

TCE was selected as a reference chemical for these studies, recognizing that diffusion coefficients in air and water for other CHCs are within about a factor of 2X and that Henry's Law constants might vary from TCE by as much as two orders of magnitude. Thus, simulations

were run by varying its D_{air} and D_{water} values from 0.5X to 2X TCE values, and H from 0.1X to 10X the TCE value. The effective sorption coefficient (k_s) was also varied from 0 to 10 L/kg.

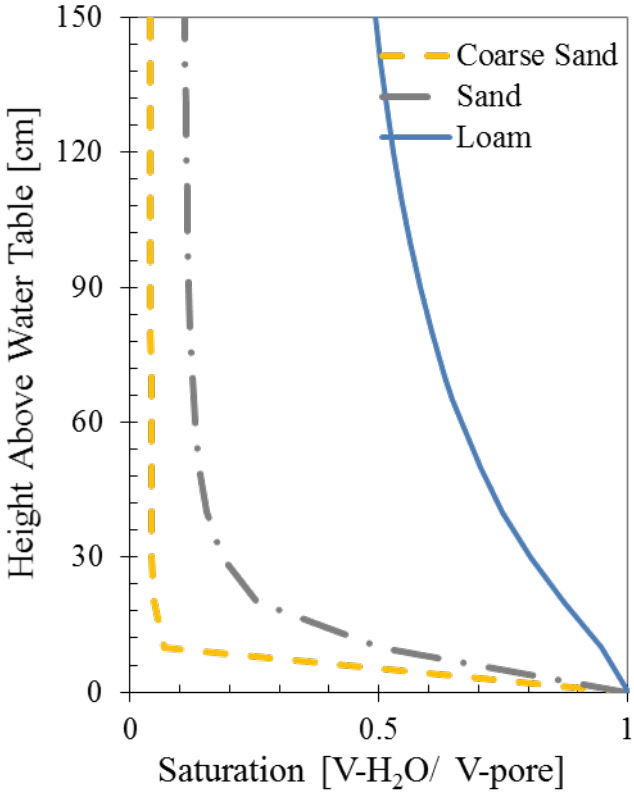

Figure 3.6. Soil saturation versus height above water table using coarse sand, sand and loam van Genuchten parameter values.

3.2 SAMPLING AND ANALYTICAL METHODS

3.2.1 Measurement of chlorinated hydrocarbons (CHCs) in indoor and outdoor air

Measurement of CHCs in indoor air was performed using the three methods below, usually with at least two methods run in parallel at all times.

1. HAPSITE portable GCMS: Near-instantaneous (1-min duration) 100-mL samples; collected, concentrated, and analyzed every 2 h using a HAPSITE portable gas chromatography/mass spectroscopy (GC/MS) unit (Inficon, Syracuse, NY);

2. Sorbent tubes: A continuous sequence of 4-h time-averaged 12-L samples concentrated on multi-bed sorbent tubes that were sent to Arizona State University (ASU) for analysis by thermal desorption and GC/MS; and

3. GC/ECD: 10-min time-averaged samples collected every 40 min; 100-500 mL concentrated on a multi-bed sorbent trap and analyzed on-site using a GC equipped with an electron capture detector (ECD).

Details of each method are provided below:

HAPSITE Portable GC/MS: Following a sample purge volume of 100 mL, 100 mL of air were pulled through a heated probe and through a multi-bed sorbent trap. The trapped chemicals were thermally desorbed and delivered to a GC column for separation and analysis by MS. The temperature program was: 55°C start, hold for 80 s, and ramp at 30°C/min to 110°C. The procedure outlined by Gorder and Dettenmaier (2011) was followed for operation of the HAPSITE, including calibration and QA/QC procedures. The method detection limit (MDL) for TCE using the HAPSITE was 0.06 ppb_v.

Sorbent Tubes and Off-site GC/MS: Air was drawn through multi-bed sorbent tube samples using two customized 20-stream gas sampling valves (SRI Instruments, Torrance, CA), a Rena model BE-3012 vacuum pump and a 0-100 mL/min vacuum-configured mass flow controller (Alicat Scientific, Tucson, AZ). Samples were collected over a 4 hour period at 50 ml/min for a total sample volume of 12 L. Sample collection was controlled by an SRI Instruments 6-channel data system and monitored using SRI PeakSimple software. Sorbent tubes (0.64 x 15.2 cm-long) were packed with Tenax-GR and Carboxen-569 and capped with Markes Difflok sampling caps (Markes International, UK). A schematic and photo of the sorbent tube collection configuration is shown in Figure 3.7. After completion of a sampling set (38 sorbent tubes, approximately 6.3 days), sorbent tubes were removed and capped with Swagelok brass caps with Teflon ferrules and shipped to ASU for analysis.

Sorbent tubes were analyzed using a Markes Ultra autosampler, a Markes Unity thermal desorber (Markes International, UK) and an HP5890 gas chromatograph (GC) with an HP5972 mass spectrometer (MS). The GC analytical column was a 60 m Restek RXI-5 capillary column. Analysis of samples on the GC/MS was performed using the selective-ion monitoring (SIM) mode. The temperature program was: 40°C start, hold for 2 min, ramp at 15°C/min to 220°C, and hold for 5 min. The MDL was calculated as 0.008 ppb_v for TCE for this method using USEPA's MDL procedure (USGS, 1999; see Table 3.5).

To reduce sample mass loss, sorbent tubes were analyzed as soon as possible upon receipt at ASU. Due to the duration of sample set collection (i.e., tubes used early in sampling set), shipping, and analytical equipment maintenance, samples could sit up to 12 days prior to analysis. To quantify potential losses that might occur during over this duration, a 12 day holding test was performed using spiked sample tubes. Three sorbent tubes were spiked with 0.1 ppb_v of a CHC mix (equivalent to 0.55 ng for TCE) and three additional tubes were spiked with 1.0 ppb_v of a CHC mix (equivalent to 5.46 for TCE). Additional sets of six spiked sorbent tubes were prepared at 4, 8, and 11 days. All tubes were then analyzed on the 12^{th} day. Focusing on TCE mass, results for this test are shown in Table 3.6. In general, the mass losses over the testing period were relatively low with similar losses observed between the shortest and longest

holding times. The greatest percent difference between spiked mass and mean calculated mass was 13.5% and this was considered within a range of acceptable analytical error.

Prior to each use, sorbent tubes were conditioned using a Markes TC-20 tube conditioner (Markes International, UK) at ASU. This involved incremental heating (180°C for 10 min, 210°C for 10 min, 230°C for 10 min, and 250°C for 30 min) of each tube with concurrent flow (15-20 mL/min) of ultra-high purity (UHP) nitrogen. Once the conditioning program was finished, tubes were allowed to cool to room temperature with a continuous nitrogen flow and then capped with Swagelok brass caps with Teflon ferrules in preparation for the next use.

Calibration of the GC/MS was performed prior to each sample set using gas standards prepared from a customized 1 ppm_v commercial gas standard (Linde Gas North America LLC, Alpha, NJ) containing a suite of chlorinated and petroleum hydrocarbon chemicals in nitrogen (see Table 3.7). Analytical accuracy for the prepared gas standard concentrations was stated as ±5% by the manufacturer. Calibration curve fittings consistently gave R^2 regressions of 0.99 or greater.

Additional QA/QC included sample blanks, trip blanks, trip spikes, and internal standards. Sample blanks were included in all calibration and sample sets. For sample sets, blanks were run at the rate of 1 per 10 samples. Target chemicals were consistently non-detectable on blanks. Similarly, trip blanks, which were routinely included in sample sets and concentrations for target chemicals were consistently non-detectable. Starting in Spring 2012, fluorobenzene was used as an internal standard on 1-in-10 samples. Recovery of fluorobenzene was consistently greater than 96%. Based sample collection time, method of collection, and equipment restrictions, it was not possible to perform duplicates as part of QA/QC for this method.

Sorbent Tubes and On-site GC/ECD: Indoor air samples collected for analysis with the on-site GC/ECD were concentrated on a multi-bed sorbent tube trap (0.64 x 15.2 cm) packed with Tenax-GR and Carboxen-569 using a Rena model BE3012 vacuum pump and a vacuum-configured 0-100 mL/min mass flow controller (Alicat Scientific, Tucson, AZ) at 50 mL/min. Sample collection time was controlled using SRI's PeakSimple software. Once collected, the sample was desorbed onto a Restek 60–m long MXT-5 column using a 2-minute, 240°C trap heating program with helium carrier gas. The MXT-5 column was then heated from 40°C to 220°C at 10°C/min and sample analysis by ECD.

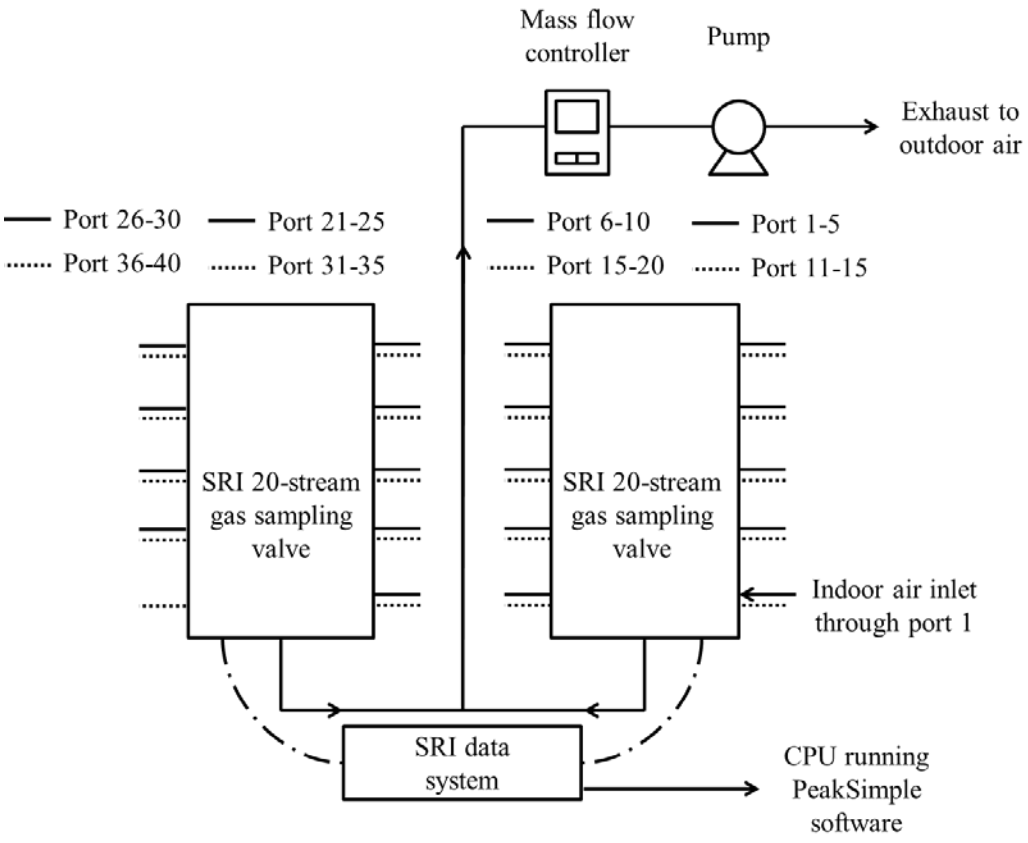

Figure 3.7. Schematic and photo of automated indoor and outdoor air sampling and concentration using multi-bed sorbent tubes.

Calibration of the GC/ECD occurred every 1-3 months at the beginning and end of on-site synoptic surveys. Calibrations were performed using gas standards prepared from a 1 ppm_v commercial gas standard containing a suite of CHCs. Replacement of the multi-bed sorbent trap occurred when calibration curves approached a 20% difference from the initial calibration using that trap. On average, trap replacement occurred every 3 months. The MDL for TCE for this method was calculated as 0.009 ppb_v (approximately 0.05 $\mu g/m^3$) using USEPA's MDL procedure (USGS, 1999). Results for MDL calculation are shown in Table 3.8.

Table 3.5. Spiked concentrations, responses, and calculated concentrations used to calculate the MDL for TCE using the sorbent tube off-site GC/MS method.

Sample	Spiked Concentration [ppb_v]	Response [area count]	Calculated Concentration [ppb_v]
1	0.05	21101	0.0515
2	0.05	21054	0.0514
3	0.05	19894	0.0487
4	0.05	19254	0.0472
5	0.05	20127	0.0492
6	0.05	18826	0.0461
7	0.05	21593	0.0526
		Average:	0.0495
		Standard Deviation (s):	0.0024
		Student's t value (t):	3.14
		MDL [ppb_v]	0.008
$MDL = s\ x\ t_{(n-1,1-\propto=0.99)}$			

Table 3.6. Results of sorbent tube holding tests for TCE mass.

Time since preparation [d]	Spiked Mass, TCE [ng]			
	0.55		5.46	
	Mean Calculated Mass [ng], n=3	Percent Difference [%]	Mean Calculated Mass [ng], n=3	Percent Difference [%]
1	0.51	7.3%	5.15	5.8%
4	0.59	7.7%	5.65	3.4%
8	0.60	9.3%	4.76	13.7%
12	0.61	9.5%	5.18	5.3%

Table 3.7. Contents, requested concentrations, and analyzed concentrations of components in the commercial gas standard from Linde Gas North America LLC (Alpha, NJ).

Compound	Requested Concentration [ppm_v]	Analyzed/Actual Concentration [ppm_v]
vinyl chloride	1.00	0.97
1,1-dichloroethene	1.00	1.03
trans-1,2-dichloroethylene	1.00	1.06
1,1-dichloroethane	1.00	1.01
cis-1,2-dichloroethylene	1.00	1.03
1,2-dichloroethane	1.00	1.00
1,1,1-trichloroethane	1.00	1.00
benzene	1.00	1.02
trichloroethylene	1.00	1.02
1,1,2-trichloroethane	1.00	1.04
toluene	1.00	1.03
tetrachloroethylene	1.00	1.01

Table 3.8. Spiked concentrations, responses, and calculated concentrations used to determine the MDL for TCE using the GC/ECD method.

Sample	Spiked Concentration [ppb_v]	Response [area count]	Calculated Concentration [ppb_v]
1	0.04	578.1	0.0406
2	0.04	549.1	0.0385
3	0.04	586.8	0.0413
4	0.04	625.7	0.0442
5	0.04	552.7	0.0387
6	0.04	506.3	0.0353
7	0.04	599.8	0.0423
		Average:	0.0401
		Standard Deviation (s):	0.0029
		Student's t value (t):	3.14
		MDL [ppb_v]	0.009
$MDL = s\ x\ t_{(n-1,1-\propto=0.99)}$			

3.2.2 **Measurement of CHCs in soil gas**

Measurement of CHCs in soil gas occurred on-site during synoptic survey events (snapshots) using a GC/DELCD (dry electrolytic conductivity detector). Depending on the sample concentration, samples were analyzed by either direct-injection onto the GC/DELCD or by pre-concentration of 500 mL of the sample on a sorbent tube prior to thermal desorption and analysis by GC/DELCD.

Collection of Soil Gas Samples: The custom-built vacuum/lung sampler shown in Figure 3.8 was used to collect the samples. Within the sampler, a vacuum environment is created around a 1-L Tedlar bag and this draws soil gas samples directly into the Tedlar bag (SKC 232-01) without passing through a pump, thereby avoiding cross contamination. The box was constructed from a Pelican case (Pelican Products, Torrance, CA), stainless steel tubing, and Swagelok parts and was connected to a RENA model BE-3012 vacuum pump.

The procedure for soil gas sampling was:

- Tedlar bags were flushed with helium gas three times and then evacuated using a 60 mL syringe prior to use.
- The soil gas sampling port was connected to the lung sampler.
- The lung sampler was opened and the Tedlar bag was connected to the internal sampling port. The valve on the Tedlar bag was then opened and the lung sampler was closed.
- The pump was turned on and approximately 100 mL of soil gas was purged from sampling lines and exhausted to flush the tubing.
- The soil gas was then routed to the Tedlar bag where an additional 100 mL of soil gas was collected to flush the Tedlar bag. This volume was then exhausted to outdoor air.
- Approximately 500 to 800 mL of soil gas was then collected. The actual volume was based on the anticipated concentration of sample and volume needed for concentration.
- The vacuum pump was then turned off and the lung sampler ventilated and opened. The valve on the Tedlar bag was closed and the bag was removed from the sampler for analysis.
- The sampling port and lung sampler were then disconnected and the sampling port was resealed.

Analysis of Soil Gas Samples: Soil gas samples were analyzed within 3 hours of collection by one of two methods as determined by sample concentration: (1) direct on-column sample injection with GC/DELCD analysis for samples with concentrations >5 ppb_v and (2) concentration on a multi-bed sorbent trap, subsequent thermal desorption and analysis by GC/DELCD for samples <5 ppb_v. For samples with concentrations >5 ppb_v, 500 µL of sample were injected into the SRI GC/DELCD with a 60-m long Restek MXT-1 column. The temperature program was: 40°C start, hold for 2 minutes, 12°C/min ramp to 220°C, and hold for 2 minutes. For samples with concentrations <5 ppb_v, 500 mL of sample were pulled from the 1-L Tedlar bag for concentration on a sorbent tube (same sorbent tubes as discussed above) using a RENA model BE-3012 vacuum pump and a vacuum-configured 0-100 mL/min Alicat mass flow controller set at 50 mL/min. After sample concentration, sample analysis followed the desorption and oven program given above for on-site GC/ECD analyses.

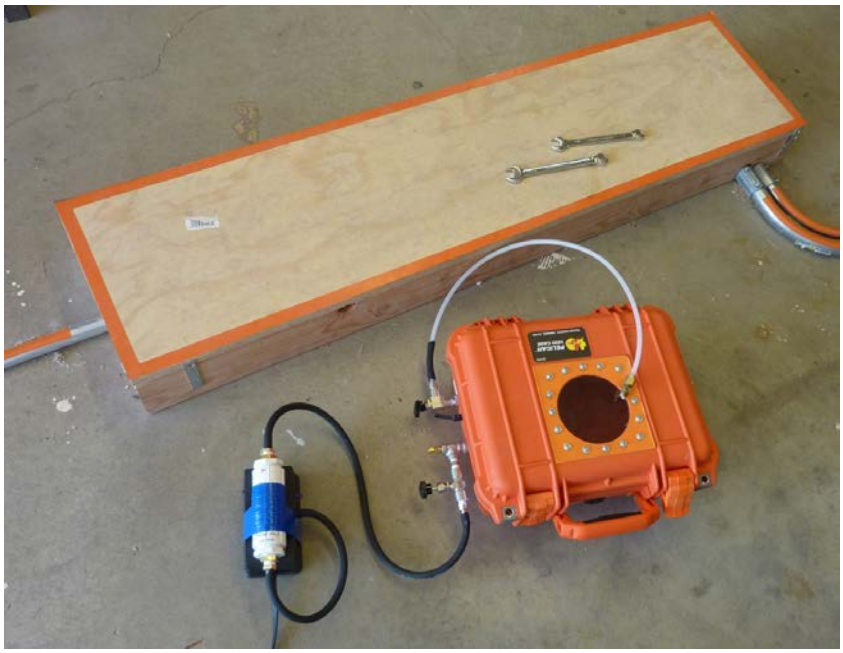

Figure 3.8. Photo of lung sampler (orange box) next to a monitoring location.

High-frequency Collection and Analysis of Soil Gas Samples Using the GC/ECD: Soil gas samples collected at high-frequency for analysis on the SRI GC/ECD followed the same procedure as outlined above for indoor and outdoor air, except that for soil gas samples, sample volumes of 500 mL or less were concentrated for analysis, since concentrations of CHCs in soil gas tended to be higher than indoor and outdoor air.

3.2.3 **Measurement of radon in indoor air and soil gas**

A Durridge RAD7 (Durridge Company, Inc., Billerica, MA) was used to measure the concentration of radon in both indoor air and soil gas. The RAD7 radon detector is a portable solid-state alpha detector with the ability to perform continuous real-time monitoring. A schematic of the RAD7 sampling assembly is shown in Figure 3.9. Prior to analysis, samples were pulled through a Drierite desiccant bed (W. A. Hammond DRIERITE Co. LTD, Xenia, OH) to ensure the relative humidity (RH) of the sample was low enough for proper detector operation (per manufacturer, no humidity correction is necessary when samples have 10% RH or less), followed by an inlet filter. The indicating desiccant was changed as necessary. When sampling indoor air and soil gas within the building, the outlet of the RAD7 assembly was discharged to outdoor air.

The RAD7 was calibrated by the manufacturer prior to initial use and then each year thereafter. The manufacturer uses a set of four control instruments as standards for the calibration of all RAD7s sold. The four control instruments are calibrated by inter-comparison with radon chambers designed by U.S. EPA. Using this method, the manufacturer claims the RAD7 accuracy to be ±5% or better. Each measurement from the RAD7 also includes a value for the

uncertainty associated with the sample; this is a 95% confidence interval based on the number of alpha particles counted during the spectral analysis.

Measurement of radon in indoor air and soil gas was conducted using two methods: (1) time-averaged samples collected over a 2-h period for continuous monitoring of indoor air and (2) an average of five 5-min cycles for Tedlar bag samples collected during synoptic soil gas sampling events. Real-time monitoring of radon concentration in indoor air was performed in the lower-level of the house at approximately 1 m above the floor. Synoptic soil gas sampling events were performed every 1-3 months during on-site synoptic surveys at the sampling locations shown in Figure 3.1.

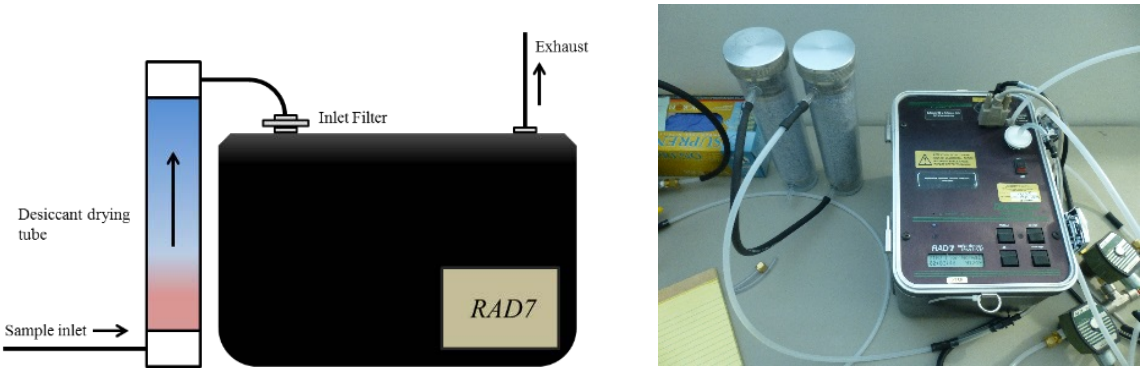

Figure 3.9. Schematic and picture of Durridge RAD7 sampling assembly used for analysis of indoor air and soil gas for radon.

Prior to initiating indoor air sampling and between each soil gas sample, the detector was purged using outdoor air. The purge function of the RAD7 uses its internal pump to pull "clean" air to flush the sample chamber from residual radon gas and moisture. For soil gas samples, the detector was purged for 5 minutes after each sample. The shallowest soil gas samples were collected first, as the radon concentrations at those depths were generally lower than in deeper soil gas (0.9 m and 1.8 m BS). When sampling took place at depths of 0.9 m or 1.8 m BS, the detector was purged for 15 minutes before returning to sample sub-slab soil gas depths.

3.2.4 **Release and measurement of sulfur hexafluoride (SF_6) tracer gas**

Release of Sulfur Hexafluoride (SF_6): SF_6 was used as a tracer for determining building air exchange rates and for studying indoor source behavior. SF_6 was continuously released to indoor air at 3-5 mL/min during all phases of the project. The SF_6 release was controlled by an Alicat 0-10 mL/min mass flow controller and monitored using SRI PeakSimple software.

Measurement of Sulfur Hexafluoride (SF_6): Two methods were used for analyzing SF_6; one for continuous indoor/outdoor air and soil gas monitoring and one for on-site synoptic soil gas surveys.

For continuous monitoring, samples were collected every 30-min using an SRI 10-stream gas sampling valve connected to an SRI 8610C Gas Chromatograph (GC). The GC was equipped with a dual mode pulse discharge detector (PDD) (Model D-2, Valco Instruments Co. Inc., Houston, TX) run in electron capture (EC) mode for SF_6 analysis. Samples were pulled through a 1-mL loop using a Rena model BE-3012 vacuum-pump and an Alicat, vacuum configured, 0-100 mL/min mass flow controller set at 50 mL/min. Samples were injected onto a washed 0.6-m (2 ft)-long molecular sieve 5A column using a helium carrier gas purified with a heated helium purifier (Model HP2, Valco Instruments Co. Inc., Houston, TX). The sample collection duration was set to ensure flushing of the sampling line prior to sample analysis. The calculated MDL for this instrument, as configured, was 0.97 ppb_v for SF_6 using USEPA's procedure (USGS, 1999). The results used to calculate the MDL are shown in Table 3.9.

Table 3.9. Spiked concentrations, responses, and calculated concentrations used to calculate the MDL for SF_6 using the GC/PDD method.

Sample	Spiked Concentration [ppb_v]	Response [area count]	Calculated Concentration [ppb_v]
1	10	408.4	10.03
2	10	422.2	10.46
3	10	405.2	9.94
4	10	430.4	10.72
5	10	410.2	10.09
6	10	419.5	10.38
7	10	427.9	10.64
		Average:	10.32
		Standard Deviation (s):	0.31
		Student's t value (t):	3.14
		MDL [ppb_v]	0.97
$MDL = s\ x\ t_{(n-1,1-\propto=0.99)}$			

Instrument calibration occurred at the beginning and end of on-site synoptic surveys (typically 1-3 months between the end of one survey and the start of the next). Due to changes in instrument sensitivity between site visits, after May 24, 2011 one port of the 10-stream gas sampling valve was dedicated to a 500 ppb_v SF_6 gas standard held in 10 L FlexFoil bags (SKC 262-10) to allow for continuous tracking and calibration of detector response. The standard was sampled once every 5 h during continuous monitoring. Calibration curves were modified as necessary based on the ratio of the sample analysis relative to the known concentration. For data collected prior to May 24, 2011, it was assumed that the sensitivity change between instrument calibrations was linear.

For on-site synoptic soil gas surveys, soil gas samples were collected in 1-liter Tedlar bags (SKC 232-01) using the lung sampler described above and analyzed using the GC/PDD configured for

500 μL direct on-column injections onto the 0.6 m molecular sieve 5A column. Samples were analyzed within 1 h of collection.

3.2.5 **Differential pressure measurements**

Differential pressure transducers (Model P300-0.4"-D, Pace Scientific Inc., Mooresville, NC) were used for continuous monitoring of differential pressures between soil gas and indoor air, between indoor and outdoor air, and other configurations as deemed necessary. The transducers contain a high and a low pressure port. When the pressure of the high port exceeds that of the low port, a positive pressure response is recorded and vice versa. Readings from the transducers were recorded on 2 min intervals using a data acquisition module (Model OMB-DAQ-56, Omega Engineering Inc., Stamford, CT).

Prior to use, all transducers were tested on-site by applying a range of positive and negative pressures to generate unique response/calibration curves for each. Initially, a range of positive pressures was applied using a nitrogen gas feed to the high ports. Pressures were controlled by feed/bypass valves and were calibrated to a Magnehelic differential air pressure gauge (Dwyer Instruments, Inc., Michigan City, IN). At each pressure measured, the differential pressure signal from each transducer was monitored/recorded. To simulate negative pressures, the tubing to the high and low ports was reversed and the process repeated. Using the applied pressure readings and the differential pressure signal, response/calibration curves were developed.

3.2.6 **Measurement of CHCs in groundwater**

Collection of Groundwater Samples. Prior to collection of groundwater samples, the depth to groundwater was measured to determine groundwater elevation and estimate water volume in the well. Groundwater wells were then purged three well-volumes using peristaltic pumps, dedicated inertial pumps, or new disposable polyethylene bailers. The use of inertial pumps or bailers was necessary when a peristaltic pump was unable to purge water without vaporization.

Groundwater samples were collected within 24 h of purging using a peristaltic pump, dedicated inertial pump, or a new polyethylene bailer. Samples were collected in 40 mL volatile organic analysis (VOA) vials and preserved with hydrochloric acid. All samples were collected with duplicates when enough groundwater was available. After collection, the samples were placed on ice and shipped to ASU for analysis.

Analysis of Groundwater Samples: Groundwater samples were analyzed for dissolved CHCs by GC/DELCD using a 42°C heated-headspace technique. For every 10 samples analyzed, a duplicate sample was analyzed to assess variability and error in sampling and analysis. The MDL for this method was 0.42 μg/L for TCE. The results used to calculate the MDL are shown in Table 3.10.

Table 3.10. Spiked concentrations, responses, and calculated concentrations used to calculate the MDL for TCE in groundwater using the GC/DELCD method.

Sample	Spiked Concentration [ppb_v]	Response [area count]	Calculated Concentration [ppb_v]
1	4	45.6	4.78
2	4	44.3	4.59
3	4	43.5	4.48
4	4	43.5	4.48
5	4	43.0	4.41
6	4	43.4	4.46
7	4	43.0	4.41
		Average:	4.52
		Standard Deviation (s):	0.13
		Student's t value (t):	3.14
		MDL [ppb_v]	0.42
$MDL = s\ x\ t_{(n-1,1-\propto=0.99)}$			

3.2.7 **Continuous monitoring of relative changes in groundwater elevation**

As indicated in Table 3.1, groundwater elevation was monitored at all GW3 discrete intervals on a continuous basis to track changes in groundwater elevation. Solinst Leveloggers (Solinst Canada, Georgetown, ON, CA) were used to record height of water above the transducers within each of the depth-discrete wells at GW3. The results were used to track relative changes in groundwater elevation, and with the ground-surface elevation of each well, could be converted to groundwater elevations with time.

3.2.8 **Soil moisture content**

Soil moisture profiles were determined from soil samples collected using a hand auger (AMS Inc., American Falls, ID). Soil samples were collected at 0.15 m (6 in) increments to a depth of 3.81 m (12.5 ft). Samples were placed in jars, sealed, and shipped to ASU for gravimetric analysis. Soil moisture content was determined as follows:

- Approximately 15 g of soil were taken from a sample jar and placed on a pre-weighed aluminum dish and the mass recorded using an analytical balance (Mettler-Toledo, LLC, Columbus, OH).

- The soil and aluminum dish were then dried in an oven at 105°C for 24 h.

- Following removal from the oven and a cooling period, the dried soil and aluminum dish were reweighed.

- The mass of dried soil was determined by subtracting the mass of the tin from the mass of dried soil plus tin.

- The mass of water was determined by subtracting the dried mass of soil plus tin from the original mass of soil plus tin.

- Soil moisture content was then calculated by taking the mass of water and dividing it by the mass of dry soil.

3.2.9 **Additional low-value data collection**

Table 3.11. Summary of data collected but determined to be of low value for this study. provides a summary of additional data collected during both natural and controlled pressure conditions from August 2010 through July 2013 ($0 < t < 1074$ d). They were reviewed and judged to be of low value for the objectives of this study. They have been archived for future use if needed.

Table 3.11. Summary of data collected but determined to be of low value for this study.

Measurement	Analytical Methods and Frequency	Sampling Media and/or Location	Data QA/QC	Comment
Real-time soil temperature	Soil temperature sensors connected to data acquisition system; reading every 2 minutes	Multiple depth discrete measurements at locations C and 1	N/A	VI impacts were dominant in winter when soils were cooler and the VI impacts were much more temporally variable in frequency and magnitude than soil temperatures. These observations indicate that soil temperature was not a key factor for VI occurrence at this site.
Real-time soil moisture	Soil moisture sensors connected to data acquisition system; reading every 10 minutes		Comparison with data from soil samples	Irregular measurements from the sensors were not believed to be accurate
Real-time soil gas O_2 concentration	O_2 sensors connected to data acquisition system; reading every 10 minutes	All multi-depth soil gas locations	Sensor calibration	O_2 measurements showed consistently elevated O_2 and little change over time

3.2.10 **Lab studies**

Design and Operation: The two physical models used in this study were 182-cm tall, 61-cm wide, and 10-cm thick stainless steel frame tanks fitted with acrylic glass on both sides. The acrylic glass provided a visual view in addition to allowing custom sample port or equipment installations. For these tests, the front window was fitted with Swagelok 1/8-in NPT x ¼-in Swagelok fittings. Rubber septa replaced the Swagelok compression ferrules and allowed for gas/water sampling from within the tank using a syringe and needle. The back window was fitted with five Decagon ECH_2O EC-5 soil moisture sensors (Decagon Devices, WA) to provide continuous monitoring of vertical soil moisture profiles within the tank. Volumetric soil moisture data were collected by an EM50 Digital/Analog data logger (Decagon Devices, WA) on 15-30 minute intervals.

The two tanks were packed with different media; one contained Quikrete® Play Sand sieved to 50 mesh plus, and the other was packed with a commercial-grade, washed 10-20 mesh silica sand.

Water table elevations were managed using an automated head control device which effected simultaneous changes in water level elevation within the tanks. Hydraulic head was controlled using a STP-MTR-23079 stepper motor and a STP-DRV-6575 stepper drive (AutomationDirect, GA) controlled by a D0-05DD PLC (Koyo, China).

Water containing constant concentrations of dissolved CHCs, including trichloroethylene (TCE), 1,2-Dichloroethane (1,2-DCA) and Tetrachloroethylene (PCE), was initially introduced and induced to flow horizontally across the tanks. Figure 3.3 shows the tank/flow configuration for the uniform horizontal flow setting. The flow field was generated using a 12-port inlet/outlet configuration. Inlet ports were manifolded together and managed by a single feed pump, while outlets were manifolded together and managed by a single head control device. Inlet water was continuously spiked with CHCs using a syringe pump and a mixing chamber. Horizontal velocities were maintained at approximately 30 cm/day.

To determine the emission rate of CHCs from water, breathing grade compressed air was used as a sweep gas across the tank headspace. Knowing the sweep gas flow rate Q_{sweep} [m^3/d] and CHC concentration in the sweep gas effluent $C_{sweep,\,i}$ [g/m^3], the emission rate can be determined:

$$E\ [g/d] = Q_{sweep}\ [m^3/d] \times C_{sweep,\,i}\ [g/m^3]$$

where the subscript i denotes different chemicals.

For the horizontal flow field experiments, CHCs emission rates were monitored during falling, rising, and cyclical water table elevation histories. For vertical flow experiments, CHCs emission rates were monitored during cyclical water table elevation histories. Operational conditions and measurements are summarized above in Table 3.3.

Sample Collection and Analysis: Water, soil gas, and sweep-gas samples were collected before, during and after the water table fluctuations. Aqueous samples (1.0 mL) were collected from

influent sampling ports and sampling ports across the face of the tank. Samples were diluted with 30 mL reverse osmosis (RO) water. Samples were analyzed using an SRI GC/DELCD with a 60-m long Restek MXT-1 column and a 42°C heated headspace technique. For analysis, 500 µL of the sample was injected on-column. The GC oven heating program was: 66°C start, hold for 2 min, ramp at 12°C/min to 220°C, and hold for 3 min. Calibrations were conducted before every sampling event and the linear calibration range for samples was between 5 and 100 µg/L.

Soil gas samples (0.1 to 0.5 mL) were collected from sampling ports after purging 5 mL. The sample was injected on-column for analysis with the GC/DELCD. GC calibration for gas sampling was conducted prior to each gas sampling event. The calibration standard was made by injection and evaporation of predetermined volumes of CHC liquids into helium in a 1-Liter Tedlar bag.

Sweep gas concentrations were analyzed at high frequency by GC/FID (SRI Instruments). Sweep gas was sampled alternately from the two tanks using a 3-way solenoid valve (ASCO, NJ) controlled by the SRI Peaksimple software and timed relay sequence. Sweep gas samples collected for analysis were first concentrated on a multi-bed sorbent tube trap (0.64 x 15.2 cm) packed with Tenax-GR and Carboxen-569 using a Rena model BE-3012 vacuum pump, and an Alicat vacuum-configured 0-100 mL/min mass flow controller set at 40 mL/min. Sample collection time was controlled using SRI's PeakSimple software. Sample desorption was at 230°C for 2.5 min with a helium carrier gas. Samples were analyzed using GC/FID and a 60-m long MXT-5 capillary column. The GC oven heating program was: 40°C start, hold for 2 min, 12°C/min ramp to 220°C, and hold for 3 min. Three point calibrations were performed before and after each set of tests using a minimum concentration of 50 $\mu g/m^3$ and a maximum concentration of 5000 $\mu g/m^3$.

4 RESULTS AND DISCUSSION

4.1 LONG-TERM HIGH-FREQUENCY MONITORING OF INDOOR AIR CONCENTRATIONS UNDER NATURAL CONDITIONS

The objectives of the long-term high-frequency monitoring of indoor air concentrations were:

a) to gain an understanding of the long-term and short-term transient behavior of indoor air concentrations at a vapor intrusion (VI) site, and

b) to evaluate whether conventional low-frequency indoor air sampling schemes used in VI pathway assessment confidently identify VI occurrence and accurately characterize long-term indoor air exposure.

4.1.1 Temporal trends in indoor air concentration data

TCE concentrations are presented below as their behavior is representative of the suite of chlorinated compounds monitored in indoor air at the study house.

Figure 4.1 presents results from February 2010 to August 2012, with time (t) = 0 being 8:00 AM on 08/15/2010; this time was selected as it was when the first synoptic sampling of the multi-level soil gas and groundwater installations occurred. As discussed in USGS (1999), the USEPA MDL determination approach emphasizes minimization of false-positives using statistical analysis of detector response, and there is value and justification to presenting results <MDL when data-rich analyses (e.g., GC/MS/SIM) are used to determine concentrations. In this case, data in the 0.01 – 0.06 ppb_v range are presented as they help discern temporal trends in indoor air concentrations; however, it should be noted that these data are qualified as being less than the MDL for that instrument.

There were periods from 2 d < t < 40 d and 47 d < t < 54 d, when indoor pressures were manipulated to create under-pressurized conditions for other studies conducted at the house. One of those studies inadvertently introduced a TCE indoor air source that was identified and removed at t = 54 d. These periods are identified and those data are shown in Figure 4.1, but the results were excluded from later analyses and assessment of indoor air sampling approaches. Also indicated in Figure 4.1 are time intervals when synoptic soil gas and groundwater sampling were conducted.

Ignoring the t = 0 d to 60 d time period, TCE concentrations in indoor air varied by about two to three orders-of-magnitude (<0.01 to 10 ppb_v). During this same time period, changes in the indoor air exchange rate were less than an order of magnitude as shown in Figure 4.2. Thus, the indoor air concentration changes must reflect changes in TCE mass entry rate to the house. Embedded within the 2.5 year sampling history are two recurring VI behaviors. There are "active" VI periods, which are prevalent in fall, winter, and sometimes into early spring; these involve varying levels of VI impacts intermixed with sporadic periods of non-detect concentrations. Figure 4.3 presents data from a representative VI-active period occurring during winter months. For this sample VI-active period, TCE concentrations increase and then decrease

over multi-day time periods, with maximum concentrations ranging from about 0.5 to 2 ppb_v. One- to four-day periods of non-detect concentrations (<0.01 ppb_v) are interspersed throughout the VI-active periods.

There also are inactive or VI-dormant periods, which are prevalent in late spring and summer; these involve mostly non-detect indoor air concentrations and sporadic one- to two-day periods of VI-activity. Figure 4.4 presents data from a representative VI-dormant period occurring during summer months. For this period, there are one- to three-week periods of non-detect concentrations and only brief periods of increased concentrations (0.05 – 1.0 ppbv) similar to those observed during the VI-active period.

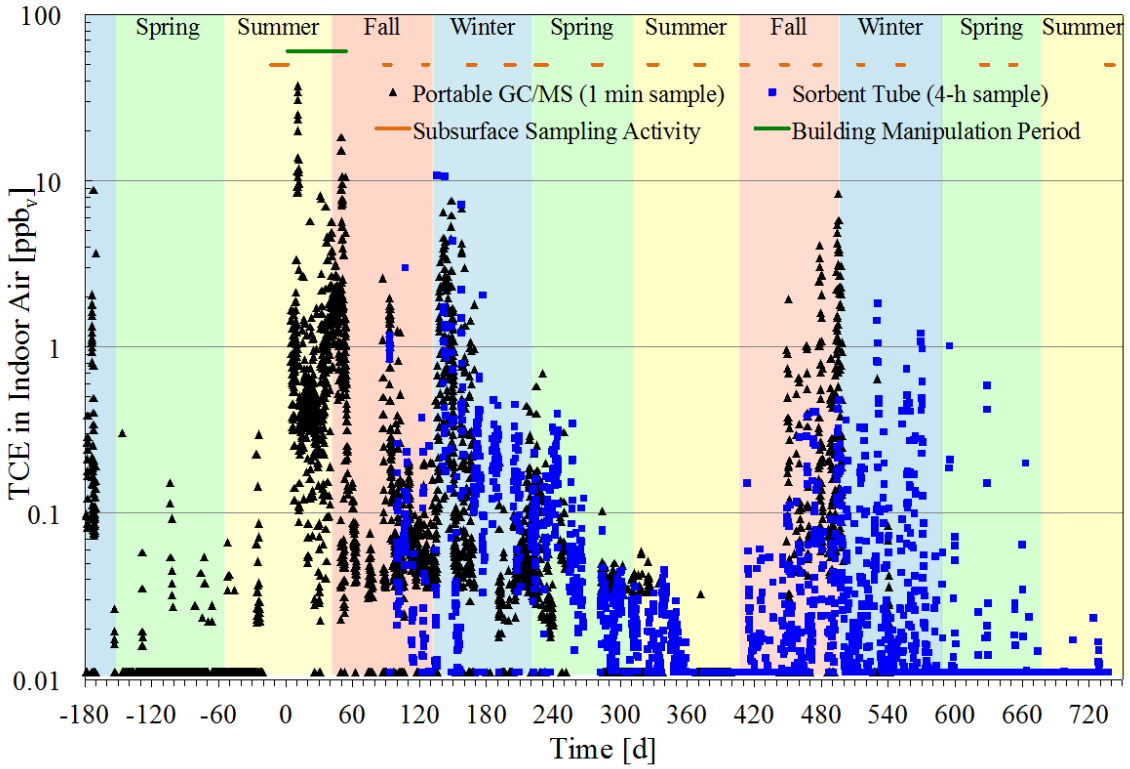

Figure 4.1. Indoor air TCE concentrations measured by portable GC/MS and sorbent tubes from February 2010 to August 2012 (note: values ≤0.011 ppb_v are plotted as 0.011 ppb_v to make it clear that samples were collected at those times); reproduced from Holton et al. (2013).

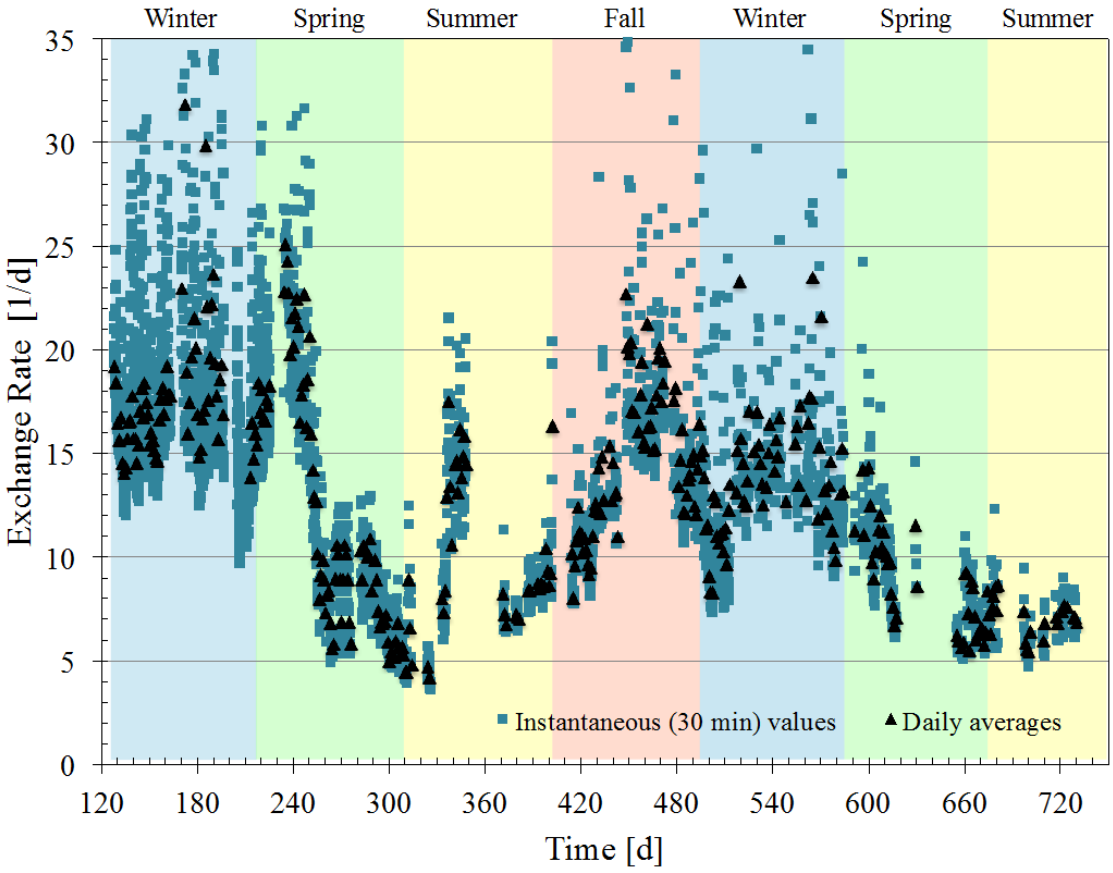

Figure 4.2. Instantaneous and daily-average indoor air exchange rate for the lower level of the study house); reproduced from Holton et al. (2013)

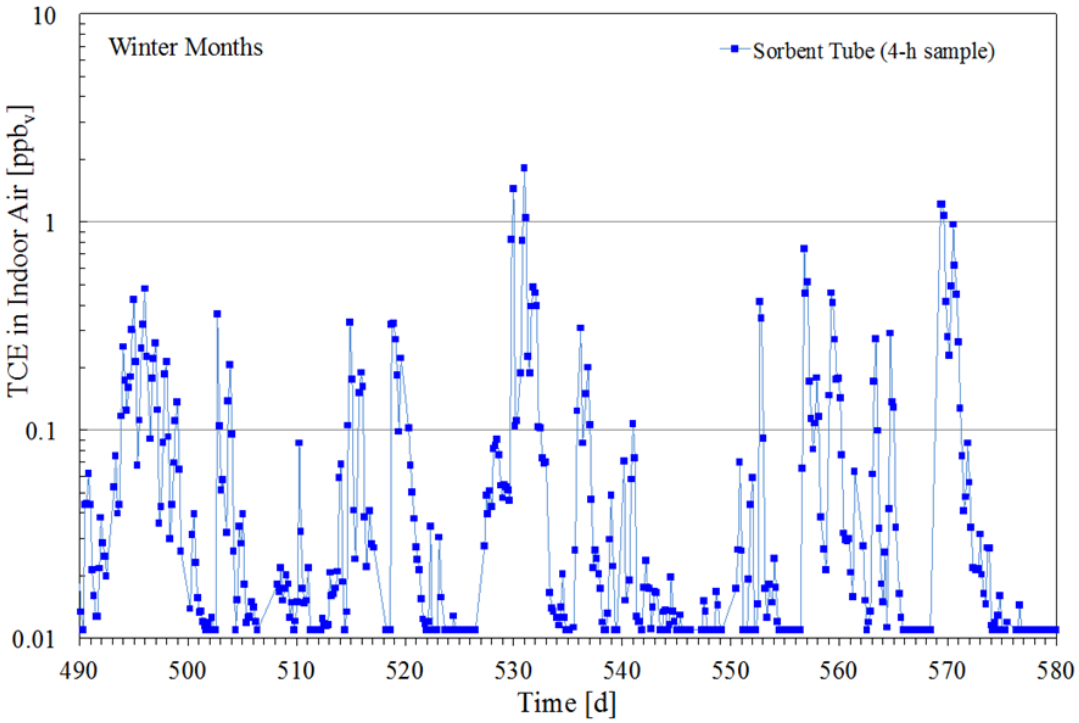

Figure 4.3. Temporal behavior of TCE in indoor air during a VI-active period (values ≤0.011 ppb_v are plotted as 0.011 ppb_v); reproduced from Holton et al. (2013)

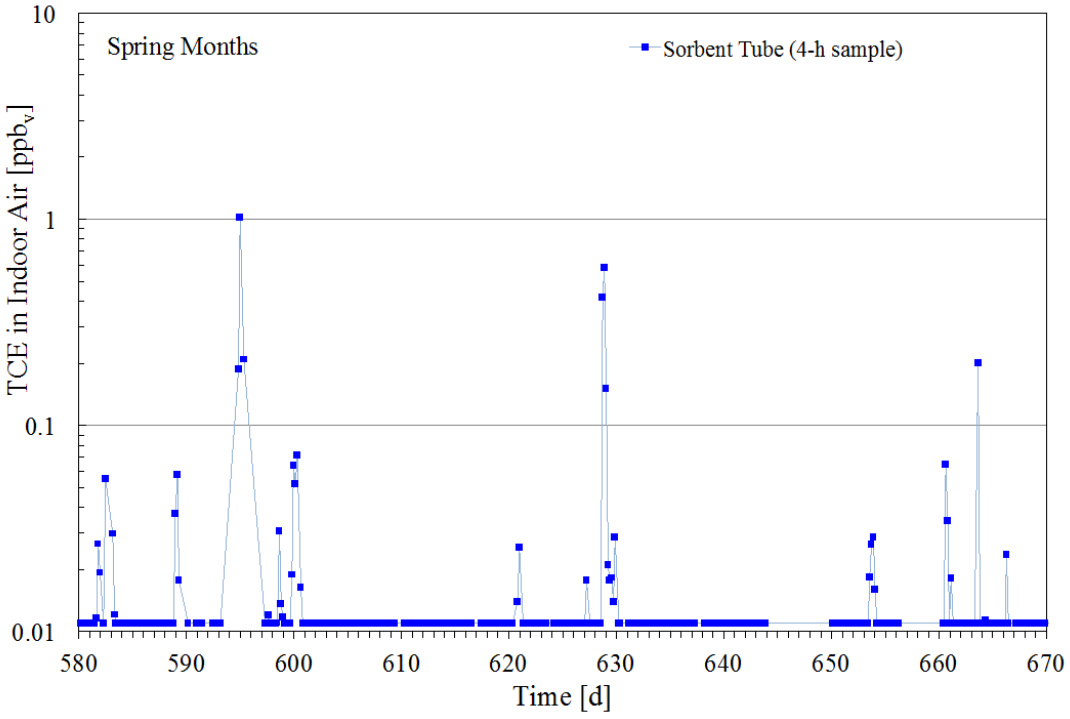

Figure 4.4. Temporal behavior of TCE in indoor air during a VI-dormant period (values ≤0.011 ppb_v are plotted as 0.011 ppb_v); reproduced from Holton et al. (2013)

4.1.2 **Implications of temporal behavior - evaluation of conventional sampling schemes**

The indoor air concentration data presented above comprise the longest and highest-frequency monitoring record to date for anthropogenic chemical impacts to indoor air at a VI site. Thus, it is unknown whether or not the data are representative of other VI-sites, and one must be cautious in extending lessons-learned below to other VI sites. Nevertheless, the data provide the first opportunity to evaluate whether or not conventional sampling approaches are likely to yield correct answers at this and any similar sites to the two primary VI-pathway assessment questions (USEPA, 2002): a) is the VI pathway complete at a site (e.g., are there indoor air impacts that are attributable to VI activity)?, and b) does the potential exposure to VI-related indoor air impacts exceed target exposure thresholds?

For the past decade, 24-h samples have been the standard for VI-pathway assessment in residential structures. Longer-term (one- to three-week) passive sorbent sampling is well validated (USEPA, 2012b), but not commonly used in the U.S. The data in Figure 4.1, therefore, were converted to a synthetic 24-h daily-average concentration data set.

The following procedure was used to create the synthetic 24-h data set presented in Figure 4.5:

i) 0 d < t < 60 d data were removed as discussed above;

ii) 24-h average concentrations were calculated separately for the portable GC/MS and sorbent tube data sets; and

iii) the two daily-average data sets were combined by averaging when two 24-h average values were available for the same day, or the single value was used when only one concentration value was available.

All 24-h average concentrations were calculated for 8 AM to 8 AM sampling periods and the value assigned to the midpoint time (8 PM) for plotting purposes. Synthetic concentrations were only calculated when actual monitoring results were available for at least 8-h of a 24-h period. To fully emulate the features of a real data set, a method detection limit was defined and used to truncate the synthetic data set at 0.01 ppb_v. Whenever the procedure above produced a 24-h concentration <MDL then that concentration was assigned a value of one-half the MDL (0.005 ppb_v) as is sometimes done in practice when manipulating VI data sets. Results <0.011 ppb_v are plotted as 0.011 ppb_v in Figure 4.5 for consistency with other figures.

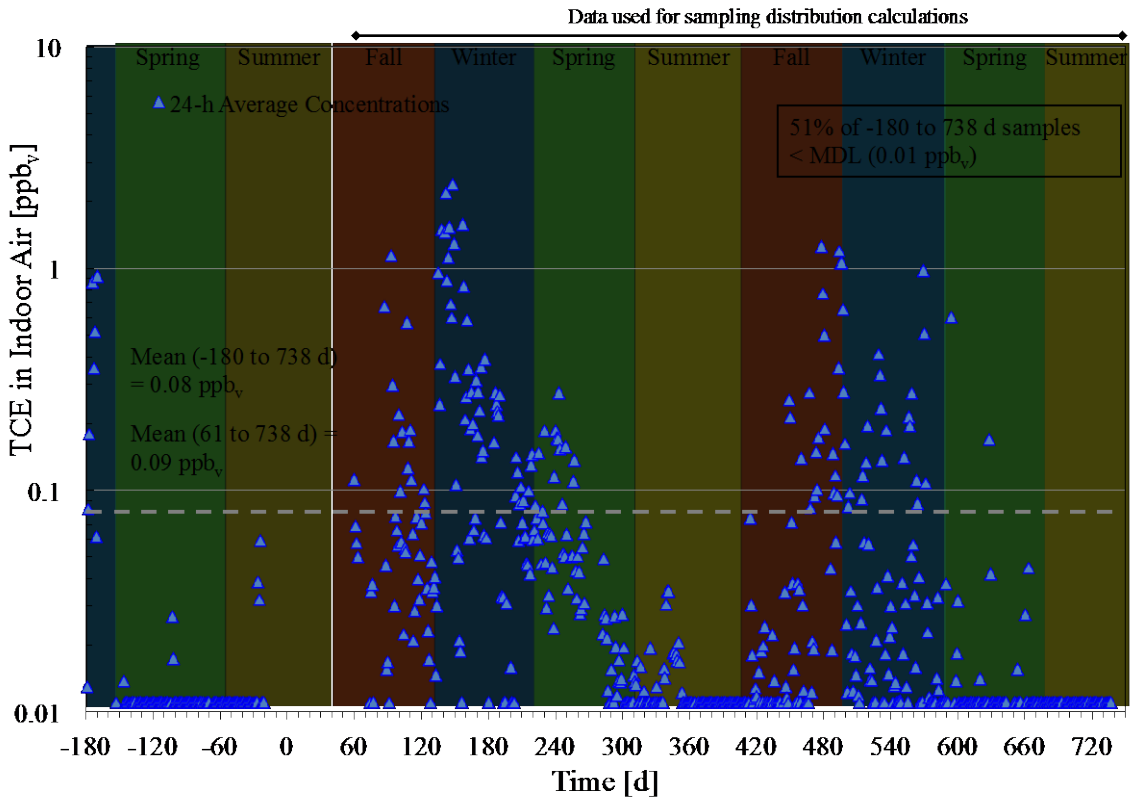

Figure 4.5. Synthetic 24-h sample data set derived from data in Figure 4.1, with the exception that data from 0 d ≤ t ≤ 60 days were excluded as they were collected during pressure testing and when a TCE source was present within the house. Note that values ≤0.011 ppbv are plotted as 0.011 ppbv); plot reproduced from Holton et al. (2013).

In the synthetic data set shown in Figure 4.5 there are 723 24-h average concentrations distributed across 858 days (84% coverage, excluding 0 d< t < 60 d). The mean and median concentrations for the synthetic data set are 0.08 and <0.01 (0.009) ppb_v, respectively. As can be seen, the 24-h average values represent the overall trends seen in Figure 4.5, with similar seasonal variability and VI-active fall-summer-spring and VI-dormant summer seasons. The peak concentration (2.4 ppb_v) is about 20% lower than in the actual sample data set due to the time-averaging, so concentrations vary by about two orders of magnitude above the 0.01 ppb_v MDL. There is a high percentage of values at or near the MDL; for example, 51% are less than or equal to the MDL and 64% are less than or equal to twice the MDL.

A seasonal comparison of the raw data and 24-h average concentration distributions is provided in Figure 4.6. The synthetic data also reasonably represent the sample concentration distributions by season as shown in this comparison,

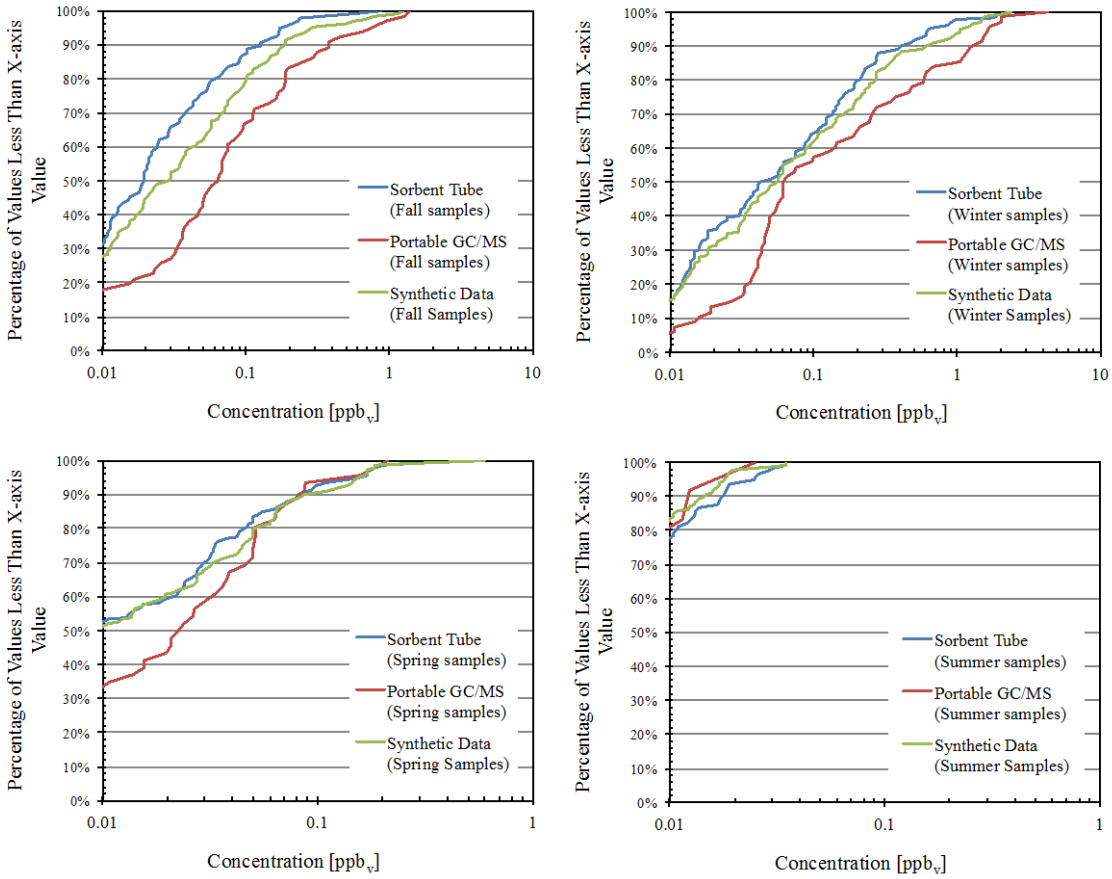

Figure 4.6. Histogram of 24-h averages for sorbent tube and portable GC/MS samples by season.

The synthetic data set was used to simulate outcomes from conventional VI sampling approaches. The data subset from 61 d < t < 738 d, which spans eight seasons, was used to generate outcomes for three simple sampling plans. For reference, the mean concentration for that time interval is 0.09 ppb_v, the maximum value is 2.4 ppb_v, and 44% of the concentrations values are less than or equal to the 0.01 ppb_v MDL.

The three simple indoor air sampling plans involve collecting: a) one sample per season (fall/winter/spring/summer) over one year, b) collecting one sample in summer and one in winter and c) collecting two samples in winter. The intent was not to explore all possible sampling plans or determine optimal plans, but rather to examine the results from three plans that are not atypical of current practice to get a sense of the possible outcomes from sparse and infrequent sampling.

Each sampling plan was simulated 5000 times to develop representative statistics. For a given realization, each seasonal sample was randomly collected from the distribution of all concentrations for that season. For example, all values in the two winter seasons shown in Figure 4.5 were combined into the one winter concentration distribution shown in Figure 4.6, and samples were pulled randomly from that distribution in each realization. Basic statistics (mean, median, quartiles) for the distributions of sampled concentrations from the 5000 realizations were compared with the statistics of the original distributions to ensure consistency.

The seasonal concentration distributions that were sampled are presented in Figure 4.7, along with the aggregate data distribution. Concentrations in this figure are normalized to the MDL as that is often an important reference in reviewing data. For example, results close to the MDL are often considered in practice to be the result of analytical variability rather than subsurface VI impacts. The MDL may be regarded as a reference for VI signal strength; it is much easier to decide if VI is occurring when all sample results are much greater than the MDL than if they are close to the MDL. As can be seen, there are fewer values ≤MDL (concentration/MDL ≤1) and more higher-concentration values (concentration/MDL ≥10) as one moves from summer to spring to fall to winter. The percentage of concentrations less than the mean is >50% for all seasons, increasing from winter to fall to spring to summer, with 100% of all summer concentrations being less than about 40% of the mean.

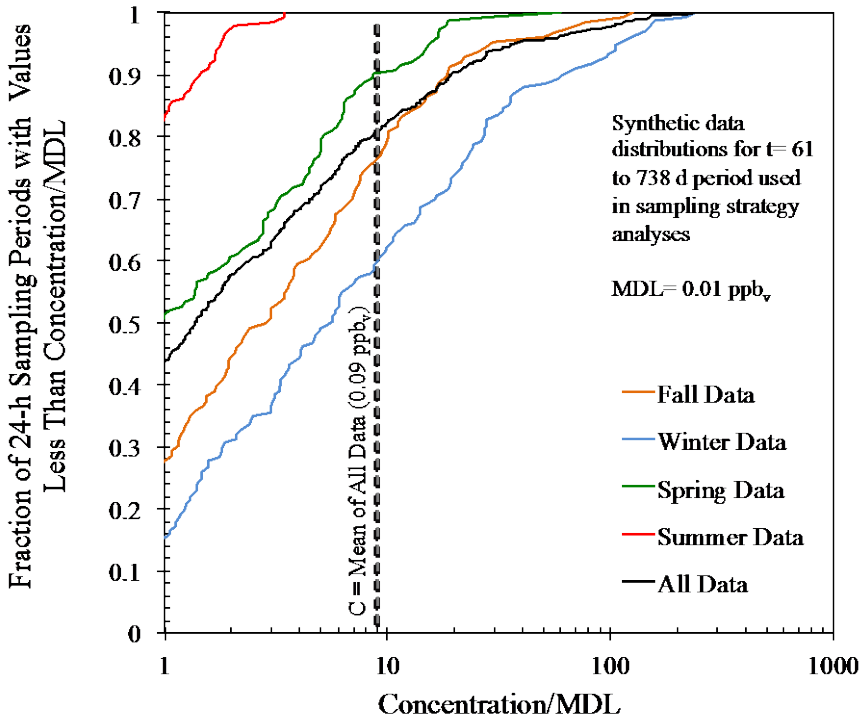

Figure 4.7. Seasonal and aggregate synthetic indoor air concentration distributions derived from the t = 61 d to 738 d synthetic data in Figure 4.4, with concentrations normalized to the MDL assigned to the synthetic data set (0.01 ppb_v); reproduced from Holton et al. (2013)

In practice, sampling results are compared against regulatory action levels, and exceedances trigger follow-on actions (e.g., additional sampling, mitigation). The synthetic data were used to study outcomes from sparse sampling using hypothetical action levels normalized to the true mean concentration for the data set, using action levels less than, equal to, and greater than the mean (action level/mean concentration = 0.2, 0.5, 1.0, 2, 5, 10).

Results are presented in Table 4.1 as probabilities of one or more samples exceeding the different action levels. Typically the action level represents a long-term average concentration that is deemed protective; however, it might also represent a threshold for acceptable short-term

exposures. For the former, we are concerned with: a) probabilities of one or more samples not exceeding the threshold when the true mean ≥ threshold (false negative condition), and b) probabilities of one or more samples exceeding the threshold when the true mean < threshold (false positive condition).

Table 4.1 shows that the probability of false negative conclusions (= 100% - values in Table 4.1) is as low as 6% and increases to 40% as the ratio of (action level/true mean) approaches unity and one exceedance is enough to trigger action. The probability of false negatives also increases significantly as the number of sample exceedances required increases. The probability of false positives is at least 10% and increases to about 40% as the ratio of (action level/true mean) approaches unity and one exceedance is enough to trigger action. The probability of false positives also decreases significantly as the number of sample exceedances required increases. There are differences between the three sampling plans, with the four season and winter-only sampling plans having the lowest false negative and highest false positive percentages.

Table 4.1. Probability of one or more indoor air samples exceeding the target concentration for a range of (target concentration/true mean concentration) ratios and three different sampling strategies; reproduced from Holton et al. (2013)

	Sampling Strategies								
	Fall, Winter, Spring, & Summer Sampling (4 samples total)					Winter & Summer Sampling (2 samples total)			Two Winter Samples (2 samples total)
	Number of Samples Exceeding the Target Concentration								
(Target/Mean) Concentration Ratio*	1	2	3	4		1	2	1	2
0.2	94%	64%	20%	1%		72%	4%	91%	51%
0.5	80%	34%	5%	0%		54%	0%	80%	28%
1	60%	14%	1%	0%		41%	0%	66%	15%
2	38%	4%	0%	0%		28%	0%	49%	9%
5	17%	1%	0%	0%		12%	0%	22%	1%
10	10%	1%	0%	0%		8%	0%	16%	1%

- *True Mean = 0.09 ppb_v for the synthetic data set*
- *MDL = 0.01 ppb_v for the synthetic data set*

For cases where the action level represents a threshold for acceptable 24-h exposures, we are concerned with probabilities of samples not exceeding the action level when the true maximum concentration ≥ action level (false negative condition). For this synthetic data set, the probability of false negative decisions (= 100% - values in Table 4.1) exceeds about 80% when the (action level/true mean) > 5. As the true maximum concentration is > 10X the true mean for this data set, there is no chance of a false positive condition.

The mean of indoor air sample concentrations is also a relevant quantity for exposure considerations. Figure 4.8 presents the distributions of mean concentrations calculated from samples for the three sampling plans, using the 5000 sampling realizations. Results are normalized to the true mean for the data set. Vertical lines that bracket an order of magnitude range about the true mean are drawn on the plot (mean of samples/true mean = 0.3 and 3.0). As can be seen, there is about a 32% probability that four-season sampling will produce a mean concentration that is ≤30% of the true mean and a smaller 8% probability that the sampling mean will be greater than three times the true mean. For the winter and summer sampling plan, there is about a 48% probability of producing a mean concentration that is ≤30% of the true mean and a smaller 11% probability that the sampling mean will be greater than three times the true mean. For the two winter samples plan, there is about an 18% probability of yielding a mean concentration that is ≤30% of the true mean and a slightly larger 22% probability that the sampling mean will be greater than three times the true mean. There is about a 60% probability that the sampling mean will be within the order-of-magnitude range about the true mean for the four-season sampling plan, a 41% probability that the sampling mean will be within the order-of-magnitude range about the true mean for the winter/summer sampling plan, and a 60% probability that the sampling mean will be within the order-of-magnitude range about the true mean for the two winter samples plan.

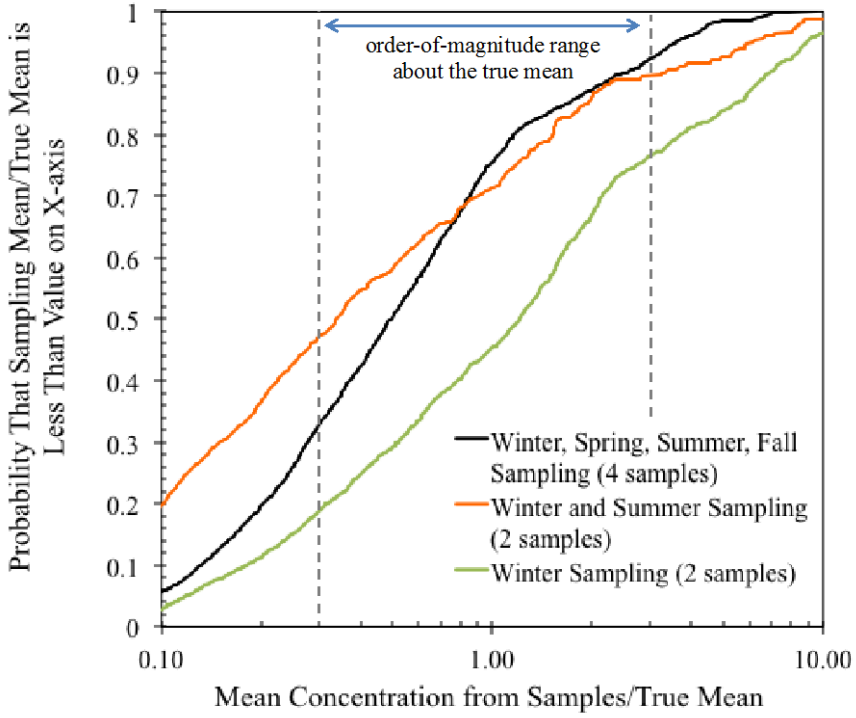

Figure 4.8. Distribution of sample means for 5000 sampling realizations and three simple sampling schemes, with concentrations normalized by the true mean for the t = 61 d to 738 d synthetic data (0.09 ppbv) shown in Figure 4.5. Data from t = 61 d to 738 d were used as this is the longest continuous period of data collection under natural conditions. As noted in Figure 4.5, data from 0 d ≤ t ≤ 60 days were excluded as they were collected during pressure testing and when a TCE source was present within the house. Reproduced from Holton et al. (2013).

4.1.3 Conclusion and caution for VI pathway assessment using sparse indoor air data sets

The results above suggest a need for discussion and linking of sampling schemes and decision rubrics in creation of future VI assessment paradigms, and examination of possible outcomes for sites with dense data sets. Use of the two simple sampling schemes illustrates that there can be relatively high probabilities of false-negative decisions and poor characterization of long-term mean concentrations with sparse data sets typical of current practice. As this is the first long-term and high-frequency data set for VI impacts from anthropogenic chemicals, similar data sets from other sites are needed to test the robustness of possible VI pathway assessment paradigms. As mentioned above, it is unknown whether or not the data from this study site are representative of other VI-sites, so caution should be exercised in extending lessons-learned at this site to other VI sites.

4.2 TEMPORAL AND SPATIAL VARIABILITY OF GROUNDWATER AND SOIL GAS CONCENTRATIONS ABOVE A DILUTE CHLORINATED SOLVENT-IMPACTED GROUNDWATER PLUME

The objective here was to gain an improved understanding of the temporal and spatial changes in groundwater and soil gas concentrations above a dilute chlorinated solvent-impacted groundwater plume. This involved over two years of systematic subsurface monitoring below the study house.

4.2.1 Spatial and temporal trends in groundwater concentrations

Figure 4.9 shows TCE concentrations at 2.7 m BS at interior sampling points from -13 d < t < 735 d. Similarly, Figure 4.10 shows TCE concentrations in shallow groundwater exterior sampling points for the same time period. For exterior sampling points, only shallow groundwater results are shown for comparison with interior sampling points. For both figures, breaks in the lines between data points represent periods where no sample was available. Data tables of groundwater concentrations, including data for other exterior monitoring points, are provided in Appendix A.

In general, TCE concentrations from interior and exterior groundwater sampling points ranged from about 1-60 μg/L. For interior sampling points, concentrations varied by about a factor of 3X or less spatially. Changes in the spatial distribution of exterior sampling points are more complex, since they are collected at slightly different elevations. Of note is the minimal temporal variability of groundwater concentrations, which suggests that changes in groundwater concentration (roughly about 2X about the mean) do not drive the orders-of-magnitude temporal changes observed in indoor air at this site.

The results for individual interior and shallow exterior groundwater sampling points during this period are summarized in Figure 4.11 as a box and whisker plot. For the figure, the end points of the boxes represent the 25^{th} and 75^{th} percentile values, the middle line is the median, and the

whiskers are the 10th and 90th percentile values. The data are separated by garage, interior, and exterior sampling points to highlight differences in the locations. Based on the interquartile range of each sampling point, the temporal variability of concentrations at most locations was about a factor of 1.5X-2.5X about the mean.

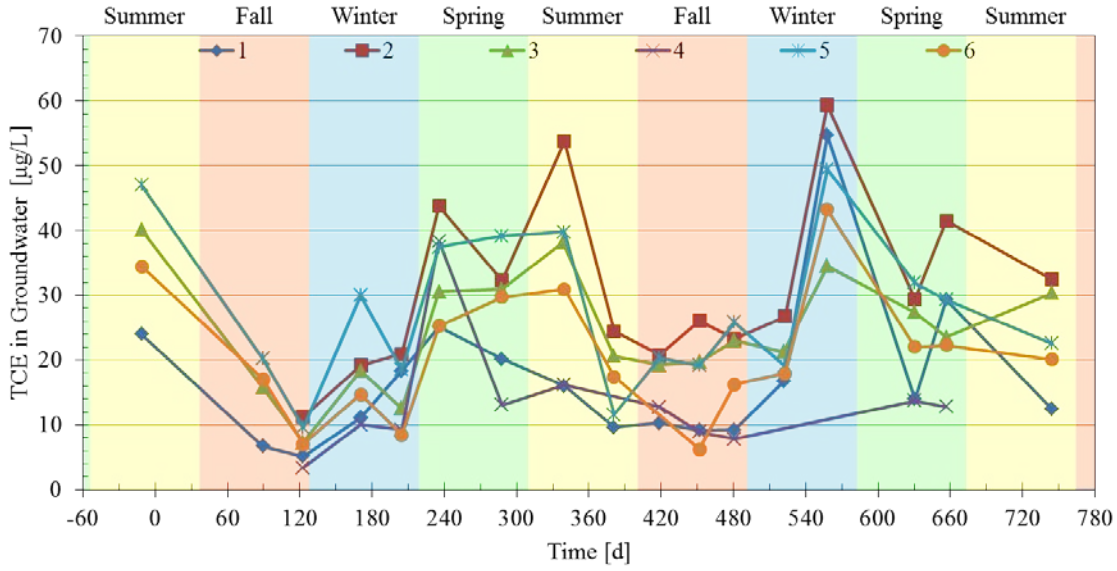

Figure 4.9. TCE groundwater concentrations for 2.7 m below-slab interior sampling points from August 2010 to August 2012.

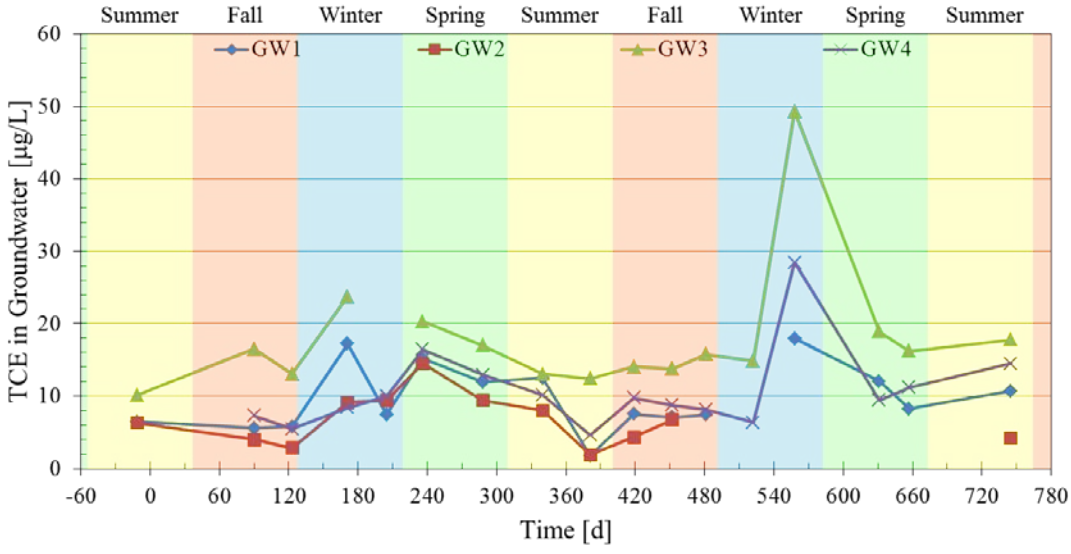

Figure 4.10. TCE groundwater concentrations at shallow exterior sampling points from August 2010 to August 2012.

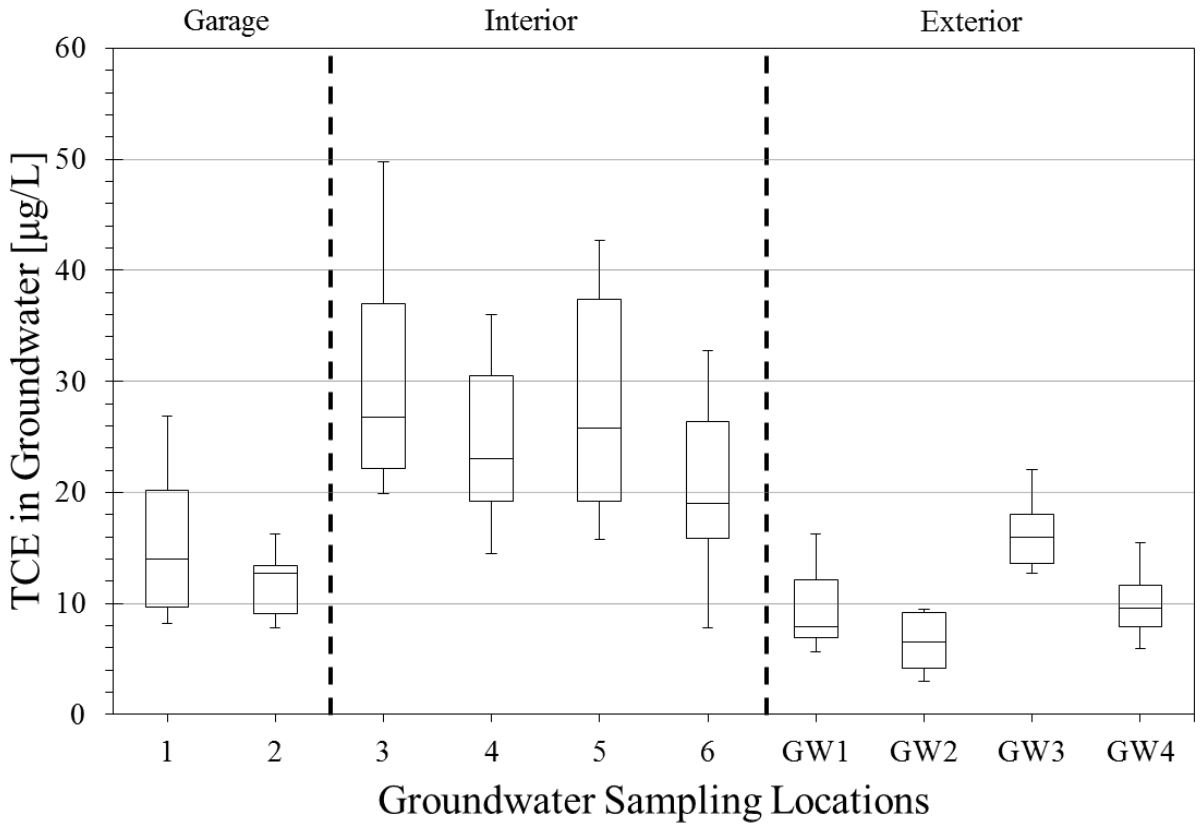

Figure 4.11. Box and whisker plot of TCE concentrations in interior and exterior shallow groundwater from August 2010 to August 2012.

4.2.2 **Spatial and temporal trends in deep soil gas concentrations**

Figures 4.12 to 4.15 contain contour plots of TCE concentrations in soil gas at 1.8 m BS depth sampling points from August 2010 through August 2012. The plots, along with those presented from shallower depths, were generated using Surfer 12 software (Golden Software, Golden, CO). The Kriging gridding method provided in the software was used to interpolate soil gas concentrations between sampling points. The plots are placed in sets of four to accommodate their size and allow for easier visual inspection.

In general, Figures 4.12 to 4.15 show a lateral concentration gradient from the northwest corner to southeast corner of the yard. This trend reflects the variation in ground surface elevation across the property; the house is built into a hillside that slopes down from north to south. As such, the 1.8 m BS depth sampling points in the backyard are further below ground surface than those beneath the building footprint or in the front yard.

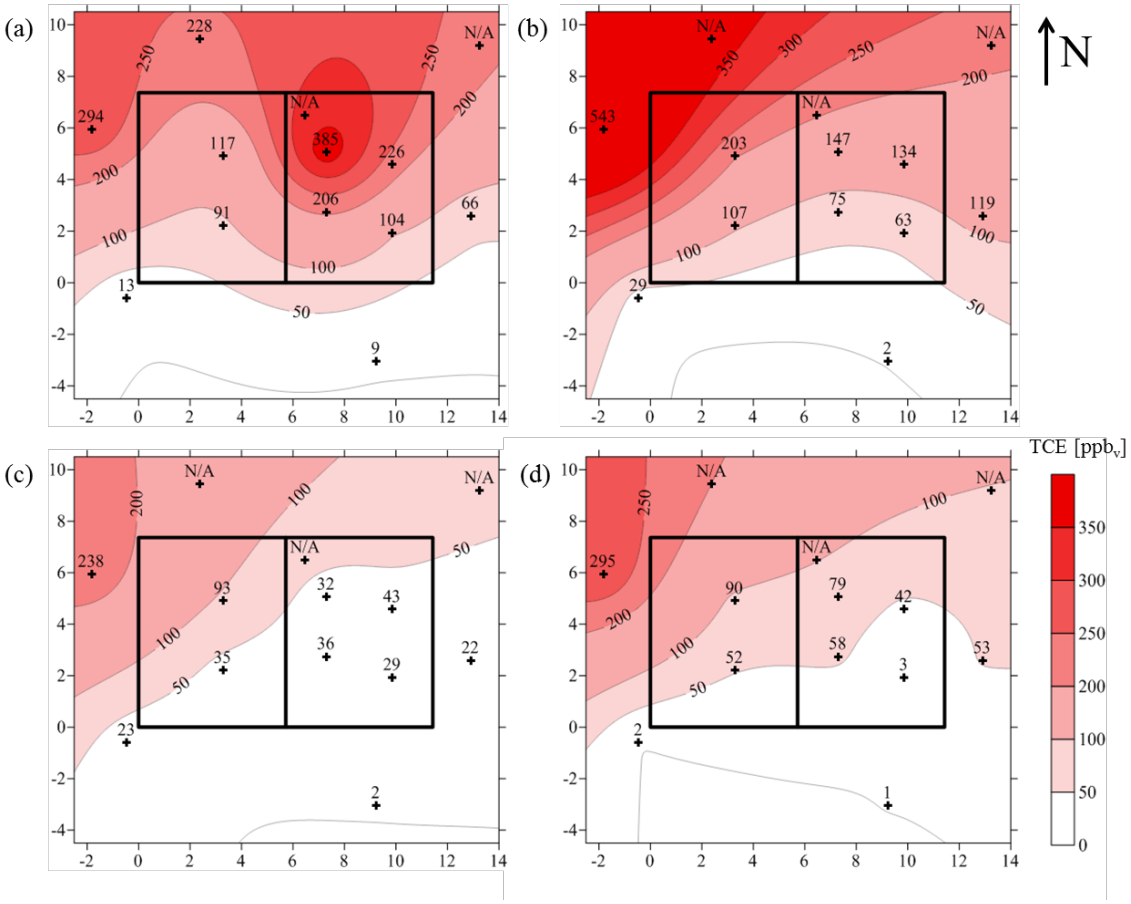

Figure 4.12. Soil gas concentration contour plots for the 1.8 m below-slab depth sampling points from (a) August 2010, (b) November 2010, (c) December 2010, and (d) March 2011.

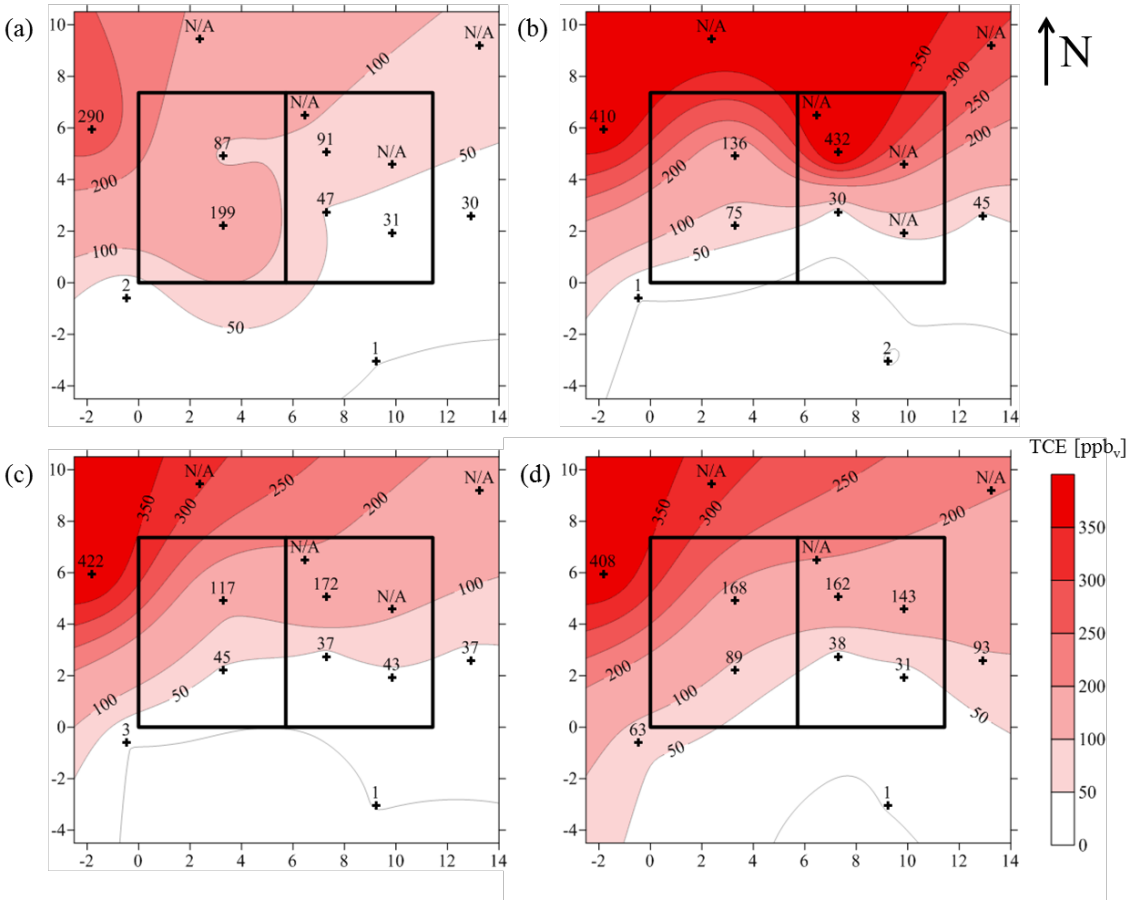

Figure 4.13. Soil gas concentration contour plots for the 1.8 m below-slab depth sampling points from (a) April 2011, (b) May 2011, (c) July 2011, and (d) August 2011.

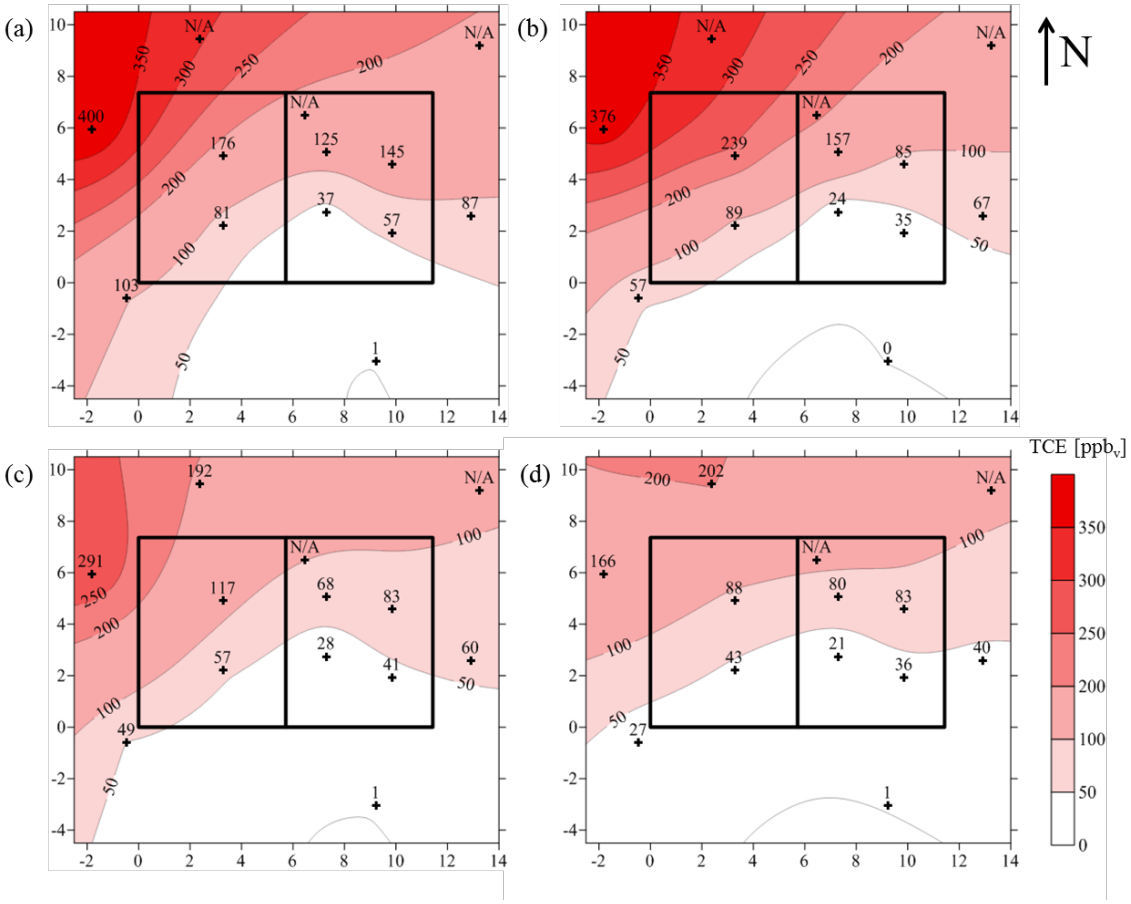

Figure 4.14. Soil gas concentration contour plots for the 1.8 m below-slab depth sampling points from (a) September 2011, (b) November 2011, (c) December 2011, and (d) January 2012.

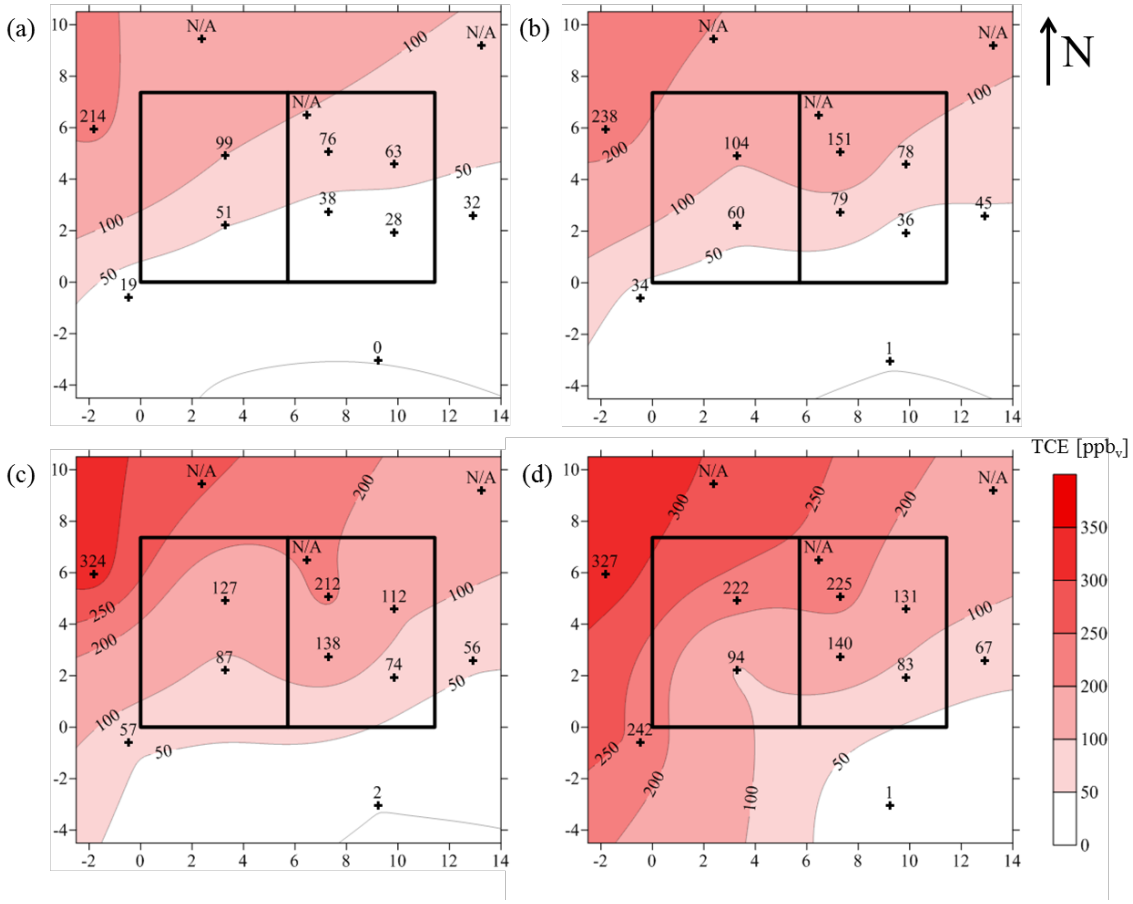

Figure 4.15. Soil gas concentration contour plots for the 1.8 m below-slab depth sampling points from (a) February 2012, (b) April 2012, (c) May 2012, and (d) August 2012.

Figure 4.16 provides a summary of the soil gas concentration data at 1.8 m BS depth sampling points in a box and whisker plot. Similar to the box and whisker plot shown for groundwater concentrations, the end points of the boxes represent the 25th and 75th percentile values, the middle line is the median, and the whiskers are the 10th and 90th percentile values. Locations A and B are not included in the plot, since water was often present at 1.8 m BS for those locations.

Overall, with the exception of location E, the concentrations at individual sampling points varied similarly over time at garage, interior, and exterior locations from a factor of about 2X to 5X between the 10th and 90th percentile values. The concentrations at locations D and E stand out in this plot as location D concentrations are about two-orders of magnitude lower than other locations and location E concentrations varied more between sampling events than other locations

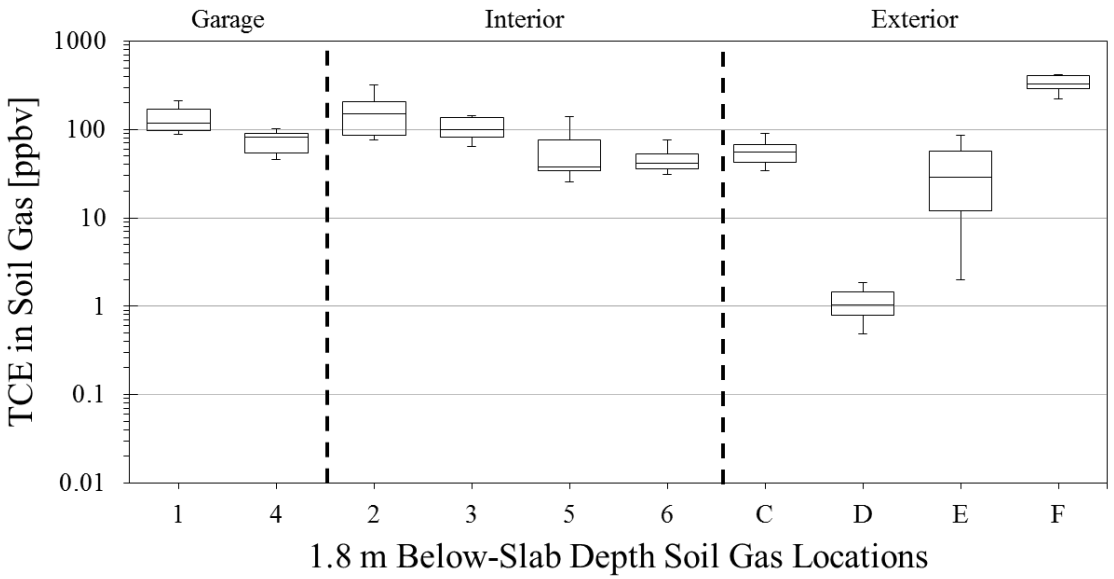

Figure 4.16. Box and whisker plot for TCE concentrations in soil gas at the 1.8 m below-slab depth sampling points from August 2010 to August 2012.

4.2.3 **Spatial and temporal trends in mid-depth soil gas concentrations**

Figures 4.17 to 4.20 show contour plots of TCE concentrations in soil gas at 0.9 m BS depth sampling points. Similar to sampling points at 1.8 m BS depth, the concentration results for 0.9 m BS depth show a concentration gradient from the northwest corner of the backyard to the southeast corner of the front yard; however, it is less distinct than that at 1.8 m BS due to spatial changes in the soil gas distribution that occurred over time.

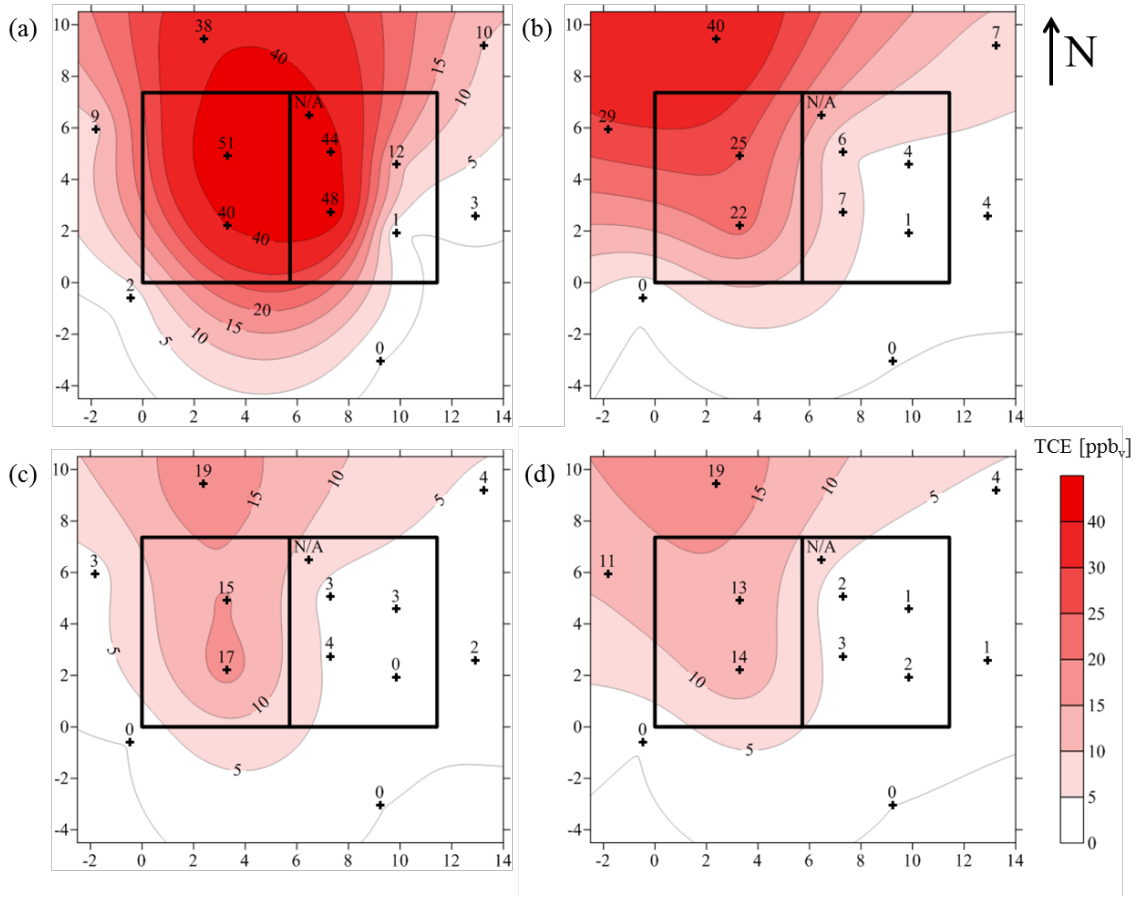

Figure 4.17. Soil gas concentration contour plots for the 0.9 m below-slab depth sampling points from (a) August 2010, (b) November 2010, (c) December 2010, and (d) March 2011.

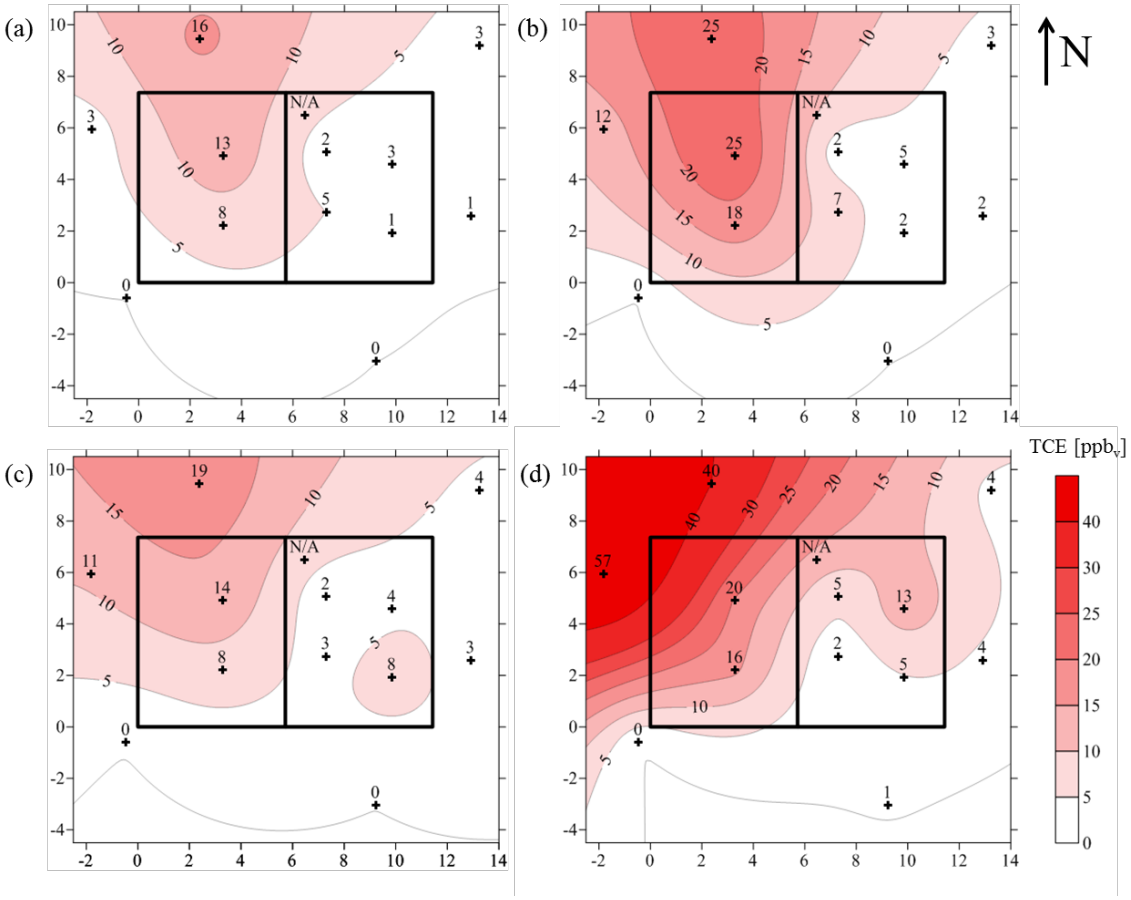

Figure 4.18. Soil gas concentration contour plots for the 0.9 m below-slab depth sampling points from (a) April 2011, (b) May 2011, (c) July 2011, and (d) August 2011.

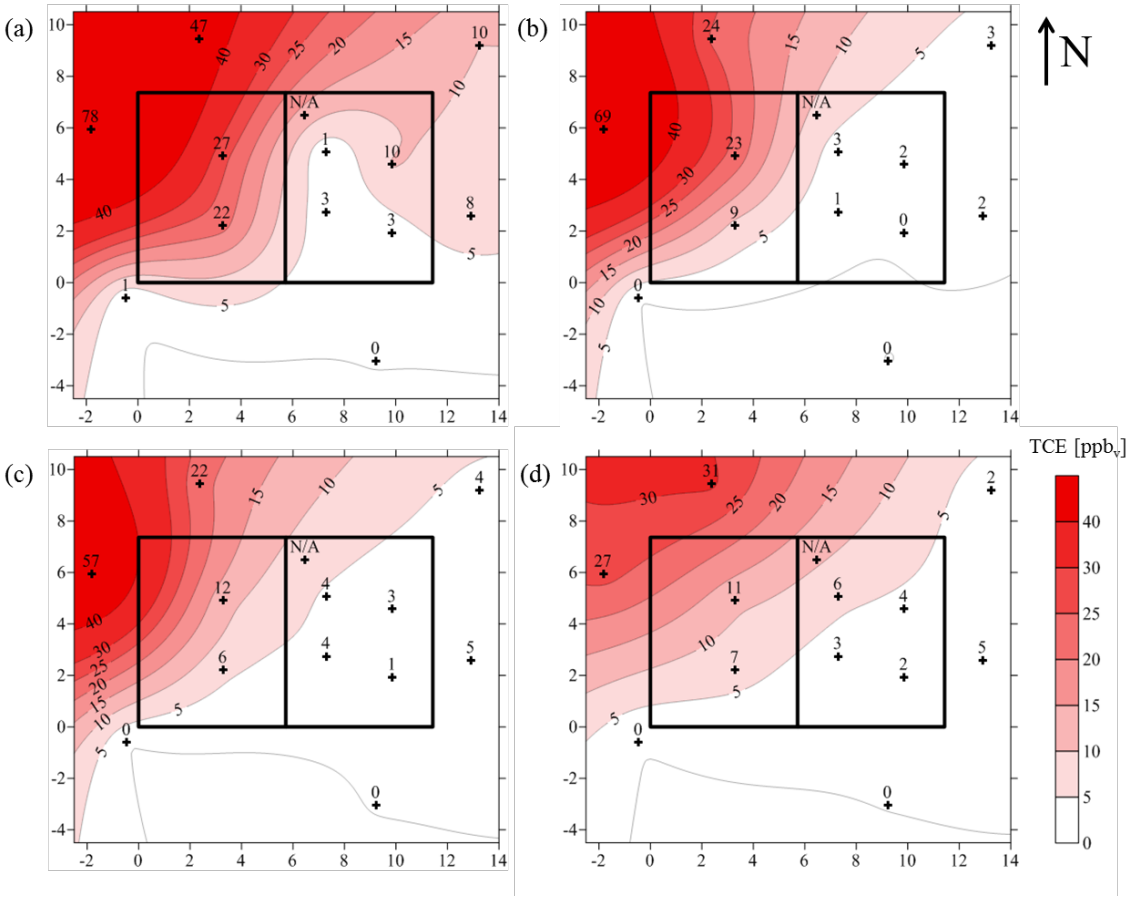

Figure 4.19. Soil gas concentration contour plots for the 0.9 m below-slab depth sampling points from (a) September 2011, (b) November 2011, (c) December 2011, and (d) January 2012.

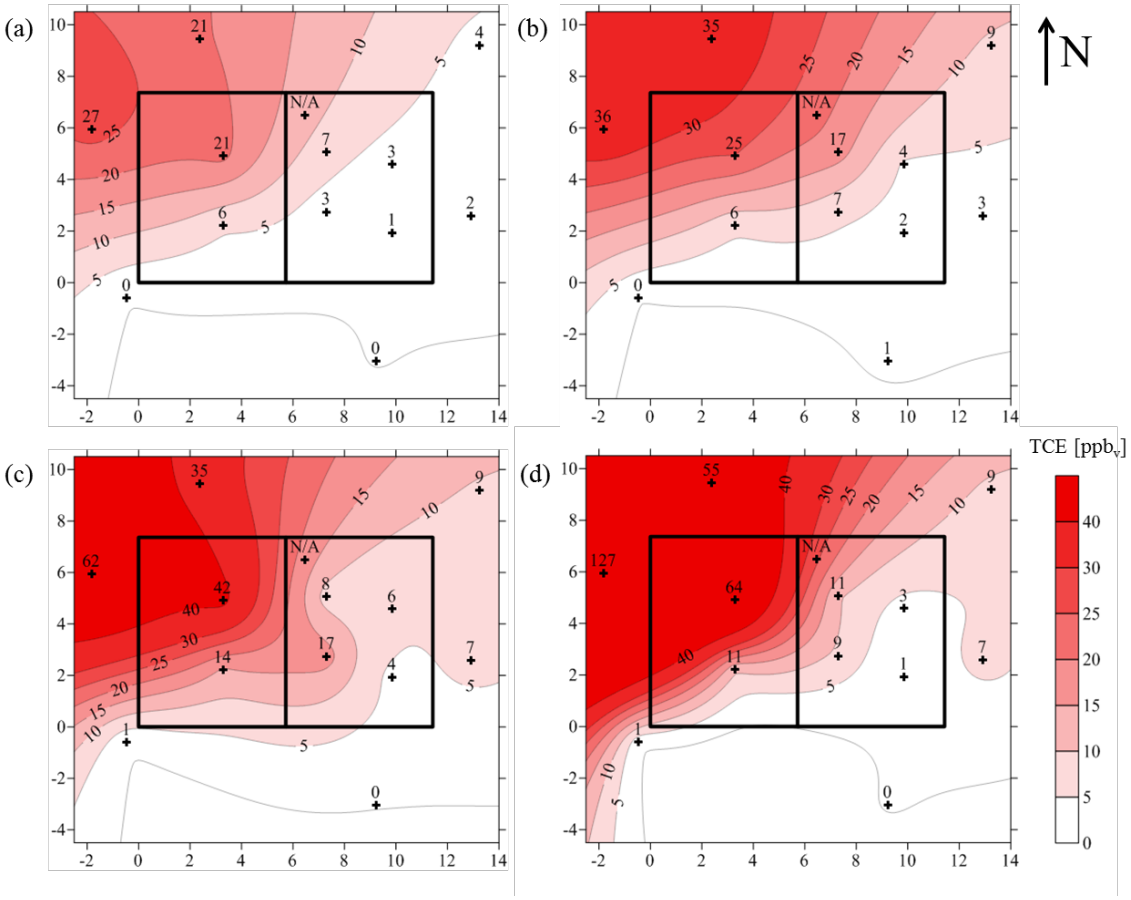

Figure 4.20. Soil gas concentration contour plots for the 0.9 m below-slab depth sampling points from (a) February 2012, (b) April 2012, (c) May 2012, and (d) August 2012.

Figure 4.21 shows a summary a summary of the soil gas concentration data at 0.9 m BS depth in a box and whisker plot. In comparison to Figure 4.16, differences between garage, interior, and exterior sampling point concentrations are more apparent, with concentrations at garage sampling points varying by a factor of about 4X, interior sampling points varying by 5X to 12X, and exterior locations varying by 2X to 12X based on the 10th and 90th percentile values.

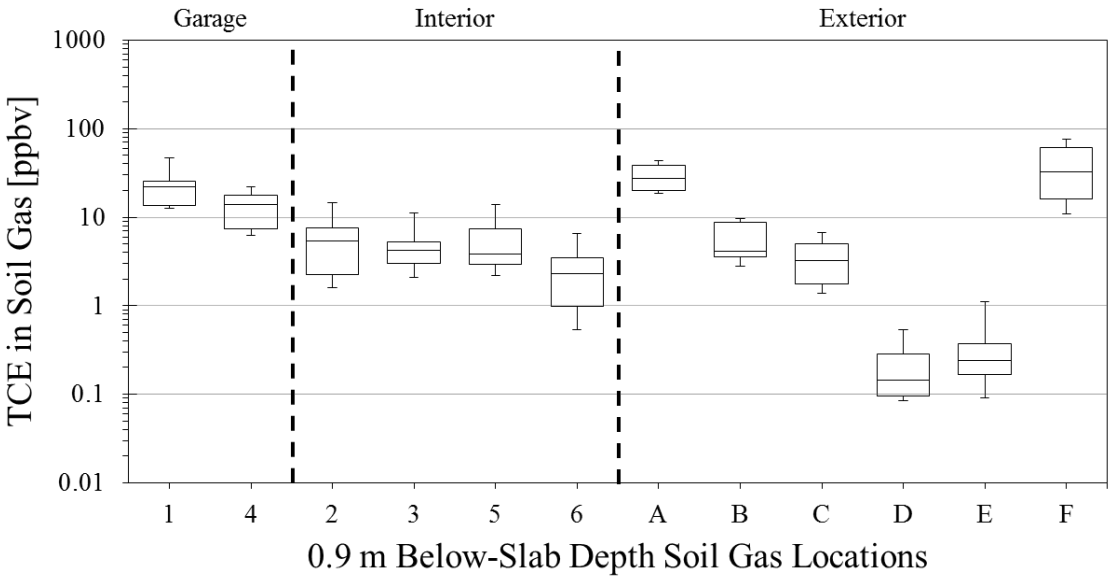

Figure 4.21. Box and whisker plot of TCE concentrations in soil gas at the 0.9 m below-slab depth sampling points from August 2010 to August 2012.

4.2.4 **Spatial and temporal trends in shallow soil gas concentrations**

Figures 4.22 to 4.25 show contour plots of TCE concentrations in soil gas at SS depth sampling points. In general, the distribution of soil gas concentrations at SS depth sampling locations is quite different from the deeper sampling points, with more obvious changes over time. In general, SS soil gas concentrations are all less than their corresponding 0.9 m BS depth sampling points, but there are occasions where the concentration in sub-slab depth soil gas is greater than at the 0.9 m BS depth. Unlike the deeper sampling points, the location of the highest sub-slab soil gas concentration changed from survey to survey.

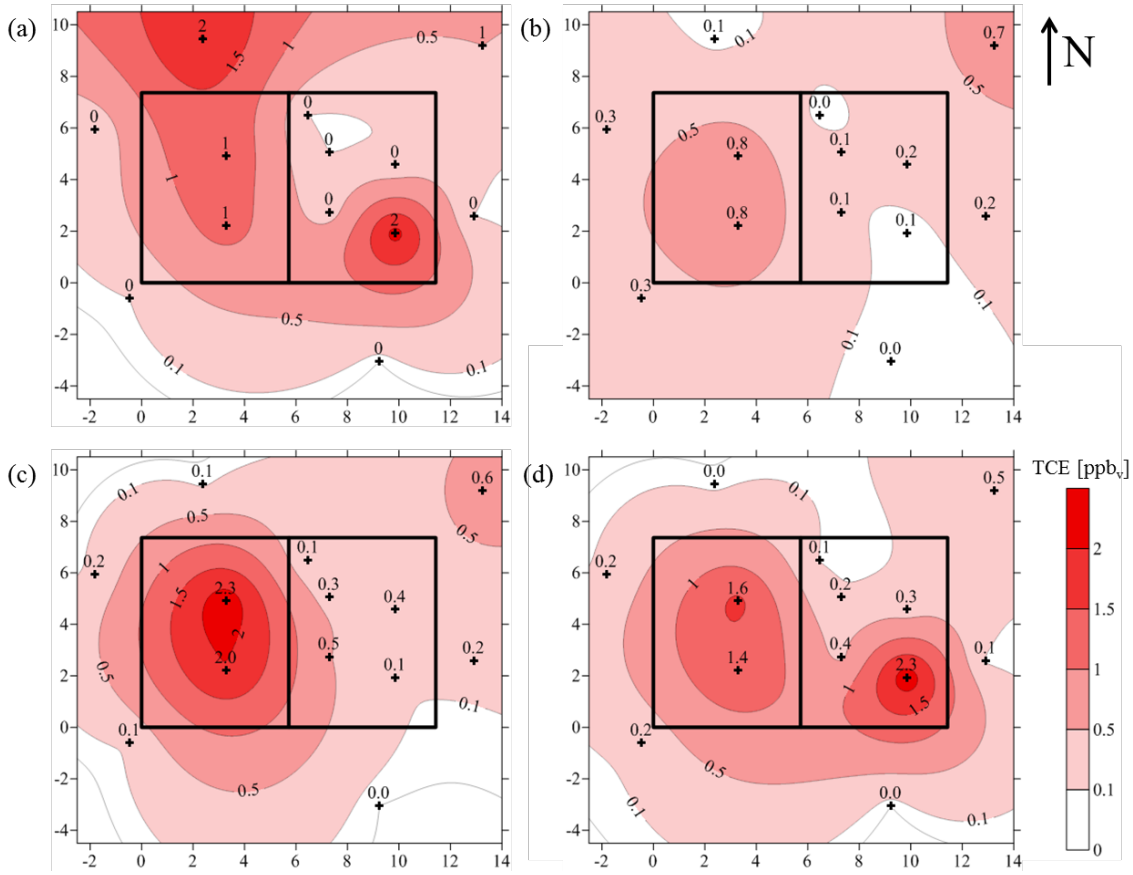

Figure 4.22. Soil gas concentration contour plots for the sub-slab depth sampling points from (a) August 2010, (b) November 2010, (c) December 2010, (d) and March 2011.

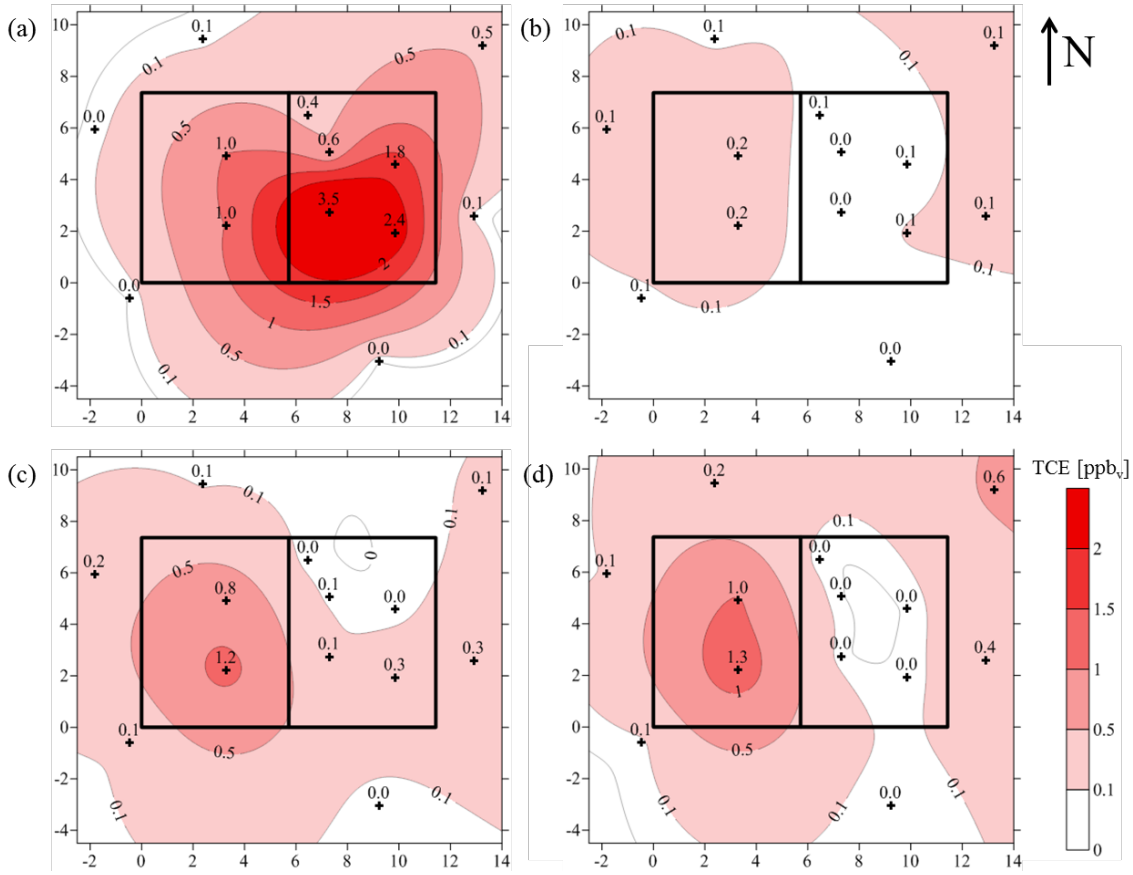

Figure 4.23. Soil gas concentration contour plots for the sub-slab depth sampling points from (a) April 2011, (b) May 2011, (c) July 2011, and (d) August 2011.

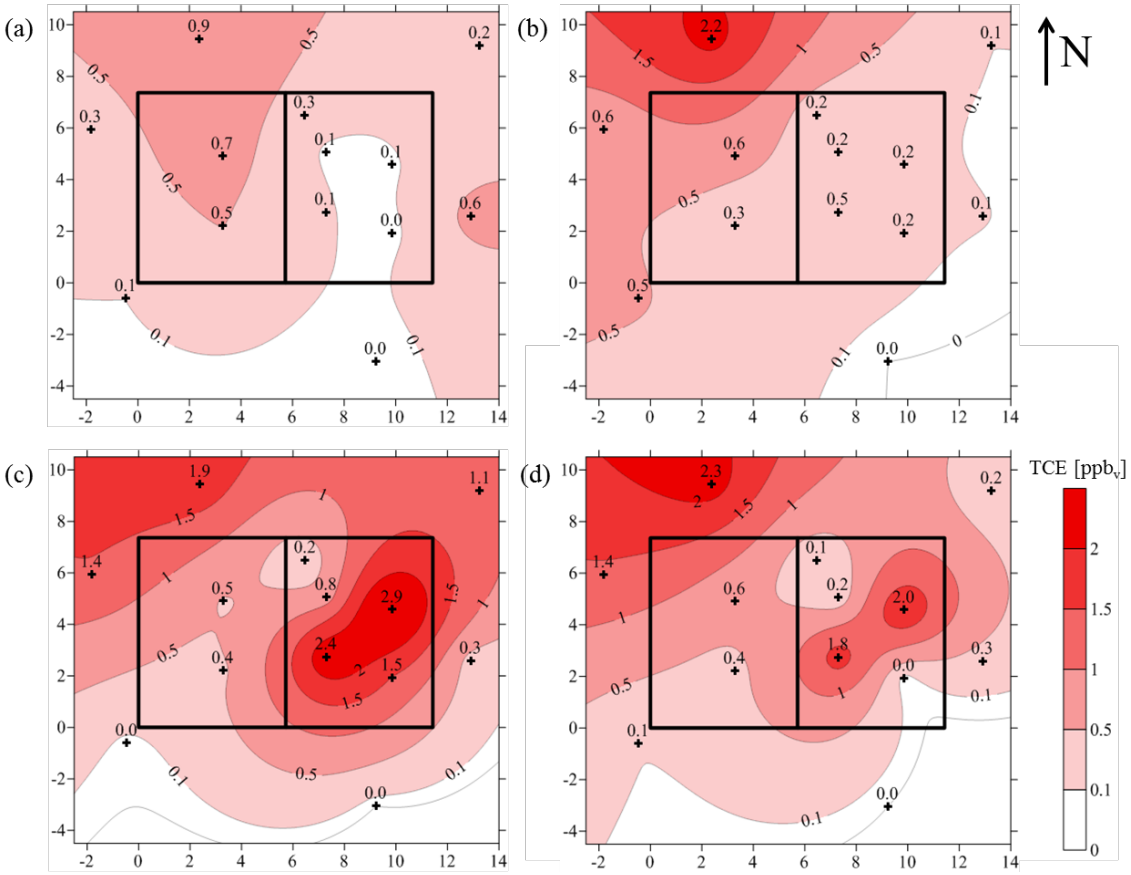

Figure 4.24. Soil gas concentration contour plots for the sub-slab depth sampling points from (a) September 2011, (b) November 2011, (c) December 2011, and (d) January 2012.

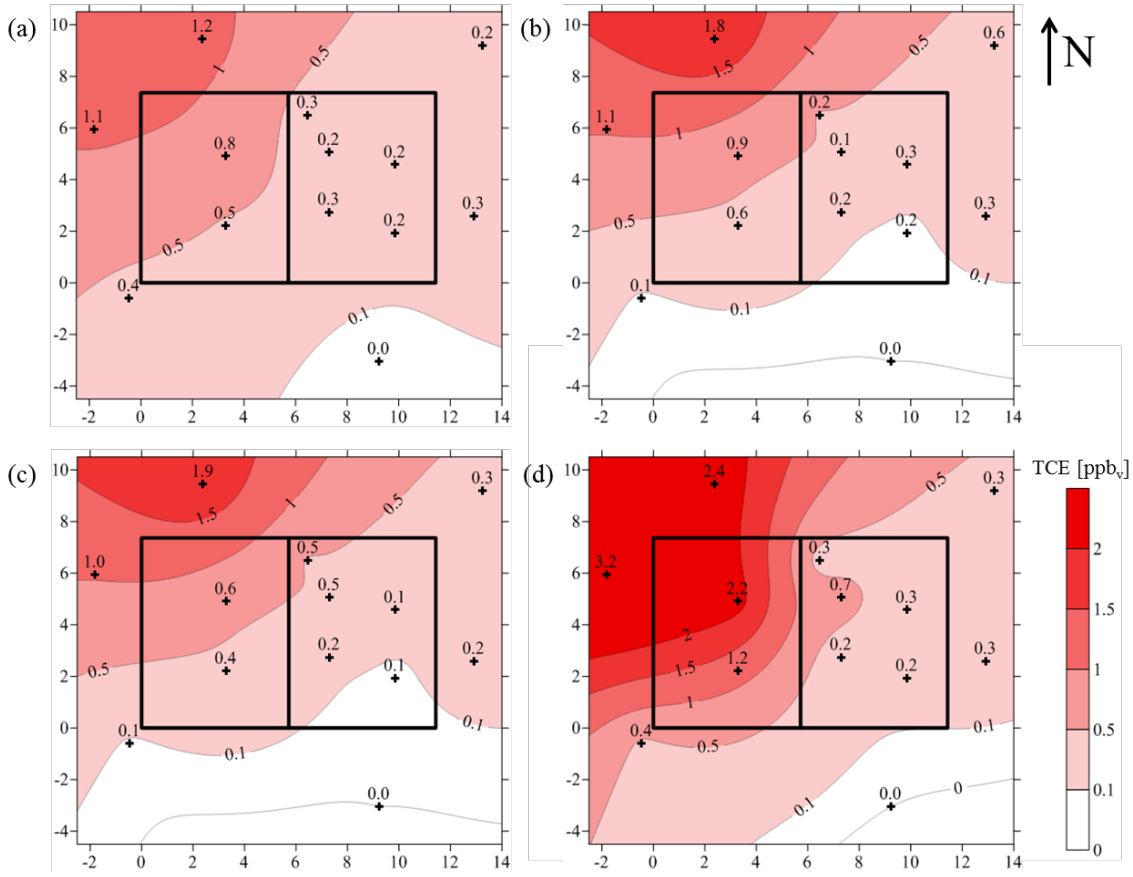

Figure 4.25. Soil gas concentration contour plots for the sub-slab depth sampling points from (a) February 2012, (b) April 2012, (c) May 2012, and (d) August 2012.

Figure 4.26 presents a summary of the soil gas concentration data at SS depths in a box and whisker plot created using the same format as outlined above. Location D is not included in the summary, since a SS depth sampling location at D would be above ground surface. Compared to the deeper sampling locations, concentrations at SS depths varied considerable more from 4X to over one order-of-magnitude based on the 10th and 90th percentile values. Soil gas concentrations at garage and exterior sampling points generally saw less variation than interior sampling points. The exception to this was location A, where the interquartile range was greatest.

It is important to note that the box and whisker plots, while giving a general idea of the variation that occurred in soil gas during the study, do not show the spatial variation that occurred over time. Appendix A.4 provides additional soil gas monitoring results, including multi-depth contour plots, to further highlight the changes in the spatial distribution of soil gas that occurred over time.

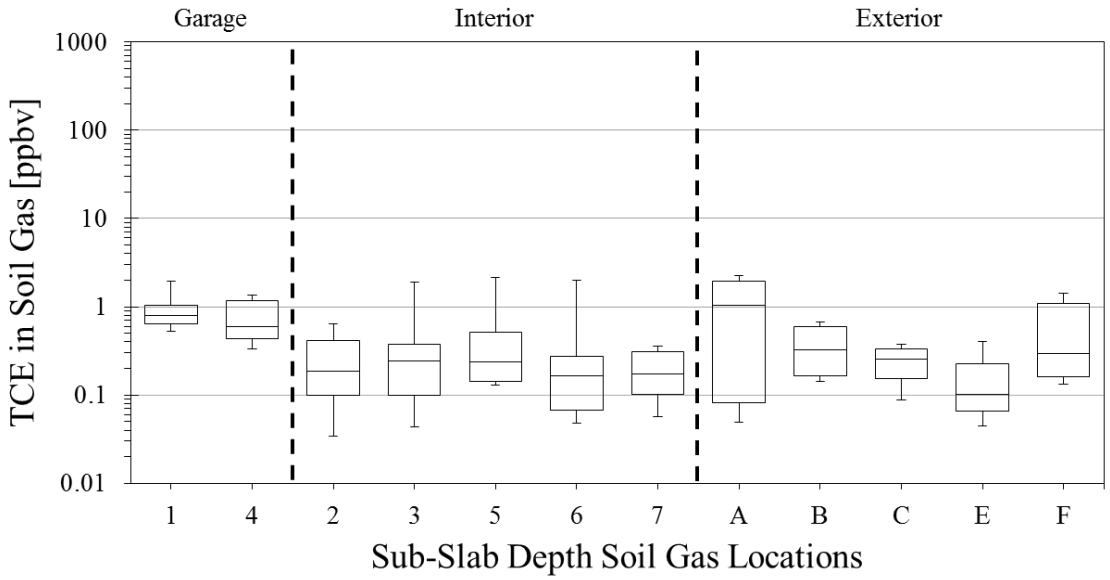

Figure 4.26. Box and whisker plot of TCE concentrations in soil gas at the sub-slab depth sampling points from August 2010 to August 2012.

4.2.5 **Trends in soil gas data**

The data presented above demonstrate that temporal and spatial variability of TCE concentrations in soil gas increased as the sampling point moved closer to the building foundation and ground surface. This observation is supported by the increasing interquartile range of the data shown in Figures 4.16, 4.21, and 4.26. This behavior is expected, since dynamic changes in the environmental and building conditions will have the greatest influence on soil gas closest to the building foundation and surface.

Table 4.2 provides a summary of relevant statistics for the soil gas data at each depth. The significance of the temporal variability observed at each soil gas sampling location and depth was evaluated by looking at the ratio of (90^{th} percentile – 10^{th} percentile)/median values. On the whole, this ratio increases in value from deep soil gas to shallow soil gas and interior locations show the largest values at the SS sampling depth. Locations B and C do not follow this trend, however, as location B didn't see a significant change between the two available sampling depths and the value decreases from 0.9 m BS depth to SS depth at location C.

As mentioned above, to further evaluate temporal and spatial changes in soil gas concentrations, real-time monitoring was performed at several sampling locations during the study. Figures 4.27 and 4.28 show results from real-time monitoring of soil gas at SS and 0.9 m BS sampling depths at locations 1 and 6, respectively. These data were collected over a one-year period from 281 d < t < 607 d. Additional real-time soil gas monitoring results are shown in Appendix A.4.

Table 4.2. Summary statistics for each soil gas sampling location and depth.

	Concentrations (ppb_v) for Sub-slab Depth Sampling Points												
	Garage		Interior					Exterior					
	1	4	2	3	5	6	7	A	B	C	D	E	F
Median	0.79	0.59	0.19	0.24	0.24	0.16	0.17	1.03	0.33	0.25	NS	0.10	0.29
10^{th} Percentile	0.53	0.33	0.03	0.04	0.13	0.05	0.06	0.05	0.14	0.09	NS	0.04	0.13
90^{th} Percentile	1.96	1.36	0.65	1.92	2.16	1.98	0.36	2.23	0.67	0.37	NS	0.41	1.43
(90^{th} Percentile - 10^{th} Percentile)/Median	1.8	1.7	3.3	7.8	8.5	11.7	1.7	2.1	1.6	1.1	NS	3.6	4.4
	Concentrations (ppb_v) for 0.9 m Below-slab Depth Sampling Points												
	Garage		Interior					Exterior					
	1	4	2	3	5	6	7	A	B	C	D	E	F
Median	22.2	13.8	5.4	4.2	3.9	2.3	NS	27.7	4.1	3.3	0.14	0.24	32.7
10^{th} Percentile	12.6	6.3	1.6	2.1	2.2	0.5	NS	18.6	2.8	1.4	0.08	0.09	10.9
90^{th} Percentile	46.5	22.0	14.6	11.2	13.9	6.5	NS	43.6	9.6	6.7	0.54	1.11	75.3
(90th Percentile - 10th Percentile)/Median	1.5	1.1	2.4	2.2	3.0	2.6	NS	0.9	1.6	1.6	3.2	4.3	2.0
	Concentrations (ppb_v) for 1.8 m Below-slab Depth Sampling Points												
	Garage		Interior					Exterior					
	1	4	2	3	5	6	7	A	B	C	D	E	F
Median	116.9	81.1	150.6	98.6	37.8	41.4	NS	NS	NS	55.7	1.0	28.6	325.4
10^{th} Percentile	89.1	46.3	77.0	64.8	25.6	30.8	NS	NS	NS	34.1	0.5	2.0	221.5
90^{th} Percentile	212.6	101.5	320.7	144.9	139.0	76.1	NS	NS	NS	90.3	1.8	86.9	418.1
(90^{th} Percentile - 10^{th} Percentile)/Median	1.1	0.7	1.6	0.8	3.0	1.1	NS	NS	NS	1.0	1.3	3.0	0.6

*NS = No sample available at this depth

The real-time soil gas results in Figures 4.27 and 4.28 agree with the results from the corresponding synoptic soil gas surveys. For location 1, sub-slab and 0.9 m BS soil gas varied similarly overtime with data from 0.9 m BS varying by a factor of 4X and sub-slab soil gas varying by a factor of 6X. In general, the differences between sub-slab and 0.9 m BS soil gas concentrations at location 1 were consistent in time with a little more than an order-of-magnitude variation. The results at location 6 were significantly more variable than location 1 with sub-slab soil gas varying by over two orders-of-magnitude and 0.9 m BS soil gas varying by over one order-of-magnitude. During several periods, the concentration of sub-slab soil gas at location 6 fluctuated between levels above and below those measured at 0.9 m BS. These events can also be seen when comparing the soil gas contours for sub-slab and 0.9 m BS depths from December 2011 (Figures 4.19 and 4.24).

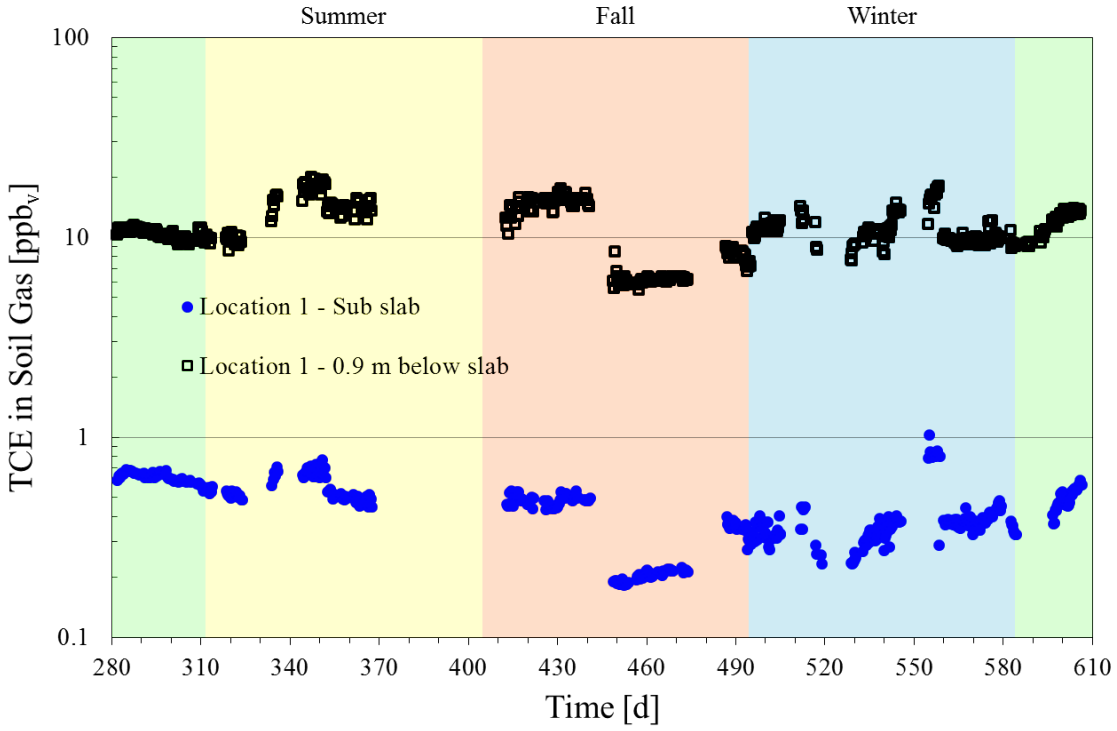

Figure 4.27. TCE concentration in sub-slab and 0.9 m below-slab soil gas at location 1 from May 2011 to April 2012.

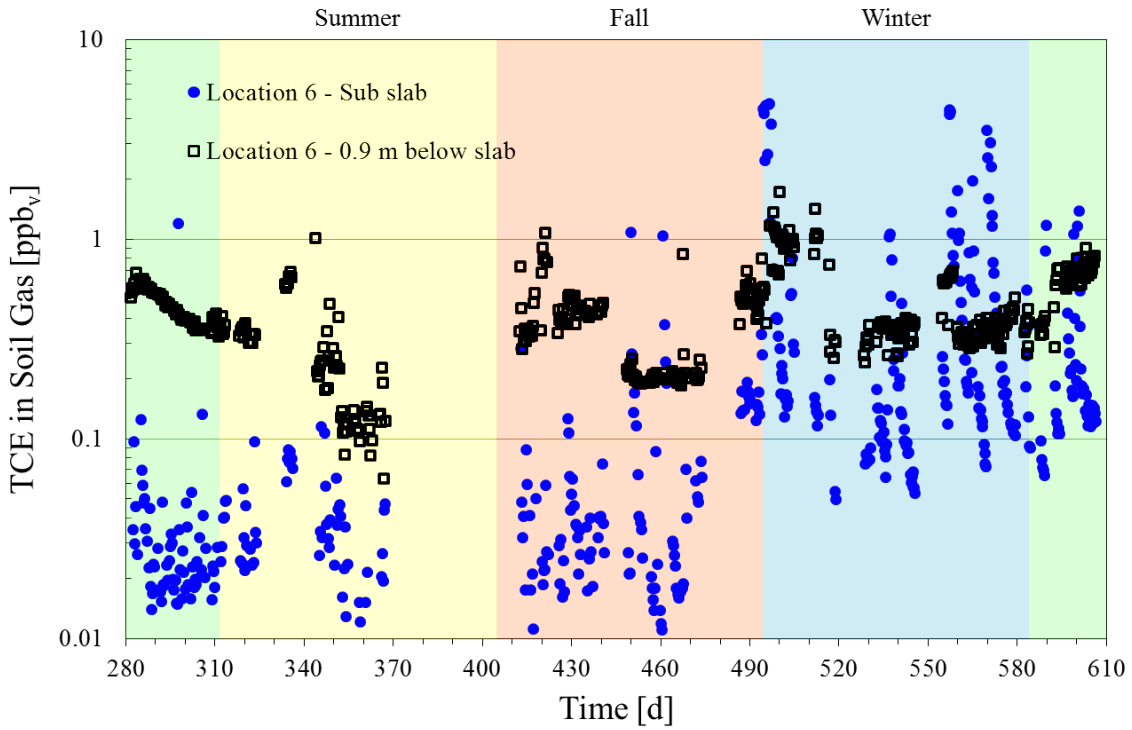

Figure 4.28. TCE concentration in sub-slab and 0.9 m below-slab soil gas at location 6 from May 2011 to April 2012.

4.2.6 **Implications for Pathway Assessment**

The spatial and temporal variability in the data presented above suggest that caution is needed when using typical site characterization data to assess the potential for vapor intrusion. Deeper soil gas concentrations and the shallow groundwater concentrations from interior and exterior sampling points showed greater consistency through time than near-surface and sub-slab soil gas data, and therefore might be more reliable for use when screening for the potential of vapor intrusion. The validity of this statement is dependent on the accuracy of approaches for extrapolating these data to indoor air concentrations and more study is needed on that topic. There was spatial variability in these deeper concentrations at the study site, so multiple locations about a building should be considered.

As this is the first study to couple long-term monitoring of groundwater, soil gas, and indoor air at a vapor intrusion site, it is not known if the observed behavior is representative of other sites. However, it is clear that conventional approaches would likely be inadequate for assessing VI impacts at this site and that alternate approaches need to be studied further and adopted by guidance.

4.3 CREATION OF A SUB-SLAB SOIL GAS PLUME BY AN INDOOR AIR SOURCE AND ITS DISSIPATION FOLLOWING SOURCE REMOVAL

The goal of this study was to gain a better understanding of the significance, dynamics, and longevity of indoor source-created soil gas CHC storage, and its potential to confound VI pathway assessment. This involved the controlled indoor release of sulfur hexafluoride (SF_6) in the lower level of the study house and the monitoring of SF_6 in indoor air and soil gas over a two-year period. The field experiment results were supplemented with mathematical modeling to see if the modeling might be useful for simulating behavior under other field conditions.

4.3.1 **Long-term Indoor Source Release**

The results presented below are placed on a timeline consistent with previous field experiments and monitoring results, where time (t) = 0 is 8:00 AM on 8/15/2010.

Figure 4.29 presents daily 24-h average differential pressures measured between sub-slab soil gas and indoor air at location 5 for the time period 120 d < t < 735 d. Positive values indicate flow from the subsurface to indoor air. Vertical bars extending from each daily data point span the 10^{th} and 90^{th} percentile values for that day. During this period, 24-h average differential pressures ranged from -0.9 to 0.8 Pa with 10^{th} and 90^{th} percentile values ranging from -3.3 to 3.0 Pa. Bidirectional flow within a 24-h period, as indicated by a vertical bar spanning both positive and negative values, occurs for 59% of the 24-h periods. These results are representative of the other indoor sub-slab monitoring locations. The 24-h average differential pressures and daily ranges shown here are similar to observations for other residential buildings under natural conditions (McHugh et al., 2006).

Figure 4.30 presents daily 24-h average indoor air SF_6 concentrations with vertical bars spanning the daily maximum and minimum values. The 24-h average values were only calculated for days with at least four samples and are plotted at 8:00 PM on each day. As mentioned above, an inline calibration gas standard was used to monitor and correct for changes in instrument sensitivity starting on t = 282 d. The data before this period still reflect the general behavior of SF_6 in indoor air. SF_6 release was suspended during two periods for source removal testing and the data from those periods, 630 d < t < 655 d and 681 d < t < 697 d, are highlighted in the figure.

Daily 24-h average indoor air SF_6 concentrations varied by a little more than a factor of five during the long-term release study with smaller daily and seasonal fluctuations. The highest concentrations occurred in the late spring to early fall months and the lowest concentrations during the late fall to early spring. As the SF_6 release rate was constant during the study period, temporal changes in indoor air concentrations reflect changes in indoor air exchange rate with time.

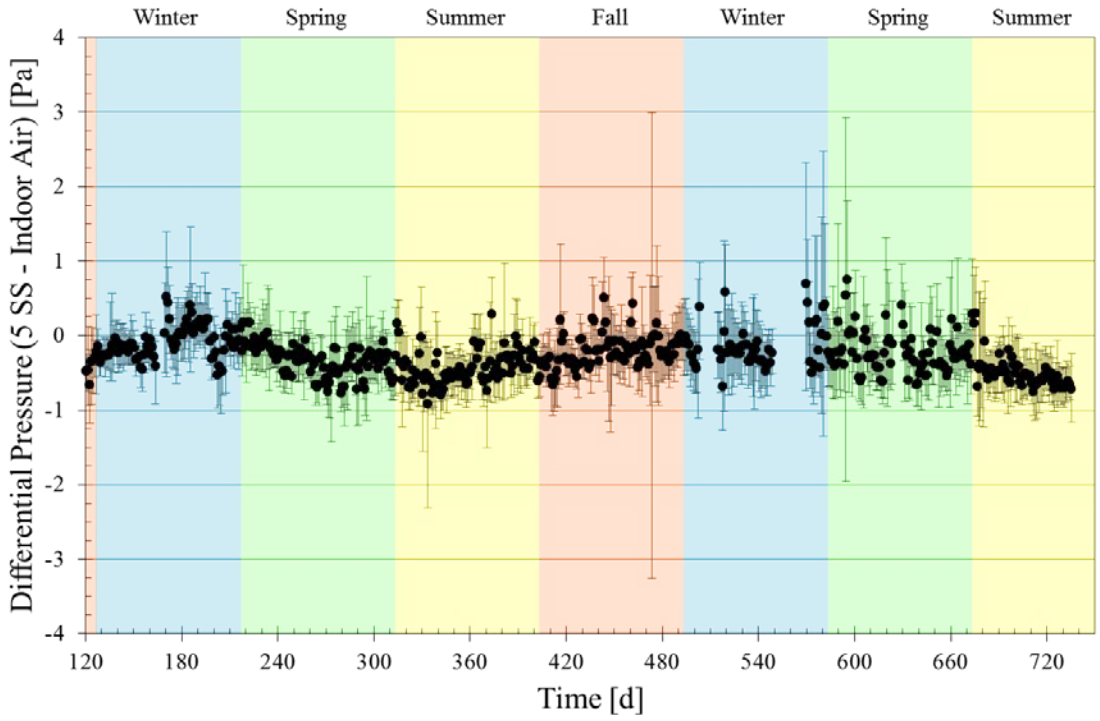

Figure 4.29. Daily 24-h average differential pressures measured between soil gas and indoor air at location 5 with error bars spanning the 10th and 90th percentile of the real-time data.

Figure 4.30 also presents daily 24-h average sub-slab soil gas SF_6 concentrations at location 3 from 234 d < t < 730 d. The plot includes error bars that span the daily maximum and minimum values. Real-time soil gas sampling also occurred at locations 2 and 6, but the results from location 3 are presented here as they are the most complete. Similar to indoor air concentrations, a seasonal trend is apparent in the sub-slab soil gas data with the highest SF_6 concentrations occurring in the late spring to early fall months and the lowest concentrations occurring during the late fall to early spring. Daily 24-h average SF_6 concentrations in sub-slab soil gas at location 3 varied by about an order-of-magnitude for this period. In general, SF_6 concentrations in soil gas were lower than indoor air concentrations during the long-term release study.

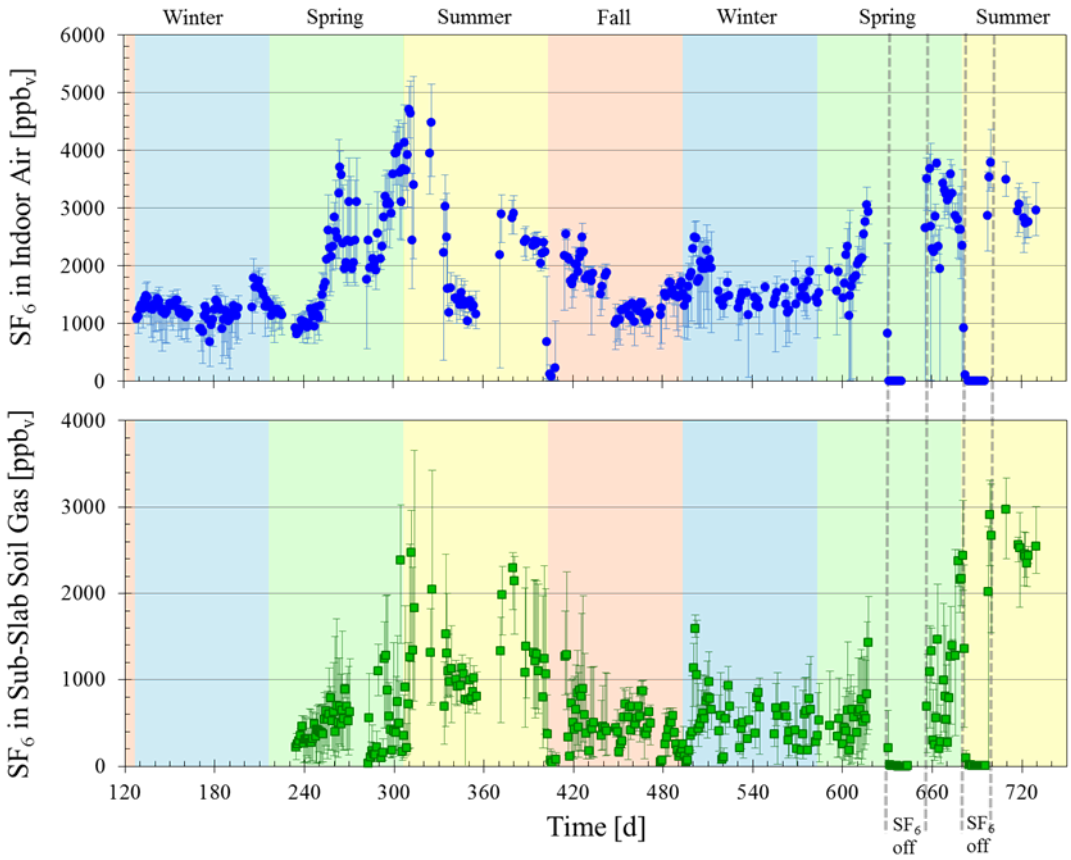

Figure 4.30. Daily 24-h average SF_6 concentrations in indoor air and sub-slab soil gas at location 3 from with error bars spanning the daily maximum and minimum values.

As discussed above, synoptic multi-depth soil gas surveys occurred every 1-3 months to gain an understanding of the temporal and spatial variation of SF_6 in the subsurface. To illustrate the temporal changes that were observed in soil gas during the long-term release of SF_6, the mass of SF_6 beneath the house was estimated for each survey using five different estimation methods. SF_6 concentrations in soil gas were multiplied by representative soil volumes and the results summed. Representative volumes for each indoor sampling location were determined by first dividing the house footprint into sub-region areas each containing a single sampling location. The vertical component of each volume was determined by treating the subsurface below the foundation as having three layers (0-46 cm, 46-137 cm and 137-183 cm BS). The concentration of SF_6 in exterior soil gas sampling locations was often 1-3 orders-of-magnitude lower than the interior sampling locations, thus exterior results were not included in the mass estimation.

Figure 4.31 presents the average SF_6 mass estimate for ten separate synoptic soil gas surveys from 197 d < t < 623 d with error bars spanning the range of estimated values. During this period, the average SF_6 mass estimate ranged from 0.03 to 1.07 g and followed a similar seasonal pattern as was observed for the real-time monitoring of indoor air and soil gas concentrations.

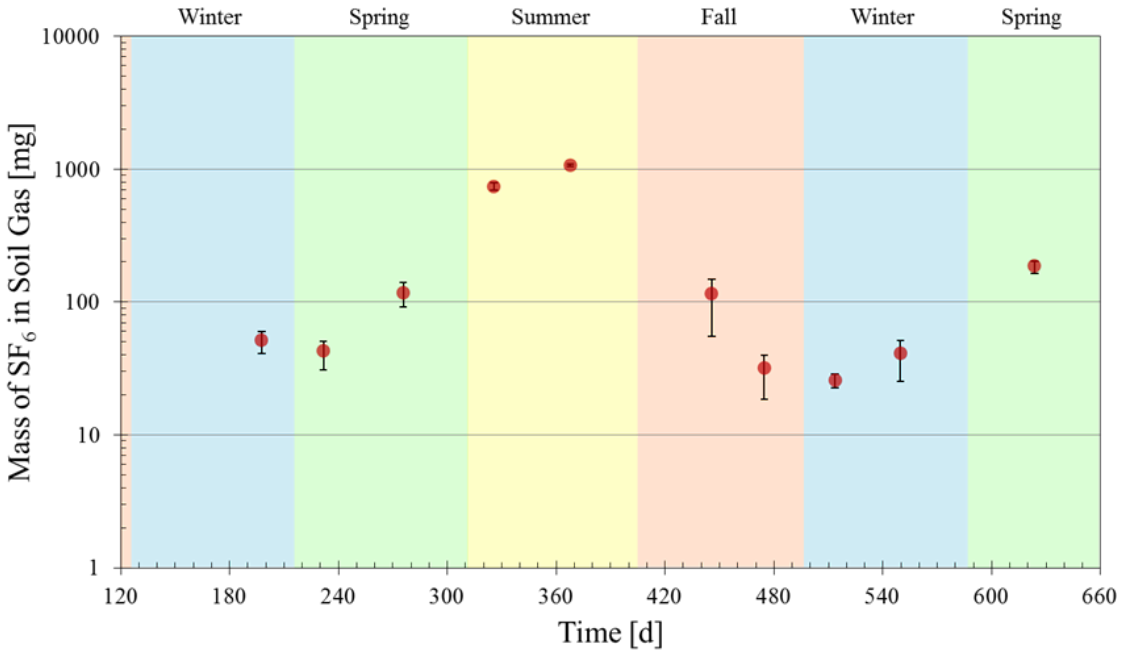

Figure 4.31. Average estimate mass of SF_6 in soil gas below the study house from synoptic soil gas survey data with error bars spanning the range of estimated values for each event.

Figures 4.32 and 4.33 show multi-depth soil gas concentration contour plots from the t = 329 d and t = 515 d sampling events, respectively. These two surveys show times when the estimated mass of SF_6 in the subsurface was high and low. For the t = 329 d event (Figure 4.32), the estimated mass of SF_6 in the subsurface was 750 mg and for the t = 515 d event (Figure 4.33) the estimated mass of SF_6 in the subsurface was 30 mg. The 30-d average indoor air SF_6 concentration prior to the t = 329 d and t = 515 d events was 5705 ppb_v and 1801 ppb_v, respectively. The multi-depth soil gas concentration contour plots further illustrate the temporal changes of SF_6 in the subsurface and highlight some of the spatial changes in SF_6 distribution that were observed.

The indoor air and soil gas concentration data presented above demonstrate that indoor sources can lead to subsurface soil gas plumes and that the extent and mass of these plumes can change with time.

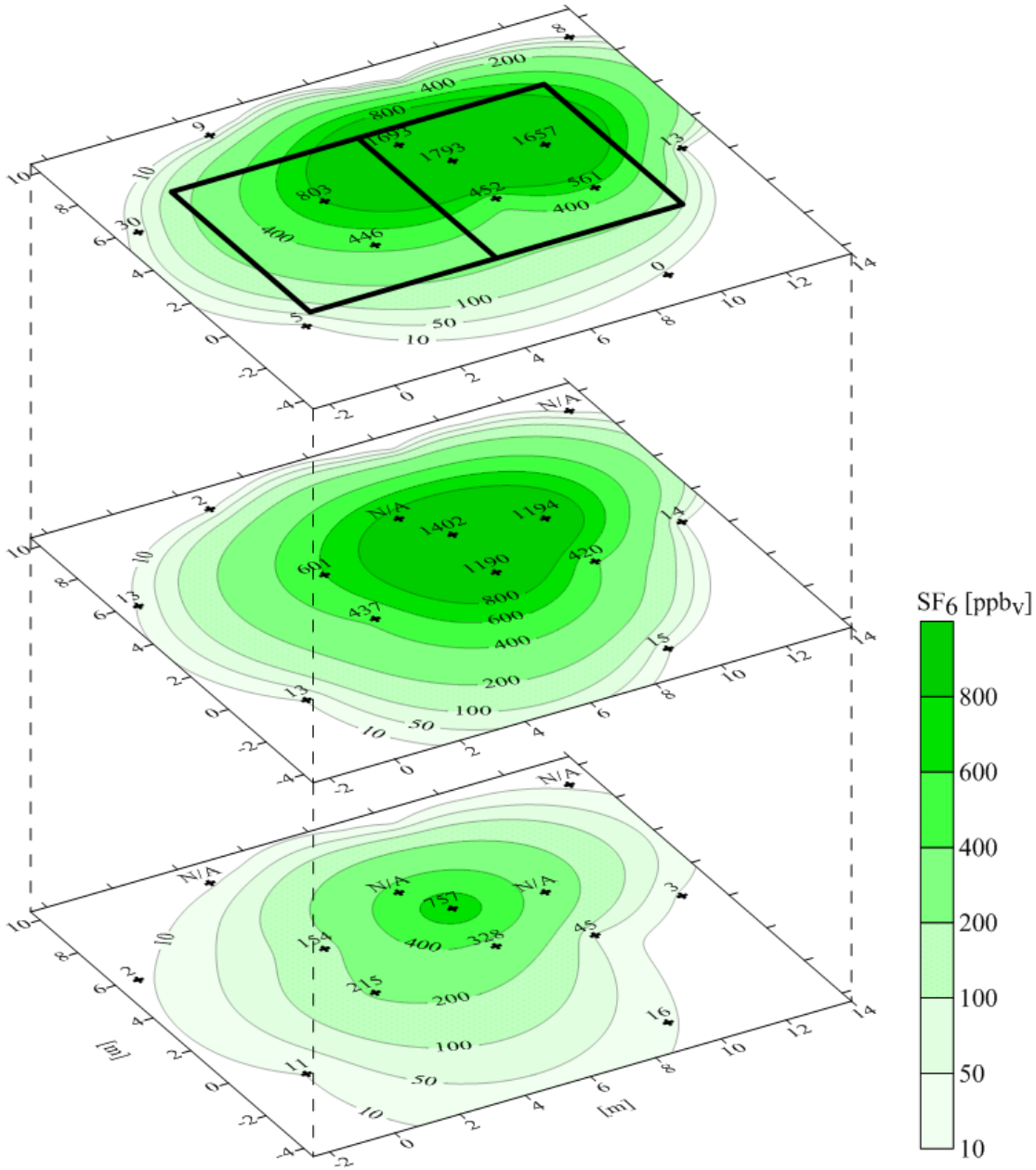

Figure 4.32. SF_6 concentration contour plots for soil gas at sub-slab, 0.9 m BS, and 1.8 m BS depths from t = 329 d.

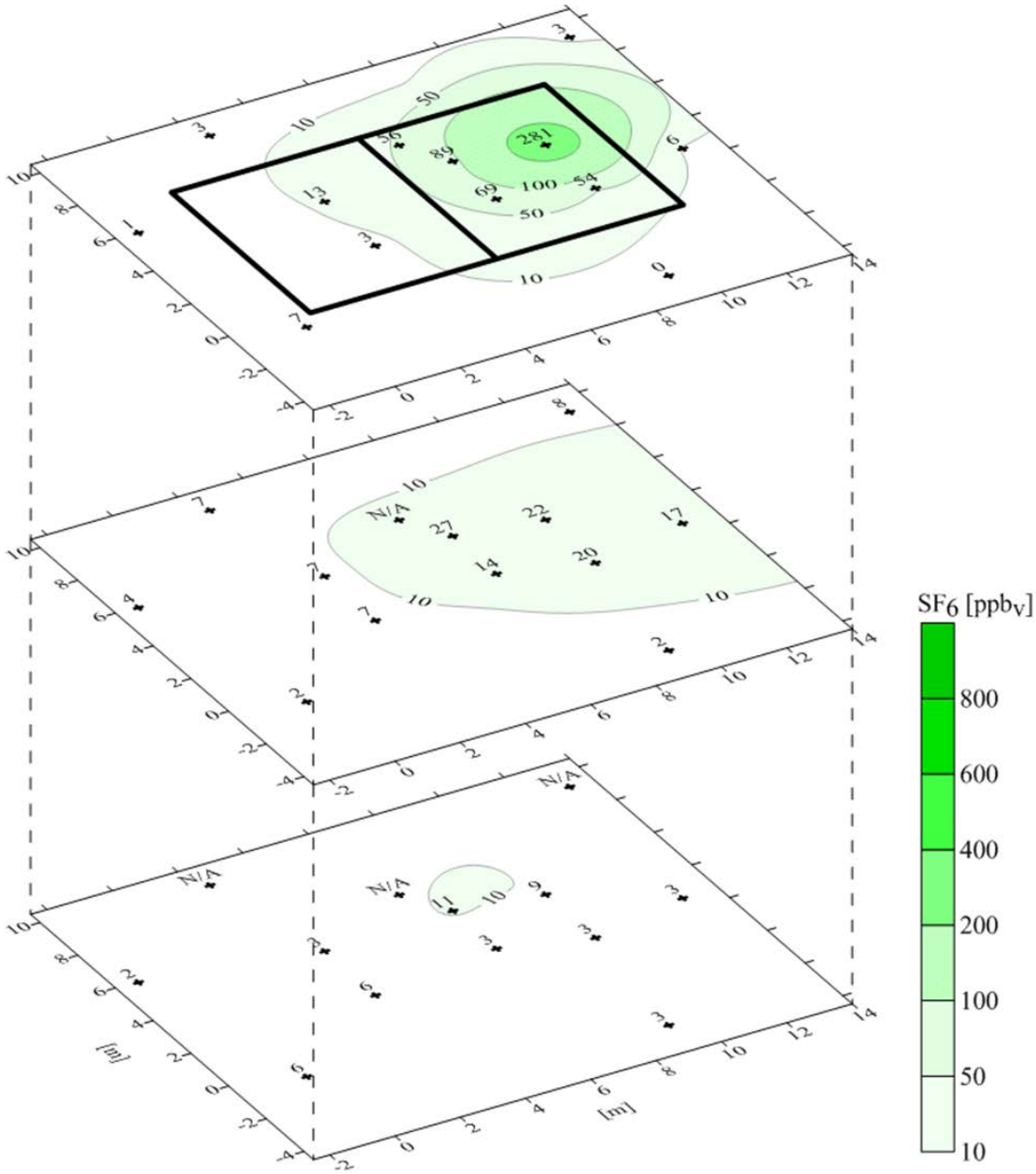

Figure 4.33. SF_6 concentration contour plots for soil gas at sub-slab, 0.9 m BS, and 1.8 m BS depths from t = 515 d.

4.3.2 **Indoor source removal tests**

The indoor source removal experiments were designed to simulate the removal of indoor sources that may occur during or prior to VI site investigations.

Figure 4.34 presents the SF_6 concentration response in indoor air and soil gas at location 3 at sub-slab and 0.9 m BS depths from 655 d < t < 695 d to the introduction and removal of SF_6 in indoor air. It is evident that indoor air responded quickest to the release of SF_6, with

concentrations reaching over 3000 ppb_v within 5 h of introduction. Sub-slab soil gas also responded relatively quickly, with concentrations reaching over 1000 ppb_v in about 29 h. The concentration in soil gas at 0.9 m BS responded more slowly, requiring over 22 d to reach 1000 ppb_v. Prior to stopping the SF_6 release, the SF_6 concentration in indoor air and soil gas at sub-slab and 0.9 m BS depths were similar and within a factor of two. After stopping the release of SF_6 on t = 680 d, indoor air and sub-slab soil gas responded quickly with concentrations dropping to below 10 ppb_v in less than 72 h and 96 h, respectively. As with the initial release, soil gas at 0.9 m BS responded more slowly, with concentrations remaining above 150 ppb_v 15 d after halting the SF_6 release.

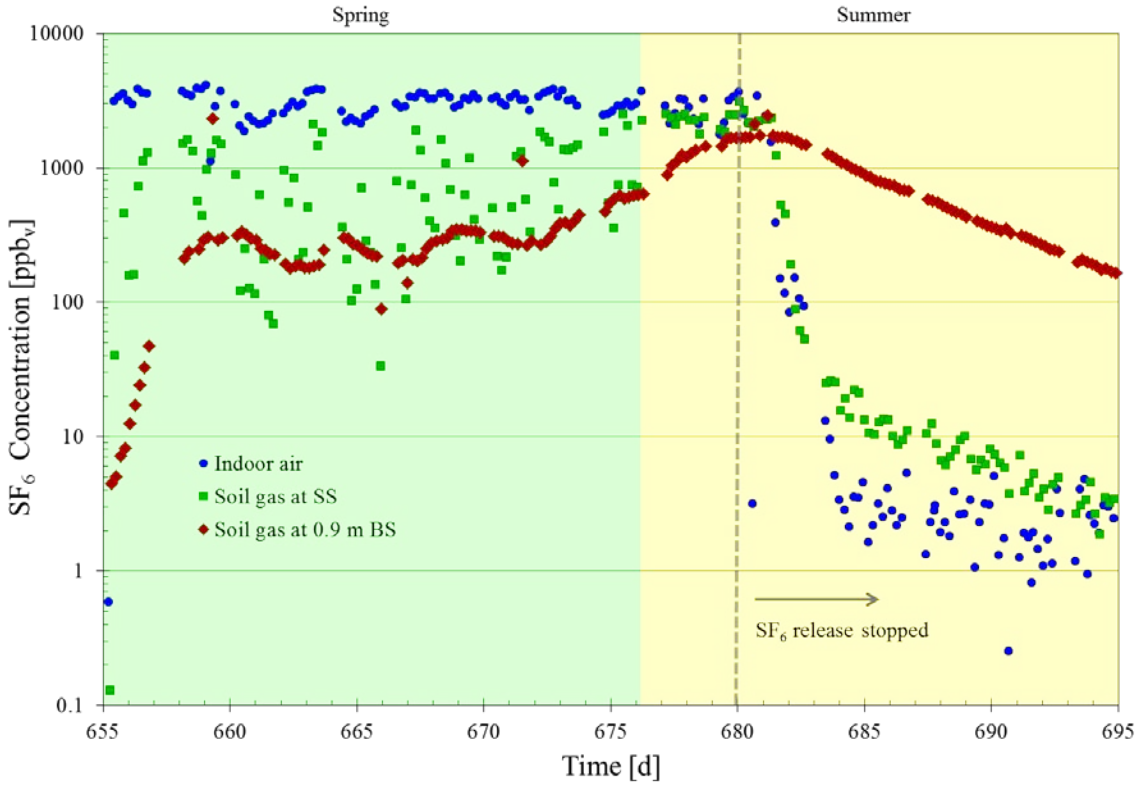

Figure 4.34. Instantaneous SF_6 concentrations in indoor air and sub-slab and 0.9 m BS soil gas at location 3 showing the results of introduction and removal of an indoor source.

The above results were obtained while the land drain lateral was connected without restriction to the neighborhood land drain. As discussed above, the subsurface infrastructure was modified on t = 1072 d with the installation of a valve on the land drain lateral and additional indoor source removal testing was performed.

Figure 4.35 shows the results of indoor source removal on concentrations in indoor air and soil gas at sub-slab and 0.9 m BS depths at location 3 from 1460 d < t < 1512 d after the land drain lateral was modified and its valve was closed. Similar to the results shown in Figure 4.34, prior to source removal (t = 1467 d) the concentrations of SF_6 in indoor air and soil gas at both depths

were within a factor of two. Upon stopping the release of SF_6 (t = 1467 d), indoor air concentrations dropped to near or below 10 ppb_v within 72 h, similar to the previous case with the open land drain connection. In contrast, sub-slab soil gas SF_6 concentrations did not decrease below 10 ppb_v until about 23 d after stopping the indoor SF_6 release. As before, concentrations of SF_6 in soil gas at 0.9 m BS decreased slowest with concentrations falling below 100 ppb_v after approximately 40 d. Near the end of the test, concentrations in sub-slab soil gas again increased to above 10 ppb_v, which may be indicative of contributions from deeper soil gas (i.e., 0.9 m BS soil gas). Results from locations 2 and 6 are also provided in Figures 4.36 and 4.37 and show similar results.

The differences observed in the removal tests from 655 d < t < 695 d and 1460 d < t < 1512 d highlight the impact of the lateral pipe and land drain system on subsurface dynamics; however, they also reveal potential erroneous VI pathway assessment outcomes following indoor source removal at sites where indoor sources are removed and then sampled within a few days. If sampling was performed 24-72 h after indoor source removal at the study house (with or without the lateral drain connected), the paired indoor air and sub-slab results could be interpreted to be indicative of a subsurface VI source as the soil gas concentrations were greater than indoor air concentrations.

4.3.3 **Indoor source modeling studies**

Modeling was performed using the three-dimensional, multicomponent, numerical model developed by Abreu and Johnson (2005) and updated by Luo (2009). It was modified to include indoor source release to indoor air at a constant emission rate. The objective of these simulations was to examine if modeling would mimic the field results and possibly provide insight about indoor source removal under scenarios that are different from the field conditions in this study. To do this, the simulation involved two time periods: (a) creation of the subsurface soil gas plume at a constant differential pressure between outdoor air and indoor air (i.e., disturbance pressure) for 30 d and (b) removal of the indoor source and continued monitoring at a constant disturbance pressure for 60 d. Table 4.3 provides details of the four scenarios simulated. Input parameters used to run the simulations are summarized in Appendix A.5. A plan view schematic of the model domain and foundation cracks is shown in Figure 4.38 and it includes the simulated sampling locations from which results are presented below.

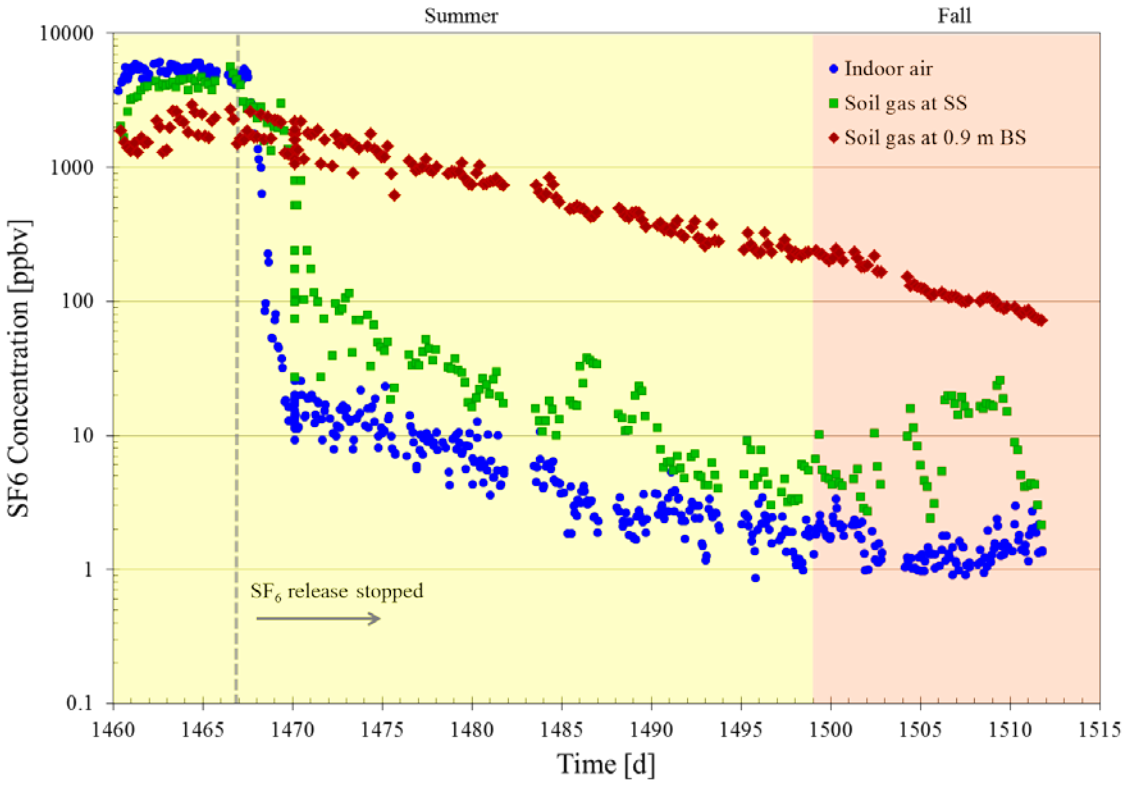

Figure 4.35. Instantaneous SF_6 concentrations in indoor air and soil gas at sub-slab and 0.9 m BS depths at location 3 showing the results of indoor source removal with the land drain lateral pipe valve closed.

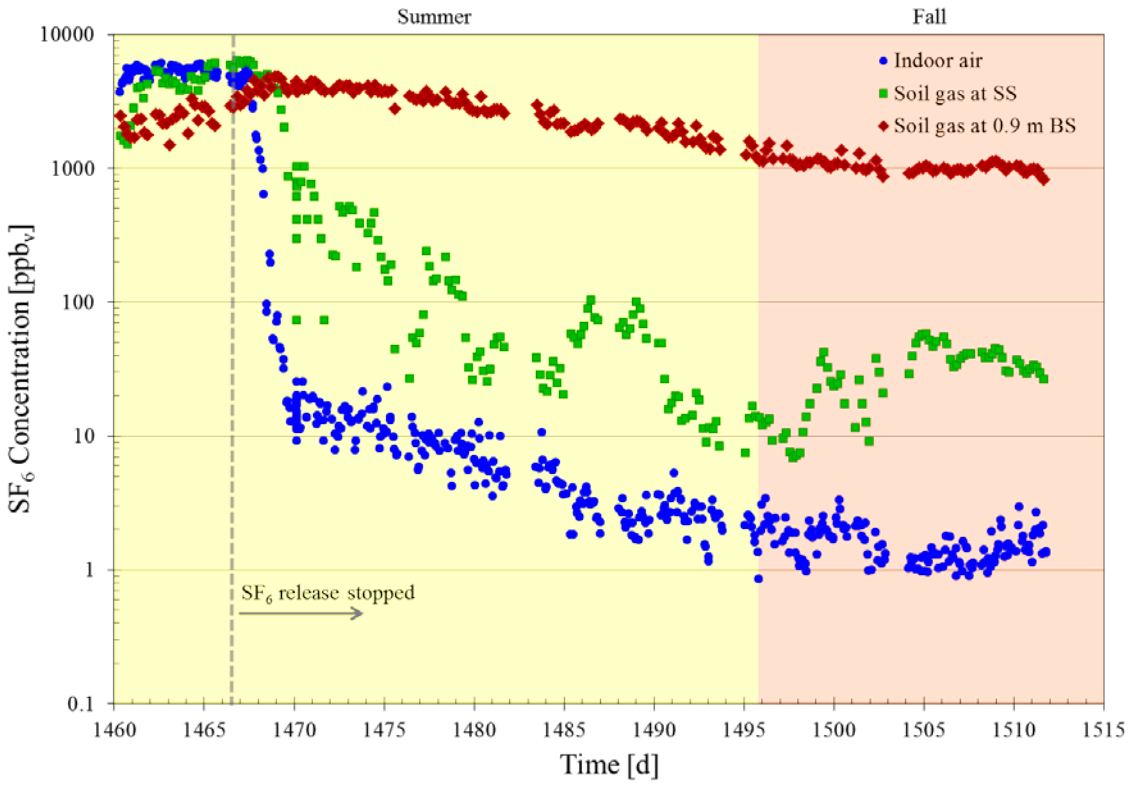

Figure 4.36. Instantaneous SF_6 concentrations in indoor air and soil gas at sub-slab and 0.9 m BS depths at location 2 showing the results of indoor source removal with the land drain lateral pipe valve closed.

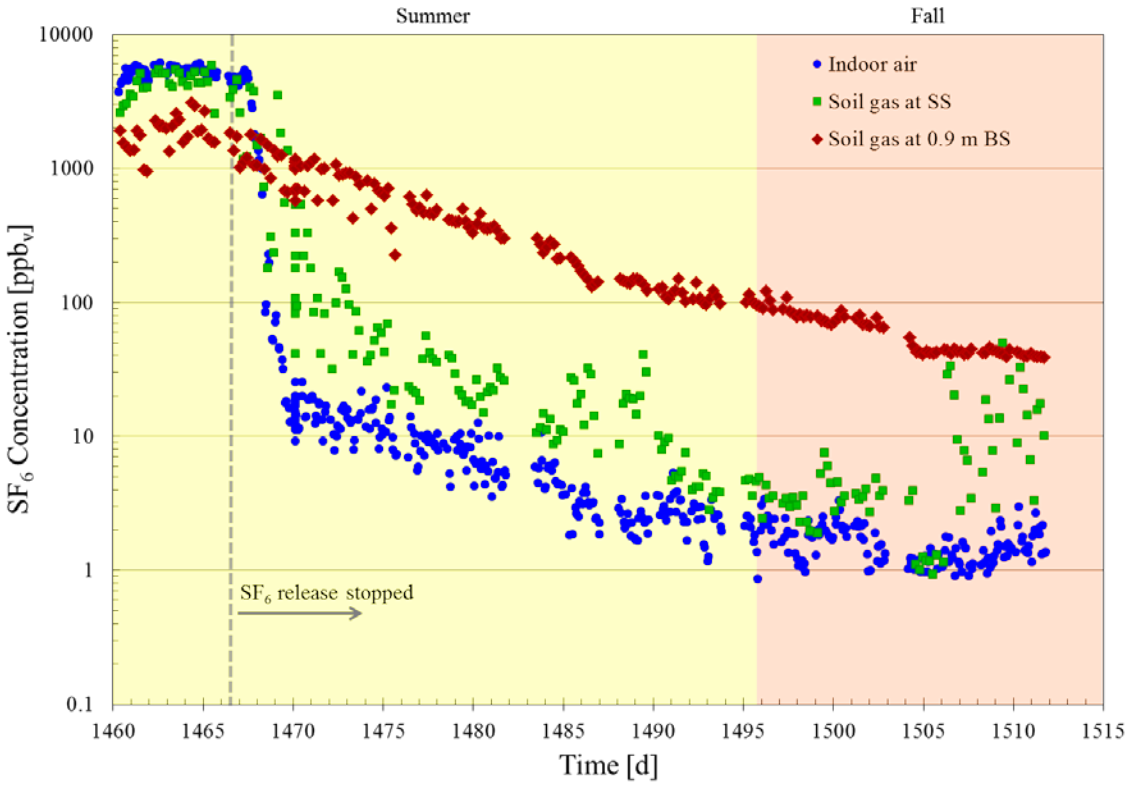

Figure 4.37. Instantaneous SF_6 concentrations in indoor air and soil gas at sub-slab and 0.9 m BS depths at location 6 showing the results of indoor source removal with the land drain lateral pipe valve closed.

As shown in Table 4.3, the subsurface soil gas plume was generated with a pressure differential between outdoor and indoor air of -2 Pa (advective flow into the subsurface). Figure 4.39 shows the resulting subsurface soil gas plume after 30 d of indoor source release at sub-slab (0.15 m below building slab), 1 m BS, and 1.8 m BS depths. SF_6 soil gas concentrations at the end of the release phase were greatest below the building foundation and along the perimeter crack.

For the second phase of the simulation, the indoor source was removed and a range of different pressure differentials were selected to observe the effects of source removal under different building pressure under- and over-pressurization conditions. Figure 4.40 and 4.41 show the results for over- and under-pressurization simulations 1 and 4, respectively. The plots show SF_6 concentrations in indoor air and soil gas at location A and B highlighted in Figure 4.38. For location A, soil gas is shown at sub-slab (0.15 m below building slab) and 1 m BS depths. For location B, only sub-slab soil gas is presented since concentrations at 1 m BS were within 10% of sub-slab values.

Table 4.3. Summary of indoor source modeling scenarios.

	Creation of Subsurface Soil Gas Plume			**Removal of Indoor Source**	
Simulation #	Indoor source* emission rate [g/s]	Disturbance pressure ($P^{outdoor}$-P^{indoor}) [Pa]	Simulation time [h]	Disturbance pressure ($P^{outdoor}$-P^{indoor}) [Pa]	Simulation time [d]
1	4.00E-04	-2	30	-2	60
2	4.00E-04	-2	30	2	60
3	4.00E-04	-2	30	5	60
4	4.00E-04	-2	30	10	60

*Chemical-specific properties of sulfur hexafluoride (SF_6) were used in simulations

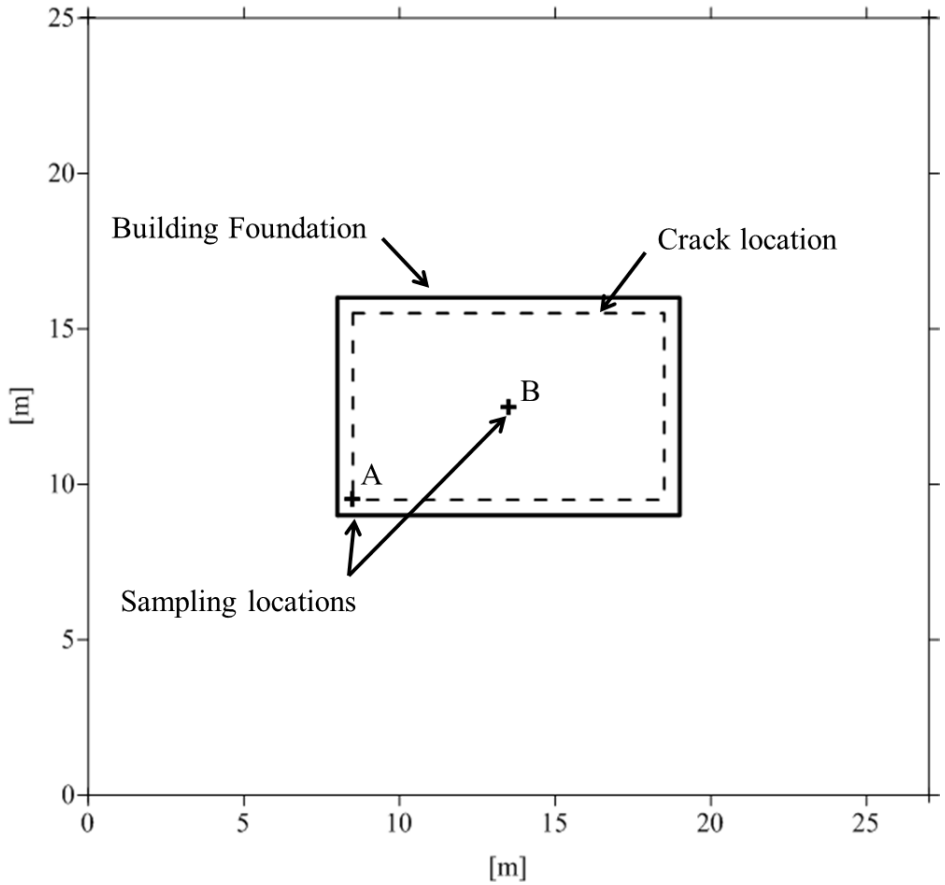

Figure 4.38. Plan view schematic of model domain, including sampling locations.

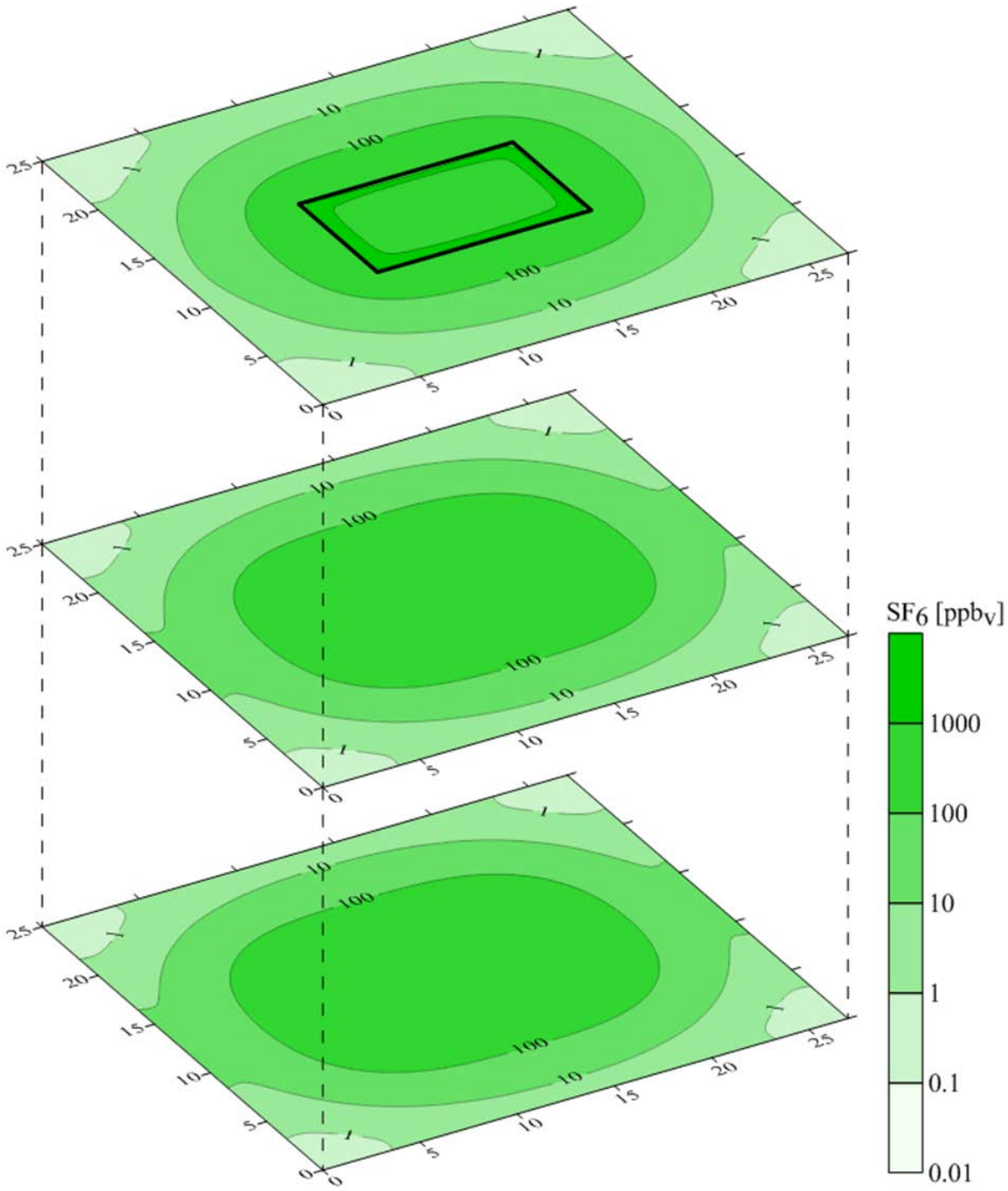

Figure 4.39. Contour plots of simulated SF_6 soil gas concentrations at depths of sub-slab (SS), 1 m BS, and 1.8 m BS following 30 d of indoor source release with a -2 Pa over-pressurization condition.

Figures 4.40 and 4.41 show similar outcomes following indoor source removal. For both simulations, indoor air concentrations decrease by over two orders-of-magnitude within 12 h of indoor source removal. Soil gas concentrations decrease faster for under-pressurization simulation 4 (Figure 4.41); however, in both cases, sub-slab concentrations take over 120 h to drop an order-of-magnitude and 1 m BS concentrations take over 5 d to drop an order-of-magnitude at location A. The soil gas results at location B are also similar for both simulations, but differ from those of location A with nearly uniform concentrations at each depth. The results at location B increase slowly for over 5 d before steadily decreasing.

The simulation results for location A are most similar to the removal test results from the field studies. For example, prior to removal of the indoor source, SF_6 concentrations in indoor air and soil gas at location A were within a factor of two. After removal of the indoor source, sub-slab soil gas concentrations decreased to levels below those of 1 m BS. The results from location B are quite different than the results from the field studies, but still indicate that indoor source-created soil gas plumes can remain in the subsurface for extensive periods after indoor source removal. The difference between location A and B is related to their proximity to the crack; thus location B sees significantly less advective flow than location A.

4.3.4 **Implications of indoor sources and their removal for VI pathway assessment**

The study results presented above demonstrate that indoor sources can cause subsurface vapor clouds and that the spatial extent and mass in those clouds can vary temporally. The results also show that subsurface vapor clouds from indoor sources can impact soil gas below sub-slab sampling points.

The field and modeling results covering indoor source removal demonstrate that the recommended 24-72 h waiting period after removal is inadequate. Under both field and modeling studies, concentrations of SF_6 in indoor air fell over two orders-of-magnitude within 72 h, but SF_6 persisted in sub-slab and deeper soil gas during the same period. These results suggest that the waiting period for indoor air sampling after indoor source removal could be 72 h or greater; however, significantly longer waiting periods are likely necessary for soil gas.

The field and modeling studies discussed here cover a simple scenario where only an indoor source is present. The addition of subsurface sources of the same chemical, a scenario not uncommon for VI site investigations, could make data interpretation even more difficult. Going forward, practitioners should consider waiting periods longer than 3 days before sampling is performed. When indoor sources cannot be removed or can only be removed for a limited time, practitioners should consider alternate investigation strategies, such as use of controlled pressure method testing (discussed below) to help distinguish contributions to indoor air from indoor and subsurface sources.

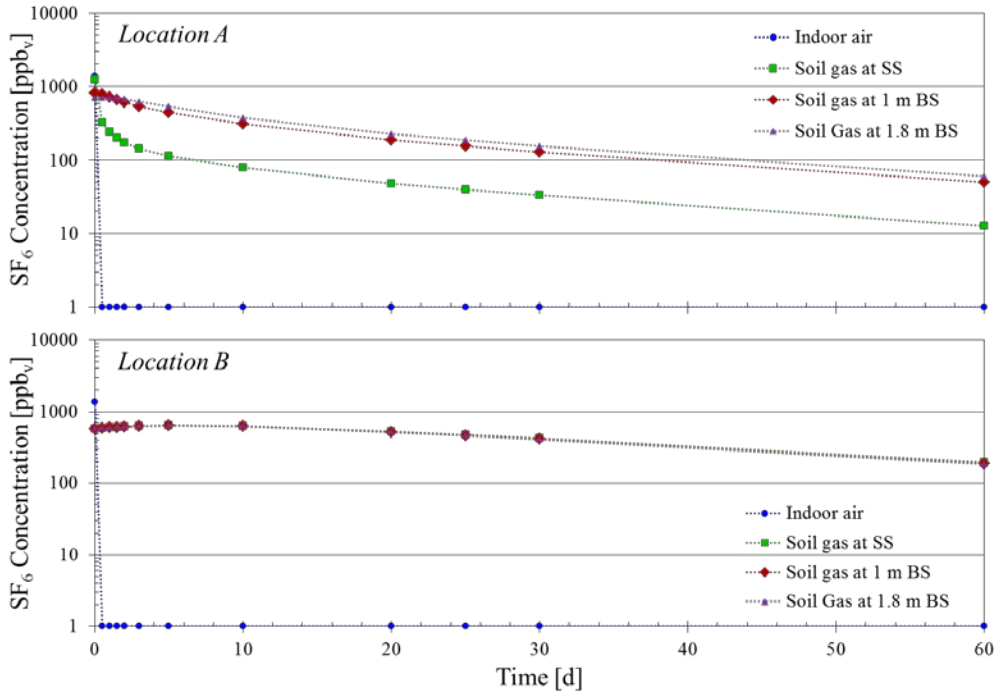

Figure 4.40. Simulation 1 (over-pressurization following indoor source release stop) results showing SF_6 concentrations in indoor air and soil gas at sub-slab (SS) and 1 m BS depths at locations A and B following indoor source removal.

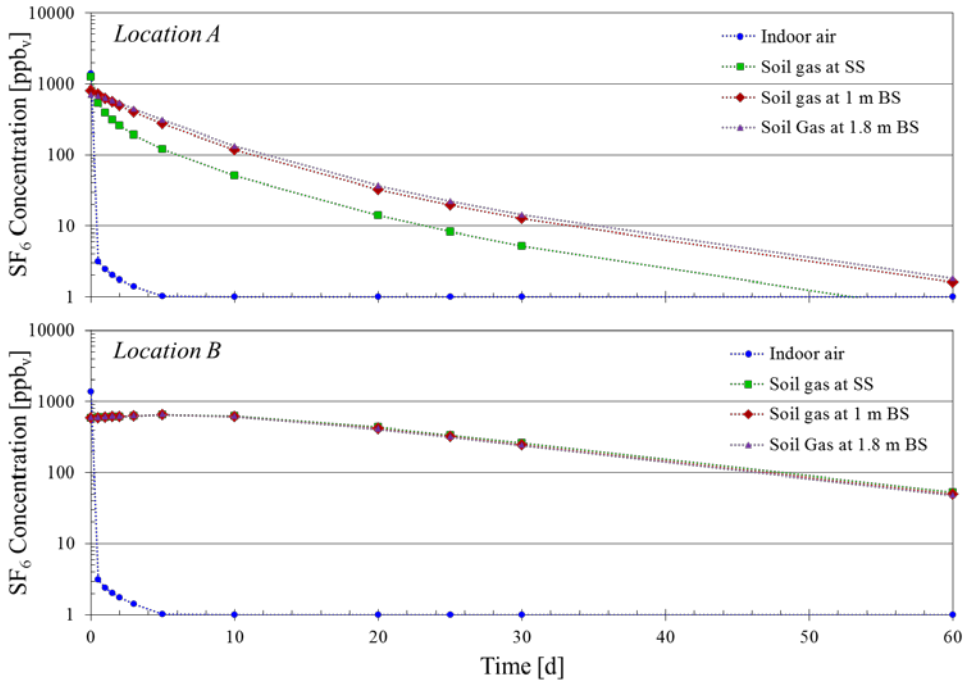

Figure 4.41. Simulation 4 (under-pressurization following indoor source release stop) results showing SF_6 concentrations in indoor air and soil gas at sub-slab (SS) and 1 m BS depths at locations A and B following indoor source removal.

4.4 LONG-TERM EVALUATION OF THE CONTROLLED PRESSURE METHOD FOR ASSESSMENT OF THE VAPOR INTRUSION PATHWAY

The objective of the long-term evaluation of the controlled pressure method (CPM) was a) to gain an understanding of the transient behavior of CHC and radon indoor air concentrations and emission rates under CPM test conditions and b) to evaluate whether CPM results can be used to confidently assess chronic (multi-year) and acute (multi-week) exposures.

4.4.1 CPM Test Data and Emissions

For the time period 780 d < t < 1045 d emphasized below, the mean 24-h average differential pressure was 11 ± 4 Pa for the outdoor to indoor air measurement and 5.2 ± 0.8 Pa for the sub-slab to indoor air measurement at location 5 (Figure 3.2) are shown in Figure 4.42. Both indicate advective soil gas flow into the building. Location 5 results are representative of other indoor living space sub-slab monitoring locations. The range in values across each 24-h period was on average 4.4 Pa for the indoor-outdoor measurement and 1.3 Pa for the sub-slab to indoor air measurement, using the 10th and 90th percentile values of the data from each 24-h period to define the range. The greater daily variation in differential pressures between outdoor and indoor air reflects occasional wind effects on the open-ended tubing running outdoor from one port of the differential pressure sensor; it was noted that the largest differentials correlate with increased wind speed.

Figure 4.43 presents CPM test TCE and radon indoor concentrations and building flow rates Q_B calculated using the known tracer gas release rate (Q_{tracer}) and concentration ($C_{tracer,\ released}$), and the resulting measured indoor air tracer gas concentration ($C_{tracer,\ indoor}$), where $Q_B = Q_{tracer} \times C_{tracer,\ released}/C_{tracer,\ indoor}$). Daily average values are plotted with error bars spanning the maximum and minimum real-time values in each day. For 780 < t < 1045 d, the mean 24-h average values are 9.3 ± 1.8 μg/m^3 for TCE, 5.0 ± 1.1 pCi/L for radon, and 15 ± 3 m^3/min for Q_B. The latter was relatively stable, with an average daily variability of 28% and an average value that was about 66% of the blower manufacturer's flow rate specification.

Real-time emission rates (E) were calculated using the building flow rate and indoor air concentrations, with $E = Q_B \times C_{indoor}$. Because the TCE, radon, and SF_6 samples are not collected at exactly the same time or frequency, the SF_6 sample closest in time to each TCE and radon concentration was used, provided it was within 0.5 d. The real-time emission results were then processed to produce the 24-h average values presented in Figure 4.44. As in Figure 4.43, error bars span the daily maximum and minimum real-time values. The emission rate is not a metric currently used in VI pathway assessment; however, comparison of emission rates under CPM and natural conditions is of interest in assessing how CPM tests alter VI behavior.

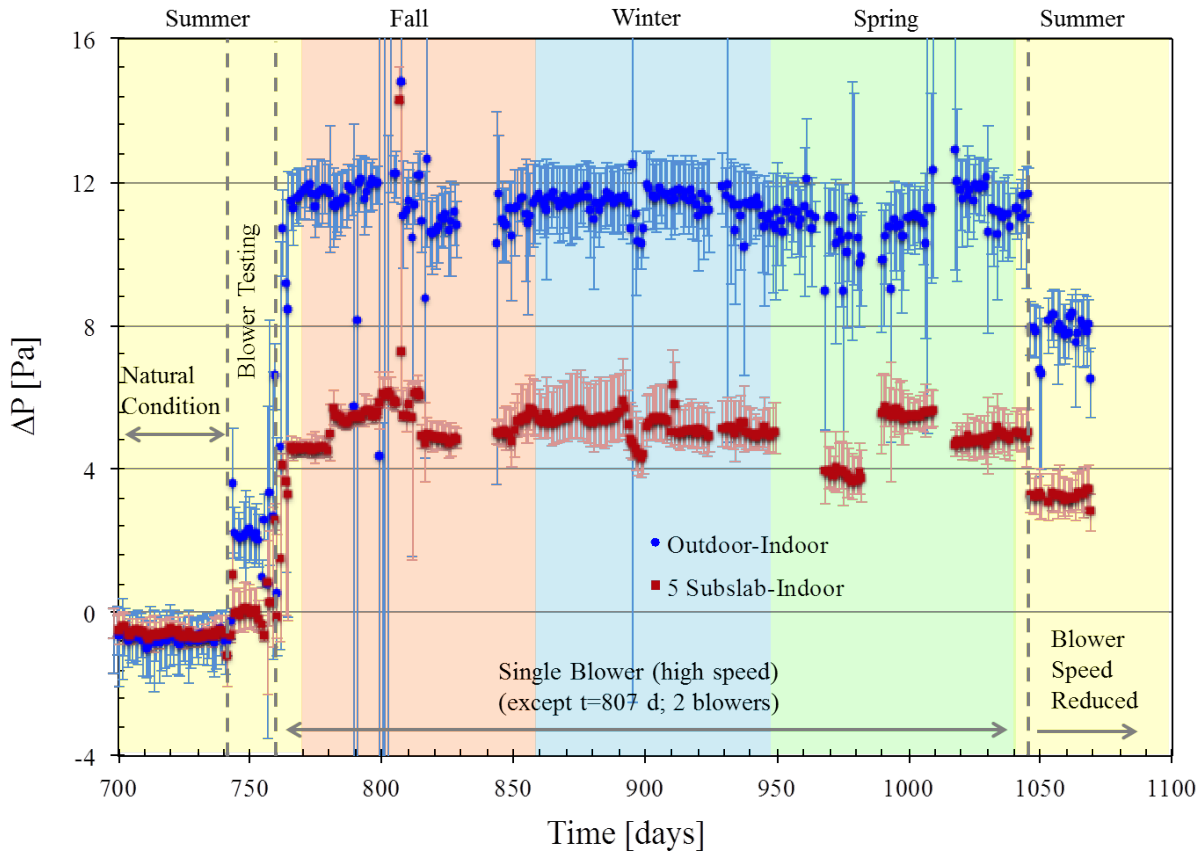

Figure 4.42. 24-h average differential pressure values between indoor air and outdoor air, and indoor air and sub-slab soil gas at location 5 (see Figure 3.2), with error bars spanning the 90th and 10th percentile of the daily data sets.

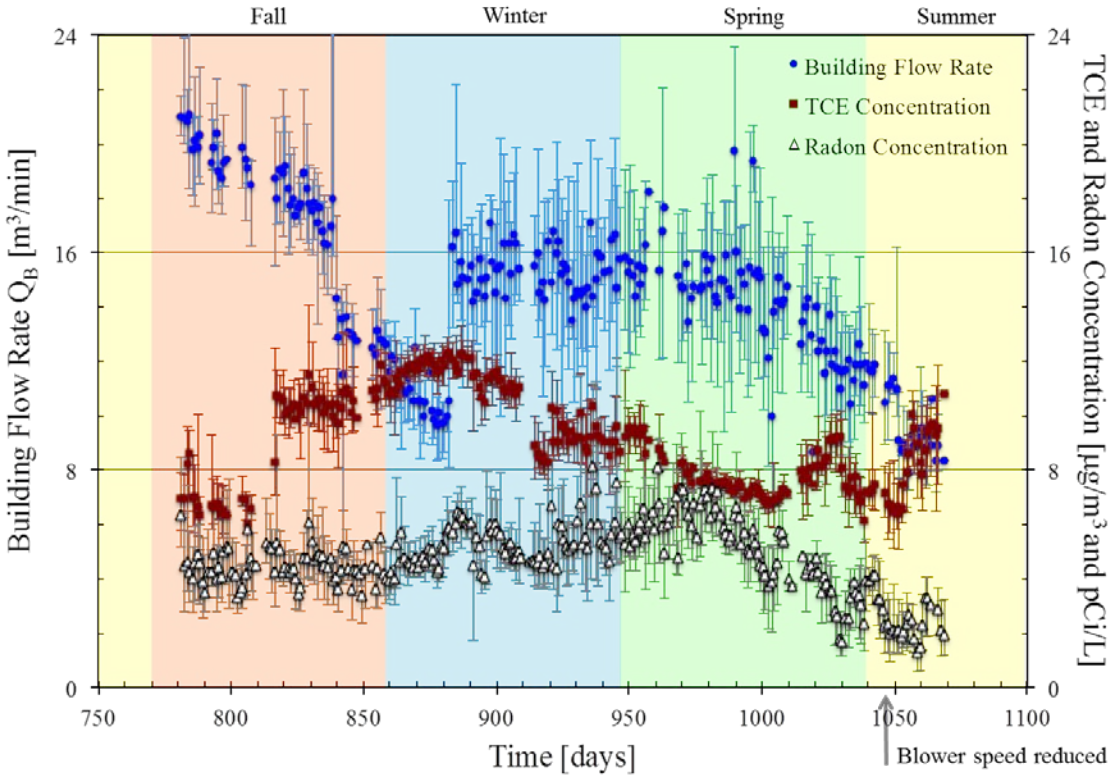

Figure 4.43. Daily average indoor air TCE and radon concentrations and building flow rate values with error bars spanning the maximum and minimum real-time values for each day during CPM testing; reproduced from Holton et al. (2015).

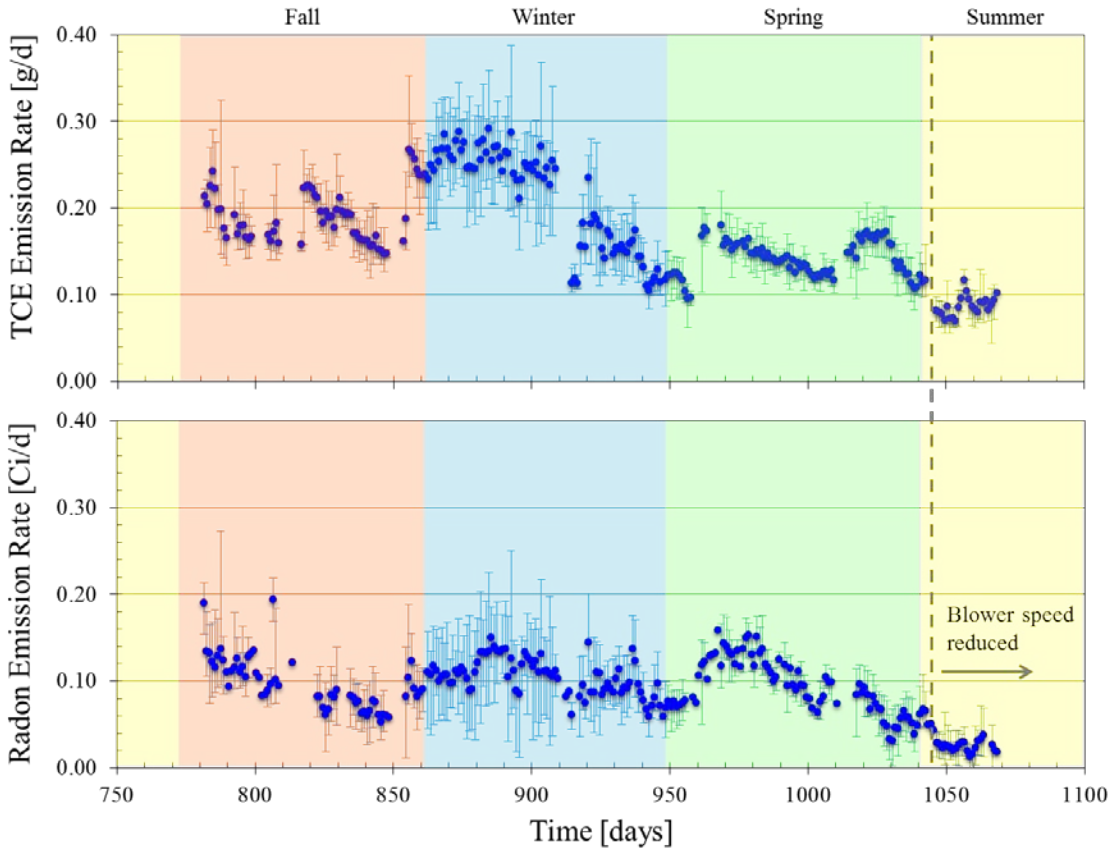

Figure 4.44. Daily average emission rates of TCE and radon with error bars spanning the maximum and minimum real-time values during CPM testing; reproduced from Holton et al. (2015).

4.4.2 **Time Dependence of CPM Test Results**

As discussed above, there is interest in determining if CPM results are temporally variable day-to-day or season-to-season. Tables 4.4 and 4.5 summarize characteristics of the concentrations and emission rate data, respectively, for the 780 < t < 1045 d period spanning Fall, Winter, and Spring seasons and the beginning of Summer. In these analyses and in Figures 4.39–4.41, seasons start September 22nd (Fall), December 21st (Winter), March 20th (Spring), and June 21st (Summer). Tables 4.4 and 4.5 include quantities of interest for both the real-time and processed 24-h average data sets because practitioners might consider CPM test durations from 2-24 h, and there is interest in assessing whether or not there are significant differences between instantaneous and time-weighted sampling results.

Overall, the results indicate that the TCE and radon concentrations and emission rates were relatively consistent with time, both across the 265 d duration of the single-blower/high-speed test and within individual 24-h periods, especially in comparison to the multiple orders of magnitude temporal variability reported by Holton et al. (2013) for the test home under natural

conditions. For example, with respect to indoor concentrations: a) the maximum 24-h average TCE concentration (12 μg/m^3) is only 2X greater than the minimum value (6.0 μg/m^3), and both are within about ±30% of the mean value (9.3 μg/m^3), b) the maximum (14 μg/m^3) real-time TCE concentration is about 3X the minimum real-time value (5.1 μg/m^3) and both are within about 50% of the mean real-time emission rate, and c) 80% of all real-time and 24-h average TCE concentrations are within about ±50% of their respective mean values. Similar results are observed for radon in that 80% of all real-time and 24-h average concentrations are within about ±30% of their respective mean values, but there is a larger spread between maximum and minimum concentrations (about 5X for the 24-h average values and about 10X for the real-time data).

As the results in Table 4.4 show, emission rates were also relatively consistent with time. The maximum 24-h average TCE emission rate is only about 3X greater than the minimum value and both are within about ±50% of the mean value, the maximum real-time TCE emission rate is about 6X the minimum real-time value, and 80% of all real-time and 24-h average TCE concentrations are within about ±50% of their respective mean values.

The significance of temporal variations within 24-h periods was assessed by looking at the ratios of maximum/minimum real-time values and (maximum – minimum)/24-h average values for each day. The former averages 1.2 and 1.7 for TCE and radon concentrations and 1.4 and 1.8 for TCE and radon emission rates, respectively. The latter averages 18% and 48% for TCE and radon concentrations and 32% and 55% for TCE and radon emission rates, respectively. This shows strong consistency in CPM results across 24-h time periods, with most daily variations between minimum and maximum values being less than about 2X.

The observation that CPM test results were similar from day-to-day and season-to-season over 265 d is significant. To the extent that these results are representative of other houses, the implication is that CPM tests only need to be conducted once per building and that selection of the test date (e.g. heating vs. cooling season) is not critical.

4.4.3 Extent to Which CPM Tests Can Be Used to Anticipate VI Impacts Under Natural Conditions

Having established that CPM results at the test house are relatively insensitive to date and time of testing, we next assess the extent to which CPM tests can be used to anticipate VI impacts under natural conditions. To do so, the 128 < t < 730 d TCE thermal desorption concentration data and SF_6 results presented in Holton et al. (2013) as well as unpublished radon data collected in that time period were used to calculate TCE and radon emissions under natural conditions (Figure 4.45). Relevant statistical characteristics of concentrations and emission rates under both natural and CPM conditions are summarized in Tables 4.4 and 4.5.

Table 4.4. Characteristics of indoor air concentration data sets under natural and controlled pressure method (CPM) conditions; reproduced from Holton et al. (2015).

Condition	Concentrations							
	TCE [µg/m^3]				Radon [pCi/L]			
	Natural Conditions* (128 to 730 d)		CPM [single blower/high speed] (780 to 1045 d)		Natural Conditions (170 to 673 d)		CPM [single blower/high speed] (780 to 1045 d)	
	Using Real-Time Data	Using Daily Avg'd Data	Using Real-Time Data	Using Daily Avg'd Data	Using Real-Time Data	Using Daily Avg'd Data	Using Real-Time Data	Using Daily Avg'd Data
Mean	0.36	0.35	9.3	9.3	0.44	0.45	5.1	5.0
Standard Deviation	2.0	1.0	1.8	1.8	0.28	0.20	1.3	1.1
Median	0.056	0.068	9.3	9.1	0.38	0.39	5.0	4.8
Maximum	57	13	14	12	4.9	1.9	12	8.2
Minimum	<0.04	<0.04	5.1	6.0	<0.25	<0.25	1.1	1.7
90th Percentile	0.77	0.81	12	12	0.70	0.68	6.7	6.3
10th Percentile	0.016	0.018	7.0	6.9	<0.25	0.28	3.6	3.7

Analysis of Real-Time Concentrations Within Each Day	TCE [µg/m^3]				Radon [pCi/L]			
	CPM [single blower/high speed] (780 to 1045 d)				CPM [single blower/high speed] (780 to 1045 d)			
	Mean	Median	Max	90th %	Mean	Median	Max	90th %
Max/Min Value for a Given Day Across All Sampling Days	1.2	1.2	1.8	1.0	1.7	1.6	3.6	2.2
(Max-Min)/Mean Value for a Given Day Across All Sampling Days	0.18	0.16	0.67	0.31	0.48	0.43	1.3	0.80

* using only thermal desorption tube data

Table 4.5. Characteristics of emission rate data sets under natural and controlled pressure method (CPM) conditions; reproduced from Holton et al. (2015).

Condition	Emission Rates							
	TCE [g/d]				Radon [mCi/d]			
	Natural Conditions* (128 to 730 d)		CPM [single blower/high speed] (780 to 1045 d)		Natural Conditions (170 to 673 d)		CPM [single blower/high speed] (780 to 1045 d)	
	Using Real-Time Data	*Using Daily Avg'd Data*	Using Real-Time Data	*Using Daily Avg'd Data*	*Using Real-Time Data*	*Using Daily Avg'd Data*	*Using Real-Time Data*	*Using Daily Avg'd Data*
Mean	$2.8x10^{-3}$	$2.6x10^{-3}$	0.18	0.18	$2.2x10^{-3}$	$2.2x10^{-3}$	0.10	0.099
Standard Deviation	$1.4x10^{-2}$	$6.9x10^{-3}$	0.05	0.05	$1.8x10^{-3}$	$2.4x10^{-3}$	0.032	0.028
Median	$3.6x10^{-4}$	$3.9x10^{-4}$	0.17	0.17	$1.8x10^{-3}$	$1.6x10^{-3}$	0.099	0.098
Maximum	$3.2x10^{-1}$	$6.2x10^{-2}$	0.39	0.29	$4.1x10^{-2}$	$1.3x10^{-2}$	0.26	0.19
Minimum	$<10^{-4}$	$<10^{-4}$	0.06	0.09	$<10^{-3}$	$<10^{-3}$	0.019	0.031
90^{th} Percentile	$6.6x10^{-3}$	$6.5x10^{-3}$	0.26	0.26	$4.2x10^{-3}$	$4.1x10^{-3}$	0.14	0.13
10^{th} Percentile	$<10^{-4}$	$<10^{-4}$	0.12	0.12	$<10^{-3}$	$<10^{-3}$	0.063	0.062

Analysis of Real-Time Emission Rates Within Each Day	TCE [g/d]				Radon [mCi/d]			
	CPM [single blower/high speed] (780 to 1045 d)				CPM [single blower/high speed] (780 to 1045 d)			
	Mean	Median	Max	90^{th} %	Mean	Median	Max	90^{th} %
Max/Min Value for a Given Day Across All Sampling Days	1.4	1.4	2.2	1.7	1.8	1.7	4.5	2.4
(Max-Min)/Mean Value for a Given Day Across All Sampling Days	0.32	0.32	0.94	0.52	0.55	0.50	1.5	0.88

* using only thermal desorption tube data

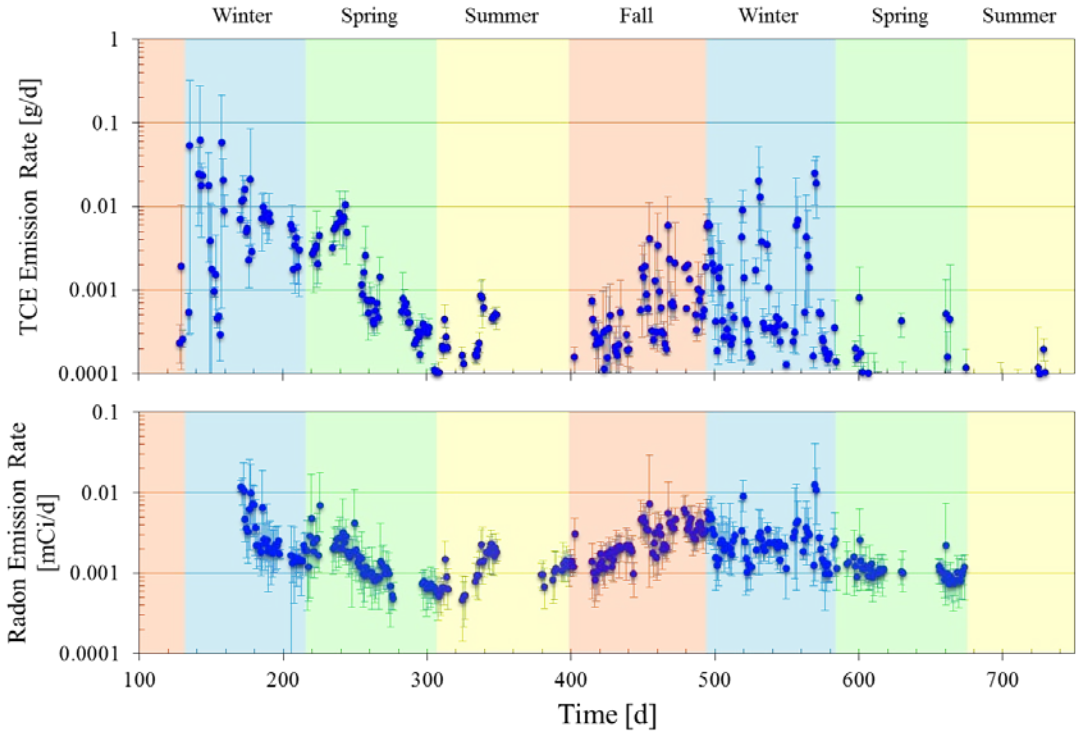

Figure 4.45. Daily average emission rates of TCE and radon with error bars spanning the maximum and minimum real-time values during natural conditions; reproduced from Holton et al. (2015).

Three key conclusions with significance to VI pathway assessment can be drawn from a comparison of the results from natural and CPM conditions. The first key conclusion from review of Tables 4.4 and 4.5 and Figures 4.44 and 4.45 is that CPM test results are comparable to or show higher emission rates and concentrations than worst-case results obtained under natural conditions. For example, the mean 24-h average CPM TCE concentration is similar to the maximum 24-h average TCE concentration under natural conditions (9.3 vs. 13 $\mu g/m^3$, respectively). The same holds true for radon concentrations (5 vs. 1.9 pCi/L) and TCE emissions (0.18 vs. 0.062 g/d). The mean 24-h average radon emission rate under CPM conditions, 0.099 mCi/d, is about an order of magnitude greater than the 0.013 mCi/d maximum 24-h average emission rate under natural conditions. The difference in behavior of TCE and radon under CPM and natural conditions observed here is possibly due to different transport pathways to indoor air, which is an ongoing focus of our study.

The second key conclusion is that CPM testing did not result in false-negative outcomes, unlike sampling under natural conditions at this house. For example, 44% of the 24-h average indoor TCE concentrations reported by Holton et al. (2013) were less than the MDL. Holton et al. (2013) used these data and examined the outcomes of two different multi-sample and multi-

season indoor air sampling schemes combined with a range of decision-making rubrics and showed that the probability of false-negative conclusions regarding vapor intrusion occurrence at the study house ranged from about 10% to 100%. In contrast, 100% of CPM testing results indicate vapor intrusion occurrence with the minimum concentration and emission rate detected being within 50% of their respective long-term mean values. Additional work is needed to determine if there is potential for false-positives at homes that overlie contamination but would not have VI impacts under natural conditions.

The third key conclusion is that CPM concentrations and emissions exceed long-term mean concentrations and emissions under natural conditions by at least an order of magnitude; therefore, CPM results over-estimate the long-term average exposure from vapor intrusion at the study house. For example, the mean 24-h average TCE CPM concentration (9.3 $\mu g/m^3$) is about 27X greater than the long-term mean 24-h average value under natural conditions (0.35 $\mu g/m^3$), the mean 24-h average radon CPM concentration (5.0 pCi/L) is about 11X greater than the long-term mean 24-h average value (0.45 pCi/L), and the mean 24-h average TCE CPM emission rate (0.18 g/d) is about 69X greater than the long-term mean 24-h average value under natural conditions (0.0026 g/d). The tendency of CPM toward over-prediction is not unexpected as the house is being artificially held in a state of constant under-pressurization while the pressure differential fluctuates in both intensity and direction under natural conditions including states of over-pressurization.

There is no known correlation between the maximum indoor concentration and the long-term average concentration. That relationship is likely building-specific and dependent on a number of factors that are not fully understood. However, the key conclusions from this study and from others (McHugh et al., 2012; Beckley et al., 2014) suggest that CPM testing could be used to conduct quick conservative screening for VI potential with a yes/no result. Buildings where the maximum concentrations of target analytes fall below screening levels could reasonably be considered to not require further investigation unless conditions significantly change. Buildings where the maximum concentrations of target analytes are above the screening levels may require additional monitoring (e.g. indoor air, differential pressure) to fully assess the long-term risk. In some cases, these buildings may be good candidates for preemptive mitigation knowing that VI is a potential concern.

4.4.4 **Need for Tracer Gas Use in CPM Testing**

There are costs associated with this CPM test component and many practitioners do not have the experience or equipment to conduct this aspect of a CPM test. Thus, future work should address the question “Are tracers necessary to attain results sufficient for risk management?" CPM testing increases the driving force for VI (building under-pressurization) and building air exchange rate relative to long-term averages under natural conditions. The former can lead to increased VI impact, while the latter leads to increased indoor air dilution and lower VI impact. Controlled tracer gas release and monitoring can be used to assess the increase in building air exchange rate under CPM conditions vs. natural conditions and it can also be used to convert indoor air concentrations to emission rates as performed above in this work.

It is likely that some will consider converting CPM concentrations to concentrations under natural conditions through consideration of building air flowrate differences between natural and CPM conditions; for example, the following linear approximation might be used:

$$C \text{ (natural condition projection) } [\mu g/m^3] = C \text{ (CPM condition) } [\mu g/m^3] \times Q_B \text{ (CPM condition) } / Q_B \text{ (natural condition estimate or measurement)} \quad (4)$$

In this study, there was about a 4X increase in the mean 24-h average Q_B value between natural conditions, 3.6 ± 8 m^3/min (128 d < t < 730 d), and the long-term CPM test, 15 ± 3 m^3/min. This Q_B information, the mean 24-h average CPM TCE and radon concentrations, and equation (4) leads to the projected concentrations 39 $\mu g/m^3$ for TCE and 21 pCi/L for radon. Both values agree less with the maximum 24-h concentrations under natural conditions (13 $\mu g/m^3$ for TCE and 1.9 pCi/L for radon) than do the mean 24-h concentrations under CPM conditions (9.3 $\mu g/m^3$ for TCE and 5.0 pCi/L for radon). Thus it appears that there are compensating effects of increased VI emission and increased dilution at the study house. Additional comparison at other study sites is needed to reach a definitive conclusion on the value of tracer delivery and measurement.

4.4.5 **Relationship of CPM Test Results to Operating Conditions**

Reaching a consensus on CPM operating conditions and duration is important for all to have confidence in CPM tests. The sensitivity of CPM results to operating conditions was not investigated in our study. The exhaust blower speed was reduced for a brief period 1045 d < t < 1067 d, during which the 24-h average indoor-outdoor pressure differential decreased from 11 Pa to 8 Pa, Q_B decreased from 15 to 9 m^3/min, the mean 24-h average indoor TCE concentration decreased from 9.3 to 8.3 $\mu g/m^3$, the mean 24-h average TCE emission rate decreased from 0.18 to 0.09 g/d, the mean 24-h average indoor radon concentration decreased from 5.0 to 2.3 pCi/L, and the mean 24-h average radon emission rate decreased from 0.099 to 0.025 mCi/d. Other information relevant to this discussion is reported in McHugh et al. (2012). They conducted a short-term CPM test in our study house and reported 5 – 6 Pa indoor-outdoor pressure differential (about half of our study), 9.5 $\mu g/m^3$ spatial mean TCE concentration vs. the 9.3 $\mu g/m^3$ temporal mean in our study, and about 2 pCi/L radon vs. the 5.0 pCi/L in our study. Their reported Q_B value (about 5 m^3/min) was about one-third of the value in our study. Thus, for the limited range of conditions applied, CPM results were dependent on operating conditions, with indoor air impacts increasing with increased under-pressurization.

4.4.6 **Implications for CPM tests**

At this study house, the CPM results were relatively constant with time, they anticipated the maximum indoor concentrations under natural conditions, and the probability of detecting VI occurrence was significantly greater than indoor air sampling under natural conditions. CPM results exceeded long-term average conditions by one to two orders of magnitude. If representative of other buildings, then the implication for practice is that CPM testing could be used at any time of the year to conduct quick screening for worst-case VI potential with a yes/no result. Additional work is needed to determine if CPM results are dependent on operating conditions, if tracer testing is a necessary component of CPM testing, if CPM tests can result in

false-negatives under different circumstances, and if long-term average exposures can be predicted from CPM test results.

This work was conducted at a chlorinated hydrocarbon-impacted site and, while CPM testing has been applied at a petroleum hydrocarbon (PHC) site (Beckley et al., 2014), it is unknown if the conclusions above extend to PHC-impacted sites.

4.5 EVALUATION OF THE IMPACT OF GROUNDWATER TABLE FLUCTUATIONS ON CHLORINATED VOLATILE ORGANIC COMPOUNDS EMISSIONS FROM GROUNDWATER

This study focused on the impact of groundwater table elevation changes on vapor emissions from dissolved groundwater sources, which is the most commonly seen vapor intrusion scenario for chlorinated hydrocarbon (CHC)-impacted sites. The objectives of this study were to: a) identifying conditions for which temporal variations in emissions will and will not be significant, and b) identifying scenarios where fluctuating groundwater tables produce emissions that are significantly different from the base-case static water table scenario.

4.5.1 **Field observation: groundwater concentration vs. water table fluctuation**

Figure 4.46 presents the groundwater table elevation at GW3 relative to the base of the building slab vs. spatially-averaged groundwater TCE concentrations beneath the building for about four years at the study site. Error bars represent standard deviations for each sampling event. On average, the groundwater table was positioned 3.3 ± 0.1 m below the building slab. A seasonal pattern in groundwater table elevations is evident; the groundwater table elevation typically increased from late winter to spring and declined during late summer to fall, with the magnitude of changes being about 0.3 m and the difference between the minimum and maximum elevations was about 0.4 m. Groundwater concentration patterns roughly mimic groundwater elevations. Increased TCE concentrations in groundwater were commonly seen when groundwater elevation was highest; with seasonal variations of about ±50% about the average concentrations. In interpreting these data, it is important to note that that samples are collected from a fixed vertical position, so apparent changes in concentration with time might reflect a non-uniform vertical concentration profile (i.e., a concentration profile that increases in concentration with depth) instead of any real concentration changes with time in the groundwater plume.

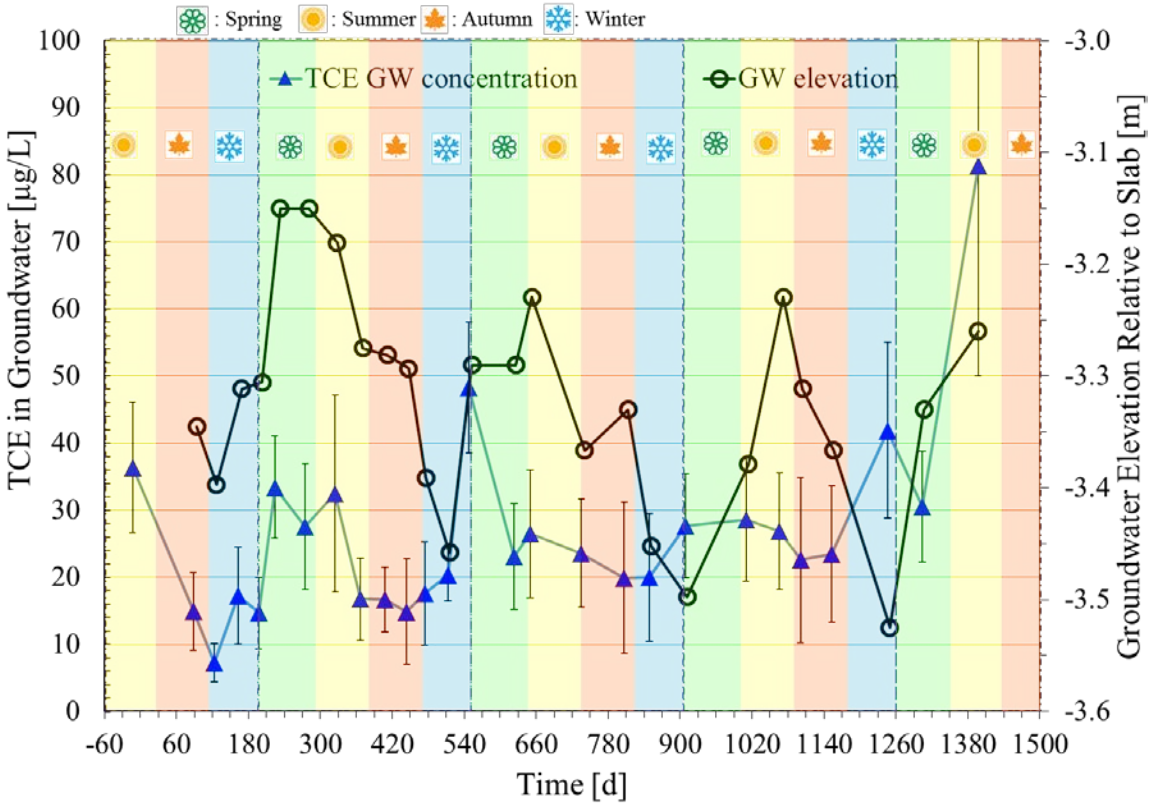

Figure 4.46. Groundwater elevation and spatially-averaged TCE groundwater concentrations. Error bars denote the maximum and minimum values for each event. Shaded color areas in background represent seasons.

4.5.2 **Field observation: soil gas concentration vs. water table fluctuation**

Figures 4.47 a-k present TCE soil gas concentrations at 0.9 m BS and 1.8 m BS and water table elevation measurements from groundwater monitoring well GW3. At locations A and B, vapor sampling was only possible at 0.9 m BS due to water saturation of the soil matrix at 1.8 m BS in those locations.

It is important to note that all soil gas sampling port elevations are referenced to the house slab and that the ground surface elevation rises from the front yard to back yard. Diffusion dominated transport theory anticipates higher soil gas concentrations for back yard sampling locations vs. front yard sampling points at similar depths.

Unlike groundwater concentrations, a correlation between soil gas TCE concentration and groundwater elevation is not visually evident. TCE concentrations at 1.8 m BS are elevated at some locations after declines in water table elevation, while others are depressed. For example, from t= 203 d to t= 447 d, 1.8 m BS TCE concentrations increased about 3X at location 1 as the

groundwater elevation dropped about 0.3 m. At location 2, on the other hand, the concentration at 1.8 m TCE decreased from 281 ppb_v to 88 ppb_v in the same period. The increase in soil gas concentrations expected with a depleting water table (McCarthy and Johnson 1993, Parker 2003, Werner and Hoehener 2002) were observed over some time periods at some locations, but that was not consistent with time at all locations. Increasing temporal and spatial variations in soil gas concentration were also found as the sampling location and depth moved closer to the building foundation and ground surface.

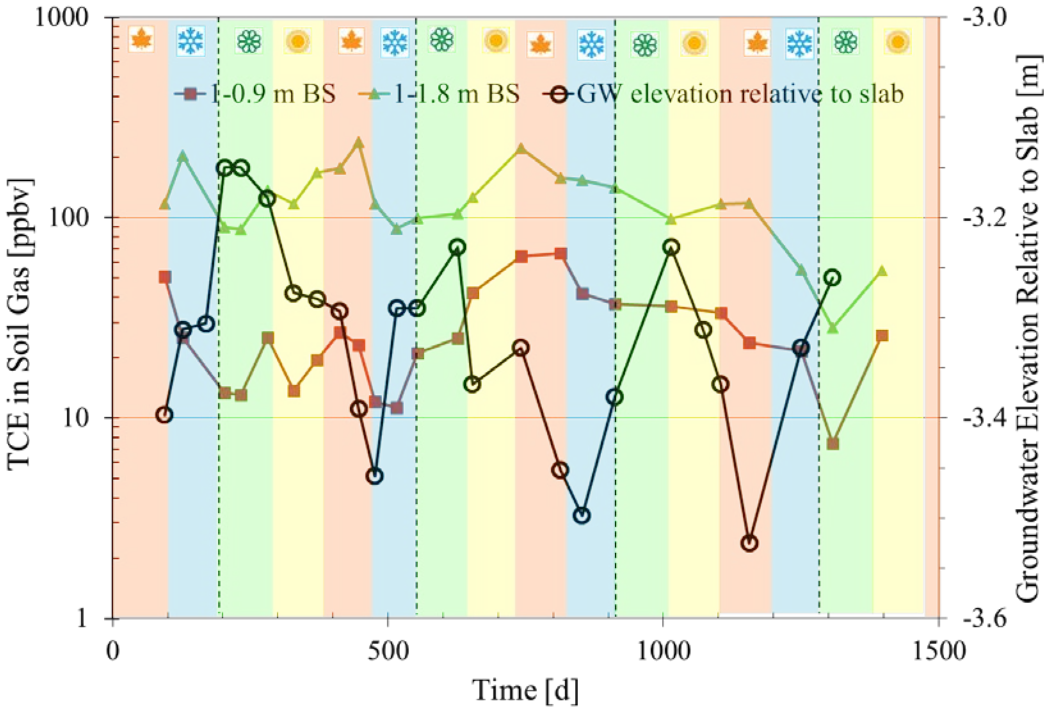

Figure 4.47 (a) TCE soil gas concentrations at location 1

: Spring : Summer : Autumn : Winter

Figure 4.47 a and b-k below. TCE soil gas concentrations at 0.9 m BS and 1.8 m BS and groundwater table elevation for interior (locations 1-6) and exterior (locations A-F) locations. Shaded background color areas indicate seasons. Conditions: 0 – 740 d, natural conditions with land drain lateral connected; 780 - 1045 d, CPM conditions with land drain lateral connected; 1071 - 1157 d, CPM conditions with land drain lateral disconnected.

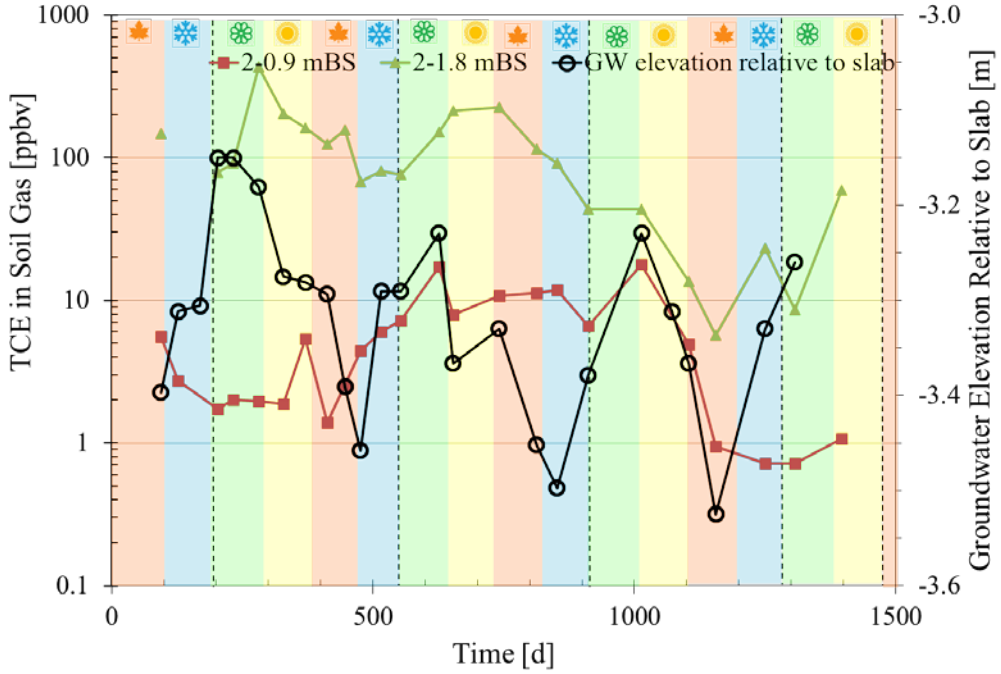

Figure 4.47 (b) TCE soil gas concentrations at location 2

: Spring : Summer : Autumn : Winter

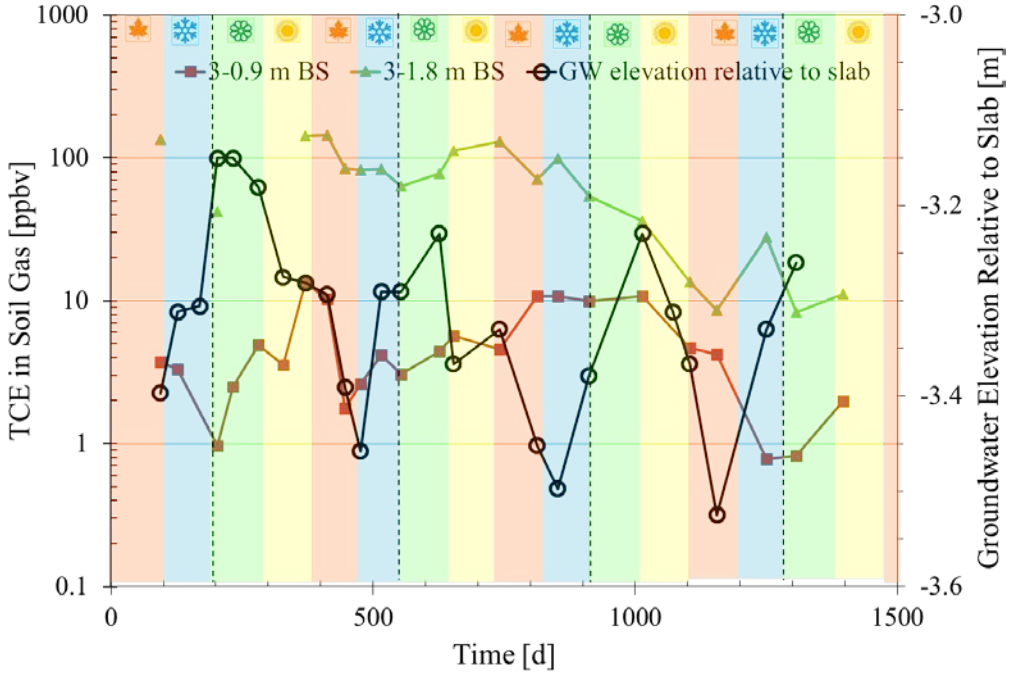

Figure 4.47 (c) TCE soil gas concentrations at location 3

: Spring : Summer : Autumn : Winter

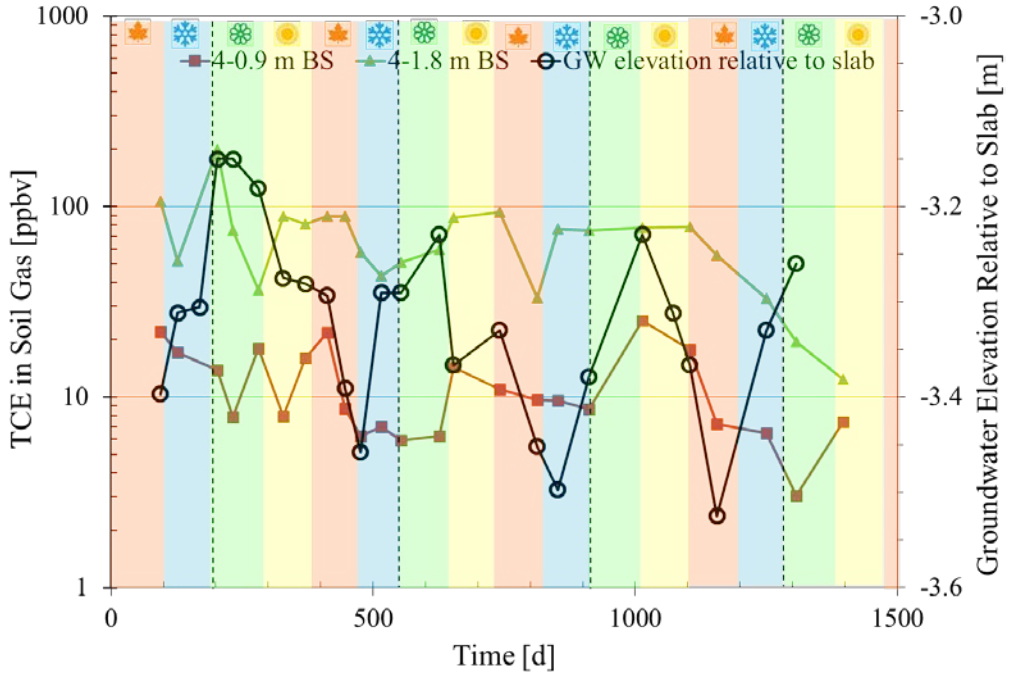

Figure 4.47 (d) TCE soil gas concentrations at location 4

: Spring : Summer : Autumn : Winter

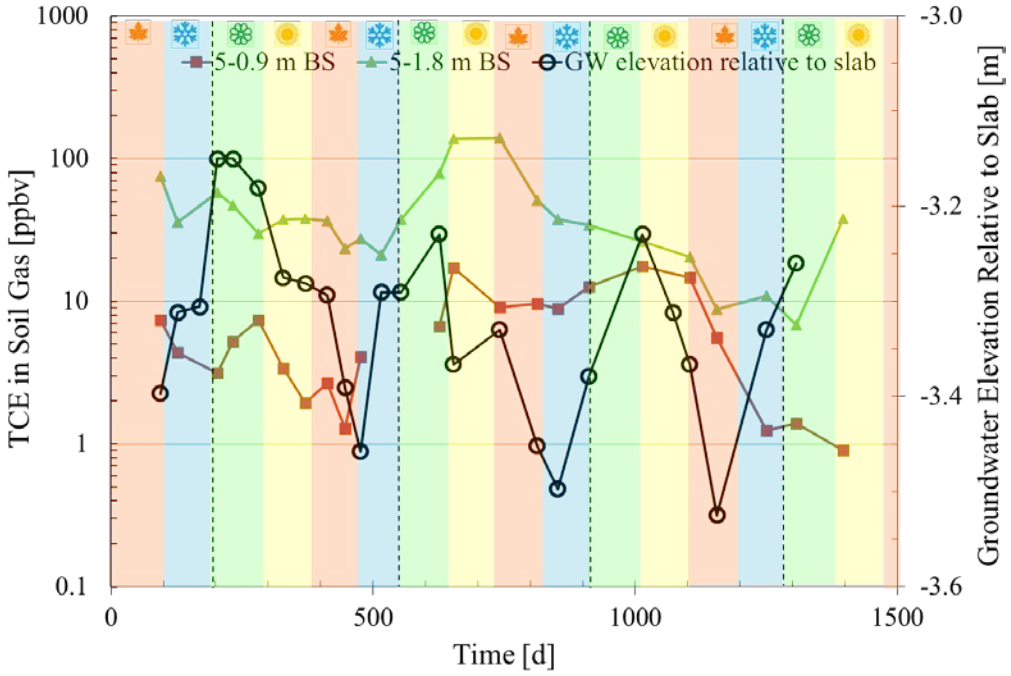

Figure 4.47 (e) TCE soil gas concentrations at location 5

: Spring : Summer : Autumn : Winter

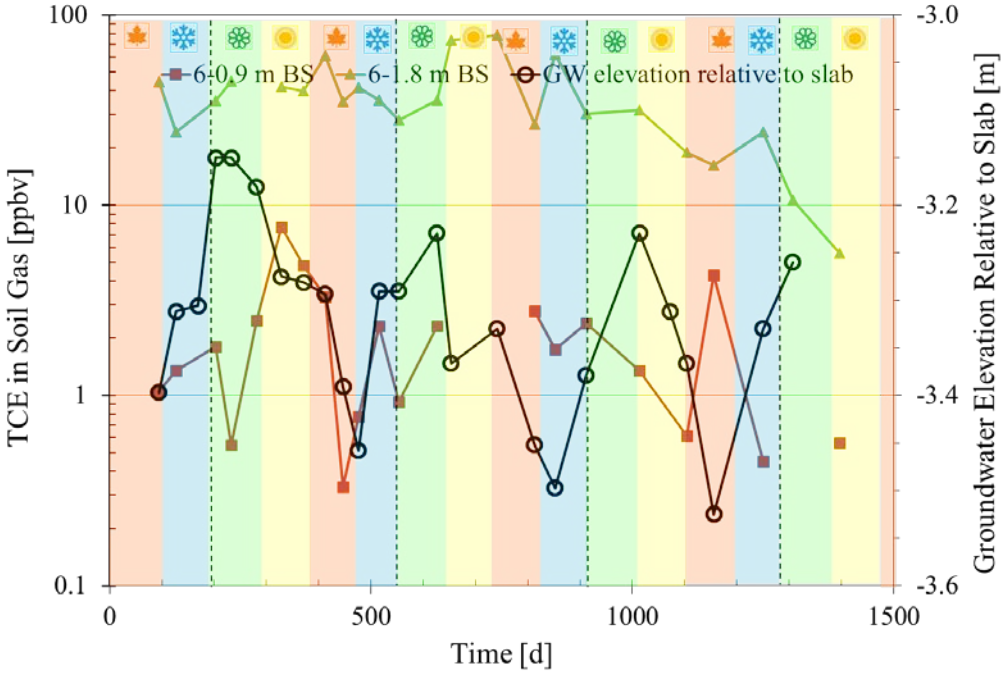

Figure 4.47 (f) TCE soil gas concentrations at location 6

: Spring : Summer : Autumn : Winter

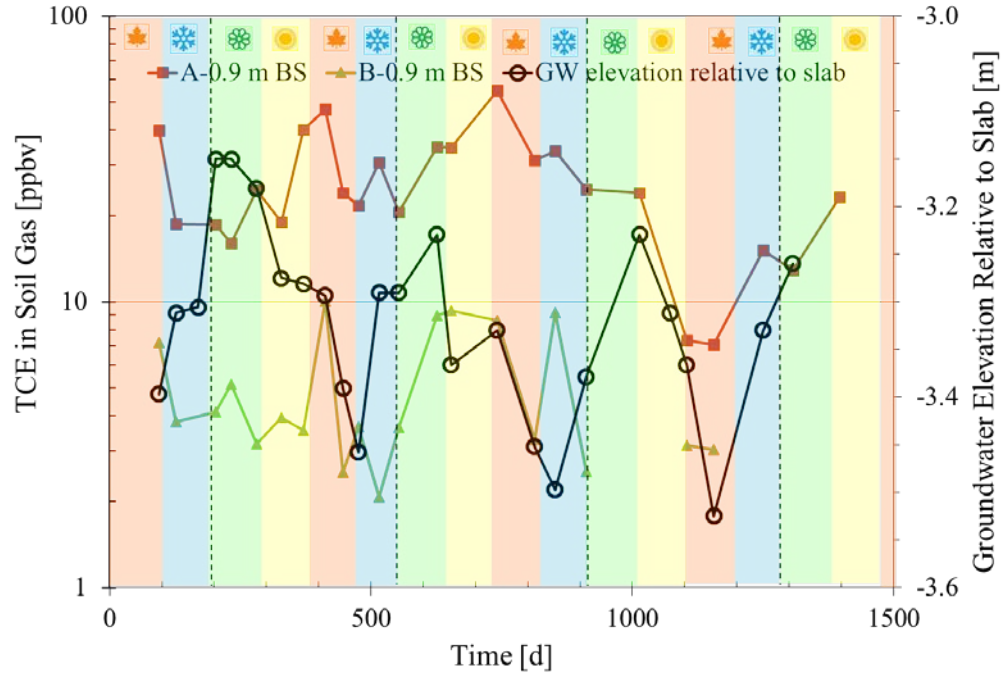

Figure 4.47 (g) TCE soil gas concentrations at location A and B

: Spring : Summer : Autumn : Winter

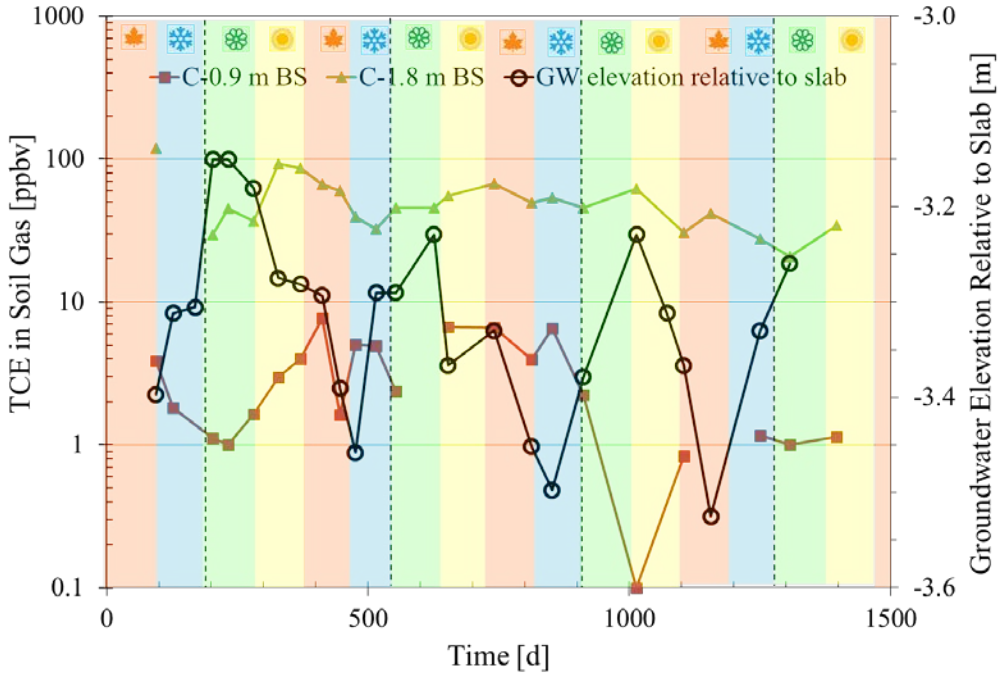

Figure 4.47 (h) TCE soil gas concentrations at location C

: Spring : Summer : Autumn : Winter

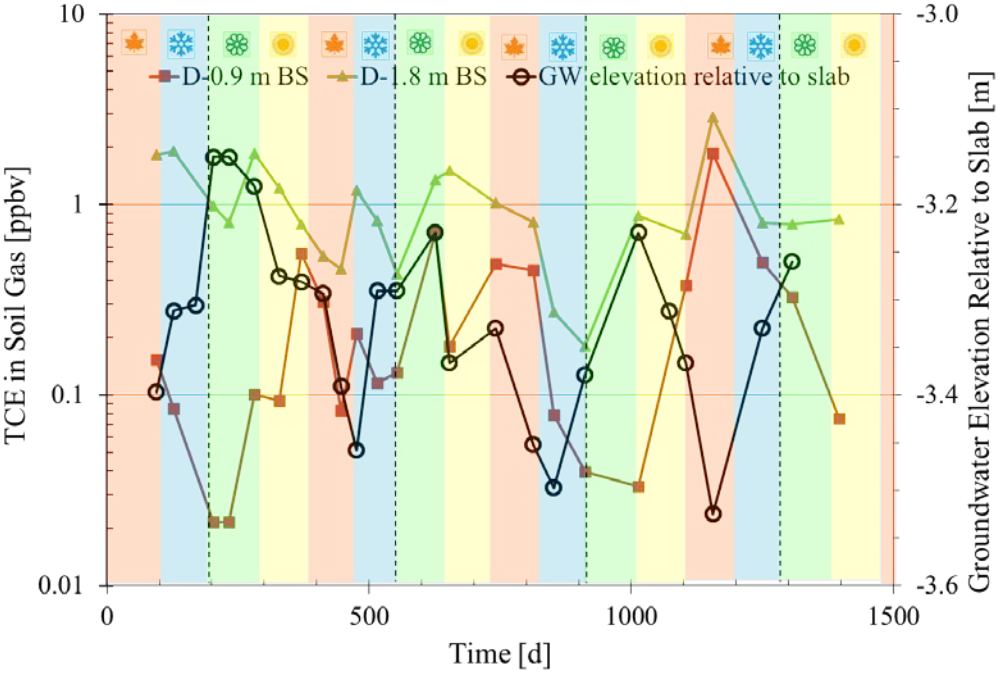

Figure 4.47 (i) TCE soil gas concentrations at location D

: Spring : Summer : Autumn : Winter

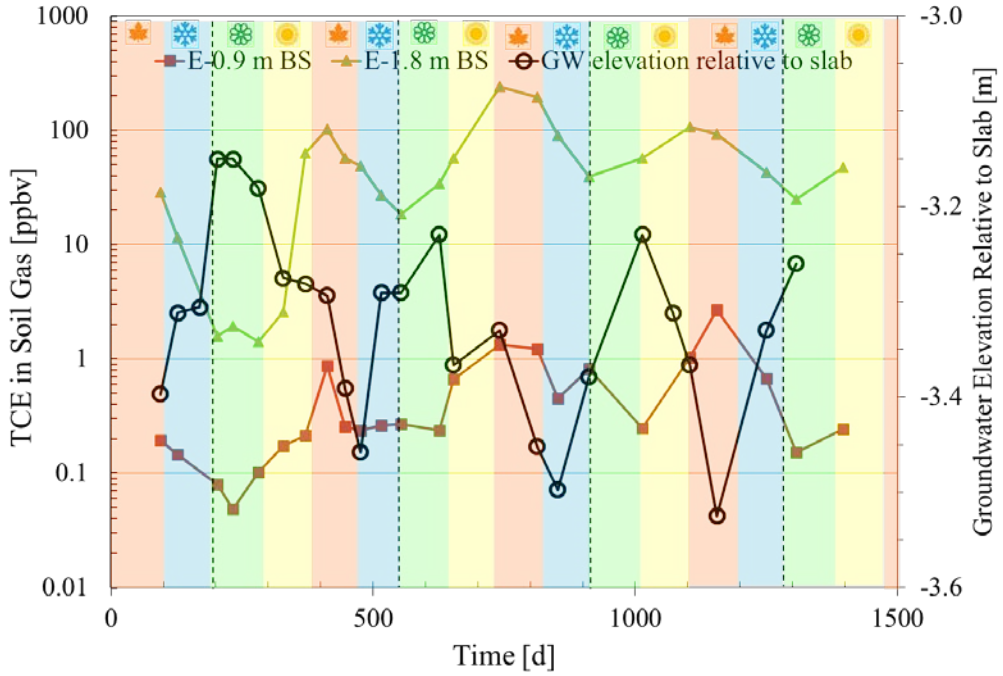

Figure 4.47 (j) TCE soil gas concentrations at location E

: Spring : Summer : Autumn : Winter

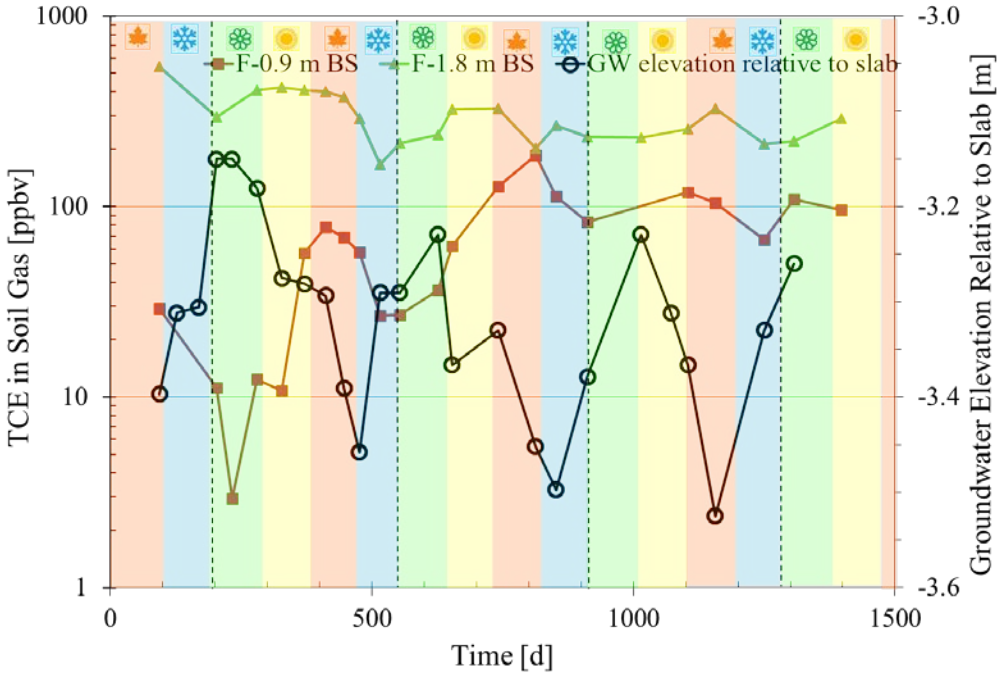

Figure 4.47 (k) TCE soil gas concentrations at location F

: Spring : Summer : Autumn : Winter

4.5.3 **Field observation: CHC emission vs. water table fluctuation**

TCE emissions from groundwater, expressed as flux rates (mass/time per unit area) were calculated using two approaches. The first approach (F_1) was based on the assumption that diffusion was the dominant vapor transport mechanism in deep soil (Johnson et al., 1991), and utilized synoptic soil gas concentrations, effective diffusion coefficients, and Fick's Law:

$$F_1 = D_i^{eff} \frac{\Delta C_{g,i}}{L_i} \tag{4-1}$$

where subscript i denotes different locations, $\Delta C_{g,i}$ is the soil gas concentration difference [M/L^3] over the vertical distance L_i [m], and D_i^{eff} [L^2/T] is the effective diffusion coefficient. D_i^{eff} values were obtained using the Johnson et al. (1998) push-pull tracer method, and results from five field surveys were averaged for use in Equation (4-1).

The uncertainty associated with this calculation is primarily due to concentration measurement errors and the compounding of those errors associated with the subtraction of two concentration values in equation (1). The average percentage difference between duplicate samples was 25.5% and D_i^{eff} and L_i were fixed values for all calculations at each sampling location i. The uncertainty in F_1 values due to concentration measurement errors is then (Harris, 2009):

$$e_i = D_i^{eff} \frac{\sqrt{\left(0.255 \times C_{g,i,0.9\ m\ BS}\right)^2 + \left(0.255 \times C_{g,i,1.8\ m\ BS}\right)^2}}{L_i} \tag{4-2}$$

The second approach (F_2) utilized indoor data collected during controlled pressure method (CPM) test conditions. As mentioned previously, from t= 1071 d to t= 1157 d, the study house was constantly under-pressurized and isolated from the land drain network. Assuming no CHC degradation during transport, then TCE emissions from groundwater are equivalent to emissions to indoor air above the groundwater, and so F_2 can be calculated:

$$F_2 = C_{indoor} \times (C^o_{tracer}/C_{tracer}) \times Q_{tracer}/A \tag{4-3}$$

where C_{indoor} is the TCE indoor air concentration [M/L^3], Q_{tracer} is SF_6 tracer release rate [L^3/T], C^o_{tracer} and C_{tracer} are release and resulting indoor SF_6 concentrations, respectively [M/L^3], and A is the building footprint area of 84.4 m^2.

Two measurements are involved in F_2 calculations. The indoor air TCE and tracer concentrations, C_{indoor} and C_{tracer}, are measured using TD GC/MS and GC/PDD respectively. These two quantities are not measured at the same time; C_{tracer} was collected approximately every 30 min and C_{indoor} was collected every 4 h and a time-averaged C_{tracer} (±4 hours about the C_{indoor} measurement) was used in Equation (4-3). Therefore, the uncertainty for C_{tracer} was estimated using the percent standard deviation ($\%S_{Ctracer}$) within that averaging time. The measurement error for TD GC/MS analyses was estimated to be <10 % based on the holding test described in section 3.2.1. The uncertainty in each F_2 value was calculated as:

$$e_{F2} = F_2\sqrt{(10\%)^2 + (\%S_{Ctracer})^2} \tag{4-4}$$

Figures 4.48 a-j present TCE emission rates per unit area calculated using the results from synoptic soil gas and groundwater table elevation sampling (method F_1), with error bars spanning the uncertainty for each calculation. Average F_1 values and the standard deviation of the average within the building footprint are shown in Figure 4.49. A statistical summary of F_1 values and uncertainties is presented in Table 4.6. The following can be concluded from a review of these figures and table:

- The temporal variation in F_1 values spans from about one to two orders-of-magnitude across all locations. For example the temporal variability is about an order of magnitude at location 1 and about two orders-of-magnitude at location 2. In reviewing the results, it is important to note that there are three different sets of operational conditions represented across the time frame presented: 0 – 740 d involved natural conditions with the land drain lateral connected; 780 - 1045 d involved CPM conditions with the land drain lateral connected; 1071 - 1157 d involved CPM conditions with land drain lateral disconnected; and after 1157 d involved natural conditions with the land drain lateral valve closed.

- The uncertainty in each F_1 value is about 40% and the standard deviation of all F_1 values at each location ranges from 34% - 131% of the average F_1 value at that location.

- The effect of closing the land drain lateral valve is evident in F_1 values vs. time for interior locations and is not evident in F_1 values vs. time for exterior locations.

- Figure 4.49 presents average interior F_1 values and their standard deviations. If this plot is divided into regions with and without the land drain lateral connection, it can be seen that any temporal variations, if they exist, are smaller than the standard deviation of the averages. Thus, at this site, changes in emission rates are at most about 50% of the time-averaged value for groundwater table elevation changes of about 0.3 m.

Figure 4.50 presents the spatial distribution of F_1 values, 1.8 m BS TCE soil gas concentrations, and TCE shallow groundwater concentrations collected under natural conditions with the land drain lateral connected for the sampling conducted $368 \text{ d} < t < 370 \text{ d}$. With the exception of one location, all F_1 emission values are within an order of magnitude and beneath the house they are within about 50% of the average value. The spatial distribution of F_1 values is similar to that of the 0.9 m BS and 1.8 m BS soil gas concentrations. While not highly spatially variable, the spatial trend in F_1 values is different than what would be expected from a relatively uniform groundwater concentration distribution and the sloped ground surface at this site; diffusion-dominated transport theory anticipates increasing emission rates with shorter distances to ground surface and the opposite is observed in this data set.

Table 4.6. Characteristics of TCE F_1 calculations under natural conditions (0<t<740 d).

	F_1 under natural pressure condition [µg/d-m^2]									
Location	1	2	3	4	5	6	C	D	E	F
Maximum	60.2	228.7	75.0	53.5	70.7	55.1	14.4	0.4	43.7	103.2
Minimum	5.8	2.5	2.4	1.4	1.8	3.6	2.5	0.03	0.2	3.5
Average	31.9	81.0	52.9	19.7	27.0	29.8	6.9	0.2	8.4	58.9
% Standard Deviation	40.3	62.4	33.9	55.6	69.1	39.1	46.1	61.1	131.9	36.1
	Uncertainty of F_1 calculation [µg/d/m^2]									
Maximum	17.1	32.4	32.1	14.7	29.2	14.1	3.8	0.2	11.2	27.9
Minimum	2.1	3.8	1.2	1.1	1.0	1.01	0.7	0.01	0.1	8.6
Average	10.0	18.7	14.2	6.0	7.6	8.0	1.9	0.06	2.2	17.7

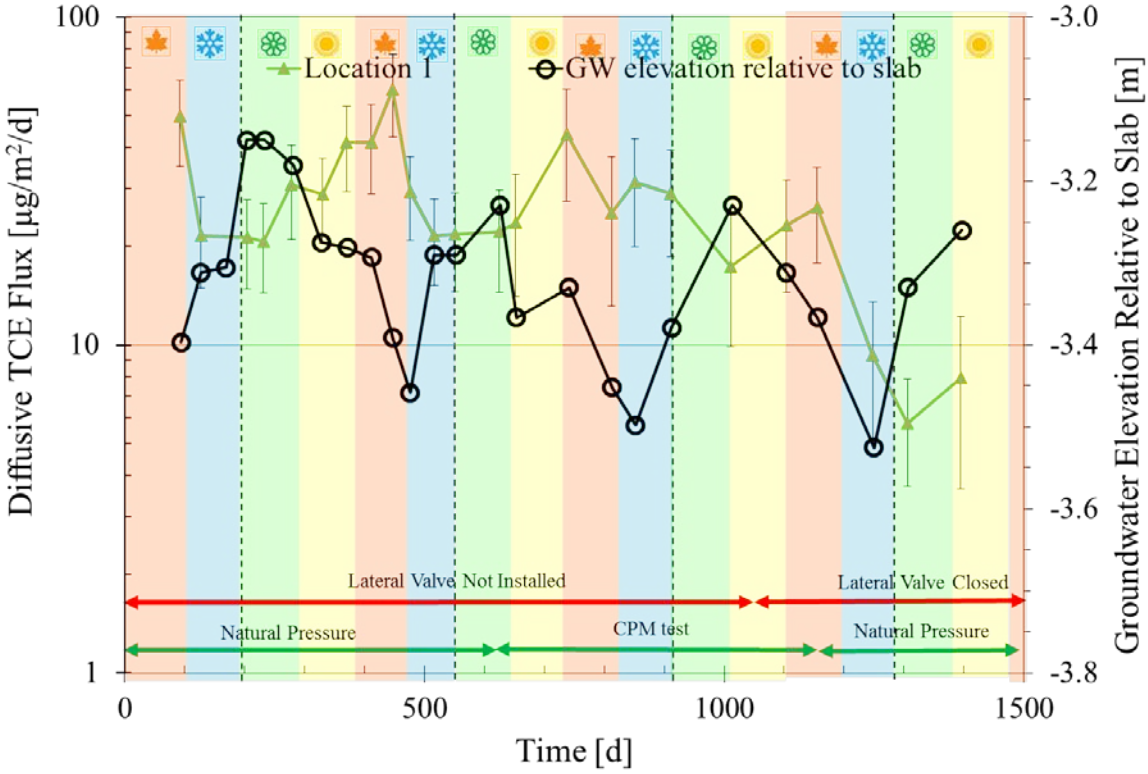

Figure 4.48 (a) TCE emissions per unit area at location1

: Spring : Summer : Autumn : Winter

Figures 4.48 a and b-j below. Calculated diffusive TCE flux F_1 values (emissions per unit area) using synoptic soil gas survey data. Error bars span the uncertainty in each F_1 value calculation associated with uncertainty in concentration measurements.

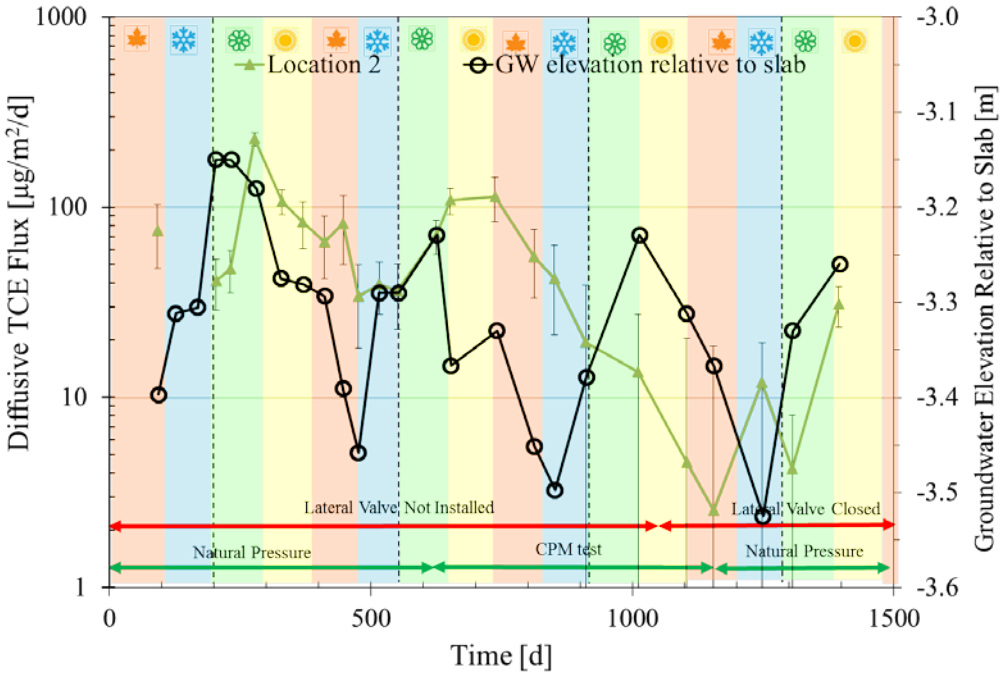

Figure 4.48 (b) TCE emissions per unit area at location 2

: Spring : Summer : Autumn : Winter

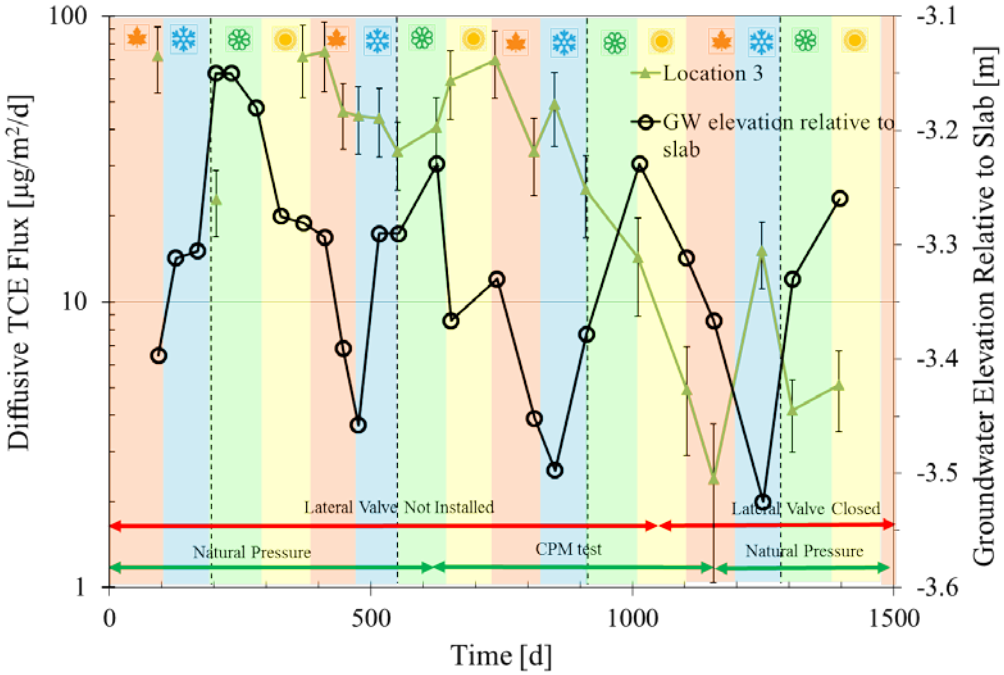

Figure 4.48 (c) TCE emissions per unit area at location 3

: Spring : Summer : Autumn : Winter

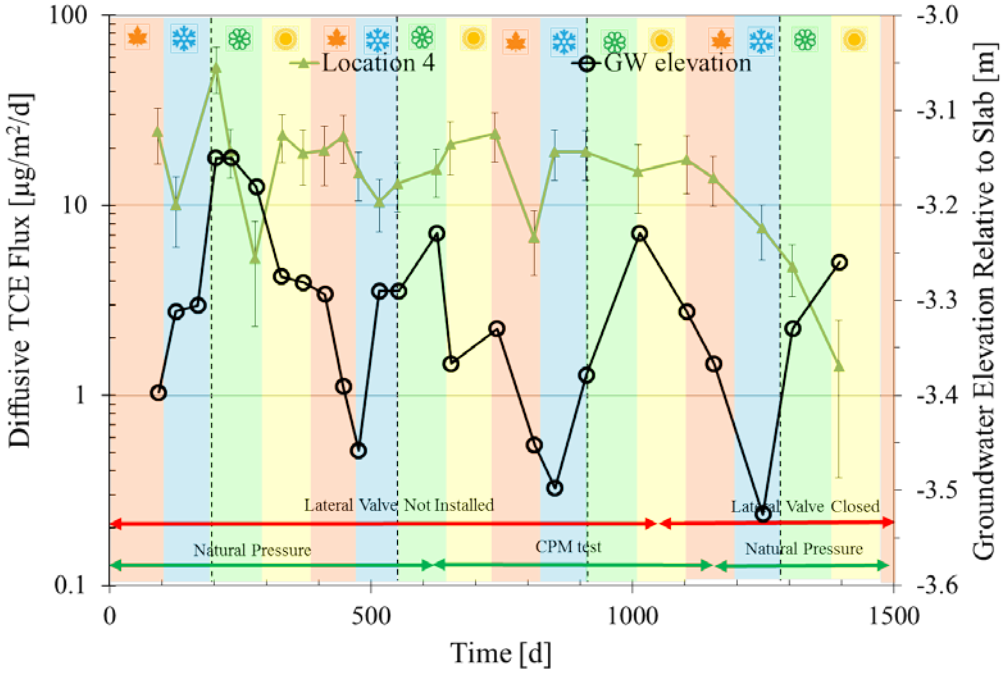

Figure 4.48 (d) TCE emissions per unit area at location 4

: Spring : Summer : Autumn : Winter

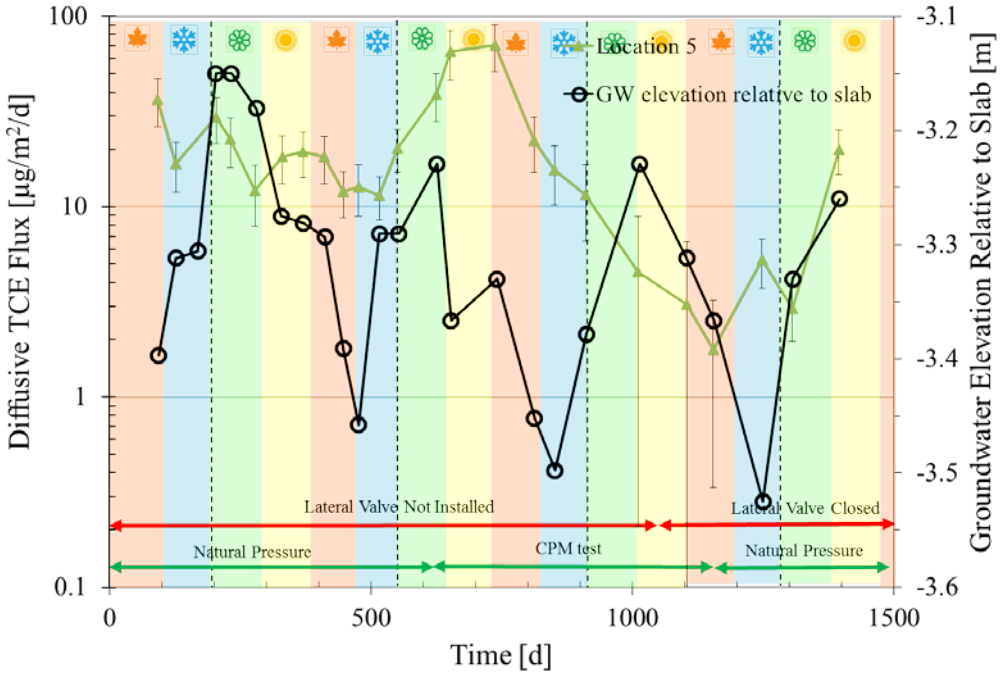

Figure 4.48 (e) TCE emissions per unit area at location 5

: Spring : Summer : Autumn : Winter

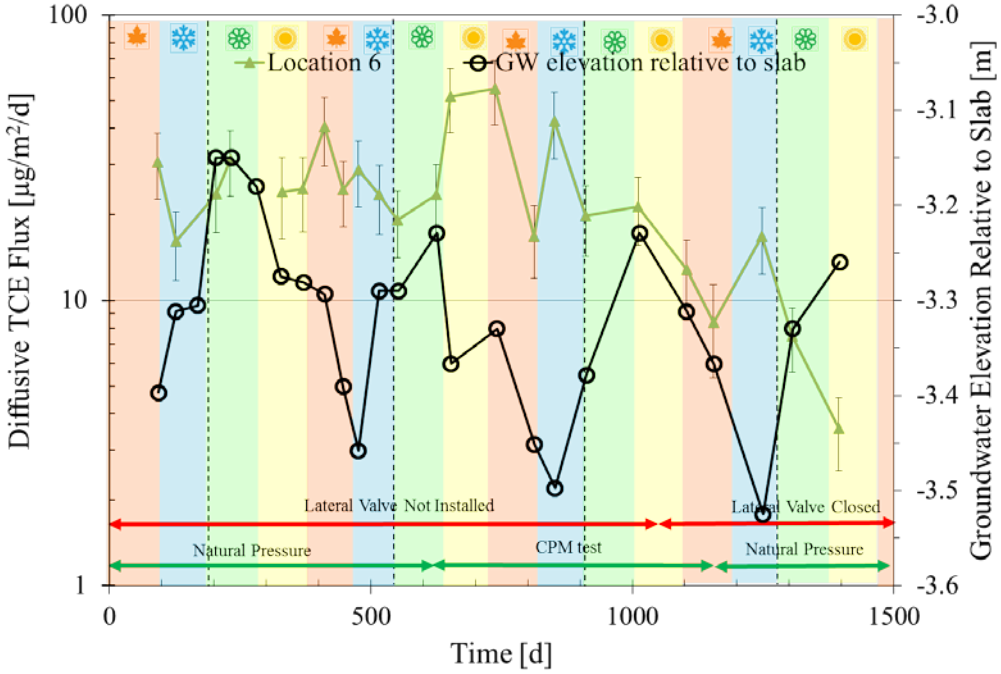

Figure 4.48 (f) TCE emissions per unit area at location 6

: Spring : Summer : Autumn : Winter

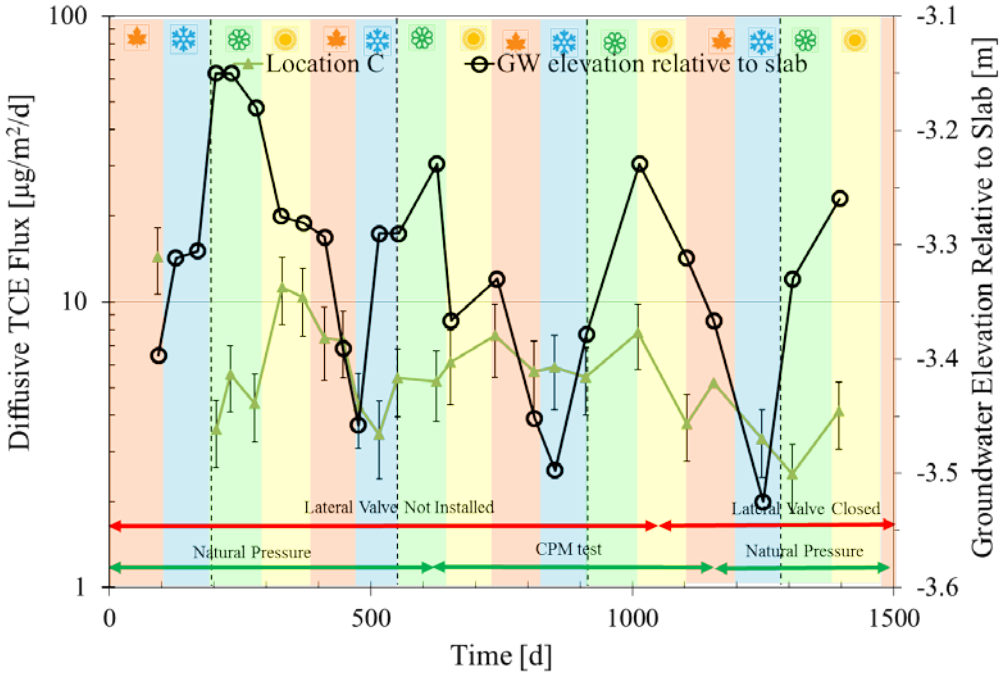

Figure 4.48 (g) TCE emissions per unit area at location C

: Spring : Summer : Autumn : Winter

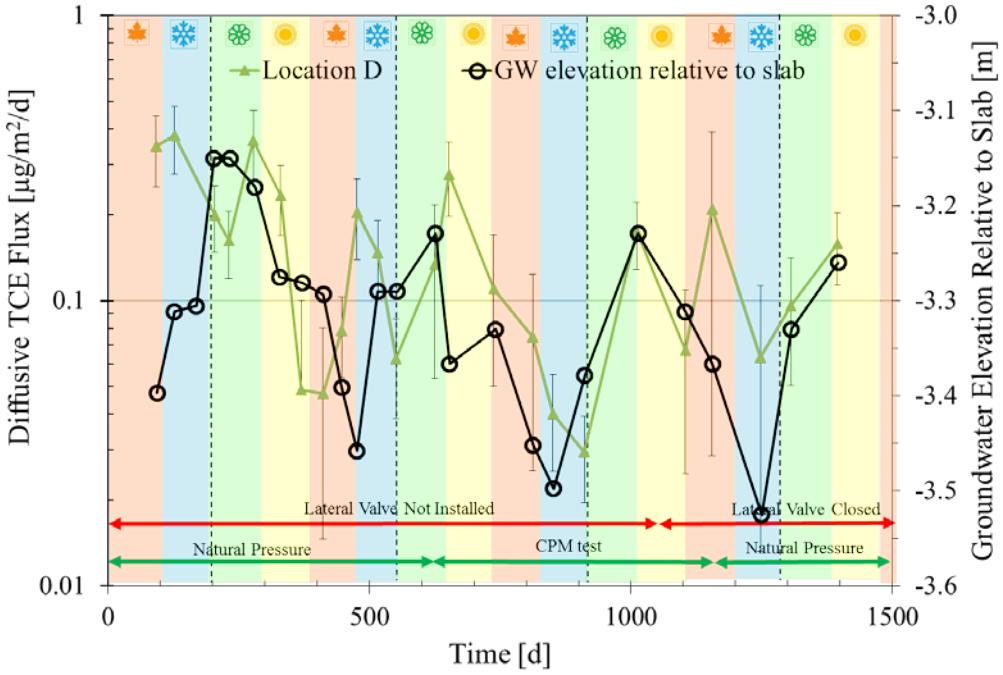

Figure 4.48 (h) TCE emissions per unit area at location D

: Spring : Summer : Autumn : Winter

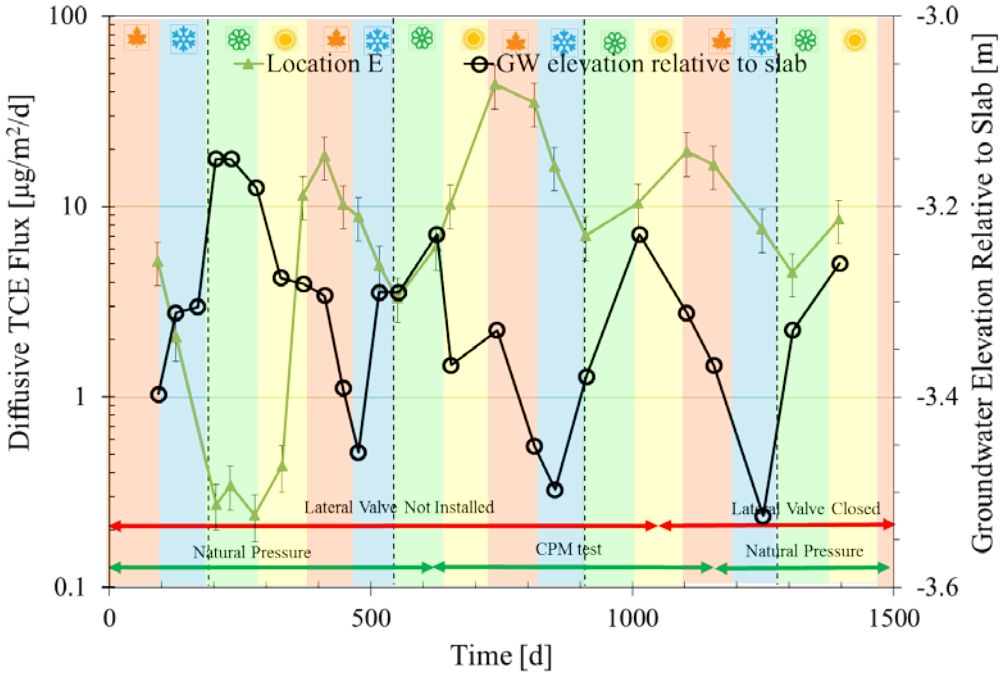

Figure 4.48 (i) TCE emissions per unit area at location E

: Spring : Summer : Autumn : Winter

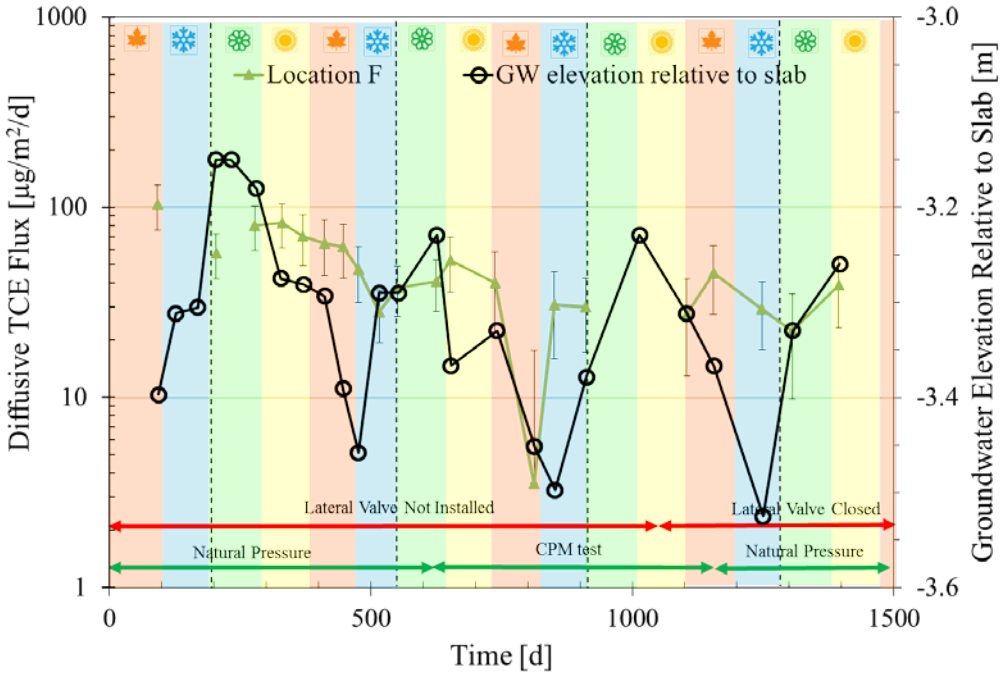

Figure 4.48 (j) TCE emissions per unit area at location F

: Spring : Summer : Autumn : Winter

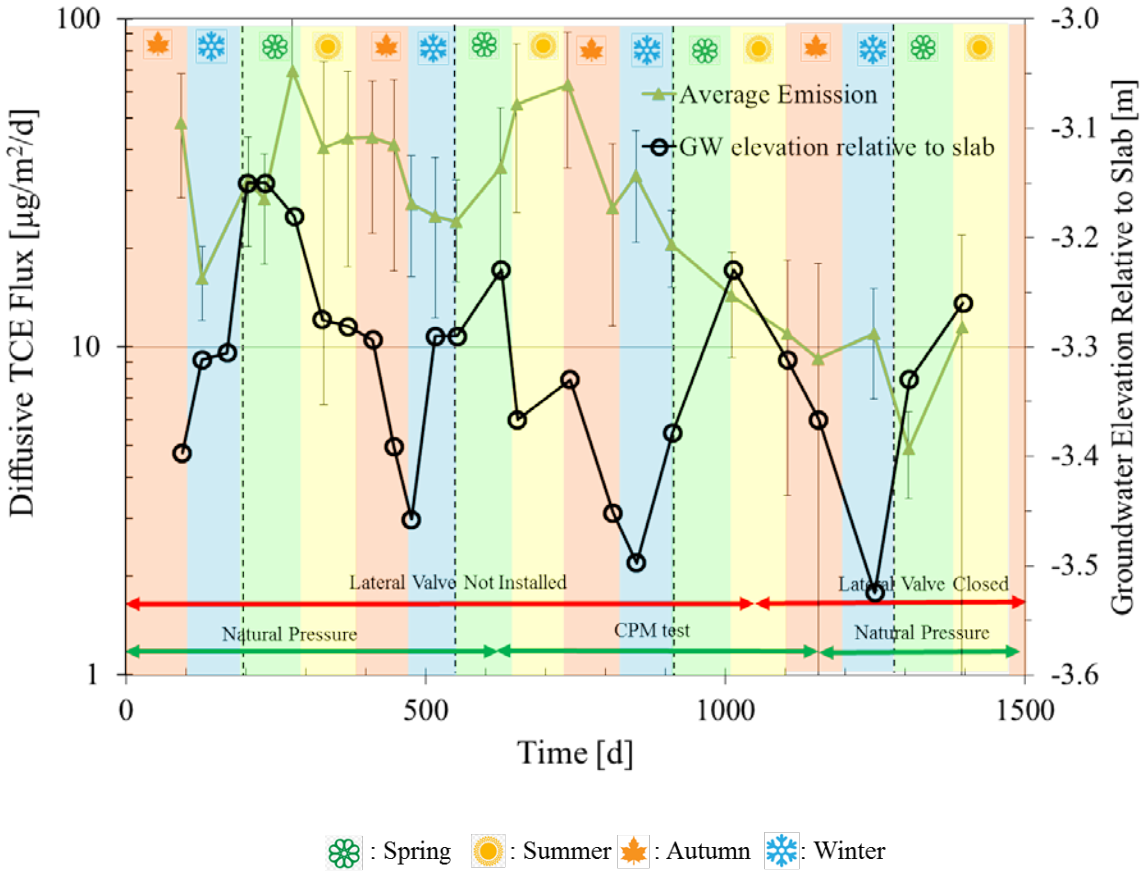

Figure 4.49. Averages of diffusive TCE flux F_1 values (emissions per unit area) for monitoring locations within the building footprint. Error bars span the standard deviation of each average value.

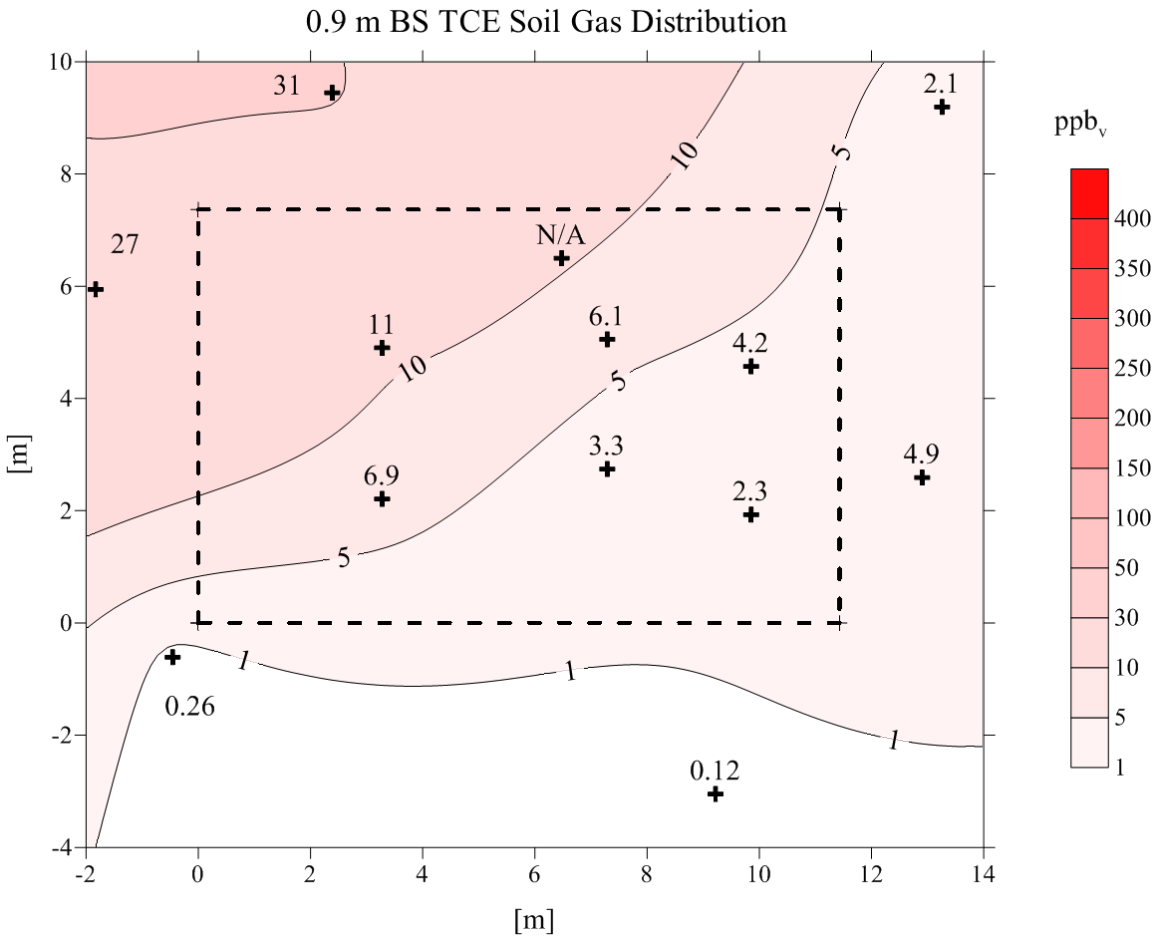

Figure 4.50 (a).

Figures 4.50 a and b-d below. Representative a) and b) 0.9 m BS and 1.8 m BS TCE soil gas concentrations, respectively, c) 2.7 m BS TCE groundwater concentrations, and d) F_1 emission rates for the t = 514 d to t = 519 d sampling event.

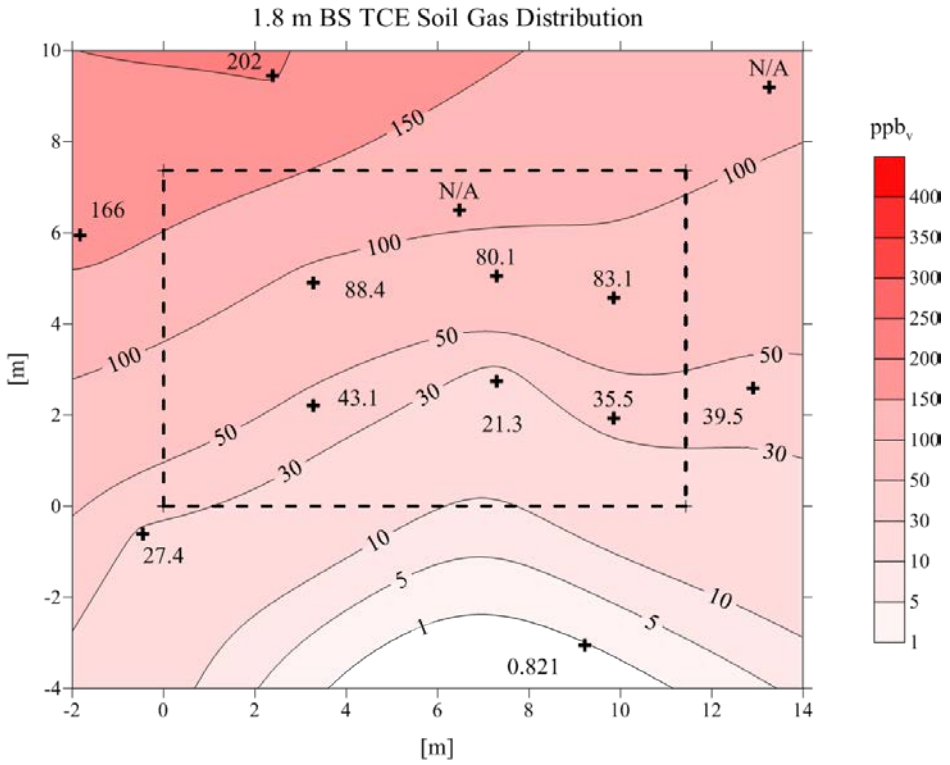

Figure 4.50 (b

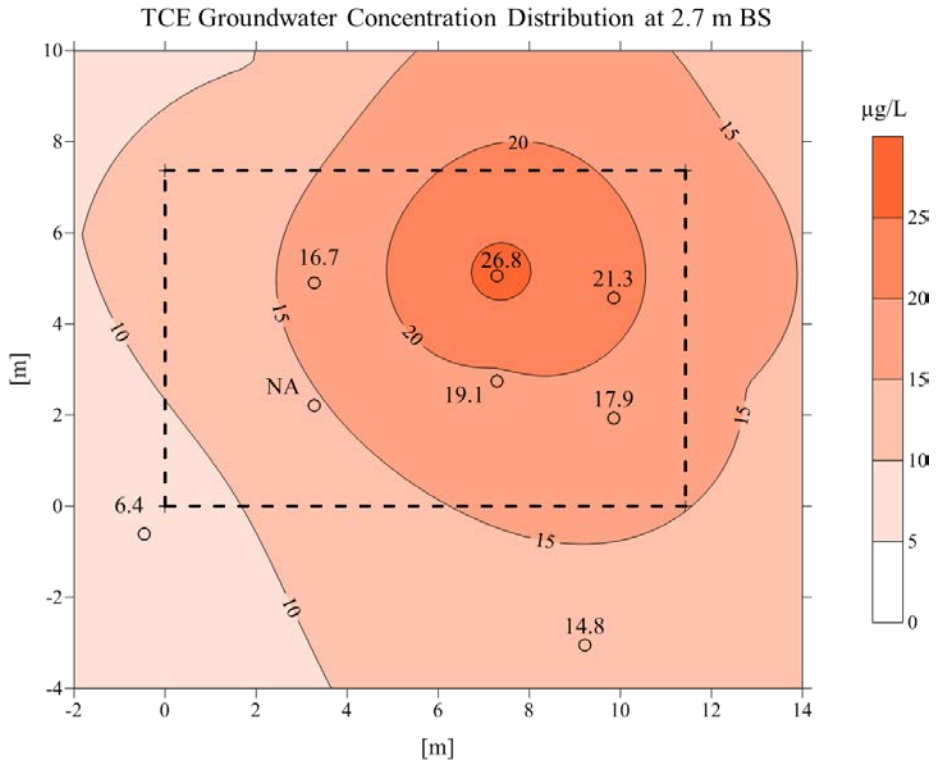

Figure 4.50 (c

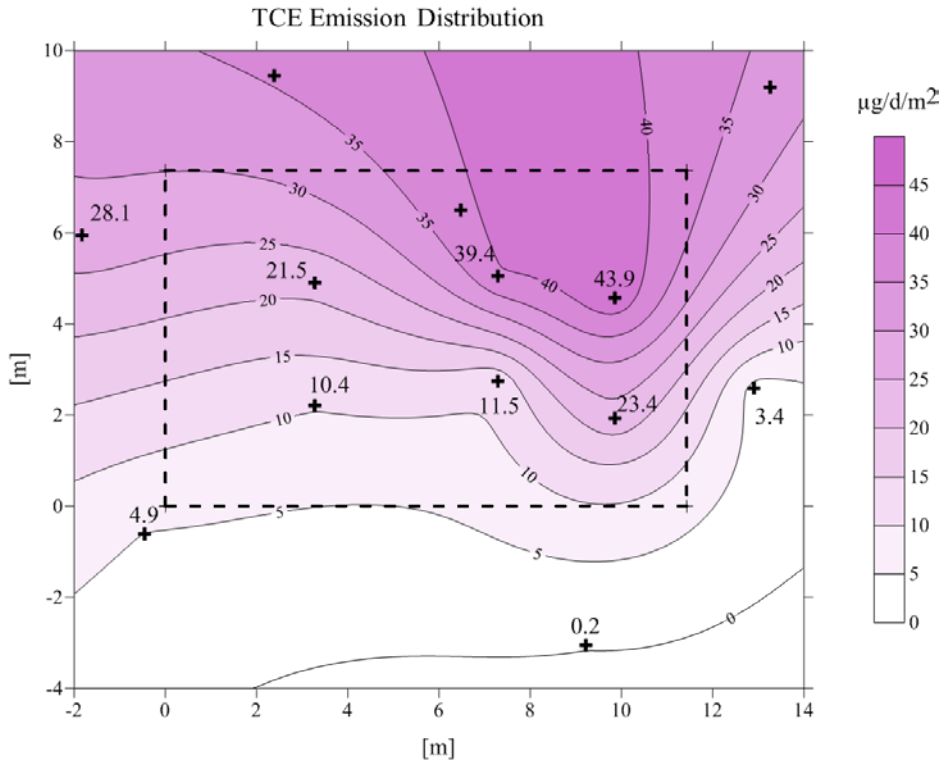

Figure 4.50 (d).

Figure 4.51 presents TCE emissions calculated for CPM test conditions using method F_2 vs. time and groundwater table elevation. The data were collected during 1071 d < t < 1157 d when the lateral drain valve was closed and the real-time groundwater table elevation data were collected every 2 h. Short-term groundwater table elevation changes ranged from about 5 cm per day to 22 cm bi-weekly, with the longer term trends following the seasonal pattern observed in the synoptic measurements.

F_2 values varied ±50% about the mean emission rate of 6.0 µg/m^2-d. The standard deviation was ±1.3 µg/m^2-d and the maximum and minimum emission rates were 8.7 and 2.1 µg/m^2-d, respectively. The F_2 results agree well with the average F_1 values within the building footprint during the same period of time (e.g. 9.2 µg/m^2-d at t = 1155 d).

In summary, both F_1 and F_2 calculation methods produced emission rates that varied by at most approximately 50% about the average emissions for groundwater table elevations that changed by about 5 cm daily and 30 cm seasonally and for consistent operating conditions. This variability about the average is similar to the 36% uncertainty in each F_1 calculation. There was a noticeable decline in F_1 values for interior sampling points when the lateral land drain valve was closed, suggesting some influence of that feature. Results for the two calculation methods were similar during the time period when both methods overlapped; the F_2 results were comparable to spatially integrated F_1 results beneath the building footprint. Temporal changes in F_2 emissions were much smaller than the 2-3 orders of magnitude changes in indoor air concentrations under natural conditions at this site (Holton, et al., 2013). Thus, it is not likely

that groundwater table elevation changes were major contributors to indoor air concentration variability at this site.

4.5.4 **Laboratory tests: single-stage water table drop and rise**

The experiments were allowed to achieve steady-state depth versus normalized soil gas concentration profiles prior to initiating water table fluctuations. In preparing the normalized concentration profiles shown in Figure 2.8, measured soil gas concentrations at the sampling locations were divided by the equivalent equilibrium vapor phase concentrations corresponding to dissolved water concentrations at the water table (=dissolved concentrations × chemical-specific Henry's Law Constant).

All normalized concentrations decrease from about one to three orders-of-magnitude across the first two sampling points above the water table. This is similar to what McCarthy and Johnson (1993) observed in their experiments; their TCE concentrations decreased over three orders-of-magnitudes across an approximately 25 cm thick capillary fringe.

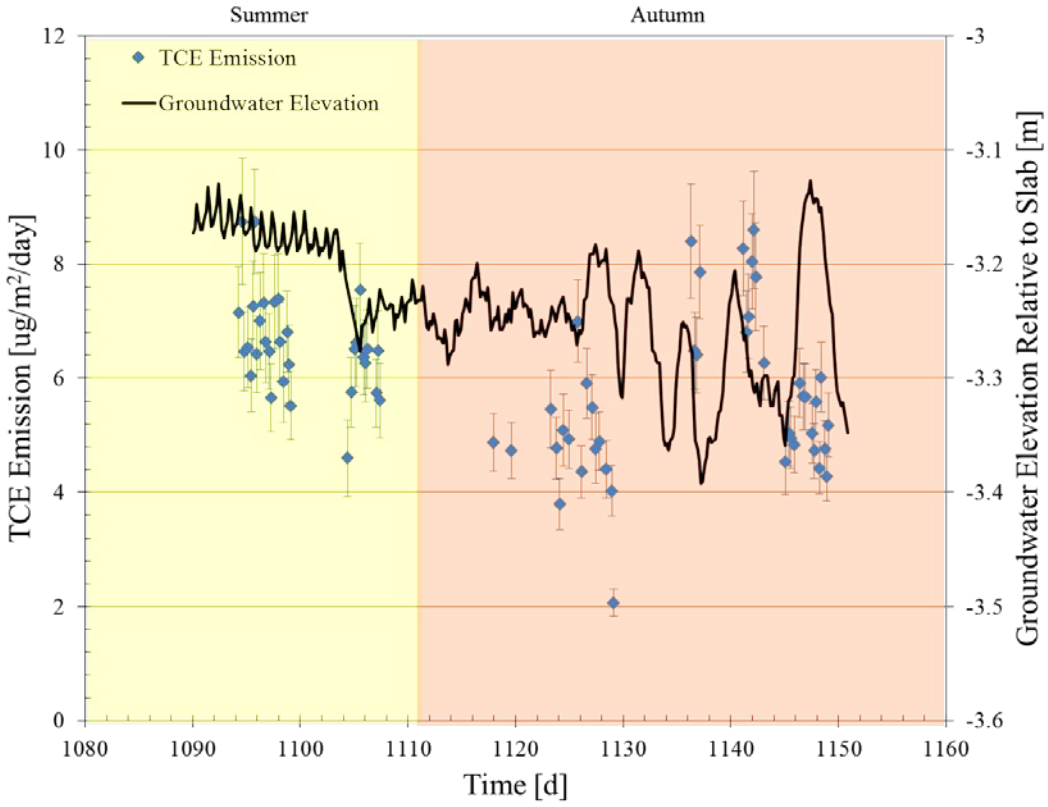

Figure 4.51. Real-time TCE emission rate per unit area (F_2) vs. groundwater table elevation during CPM test conditions when the lateral drain valve was closed. Error bars span the uncertainty in each F_2 value calculation.

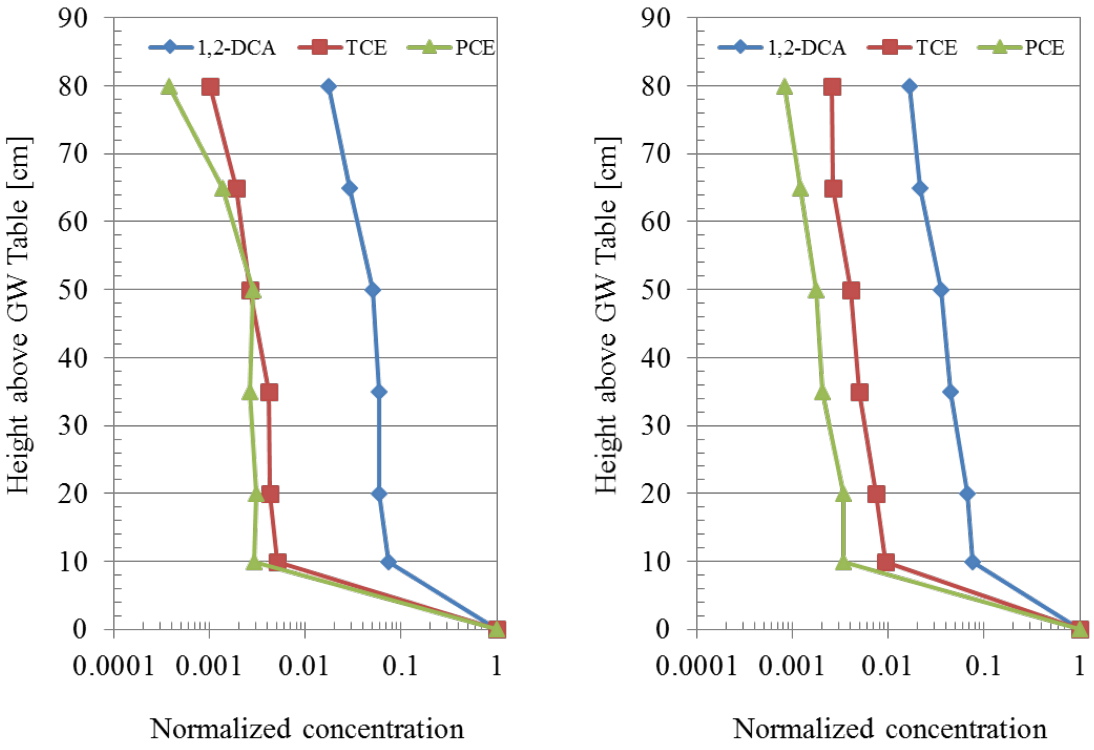

(a) Silica sand tank

(b) Play sand tank

Figure 4.52. Normalized steady-state soil gas profiles for the (a) silica sand tank and (b) play sand tank. Normalized concentrations were obtained by dividing soil gas concentrations at sampling locations by the equivalent gas phase concentrations at the water table.

Figure 4.53 a-b and 4.54 a-b present CHC emission rates and water table elevations vs. time during single-stage drops and rises in the water table, respectively. In these figures, the emission rates were normalized to the averaged steady-state emission rate before the water table elevation change. A tank leak was discovered at t=110 h in the silica sand tank during the rising water table test, and as a result data after t=100 h were discarded. Overall, CHC emission rates in both tanks increased during falling water table tests and decreased during the rising water table tests. This observation agrees with previous studies (e.g., Werner and Hohener, 2002). CHC emission rates did not return to their original level after the water table re-stabilized. With diffusion-dominated transport, steady-state emissions should be greater when the water table is 90 cm above the tank bottom vs. 60 cm above the tank bottom, because the distance to the soil surface is less. However, the opposite was observed during water table rise and drop tests. One possible explanation is that the emissions had not yet reached steady conditions when the experiment was terminated, and that appears plausible given the data trends in the single-stage water table drop tests (Figure 4.53). The explanation for the water table rise tests is that the result was an artifact

of the way the experiments were conducted. The volumetric horizontal water flow for each tank was maintained at a constant rate, so that the linear horizontal flow rate of water was 33% slower when the elevation was 90 cm above the tank bottom vs. 60 cm. This might lead to more depletion at the emission interface as the water moves across the tank, thereby leading to a lower interface concentration and lower emissions for higher water table conditions.

The CHC emissions response to the single-stage water table drop was more rapid in the more permeable silica sand tank; the CHC emissions increases peaked in ≤100 h while they generally peaked at ≥100 h in the less permeable play sand tank. In addition, slight differences were observed in the emissions increases between tanks; peak TCE emissions were 3.3X greater than steady state conditions in the silica sand tank, whereas they were only 2.9X greater in the play sand tank. Since both tanks were tested simultaneously under the same operational conditions, these variations are likely a result of the different soil properties, and are probably linked to the rate of water drainage from the soil.

4.5.5 **Laboratory tests: alternating rising/falling groundwater elevation**

Figures 4.55 and 4.56 present normalized CHC emission rates and water table elevations vs. time for water table elevation increases/decreases of 5 cm/day and 10 cm/day, respectively. In these experiments, water was continuously introduced by horizontal flow to maintain homogeneous dissolved CHC profiles across the water-saturated zone, and the change in water table elevation was about 30 cm. Four rise/fall cycles were implemented during the 5 cm/d experiment and three were implemented during the 10 cm/d experiment. Data gaps from 195 h to 225 h during the 5 cm/d experiment and from 195 h to 225 h and 403 h to 430 h during the 10 cm/day experiment were due to analytical instrument issues.

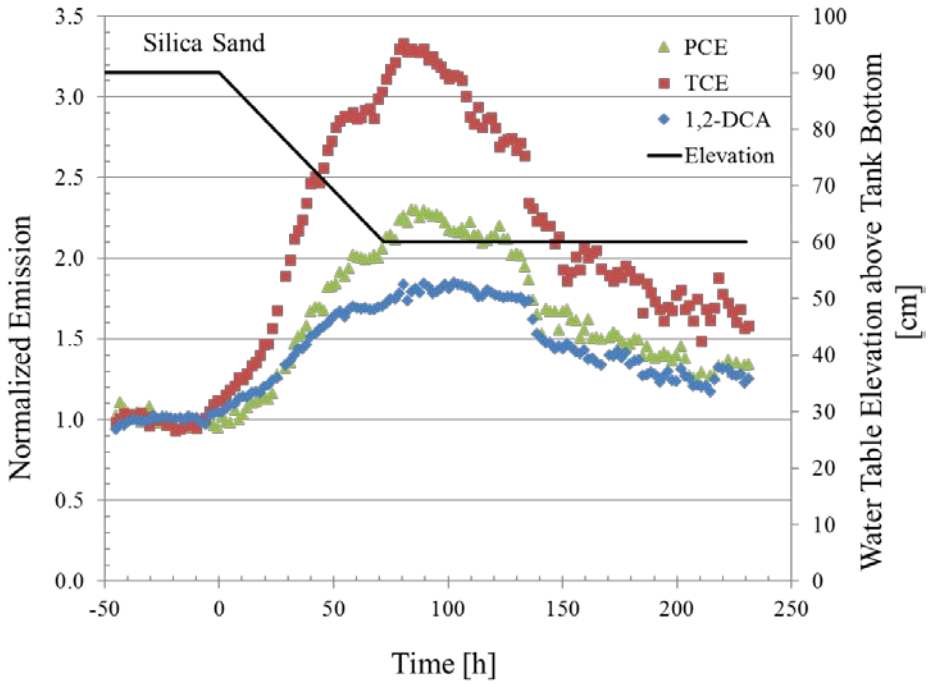

Figure 4.53 a

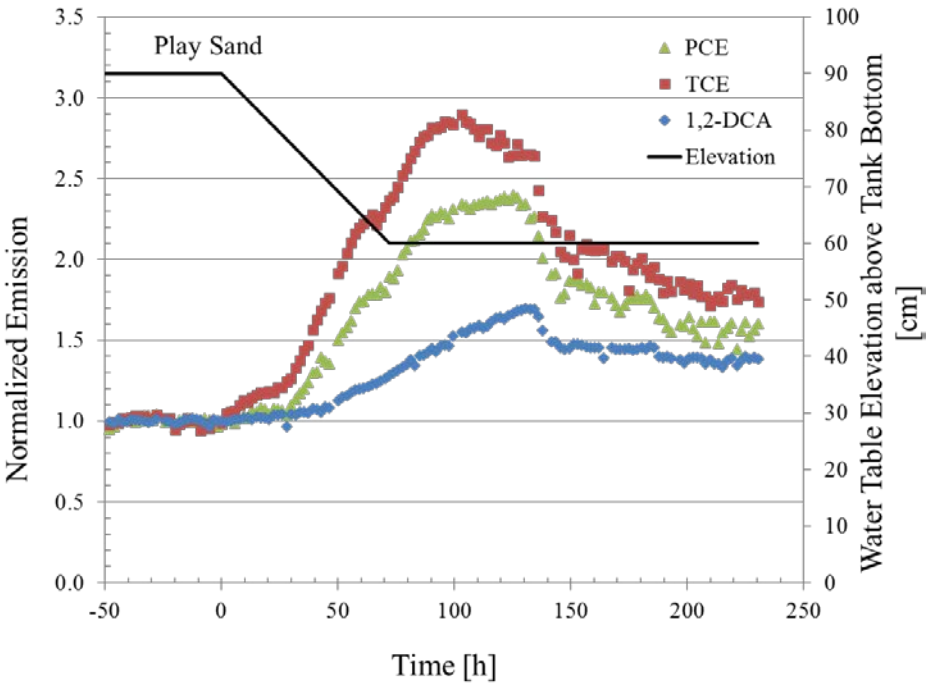

Figure 4.53 b

Figure 4.53 a-b. Normalized emissions and water table elevation vs. time in the (a) silica sand and (b) play sand tanks during the single-stage water table elevation drop test. Emissions are normalized to an averaged emission rate at steady-state before elevation changes.

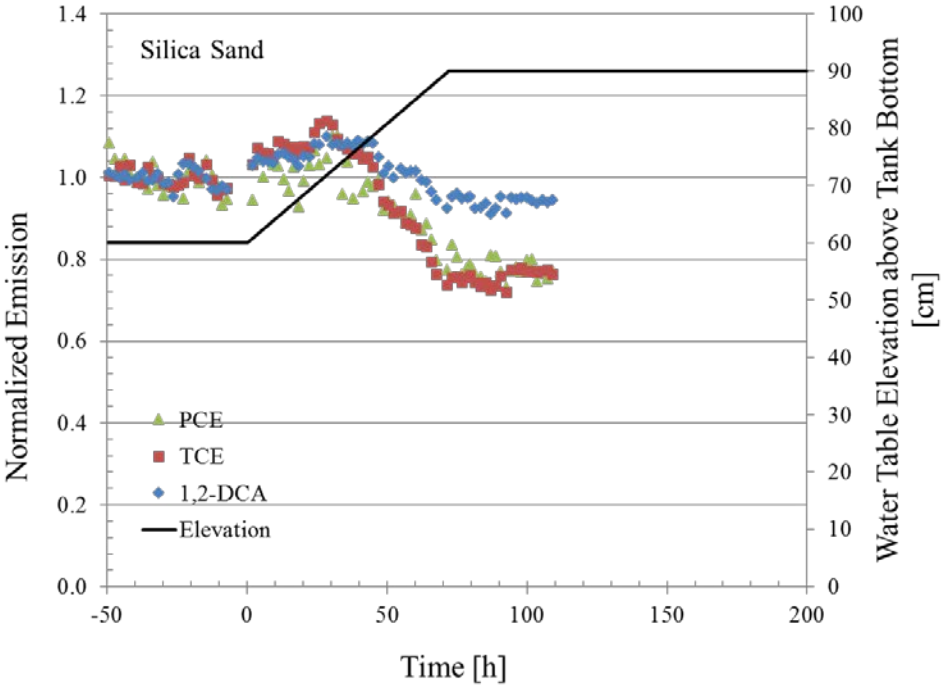

Figure 4.54 a

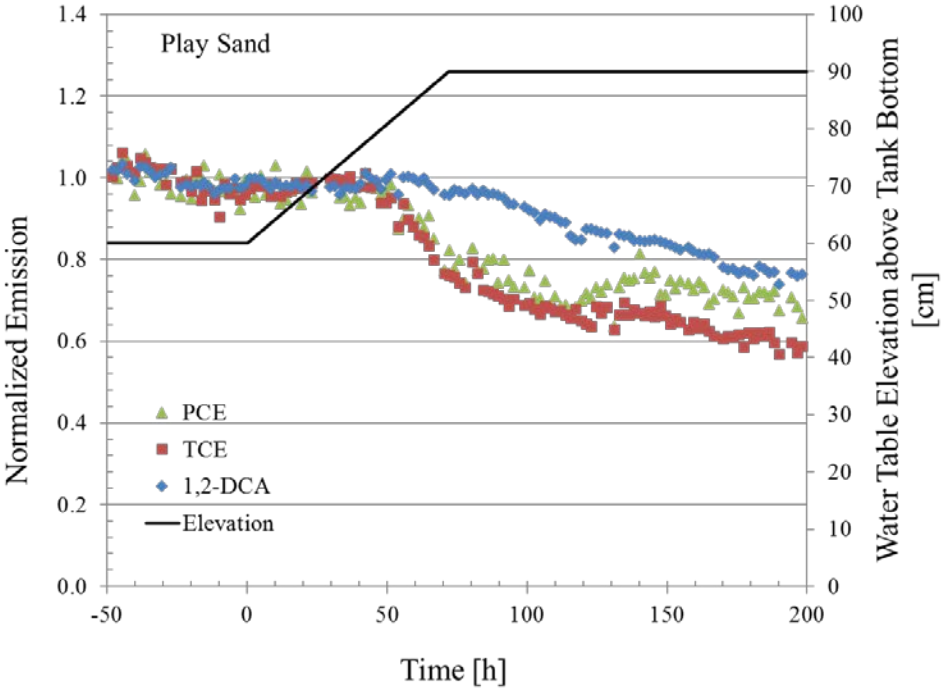

Figure 4.54 b

Figure 4.54 a-b. Normalized emissions and water table elevation vs. time in the a) silica sand and b) play sand tanks during the single-stage water table elevation rise test. Emissions are normalized to an averaged emission rate at steady-state before elevation changes.

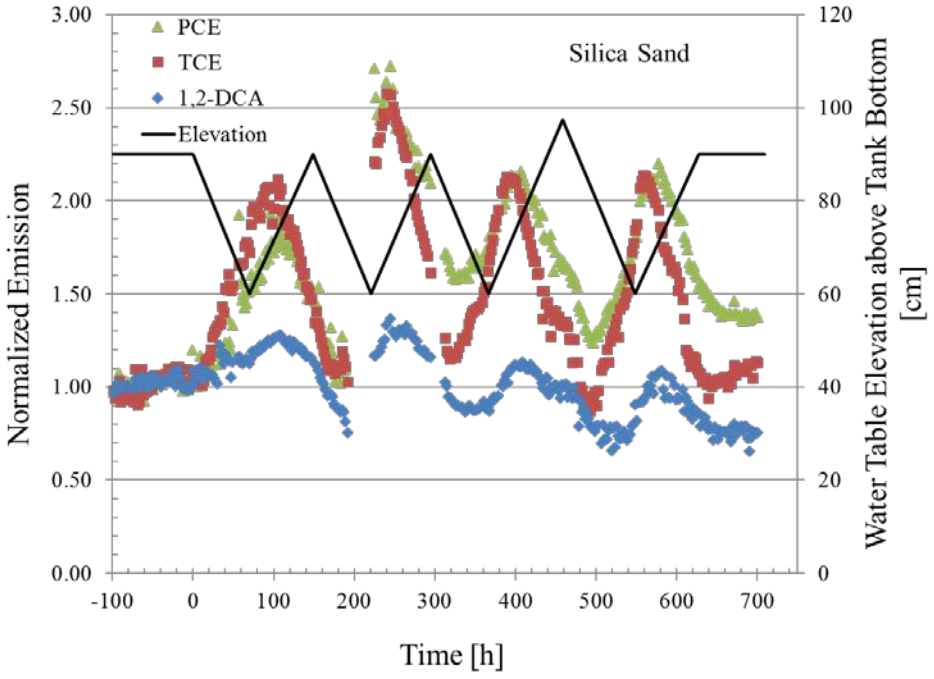

Figure 4.55 a

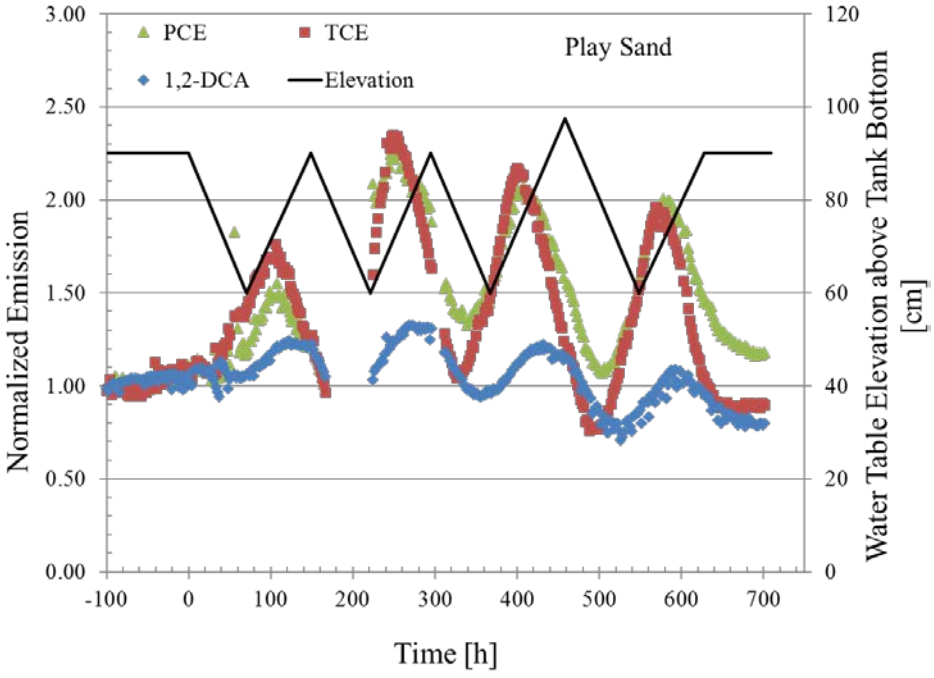

Figure 4.55 b

Figure 4.55 a-b. Normalized CHC emission rates and water table elevation vs. time during tests with 10 cm/d elevation change rate for a) silica sand and b) play sand tanks. Emissions are normalized to an averaged emission rate at steady-state before elevation changes.

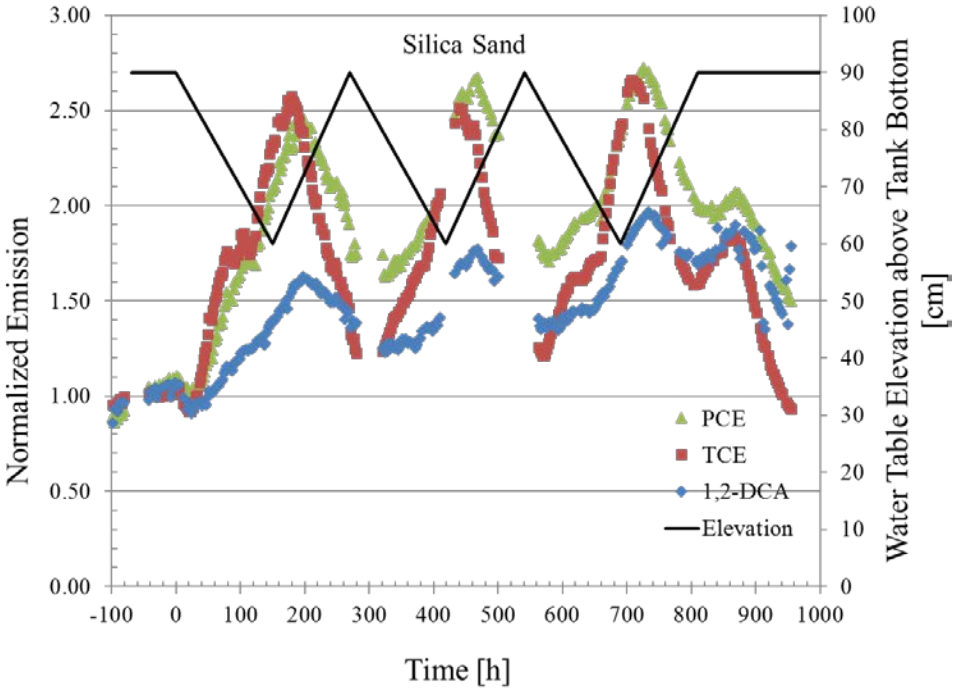

Figure 4.56 a

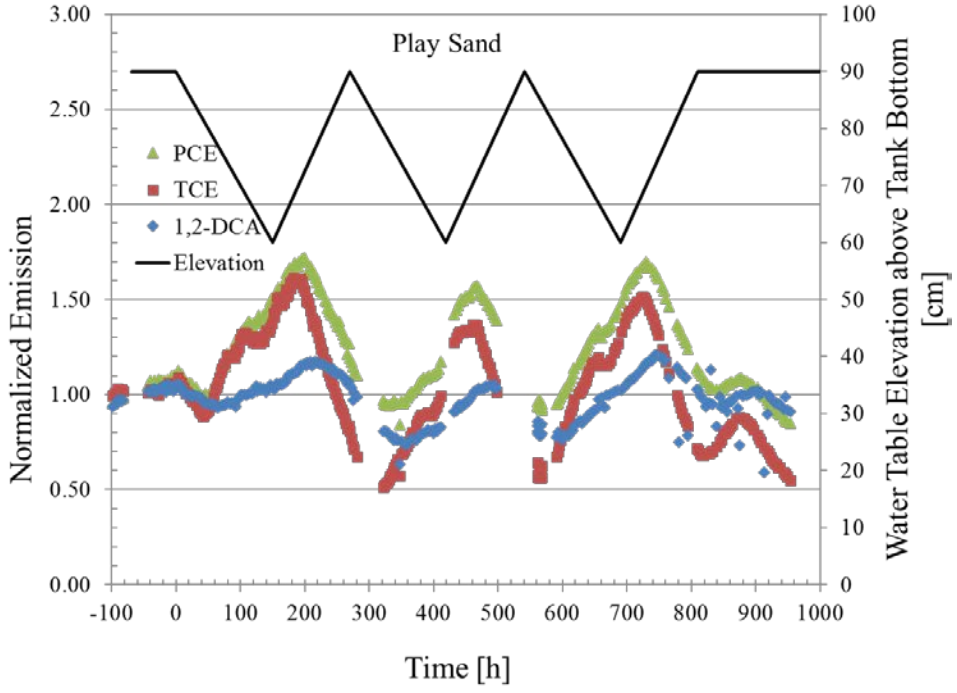

Figure 4.56 b

Figure 4.56 a-b. Normalized CHC emission rates and water table elevation vs. time during tests with 5 cm/d elevation change rate for a) silica sand and b) play sand tanks. Emissions are normalized to an averaged emission rate at steady-state before elevation changes.

The following observations were made from a review of Figures 4.55 and 4.56:

- All compounds respond to water table drops with an increase in emission rate, and that response begins shortly after the water table begins to fall.
  The TCE and PCE emissions responses to water table elevation changes were similar; the peak normalized TCE emission rates were within 10 % of the PCE peaks. The maximum increases in 1,2- DCA emissions were generally about 2X to 3X smaller than the other two CHCs. This appears to be influenced by differences in Henry's Law constants as TCE and PCE have similar H_i values and the H_i value for 1,2-DCA is 10X less than the other two (Table 3.4). In addition, the molecular diffusion coefficients are similar for all chemicals, with less than factor 2 difference across a wide range of chemicals.

- The magnitude of CHC emission increases during four 10 cm/day repeating water table fluctuations were less than in the single-stage 10 cm/day drop test (Figure 2.11). This is likely because the period of water table fluctuations was shorter than the time for emissions to peak following water table declines.

- CHC emissions increases were greater in the silica sand tank than in the play sand tank during the 5 cm/d oscillating water table level tests, but were similar for the 10/cm/d tests. For the 5 cm/d water table fluctuation cycles, the peak normalized CHC emissions in the silica sand tank were about 50% greater than those in the play sand tank. This may be a result of the differences in hydraulic conductivity between the silica sand (0.186 cm/s) and play sand (0.083 cm/s). Moisture profiles and water movement in the silica tank can respond more quickly to water head changes than in play sand tank.

- Emission responses changed when the rate of rise and fall changed from 5 to 10 cm/d. Peak normalized TCE emission rates increased from 1.50 ± 0.12 to 2.06 ± 0.26 in the play sand tank, while they were similar in the silica sand tank for both 5 and 10 cm/day.

In practice, uniform water concentration profiles with depth are unlikely to be observed aquifers. It is more probable that dissolved contaminant concentrations will decrease in approaching the water table because of depletion due to volatilization and infiltration of clean water onto dissolved groundwater plumes. For that reason, a second set of experiments was conducted in which the mass of chemical was allowed to deplete with time from the tank due to volatilization.

4.5.6 **Laboratory tests: groundwater fluctuation experiments with CHC mass depletion**

In the second type of experiments, water table fluctuations of similar magnitude and frequency as above were implemented, but they were created by adding and removing water from the tank bottom, so the CHC mass was depleting with time by volatilization and there was no horizontal

flow. Relatively uniform initial CHC distributions were created using lateral water flow and then that horizontal flow was stopped before the start of the vertical water table fluctuations.

A time progression of TCE concentration vs. depth profiles is presented in Figure 4.57. To show concentrations in both gas and water samples on the same plot, TCE concentrations are presented as "equivalent gas phase concentrations", where dissolved concentrations are converted to gas phase concentrations through multiplication by the Henry's Law constant.

At t= 0 h a strong concentration gradient exists near the water table. TCE concentrations decreased 60% and 37% within 5 cm of the water table in the silica sand and play sand tanks, respectively. This gradient was formed initially due to chemical volatilization during static water table conditions preceding the water table fluctuations.

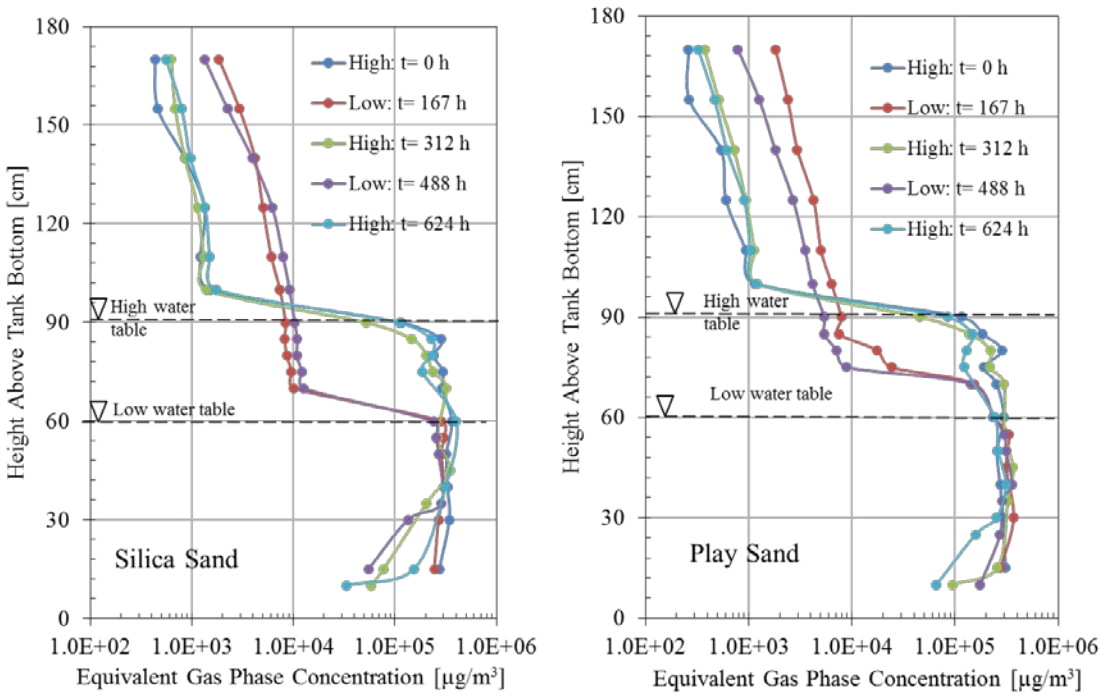

Figure 4.57. Equivalent TCE gas phase concentration profiles during water level fluctuation tests for the silica sand (left) and play sand (right) tanks. Note that "high" and "low" in the legend refer to the highest and lowest water table elevations, respectively.

Real-time measured emissions were normalized to average steady-state emissions from each tank prior to water level fluctuations. Figure 4.58 presents results during two water table elevation fluctuation cycles. For both tanks, the rate of water level change was 5 cm/d and maximum elevation changes were ± 0.3 m. Similar to the observations during uniform water concentration tests, CHC emissions changed when water table levels changed; however, in these tests the magnitude of the emissions increase decreased from the first cycle to the second. That indicates that the effect of groundwater table fluctuations will decrease with distance down-gradient in a

dissolved plume. Again, as in all other tests, the effects of water table changes on TCE and PCE emissions is greater than for 1,2-DCA.

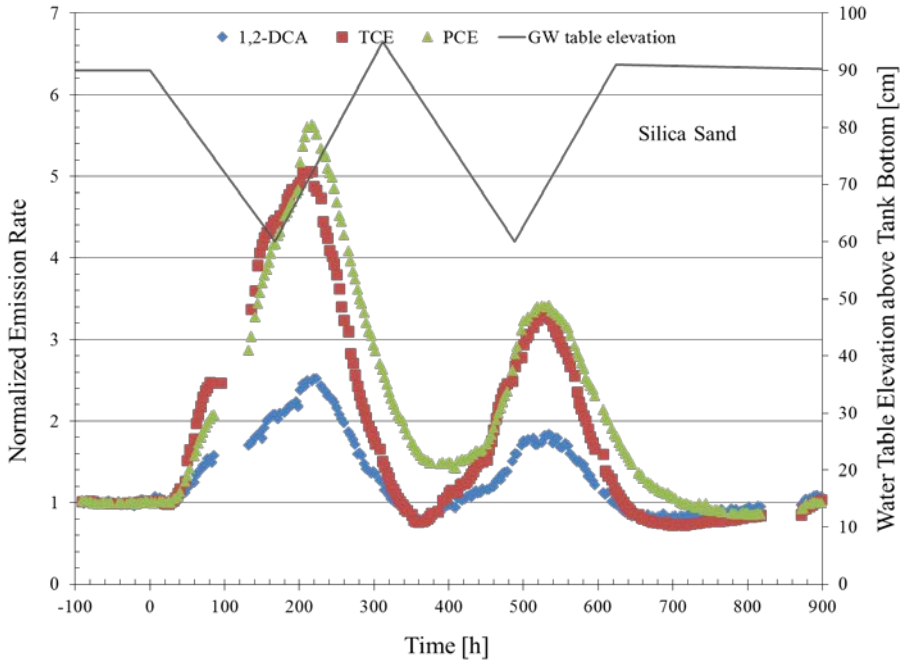

Figure 4.58 a

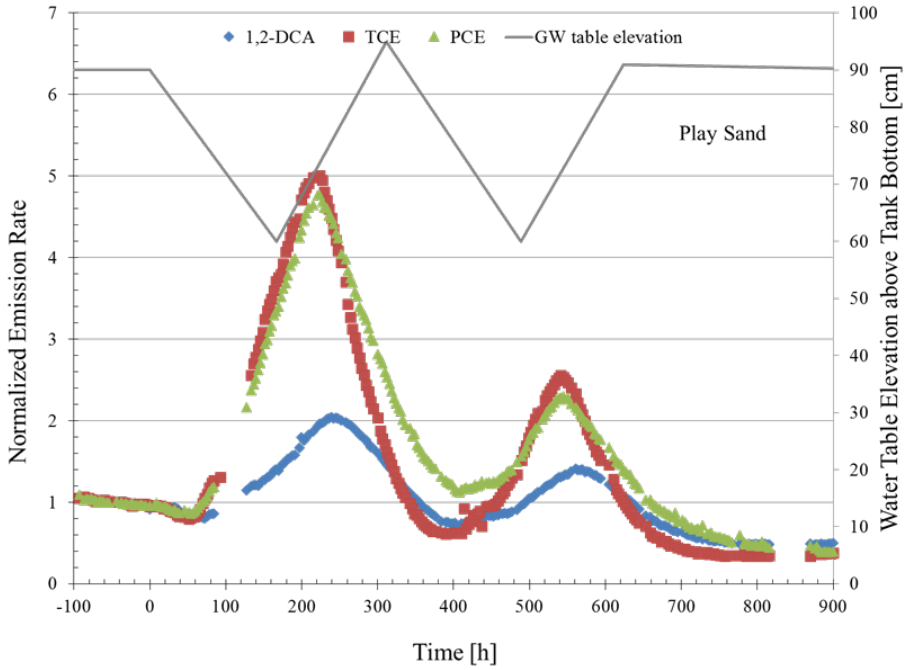

Figure 4.58 b

Figure 4.58 a-b. Normalized emission rates and water table elevations vs. time with depleting dissolved mass for the a) silica sand and b) play sand tanks. Emissions were normalized to averaged emissions from each tank prior to water level fluctuations.

In summary, the following are key observations from the laboratory studies:

- Emissions changed with changing water table elevation, with transient increases in emissions following water table declines and transient decreases in emissions following water table increases. The maximum temporary increases were <4X in the lab experiments. For reference, these are smaller than indoor air concentration changes with time reported Holton et al. (2013) but are similar to the roughly 3X seasonal variation reported by Folks et al. (2009).

- Chemical and soil properties appear to play a role in emission rate responses. For 1,2-DCA, with a Henry's law constant <1/10th of PCE and TCE values, the maximum emissions increases were about a factor of 2X to 3X less than the other two chemicals.

- Greater emissions increases were observed for the more permeable and lower capillary rise silica sand during the water table level oscillation tests.

- Water table fluctuation frequency did affect the magnitude of emission increases for the play sand tank; the magnitude increased as the water level changed faster from 5 cm/d to 10 cm/d. The rate of change in water level did not appear to impact the peak emissions from the silica sand.

- The CHC depletion test showed the development of a decreasing concentration gradient with time near the water table and corresponding reduced emission increases over time. This suggests the responses of CHC emissions to water table fluctuations may be different in different regions of a dissolved groundwater plume.

4.5.7 **Simulating vapor emissions from groundwater to soil surface with fluctuating water table**

Model inputs for HYDRUS 1-D simulations are summarized in Table 4.7. Simulation results for all scenarios, static water table ($z_{initial} + L/2$) condition emissions (E_{static}), maximum, minimum, and average emissions during fluctuation after the system reached dynamic steady state (E_{max}, E_{min}, and E_{mean}) as well as the ratios between them, are presented in Table 4.8.

Table 4.7. Summary of simulation inputs for sensitivity analyses.

HYDRUS 1-D algorithm inputs						
Time information	Initial time step [h]	0.0024	Iteration criteria	Maximum number of iteration	10	
	Minimum time step [s]	0.01		Water content tolerance	0.001	
	maximum time step [h]	200		Pressure head tolerance [cm]	1	
Time Weighing Scheme	Crank-Nicholson implicit scheme					
Space Weighting Scheme	Galerkin formulation					
Soil properties:	**Soil type: sand**		**Soil type: loam**		**Soil type: coarse sand**	
	Inputs	**Simulation ID**	**Inputs**	**Simulation ID**	**Inputs**	**Simulation ID**
Residual soil water content [cm^3-H_2O/cm^3-soil]	0.045	1-7, 10-24, 24-34	0.078	8, 25	0.016	9, 26
Saturated soil water content [cm^3-H_2O/cm^3-soil]	0.43		0.43		0.39	
Parameter *a* in the soil water retention function [1/cm]	0.145		0.036		0.6	
Parameter n in the soil water retention function [-]	2.68		1.56		3	
Saturated hydraulic conductivity [cm/h]	29.7		1.04		669.6	
Tortuosity parameter in the conductivity function [-]	0.5		0.5		0.5	
Bulk density [g/cm^3]	1.5	These values were kept as the software defaults for all simulations				
Longitudinal dispersivity [cm]	0.1					

(continued on the next page)

Table 4.7. (cont.) Summary of simulation inputs for sensitivity analyses.

Solute specific parameters:	**Inputs**	**Simulation ID**
Molecular diffusion coefficient in water, *Dwater* [cm^2/h]	0.01638	16, 33
	0.03276	1-15, 18-33
	0.06552	17, 34
Molecular diffusion coefficient in air, *Dair* [cm^2/h]	142.2	14, 31
	284.4	1-13, 16-30, 33-34
	568.8	15, 32
Adsorption isotherm coefficient, *ks* [cm^3/g]	0	1-9, 12-26, 29-34
	1	11, 28
	10	10, 27
Henry's Law constant, *H* [V-water/V-gas]	0.042	12, 29
	0.42	1-11, 14-28, 31-34
	4.2	13, 30

(continued on the next page)

Table 4.7. (cont.) Summary of simulation inputs for sensitivity analyses.

Water table fluctuation patterns:	**Inputs**	**Simulation ID**		
Fluctuation magnitude [cm]	1	4, 21		
	30	1-3, 6-20, 23-34		
	100	5, 22		
Fluctuation frequency [1/day]	1	3, 20		
	1/30	1, 4-18, 21-34		
	1/360	2, 19		
Domain information:	**Inputs**	**Simulation ID**		
Depth of modeling domain [cm]	Source 50 cm below water table		Source 100 cm below water table	
	Inputs	Simulation ID	Inputs	Simulation ID
	100	6	250	23
	200	1-5, 8-17	350	18-22, 25-34
	550	7	700	24
Initial water table elevation above bottom of the domain [cm]	50	1-17		
	200	18- 34		

Table 4.8. Model Results for Hydrus 1-D Simulations

	Simulation Number	Description	Source 50 cm below water table							
			E_{static} [g/cm^2-h] x 10^7	E_{max} [g/cm^2-h] x 10^7	E_{min} [g/cm^2-h] x 10^7	E_{mean} [g/cm^2-h] x 10^7	E_{max}/E_{static}	E_{min}/E_{static}	E_{mean}/E_{static}	E_{max}/E_{min}
	1	Reference (TCE, monthly 30 cm water table fluctuation, no adsorption)	1.55	5.04	0.634	2.50	3.25	0.41	1.61	7.95
Water table fluctuation pattern	2	Annual, 30 cm	1.55	2.54	1.24	1.83	1.64	0.80	1.18	2.04
	3	daily, 30cm	1.55	17.7	16.7	17.0	11.44	10.80	10.99	1.06
	4	Monthly, 1 cm	1.96	2.07	1.92	1.99	1.06	0.98	1.02	1.08
	5	Monthly, 100 cm	1.02	11.7	0.00692	3.33	11.45	0.01	3.26	1687
Vadose zone thickness	6	50 cm	1.55	118	4.61	53.2	76.47	2.98	34.43	25.67
	7	500 cm	1.54	2.73	2.20	2.45	1.77	1.42	1.59	1.24
Soil types	8	Loam	1.28	3.85	2.77	2.52	3.02	2.17	1.97	1.39
	9	Coarse sand	1.43	5.18	0.71	2.34	3.63	0.50	1.64	7.31
Chemical properties	10	k_s = 10 cm^3/g	1.55	2.25	2.22	2.23	1.45	1.43	1.44	1.01
	11	ks = 1 cm^3/g	1.55	3.33	1.53	2.33	2.15	0.99	1.50	2.17
	12	H= 0.042	1.50	3.10	1.59	2.33	2.07	1.06	1.56	1.95
	13	H= 4.2	1.58	5.71	0.52	2.51	3.62	0.33	1.59	10.93
	14	D_{air} = 142.2 cm^2/h	1.54	4.15	1.03	2.49	2.70	0.67	1.62	4.03
	15	D_{air} = 568.8 cm^2/h	1.56	5.94	0.53	2.55	3.81	0.34	1.64	11.14
	16	D_{water}= 0.016 cm^2/h	0.78	3.71	0.204	1.54	4.75	0.26	1.97	18.19
	17	D_{water} = 0.066cm^2/h	3.07	7.61	1.54	4.20	2.48	0.50	1.37	4.94

(continued on the next page)

Table 4.8. (cont.) Model Results for Hydrus 1-D Simulations

	Simulation Number	Description	Source 200 cm below water table							
			E_{static} [g/cm^2-h] x 10^8	E_{max} [g/cm^2-h] x 10^8	E_{min} [g/cm^2-h] x 10^8	E_{mean} [g/cm^2-h] x 10^8	E_{max}/E_{static}	E_{min}/E_{static}	E_{mean}/E_{static}	E_{max}/E_{min}
	18	Reference (TCE, monthly 30 cm water table fluctuation, no adsorption)	4.87	1.26	0.214	0.66	2.59	0.44	1.36	5.89
Water table fluctuation pattern	19	Annual, 30 cm	4.87	0.744	0.338	0.521	1.53	0.69	1.07	2.20
	20	daily, 30cm	4.87	3.82	3.67	3.74	7.84	7.54	7.67	1.04
	21	Monthly, 1 cm	5.22	0.55	0.499	0.521	1.06	0.96	1.00	1.11
	22	Monthly, 100 cm	4.2	3.36	0.00832	1.10	8.01	0.02	2.61	404
Vadose zone thickness	23	50 cm	4.87	170	7.26	66.2	348.11	14.92	135.94	23.34
	24	500 cm	4.87	0.731	0.617	0.680	1.50	1.27	1.40	1.19
Soil types	25	Loam	4.56	3.01	2.21	2.57	6.60	4.84	5.64	1.36
	26	Coarse sand	4.32	1.67	0.045	0.608	3.86	0.10	1.41	34.43
Chemical properties	27	k_s = 10 cm^3/g	4.87	0.611	0.604	0.607	1.25	1.24	1.25	1.01
	28	k_s = 1 cm^3/g	4.87	0.921	0.431	0.649	1.89	0.88	1.33	2.14
	29	H= 0.042	4.81	0.843	0.467	0.654	1.75	0.97	1.36	1.80
	30	H= 4.2	4.90	1.45	0.148	0.688	2.96	0.30	1.40	9.79
	31	D_{air} = 142.2 cm^2/h	4.86	1.04	0.270	0.616	2.14	0.56	1.27	3.86
	32	D_{air} = 568.8 cm^2/h	4.88	1.47	0.185	0.645	3.01	0.38	1.32	7.94
	33	D_{water} = 0.016 cm^2/h	2.44	0.840	0.101	0.414	3.45	0.42	1.70	8.29
	34	D_{water} = 0.066cm^2/h	9.72	2.06	0.486	1.19	2.12	0.50	1.22	4.24

Water table fluctuation pattern. The emission response to daily, monthly and annual water table fluctuations was examined under the two source zone conditions discussed above (sources 50 and 200 cm below the initial water table). Figures 4.59 and 4.60 present the chemical emissions responses to water table oscillations of different frequencies and magnitudes. In these two figures, dynamic steady state chemical emission rates are normalized to emission rates under static water table conditions for each set of conditions (E_{static} in Table 4.8). The emissions plotted here are dynamic steady state emissions and the time plotted on the x-axis is relative to the repeating water table elevation pattern and not to the initial start of the model run.

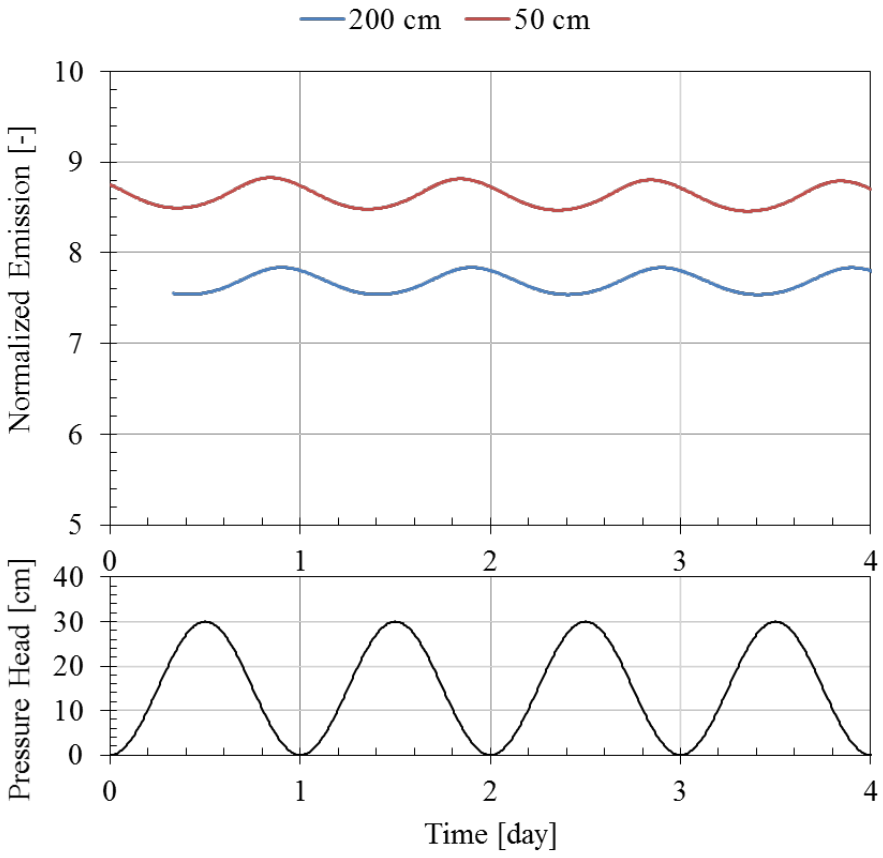

Figure 4.59 (a) – Daily fluctuation

Figure 4.59 a and b-c below. Dynamic steady state TCE emissions normalized to static water table condition emissions. Simulation results for 30 cm water table fluctuations and a contaminant source located 50 and 200 cm below the water table. Various water table fluctuation frequencies are shown (a) daily fluctuation, (b) monthly fluctuation and (c) annual fluctuation. Water pressure head is plotted relative to the initial water table elevation at the bottom boundary vs. time.

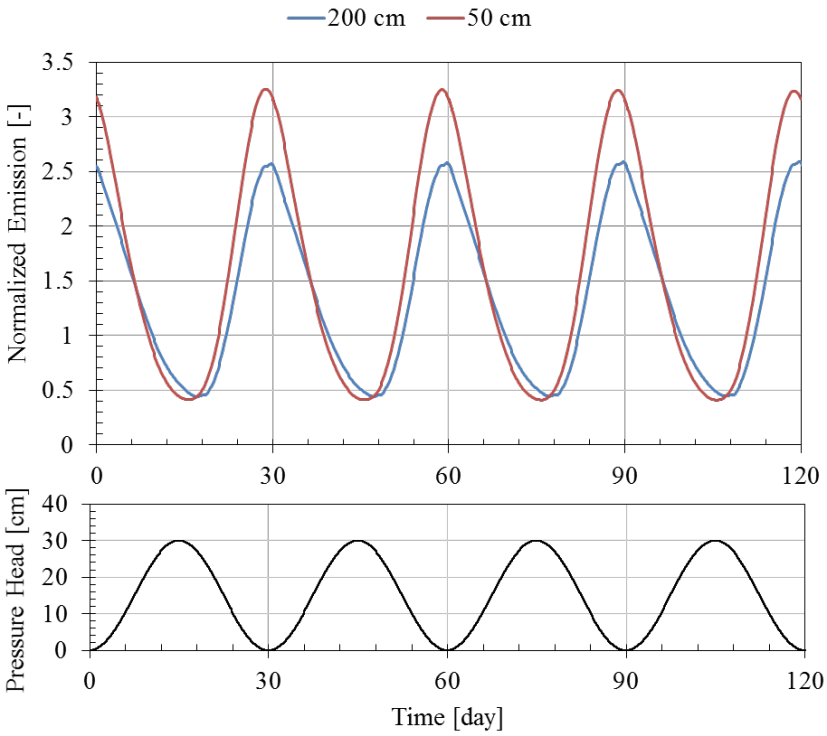

Figure 4.59 (b) – Monthly fluctuation

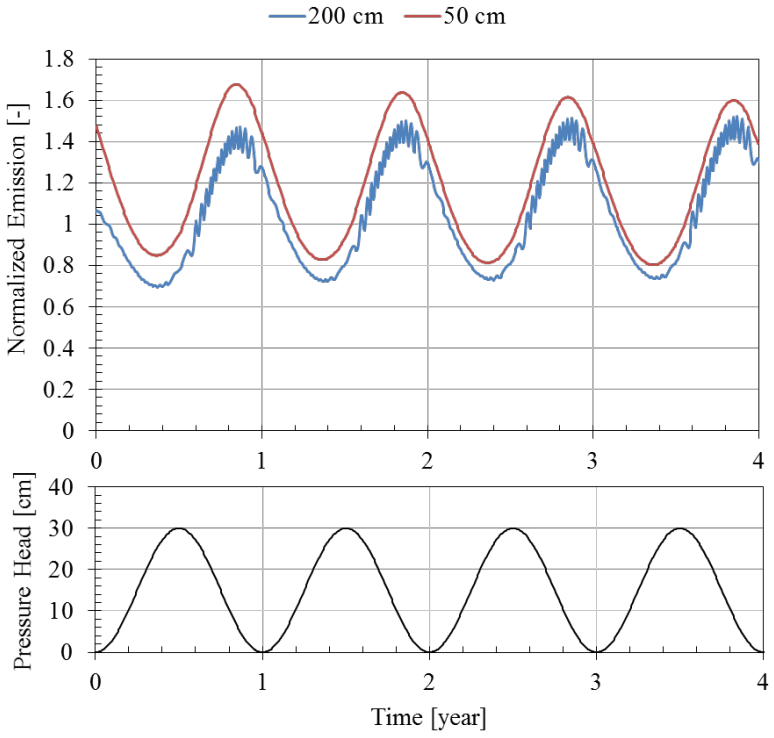

Figure 4.59 (c) – Annual fluctuation

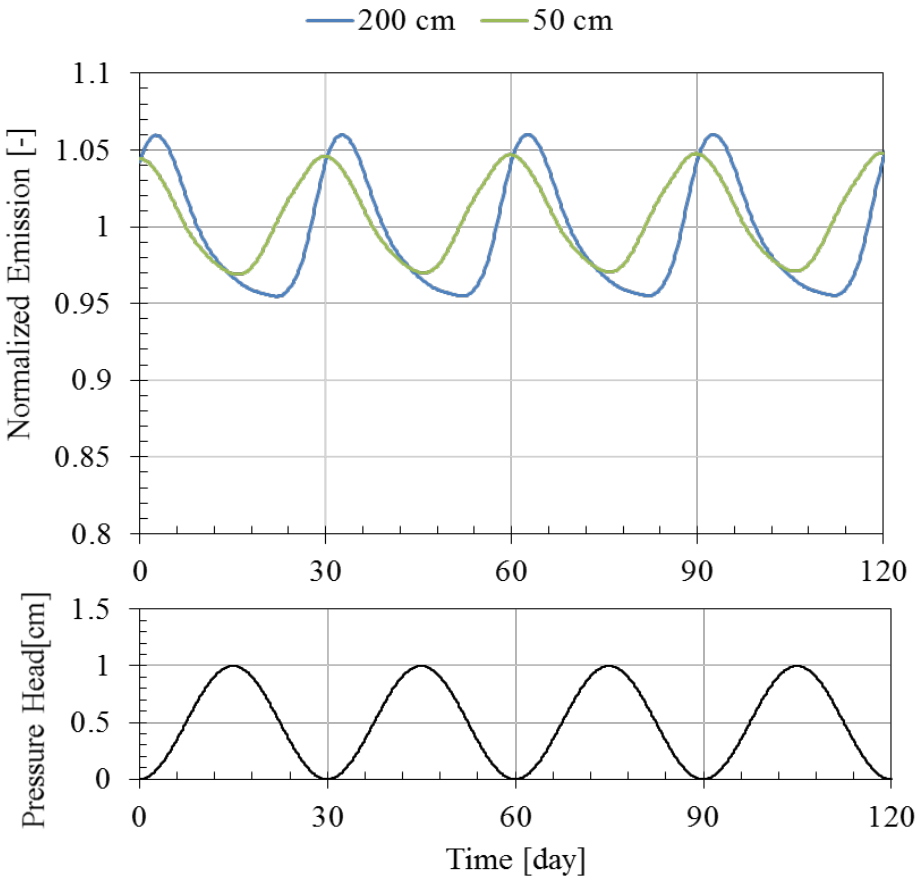

Figure 4.60 (a) – 1 cm water table fluctuation

Figures 4.60 a and b-c below. Dynamic steady state TCE emissions normalized to initial static water table condition emissions. Simulation results for monthly water table fluctuations of (a) 1 cm, (b) 30 and (c) 100 cm magnitude, where the source zone is located at 50 cm below water table and 200 cm below water table. Water pressure head is plotted relative to the initial water table elevation at the bottom boundary vs. time.

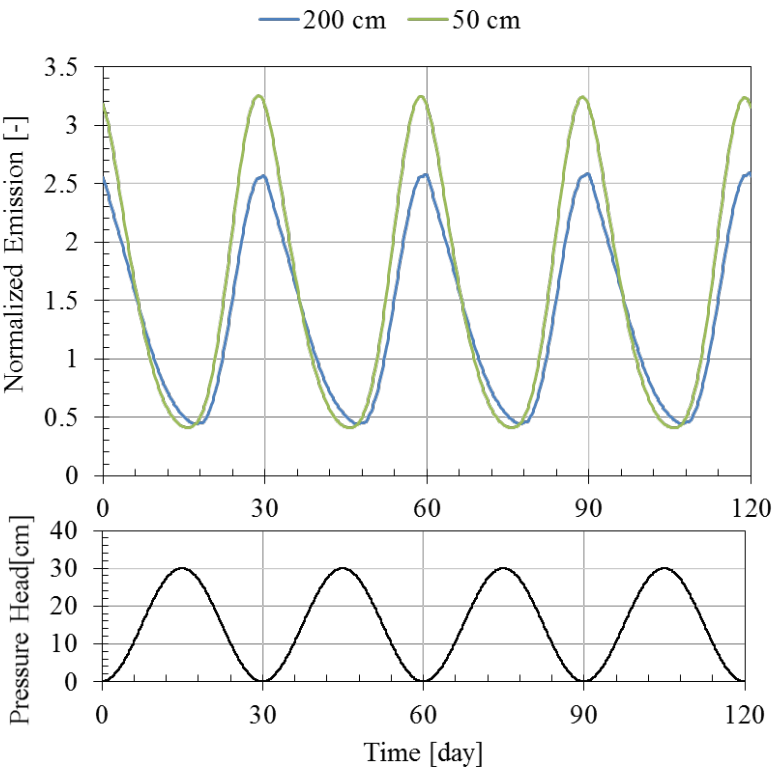

Figure 4.60 (b) – 30 cm water table fluctuations

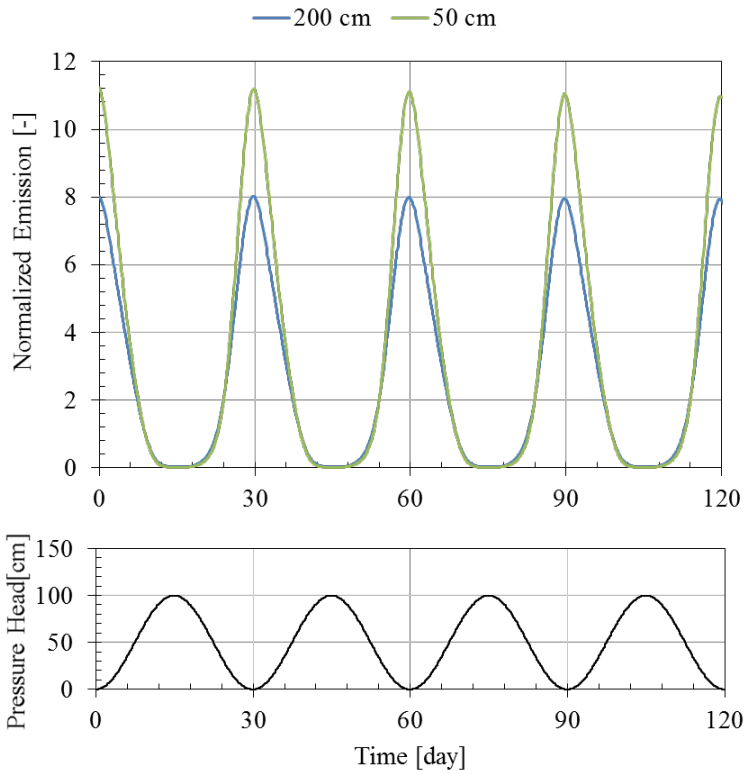

Figure 4.60 (b) – 100 cm water table fluctuations

The following observations come from those simulation results and Table 4.8:

- Larger magnitude water fluctuations over shorter periods resulted in more advective mass flux into the water table fluctuation region and result in increased long-term VOC emissions. E_{mean}/E_{static} increased with decreasing water table oscillation period (P) from years to days, and with increasing water table fluctuation magnitude (L) from 1 cm to 100 cm. The most significant increases were found at daily oscillations, for which simulated E_{mean}/E_{static} were 10.99 and 7.67 for 50 cm and 200 cm source depths below the initial water table level, respectively.

- The temporal variability in emissions can also be evaluated using E_{max}/E_{min} values. These values increased with increasing water table fluctuation magnitude from 1 cm to 100 cm. Over two orders of magnitude variation was found under 100 cm monthly water table oscillations. While E_{max}/E_{min} values were less predictable regarding oscillation frequency, the temporal changes were all less than 8X for 30 cm water table fluctuation simulations.

E_{mean}/E_{static} is >1 for all simulations. This suggests that models assuming static water table conditions will likely underestimate long-term average emissions and VI impacts, although that difference between the simulations with and without water table fluctuations is <50% for most cases modeled.

Vadose zone thickness. Figure 4.61 presents TCE emissions for 50 cm, 150 cm and 500 cm vadose zone thicknesses. E_{max}/E_{min} values increased as the depth to groundwater decreased. From a 500 cm vadose zone thickness to a 50 cm thickness, E_{max}/E_{min} increases from 1.24 to 25.6 for a source zone 50 cm below the water table, and from 1.19 to 23.3 for a source zone 200 cm below water table.

The greatest E_{mean}/E_{static} values (34.4 and 135.9) were found for simulations with 50 cm vadose zone thickness. This reflects the contributions of two factors: smaller diffusion distances that decrease significantly during the water table fluctuation cycle and less mass storage between the emission point and ground surface. Overall, the most significant temporal changes and long-term emission increases were found for simulations with $D_{vadose} =$ 50 cm, so attention should be paid when assessing shallow water table VI sites.

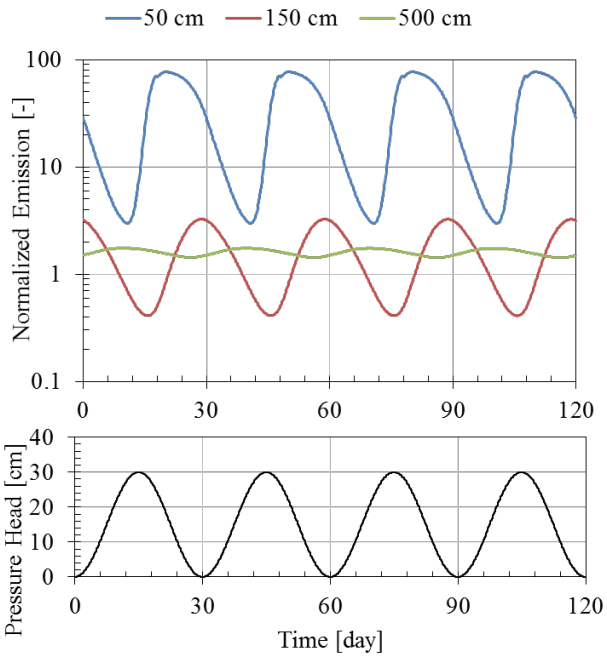

(a) Source 50 cm below water table

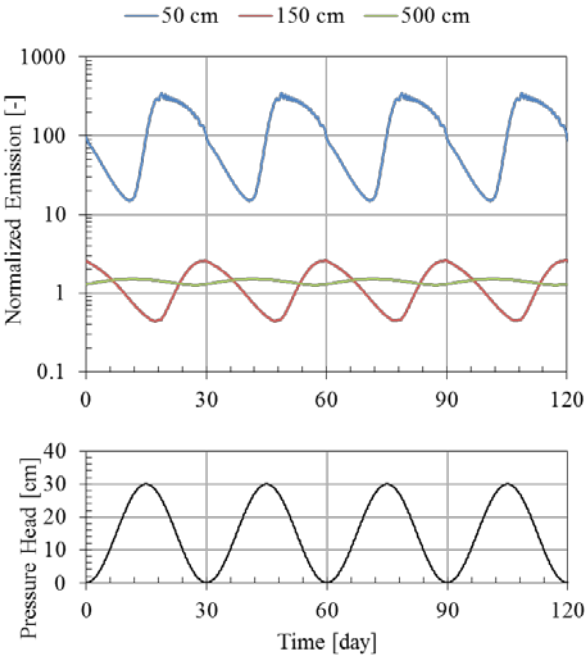

(b) Source 200 cm below water table

Figure 4.61 a and b. Dynamic steady state TCE emissions normalized to static water table condition emissions. Simulation results for scenarios with vadose zone thicknesses of 50, 150 and 500 cm where (a) the source zone is 50 cm and (b) 200 cm below water table. Water pressure head is plotted relative to the initial water table elevation at the bottom boundary vs. time.

Soil types. Simulations were run for three types of soil (coarse sand, sand, and loam) under monthly 30 cm water table oscillations. The estimated capillary rise for each is about 5 cm, 20 cm and over 200 cm, respectively. The normalized TCE emissions are shown in Figure 4.62. E_{max}/E_{min} values were greater for the coarse sand than loam - indicating more temporal variability. This is because the flow of water (up and down) responds more quickly and completely to head changes in the higher permeability soil. As the permeability decreases, the actual water level rise and fall (not the head changes) are dampened (slower and of smaller magnitude). This can be seen in the out-of-phase emissions behavior for loam in Figure 4.62.

The E_{max}/E_{min} values that were close to unity for the finer-grained loam soil are consistent with observations from the field site which had fine-grained silts and clays. The E_{mean}/E_{static} values were greater for loam than the other two types of soil – indicating greater amplification of emissions relative to a static water table case.

Chemical properties. The influences of effective absorption coefficient (k_s), Henry's law constant (H_i), and the diffusion coefficients in air and water (D_{air} and D_{water}) were tested by varying the reference chemical (TCE) properties by two orders of magnitude for H_i and 4X for diffusion coefficients. The normalized emissions are shown in Figures 4.63 to 4.66. Overall, changing the chemical properties had little effect on long-term average emission levels, as E_{mean}/E_{static} values varied less than 100 % from static water level results. In general:

- Water table fluctuations caused greater emission rate changes for more volatile chemicals. When H_i increased about 100X, the E_{max}/E_{min} values increased about 5X for both source zone conditions. This is consistent with the laboratory observations, where TCE emissions increases were greater than those for 1,2-DCA in all tests by about 2X and the H_i values differed by about 10X.

- k_s values equal to 0, 1 and 10 cm^3-H_2O/g-soil were input for monthly 30 cm water table fluctuations in sand. Partitioning between soil organic matter and water/gas can be seen as a buffering effect that reduces variation. As seen, the amplitude of TCE emissions decreased when k_s changed from 0 to 10 cm^3-H_2O/g-soil.

- As shown in Table 4.8 and Figures 4.64 and 4.65, increasing magnitude in emission fluctuations is likely to occur for lower D_{water} and higher D_{air}. Greater E_{max}/E_{min} values are found when D_{water} was set at 50% of TCE properties vs. set at 2X greater. High D_{air} values lead to greater temporal variations, approximately 10X variations were found when D_{air} value was set at 568.8 cm^2/h, whereas only 4X differences are found for the simulations using a D_{air} value of 142.2 cm^2/h.

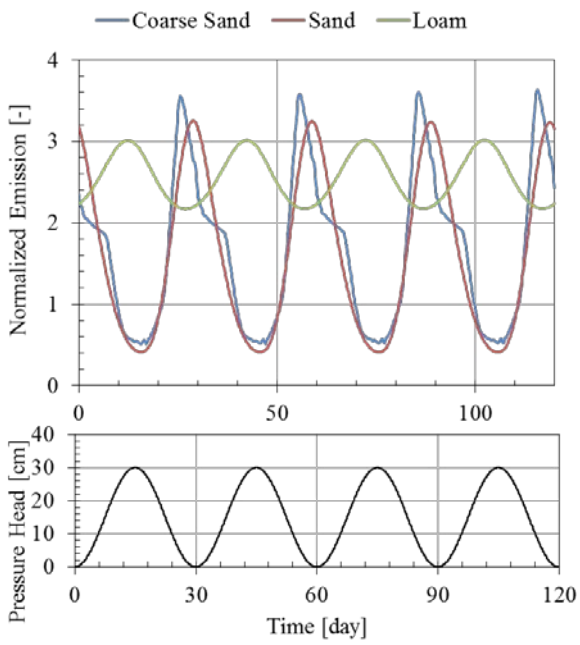

(a) Source 50 cm below water table

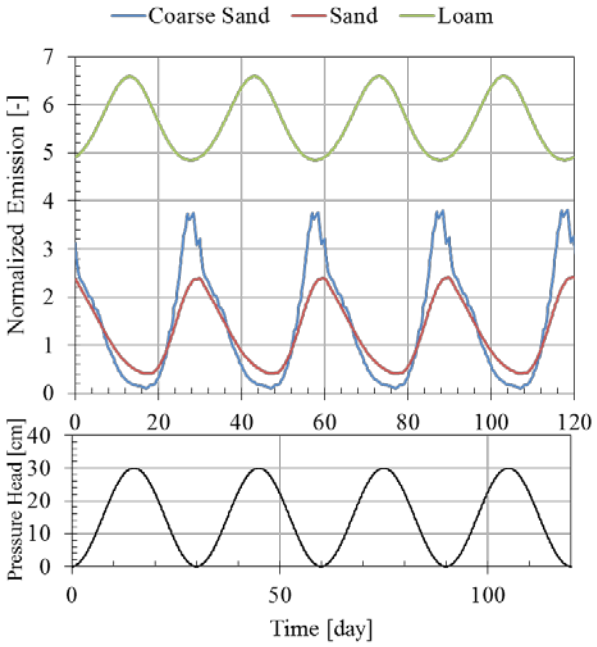

(b) Source 50 cm below water table

Figure 4.62 a and b. Dynamic steady state TCE emissions normalized to initial static water table condition emissions. Simulation results for scenarios with monthly water table fluctuations at coarse sand, sand and loam soils, and the source zone a) 50 cm below water table and (b) 200 cm below water table. Water pressure head is plotted relative to the initial water table elevation at the bottom boundary vs. time.

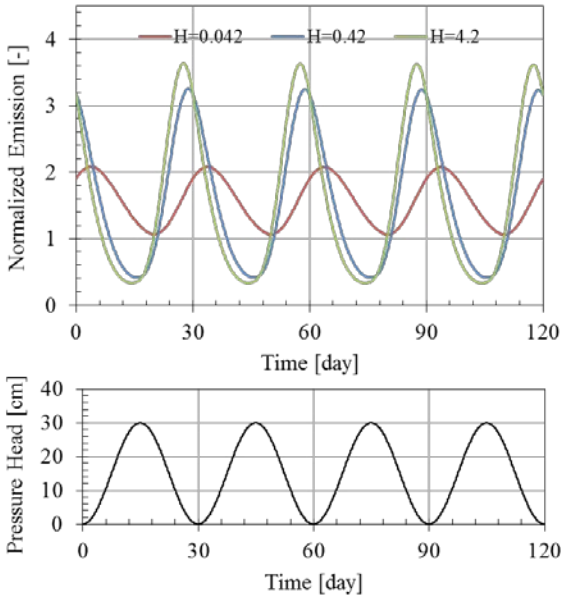

(a) Source 50 cm below water table

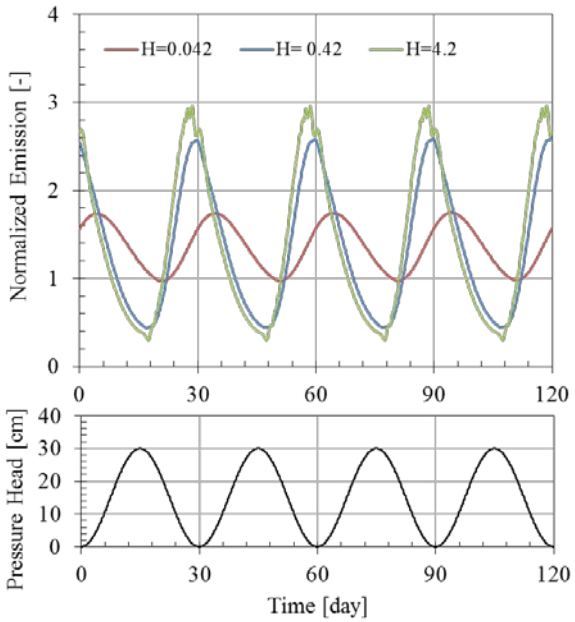

(b) Source 200 cm below water table

Figure 4.63. Dynamic steady state TCE emissions normalized to static water table condition emissions. Simulation results for scenarios with monthly water table fluctuations and Henry's Law constant values of 0.042, 0.42 and 4.2, and the source zone a) 50 cm below water table and (b) 200 cm below water table. Water pressure head is plotted relative to the initial water table elevation at the bottom boundary vs. time.

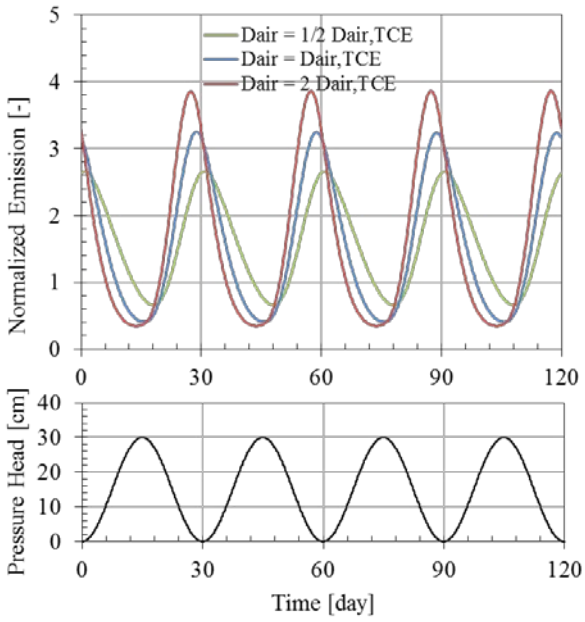

(a) Source 50 cm below water table

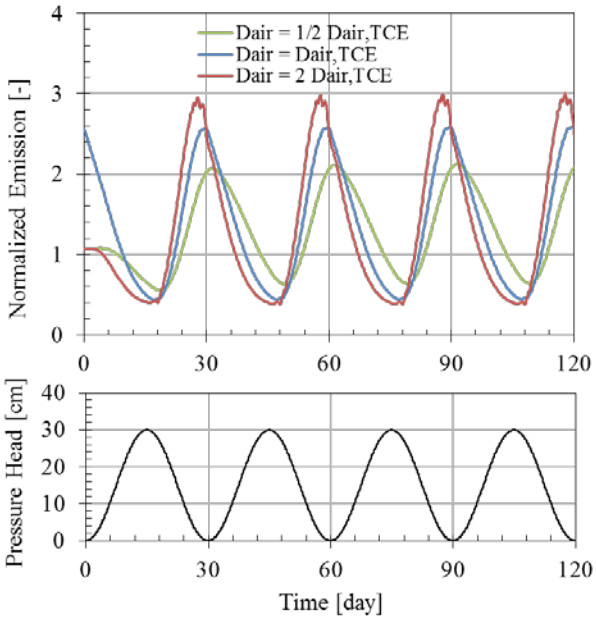

(b) Source 200 cm below water table

Figure 4.64 a and b. Dynamic steady state TCE emissions normalized to static water table condition emissions. Simulation results for scenarios with monthly water table fluctuations and chemical molecular diffusion coefficients in air of 0.142.2, 284.4 and 568.8 cm^2/h, and the source zone a) 50 cm below water table and (b) 200 cm below water table. Water pressure head is plotted relative to the initial water table elevation at the bottom boundary vs. time.

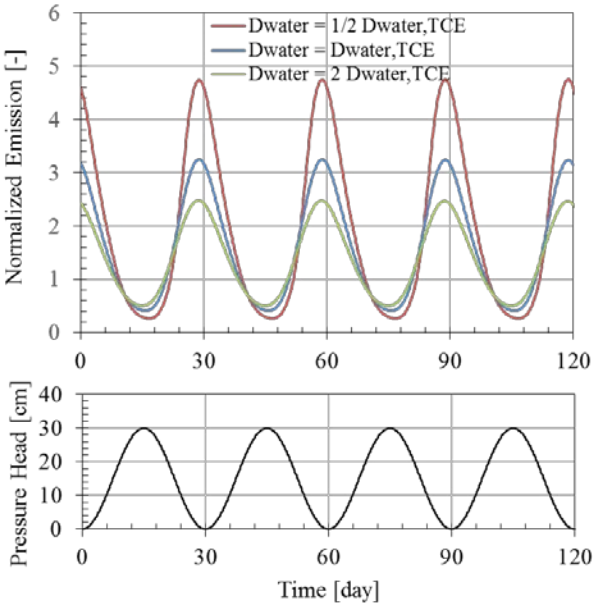

(a) Source 50 cm below water table

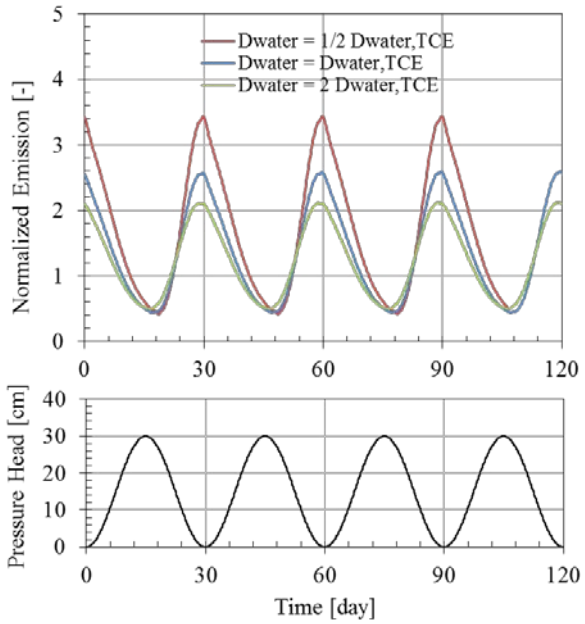

(b) Source 200 cm below water table

Figure 4.65 a and b. Dynamic steady state TCE emissions normalized to static water table condition emissions. Simulation results for scenarios with monthly water table fluctuations and chemical molecular diffusion coefficients in water of 0.016, 0.033 and 0.066 cm^2/h, and the source zone a) 50 cm below water table and (b) 200 cm below water table. Water pressure head is plotted relative to the initial water table elevation at the bottom boundary vs. time.

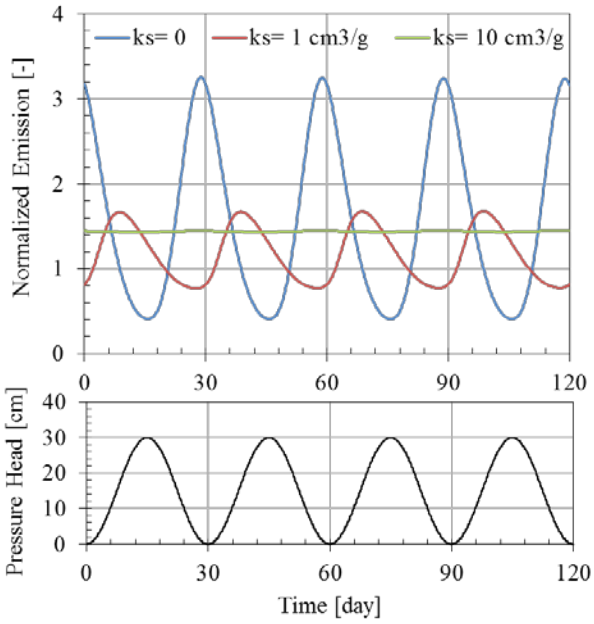

(a) Source 50 cm below water table

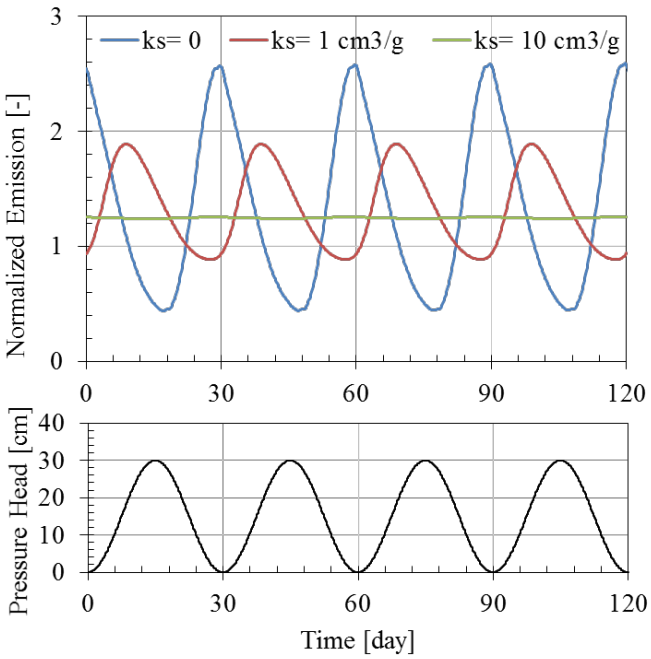

(b) Source 200 cm below water table

Figure 4.66 a and b. Dynamic steady state TCE emissions normalized to static water table condition emissions. Simulation results for scenarios with monthly water table fluctuations and effective sorption coefficients of 0, 1 and 10 L/kg, and the source zone at a) 50 cm below water table and (b) 200 cm below water table. Water pressure head is plotted relative to the initial water table elevation at the bottom boundary vs. time.

4.5.8 **Implications of water table fluctuations on VI assessment**

This section focused on improving our understanding of the connection between temporal changes in water table fluctuations and vapor intrusion (VI) impacts. With respect to the two main issues: a) identifying conditions for which temporal variations in emissions will and will not be significant, and b) identifying scenarios where fluctuating groundwater tables produce emissions that are significantly different from the base-case static water table scenario:

- Water table fluctuations will cause temporal changes in emission rates from dissolved plumes, but in many cases the short- and long-term average magnitude of these changes may be small relative to observed temporal variability in VI impacts (Folkes et al. 2009, USEPA, 2012b, Holton et al. 2013) caused by other factors like time-varying indoor-outdoor pressure differentials. For example, temporal variations in emissions calculated by two different methods for the field site were 50% or less about the long-term average, while indoor air concentrations varied by two to three orders-of-magnitude under natural conditions.

- For the scenarios examined in the simulation exercise, the long-term mean emission rate was greater, but usually within about 50% of the emissions for the static water table case. Exceptions occurred in cases with high frequency water table fluctuations (e.g., daily oscillations in simulations #3 and #20) and large water table elevation changes relative to the vadose zone thickness (e.g., simulations #6 and #23 with 30 cm fluctuations and 50 cm vadose zone; and simulations #5 and #22 with 100 cm fluctuations and 150 cm vadose zone).

- Short-term peak increases in emissions measured in laboratory experiments were less than about 4X the base case with a static water table. The E_{max}/E_{min} ratio for most simulation results was less than this as well except in conditions with greater amplitude water table fluctuations (e.g., 100 cm oscillations in simulations #5 and #22), shallower vadose zones (e.g., simulations #9 and #26 with coarse sand). It should be noted that scenarios with higher E_{max}/E_{min} ratios did not always have high long-term increases in emissions. For example, for simulation scenario #5 with E_{max}/E_{min} = 1687, the long-term mean was only 3.26X greater than the emission rate with a static groundwater table.

While more simulations are needed to explore a fuller range of conditions, the field data, lab results, and model simulation output suggest that the scenarios most likely to result in significant temporal changes in emission rates (10X or greater) and rates that are greatly amplified relative to static water table conditions are those involving water table fluctuations that are large relative to the vadose zone thickness; either because the groundwater is shallow (<1 m below ground surface) and fluctuations are moderate (e.g., 50 cm at any reasonable frequency) or because the groundwater table is deeper and the magnitude of fluctuations is larger and significant relative to the average vadose zone thickness.

5 CONCLUSIONS AND IMPLICATIONS FOR FUTURE RESEARCH AND IMPLEMENTATION

5.1 SUMMARY OF RESEARCH

Prior to this study, it was recognized that there could be temporal variability in VI pathway assessment data; however, our knowledge of temporal variability was limited to a few studies focused on high-frequency radon and quarterly and monthly VOC sampling. Thus, the significance of temporal variability and how to account for it in VI pathway assessment were poorly understood.

This project provides the first high-frequency and long-term data from a CHC-impacted VI site. The data include indoor air CHC and radon concentrations (every 2-4 h), differential pressure (indoor air - outdoor air, and indoor air - sub-foundation soil gas, every 2 min), building air exchange rates (every 20 min), synoptic soil gas and groundwater concentrations and elevations (every 1-3 months), and meteorological information (every 10 min). The data collected under natural conditions were used to assess the implications of using conventional approaches for assessing VI impacts.

Long-term high-frequency data were also collected under controlled building under-pressurization conditions. This was done to assess the potential utility of controlled pressure method (CPM) tests to replace conventional indoor air sampling under natural conditions. Those data, in combination with the data collected under natural conditions, provided the first opportunity to compare CPM test results with long-term indoor air concentrations and emission rates from monitoring conducted under natural conditions.

This study also provided an opportunity for the first field site analysis of CHC emission rates over time from groundwater with a fluctuating water table. Those results were combined with results from lab-scale experiments and modeling to assess the impact of fluctuating groundwater table elevations on emissions from dissolved groundwater plumes.

5.2 GENERAL CONCLUSIONS AND IMPLICATIONS FOR PRACTICE

This project focused on five primary research topics as discussed in the introduction to this report. These topics and their corresponding conclusions are summarized below:

<u>Temporal variability of indoor air concentrations:</u>

- Indoor air TCE concentrations spanning three orders-of-magnitude (<0.01 – 10 ppb_v) were measured, with both “active” and “inactive” VI periods (section 4.1.1). Active VI periods were prevalent in the late fall to early spring months and involved time-varying impacts with irregular periods of inactivity. In contrast, inactive VI periods were common in the late spring to early fall months and were characterized by long periods of inactivity with sporadic short-term concentration increases.

- The data were used to evaluate three typical indoor air sampling schemes and the analysis revealed that typical indoor air sampling plans are likely to mischaracterize the occurrence and magnitude of short- and long-term VI exposure at houses like the study house (section 4.1.2).

- The implication for practice is that conventional sparse point-in-time sampling protocols under natural conditions are not likely to provide robust characterization of intermediate- and long-term VI exposures at CHC sites. Thus, there is a need to utilize alternate approaches that provide more robust measures of VI occurrence and exposure, and preferably within short periods of time and at low cost. The controlled pressure method (CPM) discussed below is one alternative, and might be implemented in combination with follow-on longer-duration integrative or passive sampling at sites with CPM results that exceed threshold levels of concern.

Spatial and temporal variability in sub-slab and near-foundation soil gas:

- Results showed increasing temporal and spatial variability as the soil gas sampling point moves from the vapor source depth to ground surface, with variability of a factor of about 2X near the source and about 10X or more for sub-slab soil gas concentrations (section 4.2).

- The implication for practice is that shallow groundwater and deep soil gas concentrations may be more reliable than shallow soil gas data for screening potential VI impacts at CHC sites (section 4.2).

Indoor chemical sources:

- The indoor release of an inert tracer gas led to the creation of a soil gas plume beneath the house; thus, similar behavior is expected for indoor chemical sources (section 4.3.1).

- The implication for practice is that the detection of chemicals of concern in soil gas and indoor air should not be taken as conclusive evidence of VI impacts from subsurface sources, as is often assumed in VI pathway data analysis today.

- Indoor source removal tests and simulation results show that indoor air concentrations will likely respond quickly to source removal over several hours, but it may take several days to weeks for soil gas plumes created by indoor sources to dissipate (section 4.3.3 and 4.3.4).

- The implication for practice is that waiting times for VI pathway assessment data collection longer than the typically prescribed day or two are needed after indoor sources are removed.

Investigation of alternate assessment approaches – controlled pressure method (CPM) testing:

- Indoor air concentrations collected under CPM conditions were relatively constant over about a year and they were in close agreement with maximum indoor air concentrations under natural conditions (section 4.4.1).

- In contrast to sparse indoor air sampling under natural conditions, there were no false-negative results and the results were independent of the date and time of sampling (section 4.4.2).

- In comparison to the long-term average concentration under natural conditions, CPM results were one to two orders-of-magnitude higher (section 4.4.3).

- The presence of a significant alternative VI pathway (a buried land drain lateral pipe) was not evident in data collected under natural conditions, and was only detected during CPM testing.

- The implication for practice is that CPM testing offers a more reliable and robust short-term option for assessing VI occurrence and its maximum impact than conventional indoor air sampling under natural conditions.

Changes with time in vapor emissions from chlorinated solvent groundwater plumes:

- Lab experiments and mathematical modeling showed that groundwater table elevation changes with time can result in increased CHC emissions from dissolved groundwater plumes relative to emissions from static water table conditions (section 4.5).

- Experiments and modeling suggest that long-term average emission increases from dissolved groundwater plumes due to groundwater table elevation changes are likely to be less than 2X for most site conditions, and this is consistent with results from the study house (section 4.5.3 and 4.5.7).

- Modeling results suggest that CHC emissions from dissolved groundwater plumes can be up to about 10X greater than expected for static water table conditions under a limited set of conditions: shallow water tables (<1 m below ground surface) and high-frequency groundwater table elevation changes (daily-monthly) (section 4.5.7).

- The results suggest that groundwater table fluctuations were not a significant contributor to the one to three orders-of-magnitude concentration variability observed at the study site.

- The practical implication is that groundwater table elevation movement should not be considered a major factor in VI pathway assessment plan design at dissolved plume sites, unless the groundwater table is shallow and elevation fluctuations are frequent. It should be noted that groundwater table elevation changes could be a major factor at

sites overlying non-aqueous phase liquid (NAPL) source zones, if the water table elevation changes lead to periodic exposure and submersion of the source zone. This specific scenario was not evaluated in this work and additional study is needed.

5.3 RECOMMENDATIONS FOR FUTURE WORK

Project ER-1686 provides valuable information for improving the current VI assessment paradigm. The results also raise a number of questions that should be considered in future research projects. These include:

- *Further study of controlled pressure method testing*. CPM test results from this study and McHugh et al. (2012) suggest that CPM tests can be a valuable diagnostic tool, and a possible replacement for conventional indoor sampling under natural conditions. Well-documented tests at other study sites would be useful for advancing this method and increasing confidence in its use. Standardization of test conditions (under-pressurization, duration, use of tracer gas, etc.) and documentation of costs are also needed. Finally, the testing to date has been at one CHC-impacted site and an understanding of the utility of this diagnostic tool at petroleum hydrocarbon-impacted sites is needed.

- *Mitigation System Effectiveness at Sites with Significant Alternative VI pathways*. During the long-term CPM study, an alternate VI pathway was discovered at the study site. The presence of alternative pathways (e.g. sewer pipe VI) have been recently reported at a few other sites, leading to the suspicion that alternative pathways may play significant roles at some sites with known VI impacts. The performance of conventional VI mitigation systems at sites with significant alternative pathways should be studied, as there are conceptual scenarios for which sub-slab depressurization can lead to increased sub-slab concentrations (e.g., in the case of the study house) and where sub-slab depressurization might not have any impact on VI impacts (e.g., in the case of sewer VI).

- *Groundwater Table Elevation Fluctuations and Their Effect on VI Impacts*. This work showed negligible effect of groundwater table fluctuations on VI impacts at the field site. Modeling work suggested that the only scenarios for which effects might be significant would be at shallow groundwater sites with daily to monthly fluctuation cycles (e.g., tidally-influenced aquifers). It would be useful to study the emissions vs. time behavior at one or more sites with those conditions.

6 BIBLIOGRAPHY

Abreu, L., Johnson, P.C. (2005). Effect of Vapor Source-Building Separation and Building Construction on Soil Vapor Intrusion as Studied with a Three-Dimensional Numerical Model. *Environmental Science and Technology*, *39* (12), 4550-4561.

Abreu, L., Johnson, P.C. (2006). Modeling the Effect of Aerobic Biodegradation on Soil Vapor Intrusion into Buildings - Influence of Degradation Rate, Source Concentration, and Depth. *Environmental Science and Technology*, *40* (7), 2304-2315.

Beckley, L., Gorder, K., Dettenmaier, E., Rivera-Duarte, I., & McHugh, T. (2014). On-site Gas Chromatography/Mass Spectrometry (GC/MS) Analysis to Streamline Vapor Intrusion Investigations. *Environmental Forensics*. *15*. 243-244.

California Department of Toxic Substances Control. (2011). *Guidance for the evaluation and mitigation of subsurface vapor intrusion to indoor air (Vapor intrusion guidance).*

Dettenmaier, E. and Gorder, K. Detailed Indoor Air Characterization and Interior Source Identification by Portable GC/MS. AWMA presentation, 30 September 2010.

EnviroGroup. 2008. Redfield Site Web Site. http://www.redfieldsite.org/index.php

Ferguson, C. C., Krylov, V. V., & McGrath, P. T. (1995). Contamination of Indoor Air by Toxic Soil Vapors: A Screening Risk Assessment Model. *Building and Environment*. *30* (3); 375-383.

Folkes, D., Wertz, W., Kurtz, J., Kuehster, T. (2009). Observed spatial and temporal distributions of CVOCs at Colorado and New York vapor intrusion sites. *Ground Water Monitoring and Remediation*, *29*, 70-80.

Garbesi, K., Sextro, R. G. (1989). Modeling and field evidence of pressure-driven entry of soil gas into a house through permeable below grade walls. *Environmental Science and Technology*, *23* (12), 1481-1487.

Gorder, K. A., & Dettenmaier, E. M. (2011). Portable GC/MS Methods to Evaluate Sources of cVOC Contamination in Indoor Air. *Ground Water Monitoring & Remediation, 31* (4), 116-119.

Hers, I., Zapf-Gilje, R., Evans, D., & Li, L. (2002). Comparison, Validation, and Use of Models for Predicting Indoor Air Quality from Soil and Groundwater Contamination. *Soil and Sediment Contamination, 11* (4), 491-527.

Hers, I., Zapf-Gilje, R., Johnson, P. C., & Li, L. (2003). Evaluation of the Johnson and Ettinger Model for Prediction of Indoor Air Quality. *Ground Water Monitoring and Remediation, 23* (1), 62-76.

Hers, I., Dawson, H., Truesdale, R. (2006). Status of Generic Screening Levels –Update on Empirical Vapor Attenuation Factor Analysis. AEHS Conference. San Diego. March 16. http://iavi.rti.org/WorkshopsAndConferences.cfm EPA/AEHS.

Hodgson, A. T., Garbesi, K., Sextro, R. G., & Daisey, J. M. (1992). Soil-Gas Contamination and Entry of Volatile Organic Compounds into a House Near a Landfill. *Journal of the Air & Waste Management Association*, *42* (3), 277-283.

Holton, C.; Luo, H., Dahlen, P., Gorder, K. A., Dettenmaier, E. M.; Johnson, P. C. 2013. Temporal variability of indoor air concentrations under natural conditions in a house overlying a dilute chlorinated solvent groundwater plume. *Environmental Science and Technology, 47*, 13347-13354.

Holton, C., Guo, Y., Luo, H., Dahlen, P., Gorder, K., Dettenmaier, E., Johnson, P. C. (2015). Long-term evaluation of the controlled pressure method for assessment of

Interstate Technology & Regulatory Council. (2007). *Vapor intrusion pathway: A practical guideline*. Washington, DC: Interstate Technology & Regulatory Council.

Johnson, P. C., Ettinger, R. A. (1991). Heuristic Model for Predicting the Intrusion Rate of Contaminant Vapors into Buildings. *Environmental Science and Technology*, *25* (8), 1445-1452.

Johnson, P. C., Bruce, C., Johnson, R. L., Kemblowski, M. W. (1998). In situ measurement of effective vapor-phase porous medium diffusion coefficient. *Environmental Science and Technology*, 32, 3405-3409.

Johnson, P. C., Kemblowski, M. W., Johnson, R. L. (1999). Assessing the Significance of Subsurface Contaminant Vapor Migration to Enclosed Spaces: Site-specific Alternatives to Generic Estimates. *Journal of Soil Contamination, 8* (3), 389-421.

Johnson, P.C., Ettinger, R. A., Kurtz, J., Bryan, R., Kester, J. E. (2002). Migration of soil gas vapors to indoor air: Determining vapor attenuation factors using a screening-level model and field data from the CDOT-MTL Denver, Colorado site. *American Petroleum Institute, 16,* 1-10.

Johnson, P.C. (2005). Sensitivity Analysis and Identification of Critical and Non-Critical Parameters for the Johnson and Ettinger Vapor Intrusion Model. *Ground Water Monitoring & Remediation, 25* (1), 63-78.

Little, J. C., Daisey, J. M., & Nazaroff, W. W. (1992). Transport of Subsurface Contaminants into Buildings: An Exposure Pathway for Volatile Organics. *Environmental Science and Technology*, *26*, 2058-2066.

Luo, H. (2009). Field and modeling studies of soil gas migration into buildings at petroleum hydrocarbon impacted sites (Dissertation). Arizona State University, Tempe, AZ.

Loureiro, C. O. (1987). Simulation of the steady state transport of radon from soil into houses with basements under constant negative pressure. Ph. D. Dissertation. University of Michigan.

Loureiro, C. O., Abriola, L. M., Martin, J. E., & Sextro, R. G. (1990). Three-dimensional Simulation of Radon Transport into Houses with Basements Under Constant Negative Pressure. *Environmental Science and Technology*, *24*, 1338-1348.

McCarthy, K. A.; Johnson, R. L. 1993. Transport of volatile organic compound across the capillary fringe. *Water Resources Research, 29* (6), 1675-1683.

McHugh, T. E., De Blanc, P. C., Pokluda, R. J. (2006). Indoor air as a source of VOC contamination in shallow soils below buildings. *Soil and Sediment Contamination, 15*, 103-122.

McHugh, T. E., Beckley, L., Bailey, D., Gorder, K., Dettenmaier, E., Rivera-Duarte, I., Brock, S., MacGregor, I. C. (2012). Evaluation of vapor intrusion using controlled building pressure. *Environmental Science & Technology, 46*, 4792-4799.

Nazaroff, W. W., Fuestel, H., Nero, A. V. Revzan, K. L., Grimsruf, D. T. (1985). Radon *transport* into a detached one-story house with a basement. *Environmental Science and Technology*, *19* (1), 31-46.

Nazaroff, W.W., H. Feustel, A. V. Nero, K. L. Revzan, D. T. Grimsrud. (1985). Radon Transport into a Detached One-Story House with a Basement. *Atmospheric Environment, 19*, 31-46.

Nazaroff, W. W. (1992). Radon transport from soil to air. *Reviews of Geophysics, 30* (2), 137-160.

New York State Department of Health. (2006). *Guidance for Evaluating Soil Vapor Intrusion in the State of New York*. Troy, NY: New York State Department of Health.

New York State Department of Health. (2008). *Endicott Area Investigations - Town of Union, Broome County, New York*. Troy, NY: New York State Department of Health.

Riley, W. J., Gadgil, A. J., Bonnefous, Y. C., & Nazaroff, W. W. (1996). The Effect of Steady Winds on Radon-222 Entry from Soil into Houses. *Atmospheric Environment*, *30* (7), 1167-1176.

Robinson, A. L., & Sextro, R. G. (1995). The Influence of a Subslab Gravel Layer and Open Area on Soil Gas and Radon Entry into Two Experimental Basements. *Health Physics*, *69* (3), 367-376.

Robinson, A. L., & Sextro, R. G. (1997). Radon Entry into Buildings Driven by Atmospheric Pressure Fluctuations. *Environmental Science and Technology, 31*, 1742-1748.

Sanders, P. F., & Stern, A. H. (1994). Calculation of soil cleanup criteria for carcinogenic volatile organic compounds as controlled by the soil-to-indoor air exposure pathway. *Environmental Toxicology and Chemistry*, 13(8), 1367-1373.

U.S. Environmental Protection Agency. (2000). Johnson and Ettinger (1991) Model for Subsurface Vapor Intrusion into Buildings (3-Phase System Models and Soil Gas Models). Washington, DC: U.S. Environmental Protection Agency.

U.S. Environmental Protection Agency. (2002). *OSWER draft guidance for evaluation the vapor intrusion to indoor air pathway from groundwater and soils (Subsurface vapor intrusion guidance)*. Washington, DC: U.S. Environmental Protection Agency.

U.S. Environmental Protection Agency. (2012). *EPA's vapor intrusion database: Evaluation and characterization of attenuation factors for chlorinated volatile organic compounds and residential buildings*. Washington, DC: U.S. Environmental Protection Agency.

U.S. Environmental Protection Agency. (2012). *Fluctuation of indoor radon and VOC concentrations due to seasonal variations*. Washington, DC: U.S. Environmental Protection Agency.

U.S. Environmental Protection Agency. (2015). *OSWER Technical Guidance for Assessing and Mitigating the Vapor Intrusion Pathway from Subsurface Vapor Sources to Indoor Air*. Washington, DC: U.S. Environmental Protection Agency.

U.S. Geological Survey. (1999). *New reporting procedures based on long-term method detection levels and some considerations for interpretations of water-quality data provided by the U.S. Geological Survey National Water Quality Laboratory*. Reston, VA: U.S. Geological Survey.

Wener, D.; Hohener, P. (2002). The influence of water table fluctuations on the volatilization of contamination from groundwater. *IAHS PUBLICATION*, 213-218.

Yao, Y., Shen, R., Pennell, K. G., Suuberg, E. M. (2013). A review of vapor intrusion models. *Environmental Science and Technology, 43*, 2457-2470.

APPENDIX A: SUPPORTING DATA

A.1. Introduction

This project included field investigation, laboratory experiments and numerical modeling analyses. These generated large data sets that are impractical for presentation in this document. Since these data sets are the first of their kind, other researchers may be interested in accessing them. Some of these data have already been published (see Appendix B for publications), and others are available upon request from either Dr. Yuanming Guo (Yuanming.guo@asu.edu), Dr. Chase Holton (chase.holton@ch2m.com) or Dr. Paul C. Johnson (pcjohnson@mines.edu).

A.4. Supplemental results from groundwater, soil gas, and air monitoring during natural conditions

Overview. The information presented below is supplemental to the results in section 4, predominantly sections 4.1 and 4.2. The data were collected under natural conditions from August 2010 to August 2012 at the study site described in section 3. The data are placed on a timeline consistent with previous publications (Holton et al., 2013; Holton et al., 2015), where time (t) = 0 being 8:00 AM on 8/15/2010 and are presented in order as they occur along the vapor intrusion (VI) pathway (e.g., groundwater -> soil gas -> indoor air). For details on the materials and methods used in collecting this data, see section 3.

Groundwater. Figure A.1 shows TCE concentrations in groundwater from interior (below foundation) sampling points from -11 < t < 744 d. These results are summarized in Table A.1. Similarly, Figure A.2 shows TCE concentrations from shallow exterior (outside the foundation) sampling points from -11 < t < 744 d. Table A.2 summarizes groundwater concentration data from exterior sampling points at shallow, mid-level, and deep sampling points. For more detail on the sampling network, see section 3.

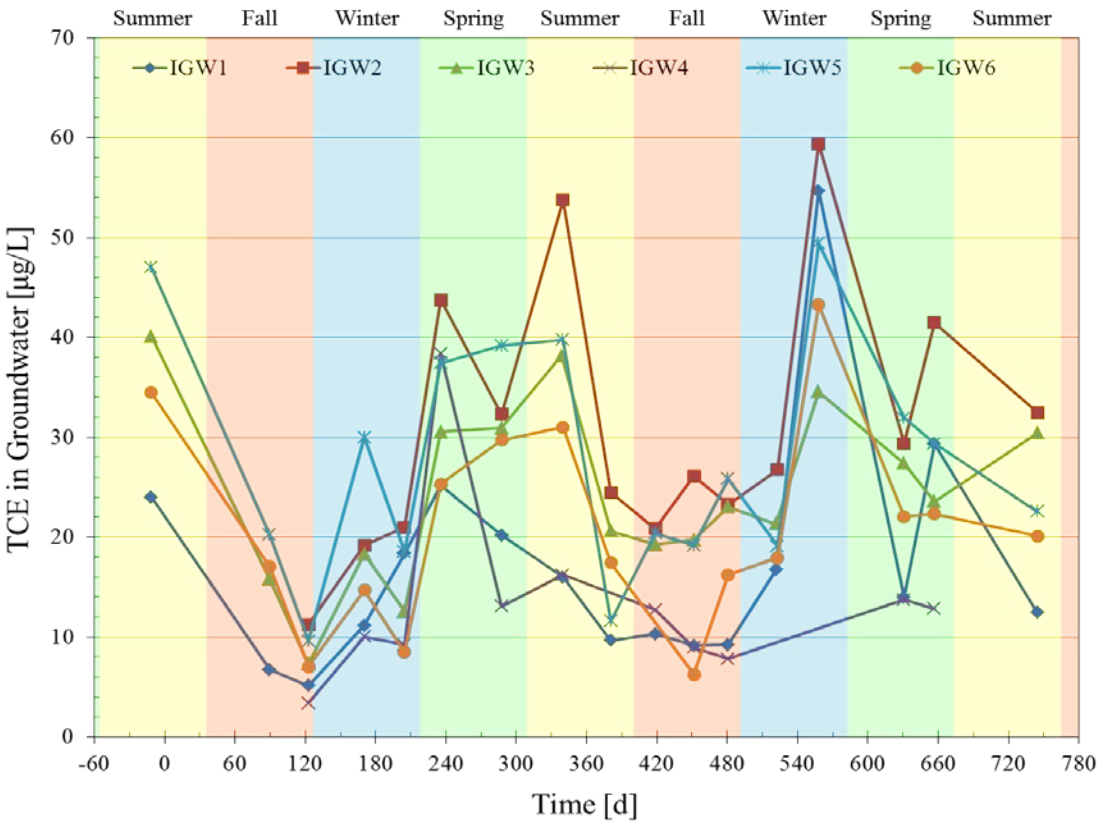

Figure A.1. TCE concentrations in groundwater at 2.7 m below-slab depth interior sampling points from August 2010 to August 2012.

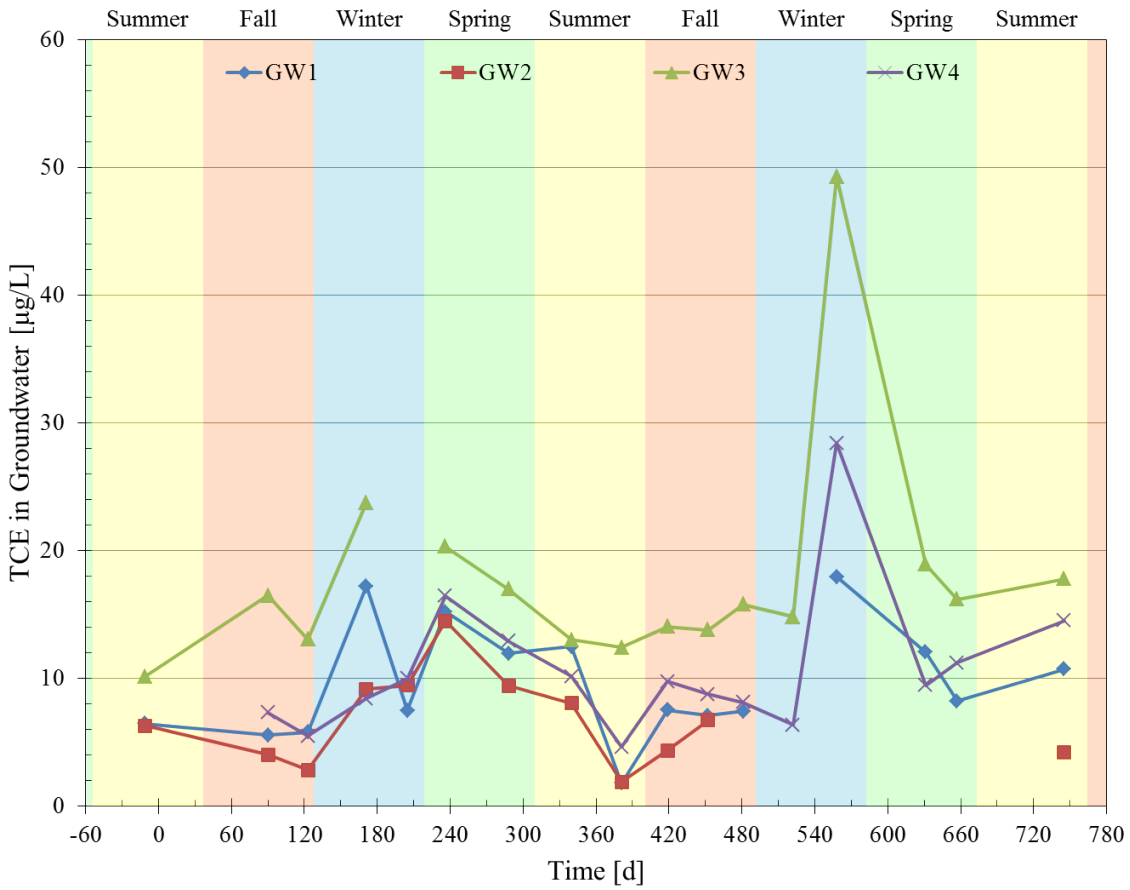

Figure A.2. TCE concentrations in groundwater at shallow exterior sampling points from August 2010 to August 2012.

Table A.1. Groundwater concentrations from samples collected at interior sampling locations and 2.7 m below-slab depths.

Date	Time [d]	TCE Concentration in Groundwater Samples [µg/L]					
		IGW1	IGW2	IGW3	IGW4	IGW5	IGW6
8/4/2010	-11	23.98	NS	40.12	NS	47.00	34.47
11/13/2010	90	6.73	NS	15.80	NS	20.22	17.05
12/16/2010	123	5.13	11.24	7.29	3.38	9.60	7.05
2/2/2011	171	11.16	19.18	18.33	10.03	29.98	14.72
3/8/2011	205	18.36	20.97	12.55	9.22	18.56	8.49
4/8/2011	236	25.17	43.75	30.54	38.40	37.44	25.31
5/30/2011	288	20.17	32.29	30.93	13.05	39.16	29.73
7/21/2011	340	15.98	53.77	38.16	16.23	39.77	30.99
8/31/2011	381	9.66	24.45	20.62	NS	11.57	17.40
10/8/2011	419	10.31	20.83	19.24	12.73	20.38	NS
11/10/2011	452	9.15	26.11	19.72	8.94	19.18	6.27
12/9/2011	481	9.23	23.26	23.04	7.83	25.84	16.24
1/19/2012	522	16.70	26.76	21.30	NS	19.09	17.93
2/24/2012	558	54.65	59.39	34.54	NS	49.42	43.26
5/7/2012	631	13.97	29.37	27.40	13.74	31.95	22.07
6/2/2012	657	29.34	41.47	23.56	12.84	29.36	22.31
8/29/2012	745	12.43	32.48	30.40	NS	22.55	20.12
Average		17.18	31.02	24.33	13.31	27.71	20.84
NS = No sample available							

Table A.2. Groundwater concentrations from samples collected at exterior locations at shallow (S), mid-level (M), and deep (D) sampling points.

Date	Time [d]	TCE Concentration in Groundwater Samples [µg/L]											
		GW1-S	GW1-M	GW1-D	GW2-S	GW2-M	GW2-D	GW3-S	GW3-M	GW3-D	GW4-S	GW4-M	GW4-D
8/4/2010	-11	6.44	71.60	13.23	6.28	25.79	2.05	10.14	22.56	22.69	NS	24.07	40.94
11/13/2010	90	5.56	23.37	10.06	4.01	19.61	3.53	16.49	28.05	12.58	7.31	9.15	27.47
12/16/2010	123	5.78	30.42	12.42	2.82	26.66	4.38	13.05	12.41	16.91	5.47	17.83	NS
2/2/2011	171	17.21	39.18	19.80	9.14	29.21	7.48	23.76	21.90	19.59	8.43	29.04	31.71
3/8/2011	205	7.48	25.10	15.39	9.43	23.64	6.75	NS	27.46	32.56	9.98	22.21	21.64
4/8/2011	236	15.23	18.20	7.75	14.48	28.64	10.67	20.31	36.85	39.35	16.45	43.54	42.18
5/30/2011	288	11.95	41.90	11.35	9.42	29.01	3.23	16.99	25.78	29.89	12.93	40.42	44.87
7/21/2011	340	12.49	42.78	22.10	8.04	32.38	4.32	13.02	20.33	26.02	10.14	33.90	70.29
8/31/2011	381	1.77	37.59	1.69	1.87	9.83	1.17	12.41	12.61	9.19	4.63	24.29	45.53
10/8/2011	419	7.51	45.82	3.57	4.36	34.05	4.83	14.04	23.03	33.24	9.74	25.87	52.63
11/10/2011	452	7.09	24.61	9.15	6.72	37.90	5.67	13.79	15.53	21.91	8.76	13.93	22.77
12/9/2011	481	7.40	42.60	10.32	NS	32.66	5.34	15.77	28.74	24.62	8.13	15.65	33.65
1/19/2012	522	NS	52.73	5.68	NS	43.70	5.82	14.83	26.90	21.40	6.35	42.77	44.37
2/24/2012	558	17.94	75.29	26.87	NS	52.14	9.07	49.31	48.77	43.30	28.42	105.57	81.49
5/7/2012	631	12.06	41.54	11.82	NS	34.58	2.95	18.91	21.15	31.02	9.44	42.45	44.37
6/2/2012	657	8.23	59.51	12.33	NS	66.90	4.25	16.20	24.14	31.49	11.21	50.85	56.17
8/29/2012	745	10.72	51.23	13.30	4.23	38.62	5.60	17.78	21.66	25.28	14.50	38.89	39.51
Average		9.68	42.56	12.17	6.73	33.25	5.12	17.93	24.58	25.94	10.74	34.14	43.72
NS = No sample available													

Soil Gas. During field survey events, soil gas was analyzed for the suite of chlorinated volatile organic compounds (CVOCs) discussed in section 3. Figures A.3-A.18 present multi-depth contour plots of TCE concentrations in soil gas at sub-slab (SS), 0.9 m below-slab (BS), and 1.8 m BS depths. The plots were generated using Surfer 12 software (Golden Software, Golden, CO). The Kriging gridding method provided in the software was used to interpolate soil gas concentrations between monitoring points.

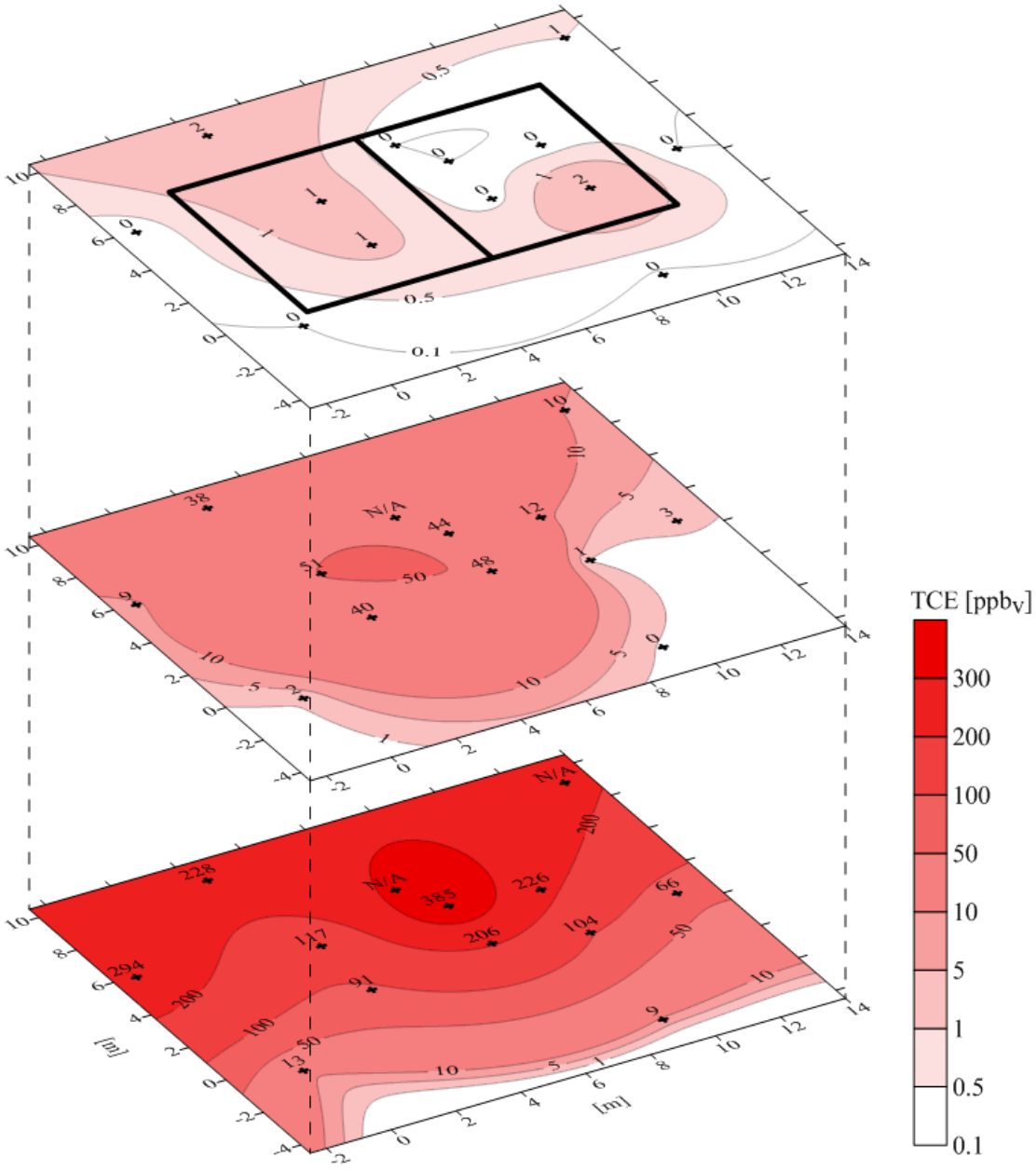

Figure A.3. Multi-depth contour plot of TCE in soil gas for samples collected and analyzed from August 7th to August 10th, 2010.

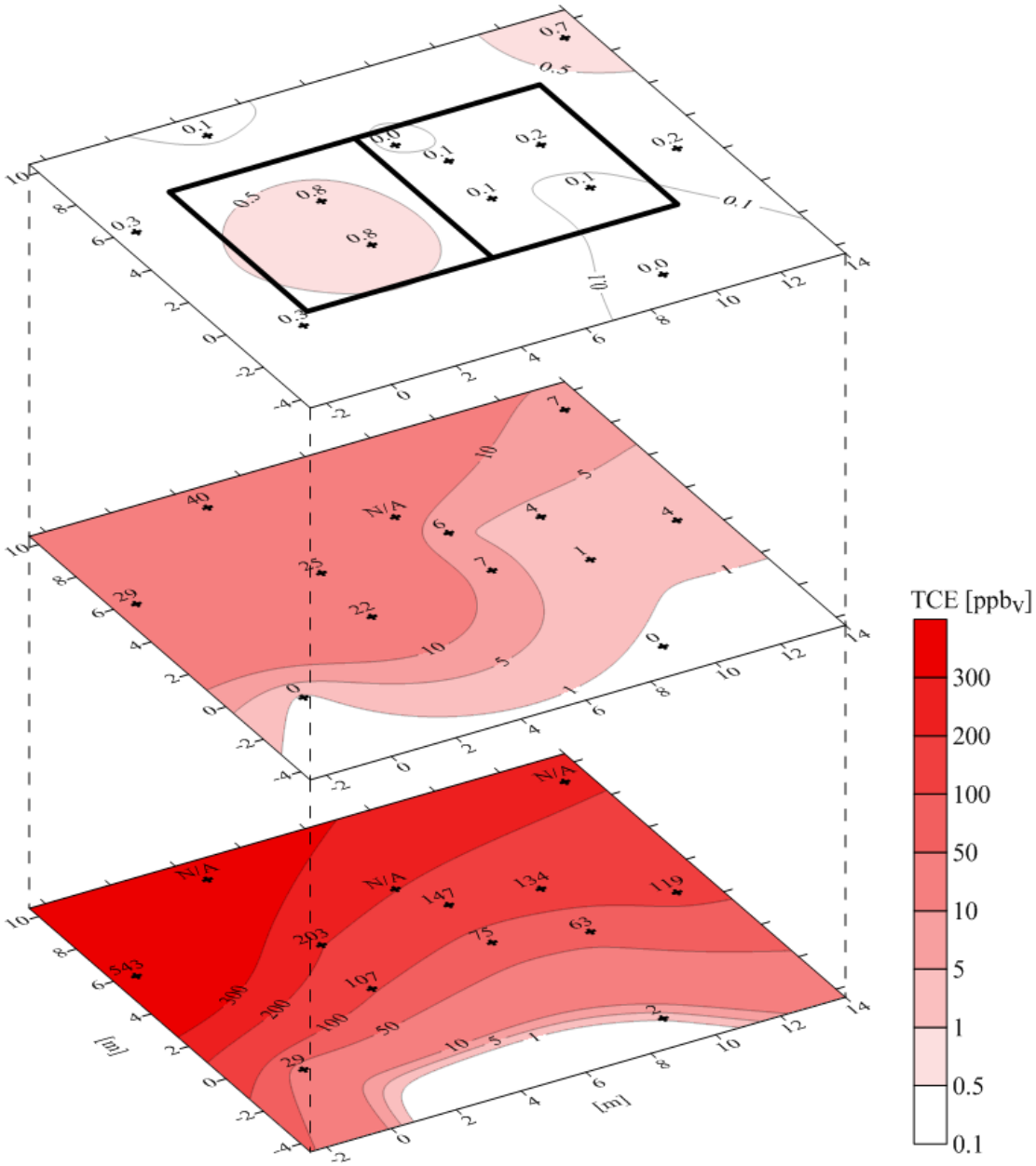

Figure A.4. Multi-depth contour plot of TCE in soil gas for samples collected and analyzed from November 13th to November 15th, 2010.

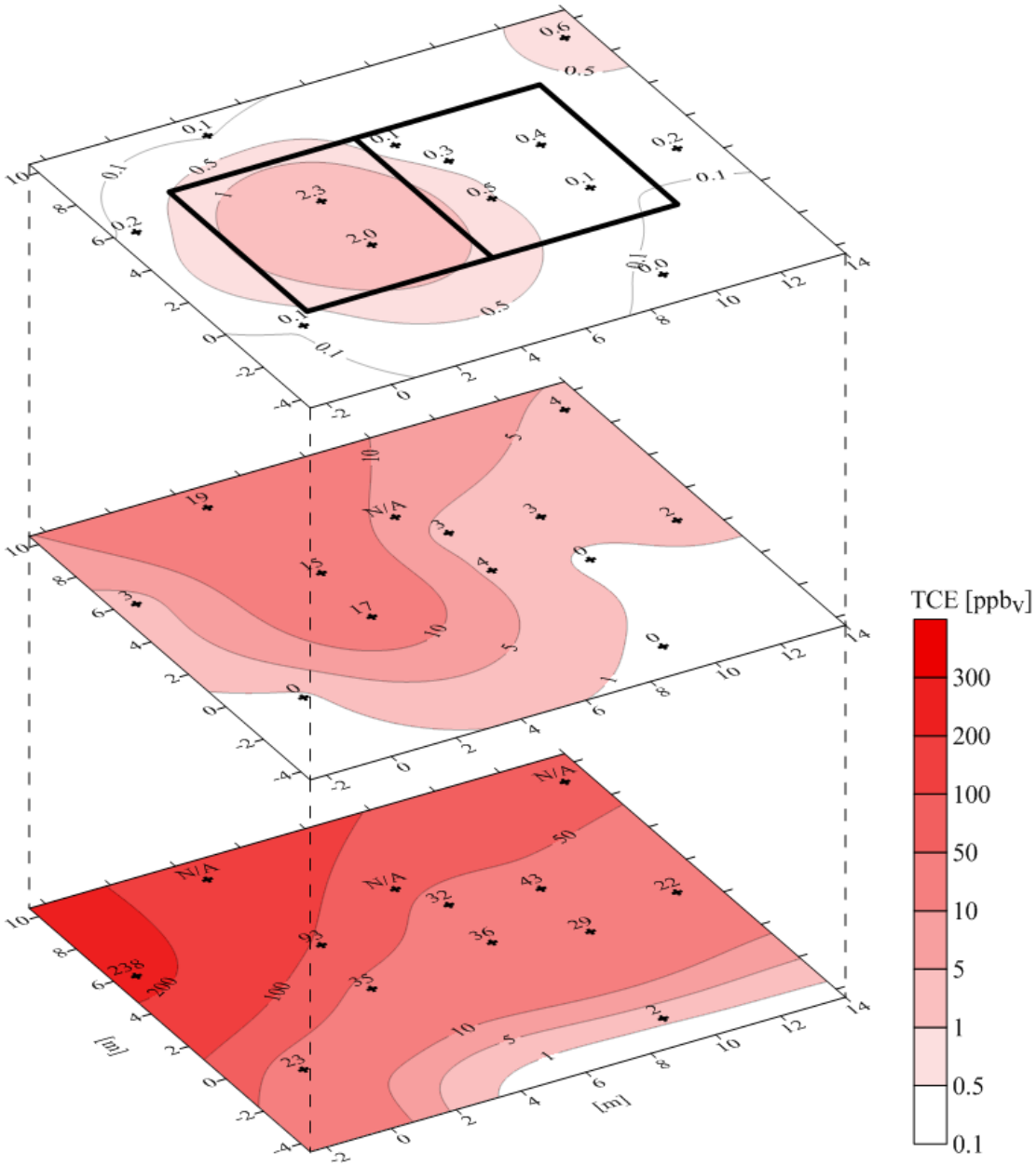

Figure A.5. Multi-depth contour plot of TCE in soil gas for samples collected and analyzed from December 17th to December 20th, 2010.

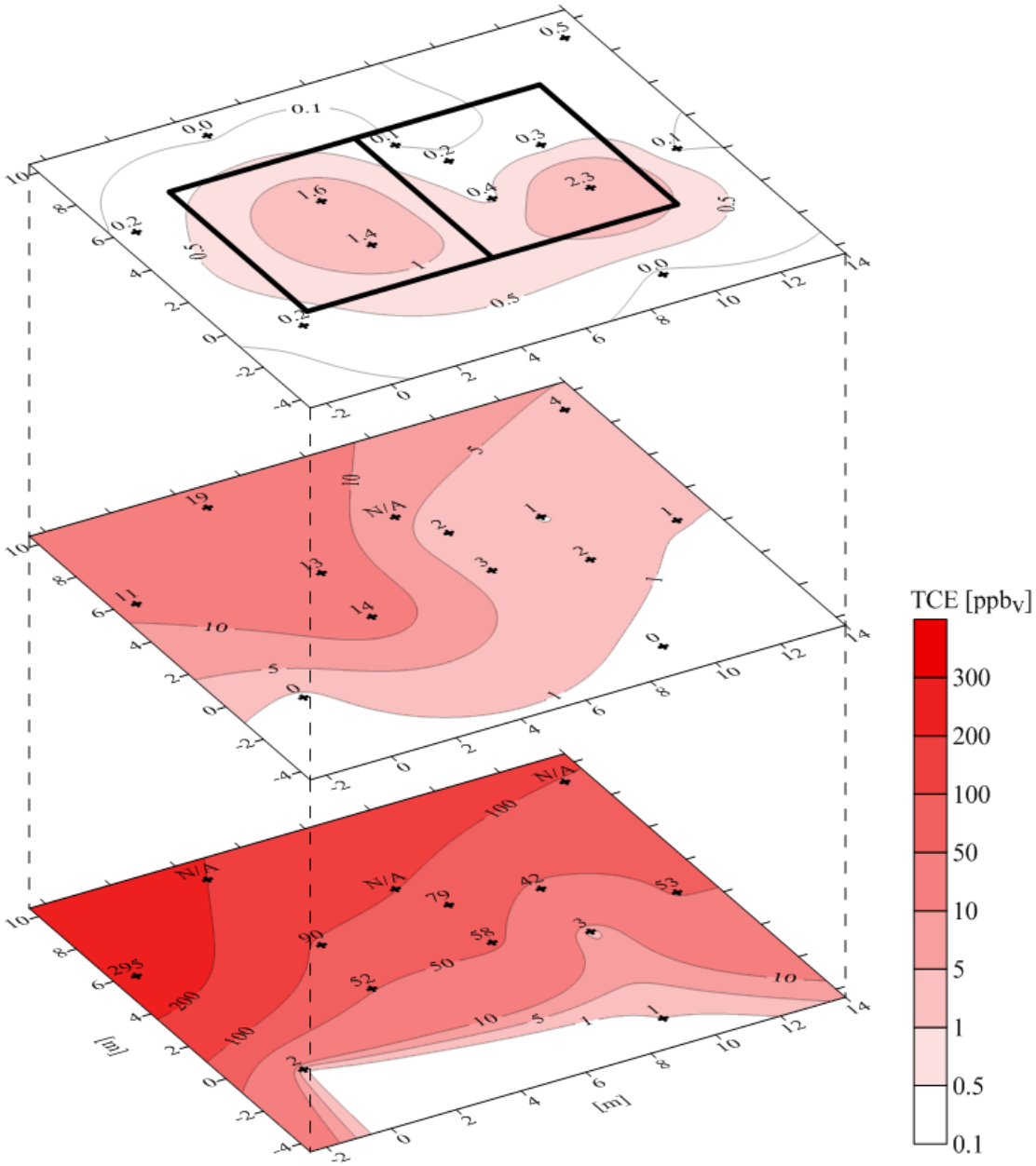

Figure A.6. Multi-depth contour plot of TCE in soil gas for samples collected and analyzed from March 1st to March 4th, 2011.

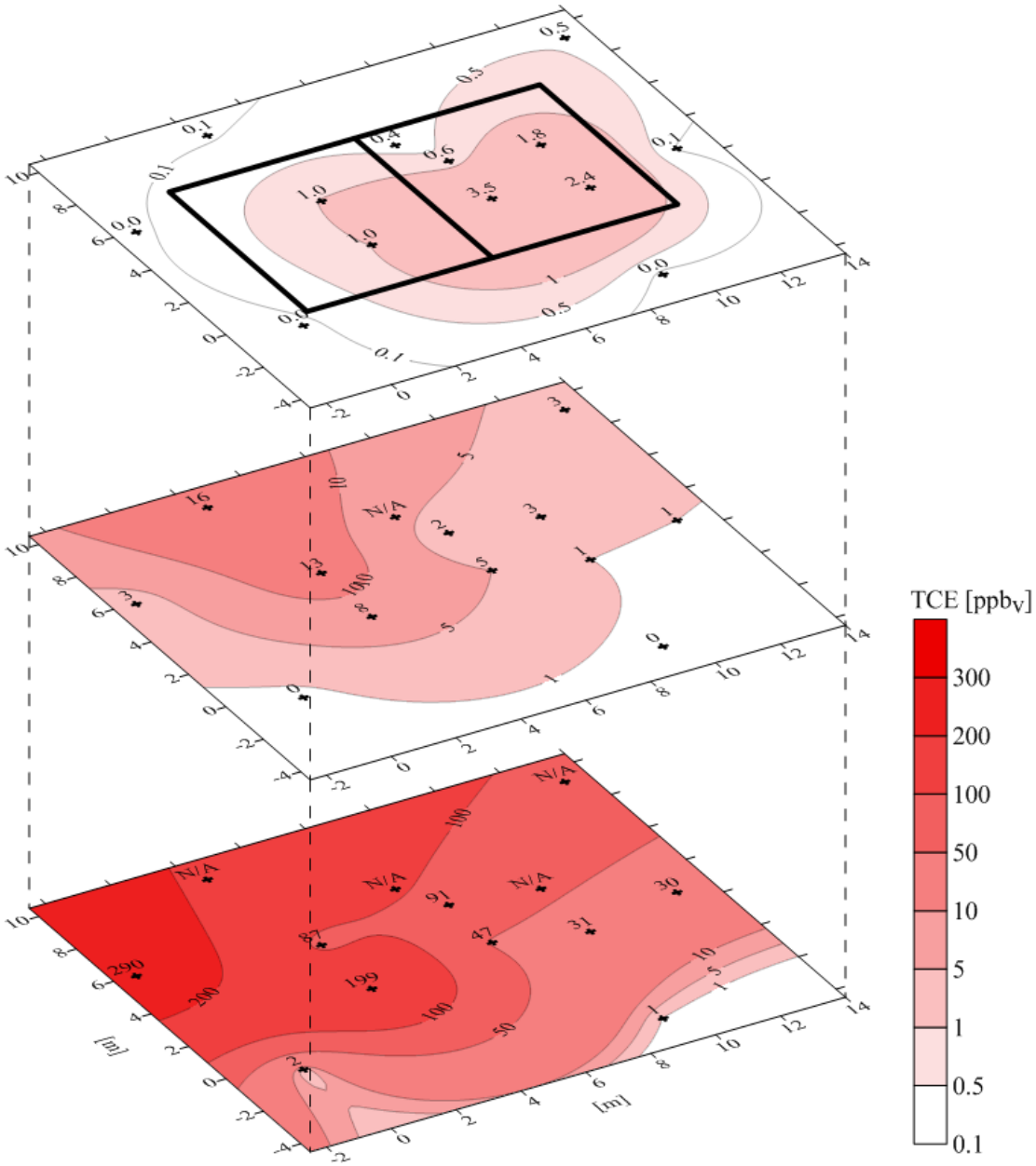

Figure A.7. Multi-depth contour plot of TCE in soil gas for samples collected and analyzed from March 31st to April 3rd, 2011.

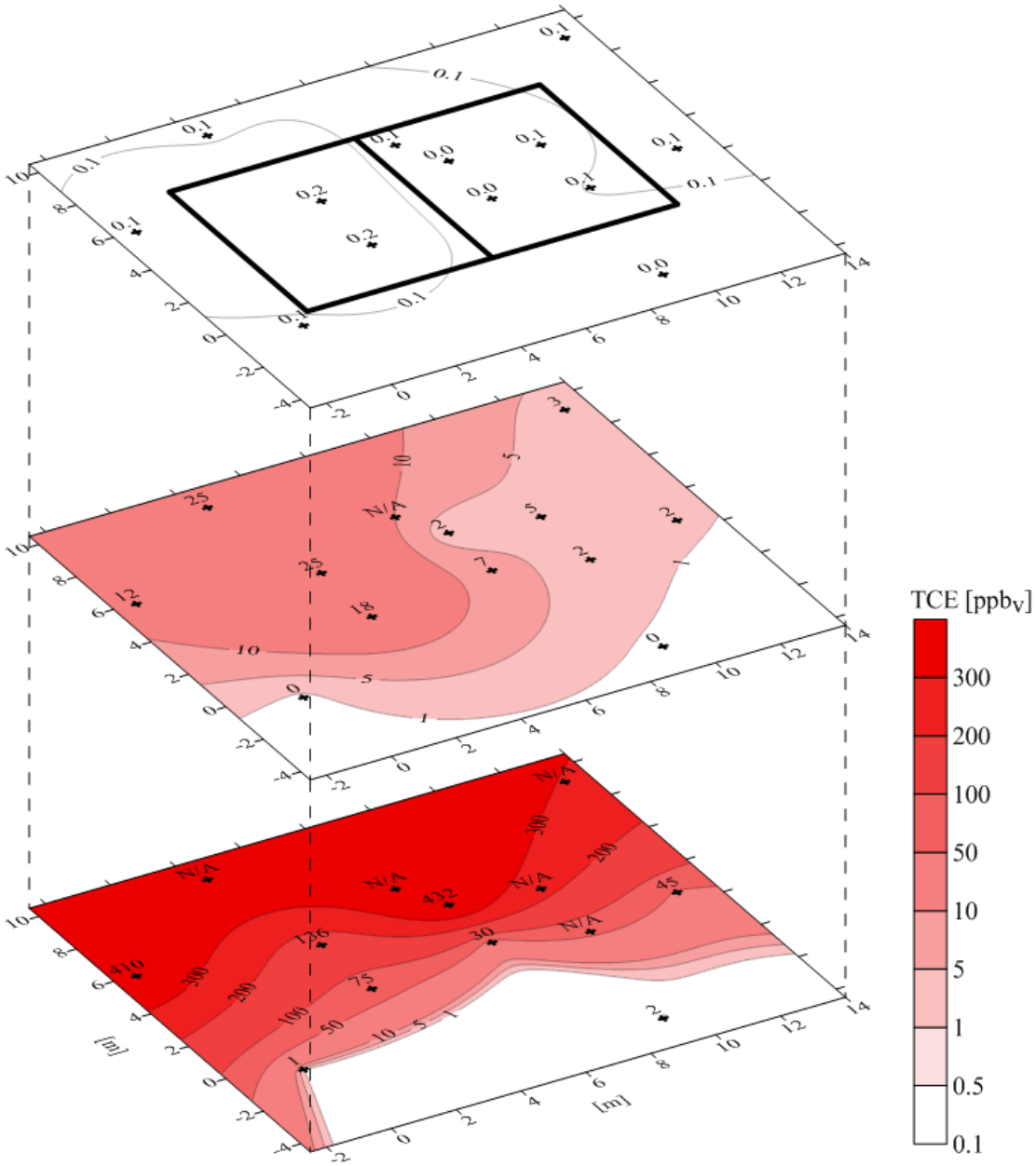

Figure A.8. Multi-depth contour plot of TCE in soil gas for samples collected and analyzed from May 18th to May 20th, 2011.

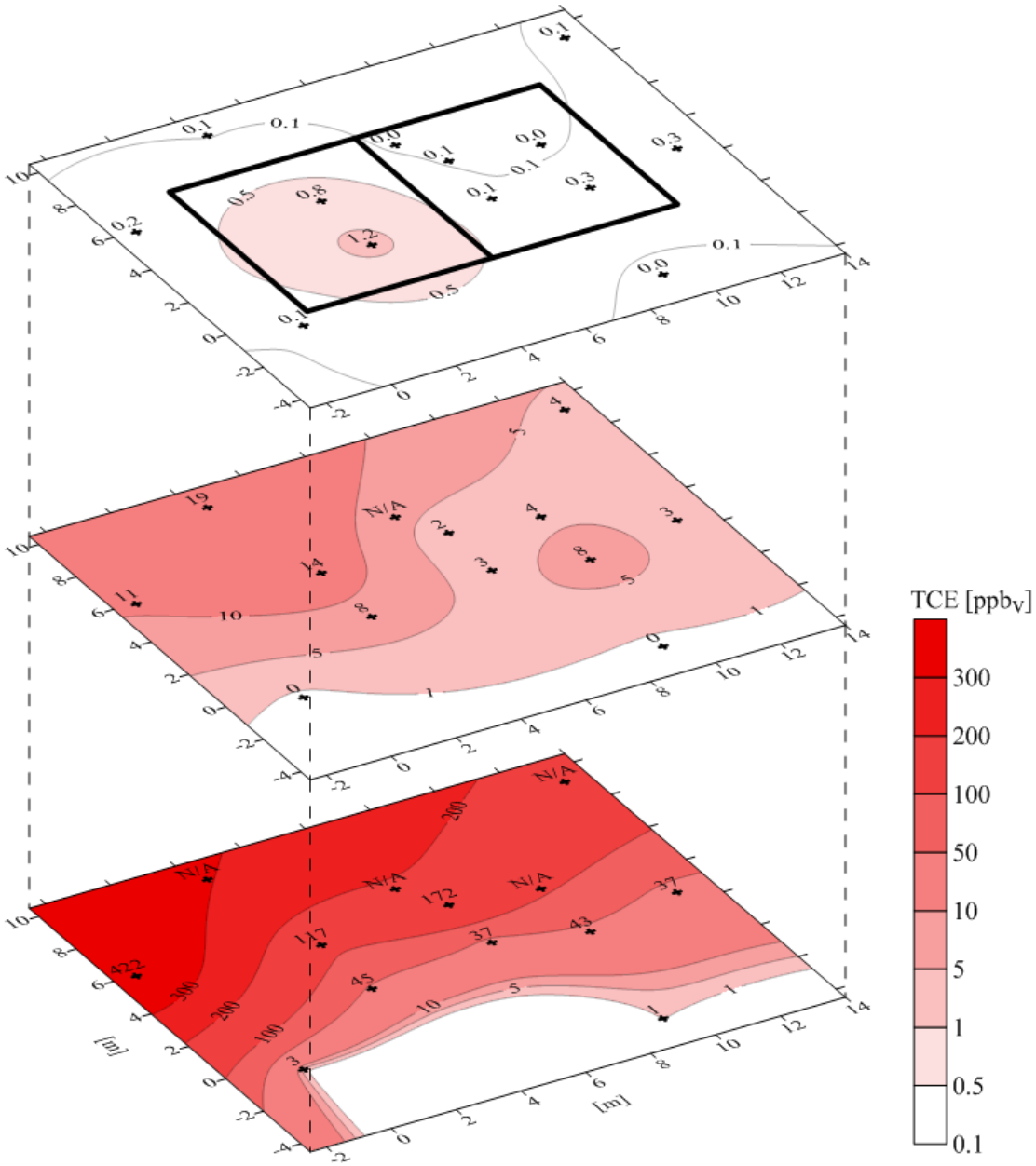

Figure A.9. Multi-depth contour plot of TCE in soil gas for samples collected and analyzed from July 7th to July 10th, 2011.

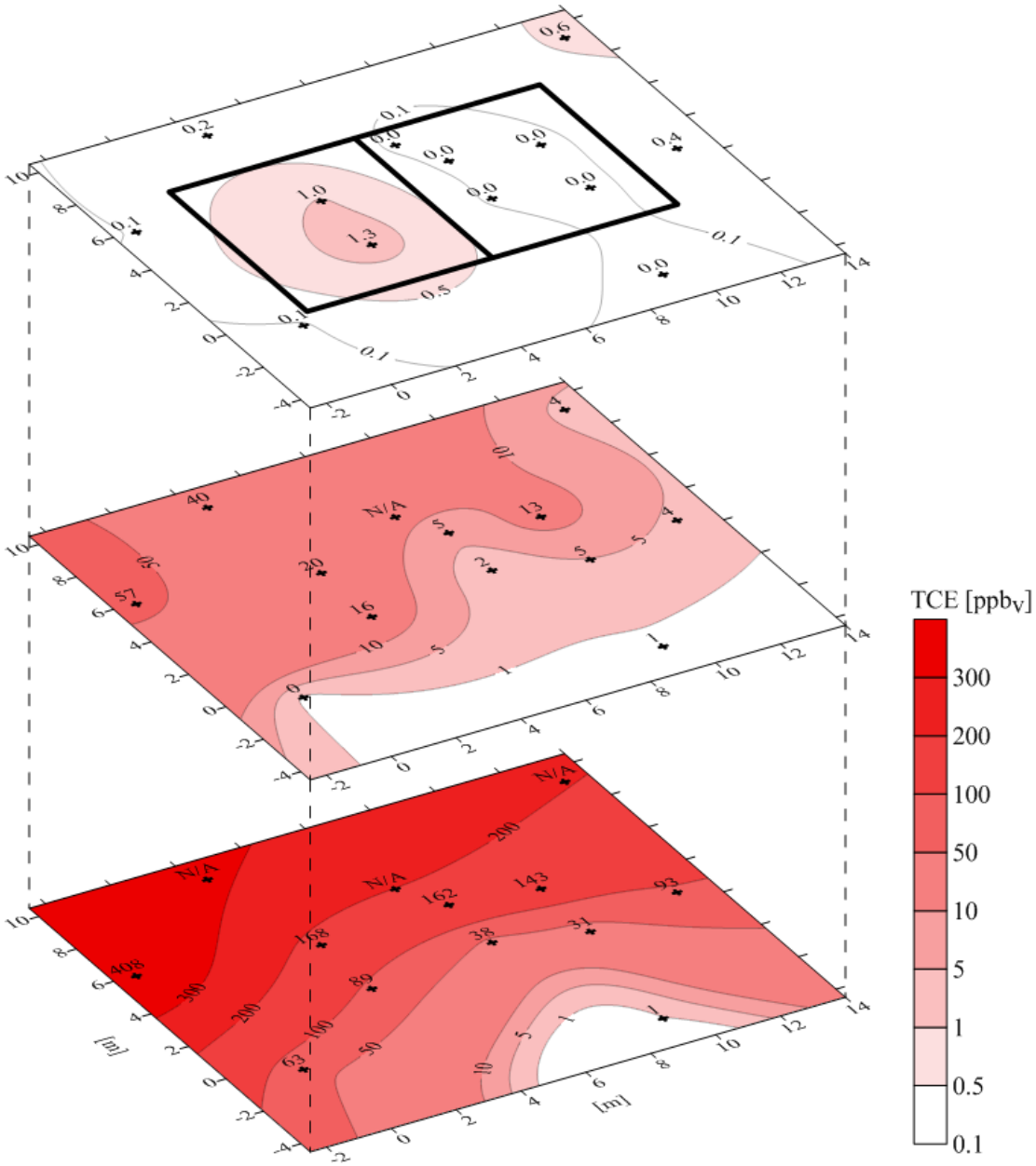

Figure A.10. Multi-depth contour plot of TCE in soil gas for samples collected and analyzed from August 18th to August 20th, 2011.

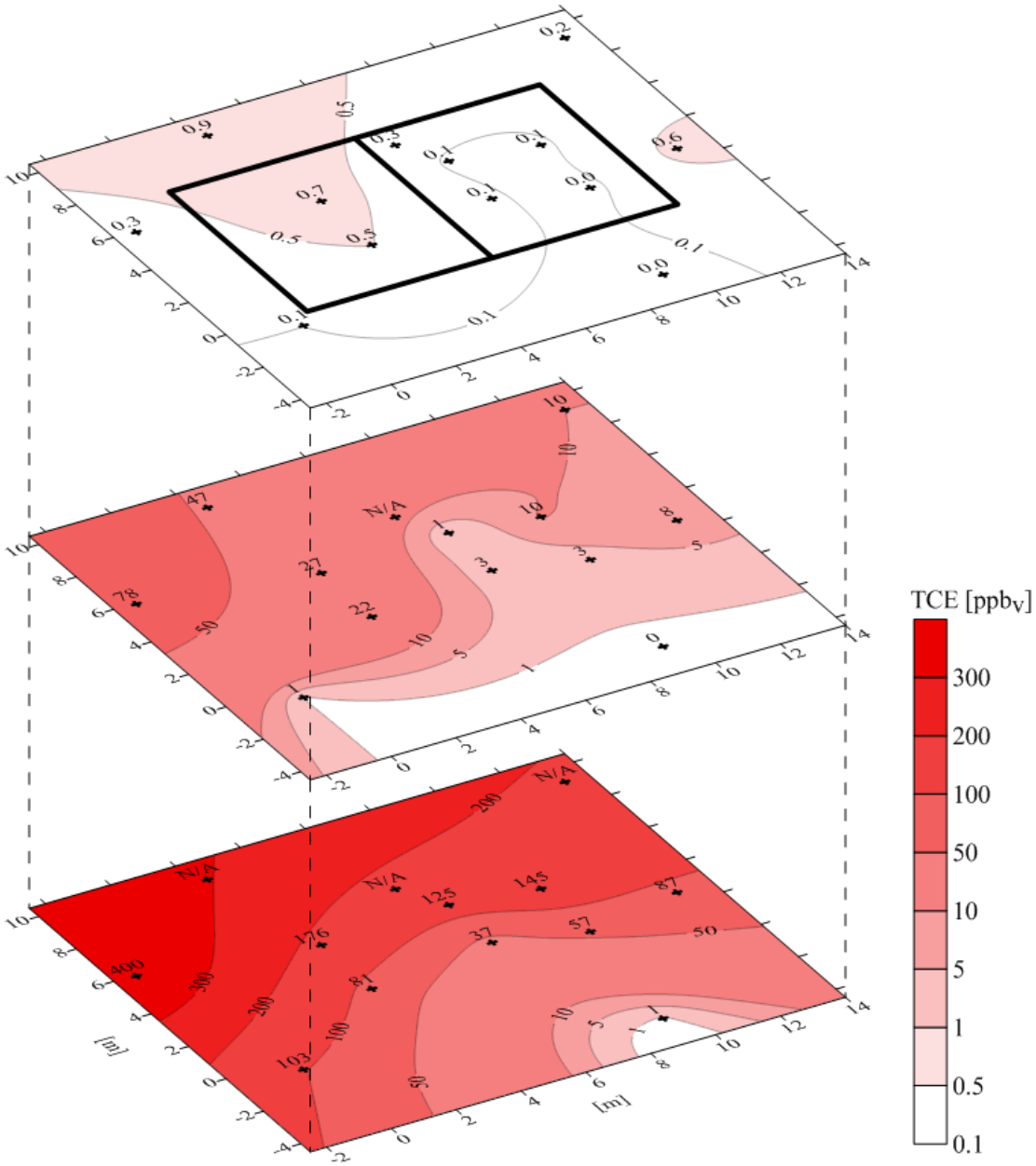

Figure A.11. Multi-depth contour plot of TCE in soil gas for samples collected and analyzed from September 29th to September 30th, 2011.

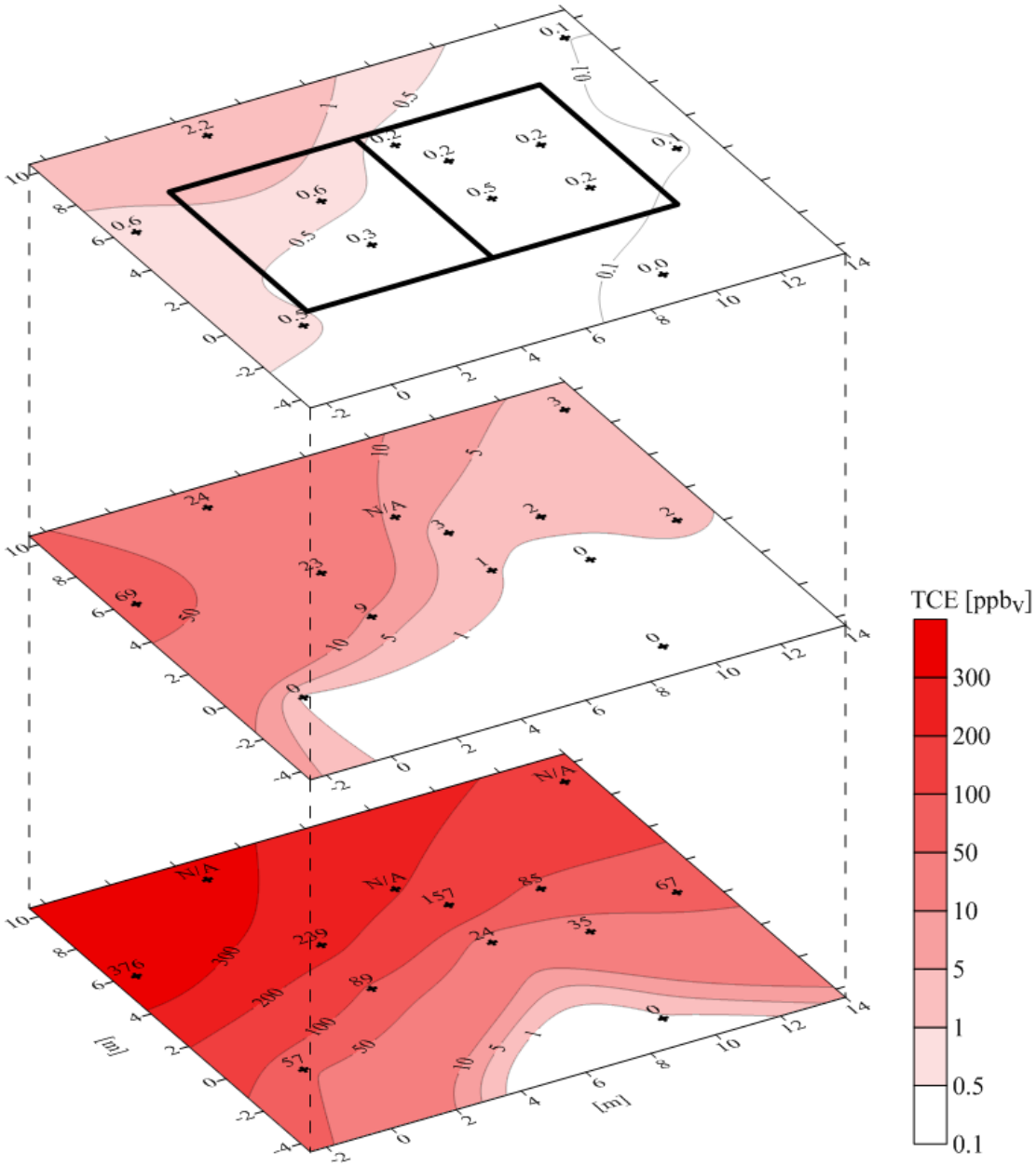

Figure A.12. Multi-depth contour plot of TCE in soil gas for samples collected and analyzed from November 4th to November 5th, 2011.

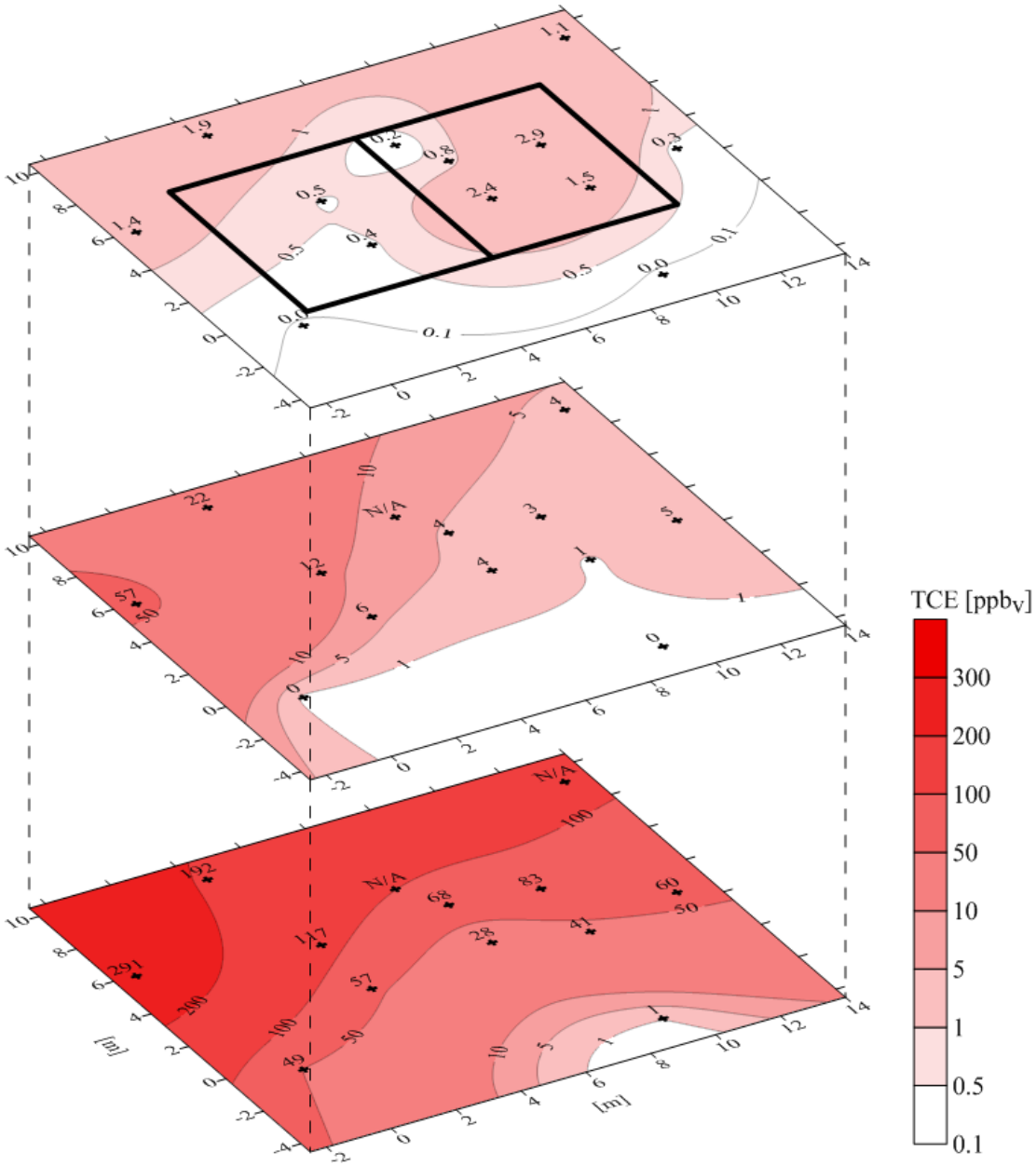

Figure A.13. Multi-depth contour plot of TCE in soil gas for samples collected and analyzed from December 3rd to December 4th, 2011.

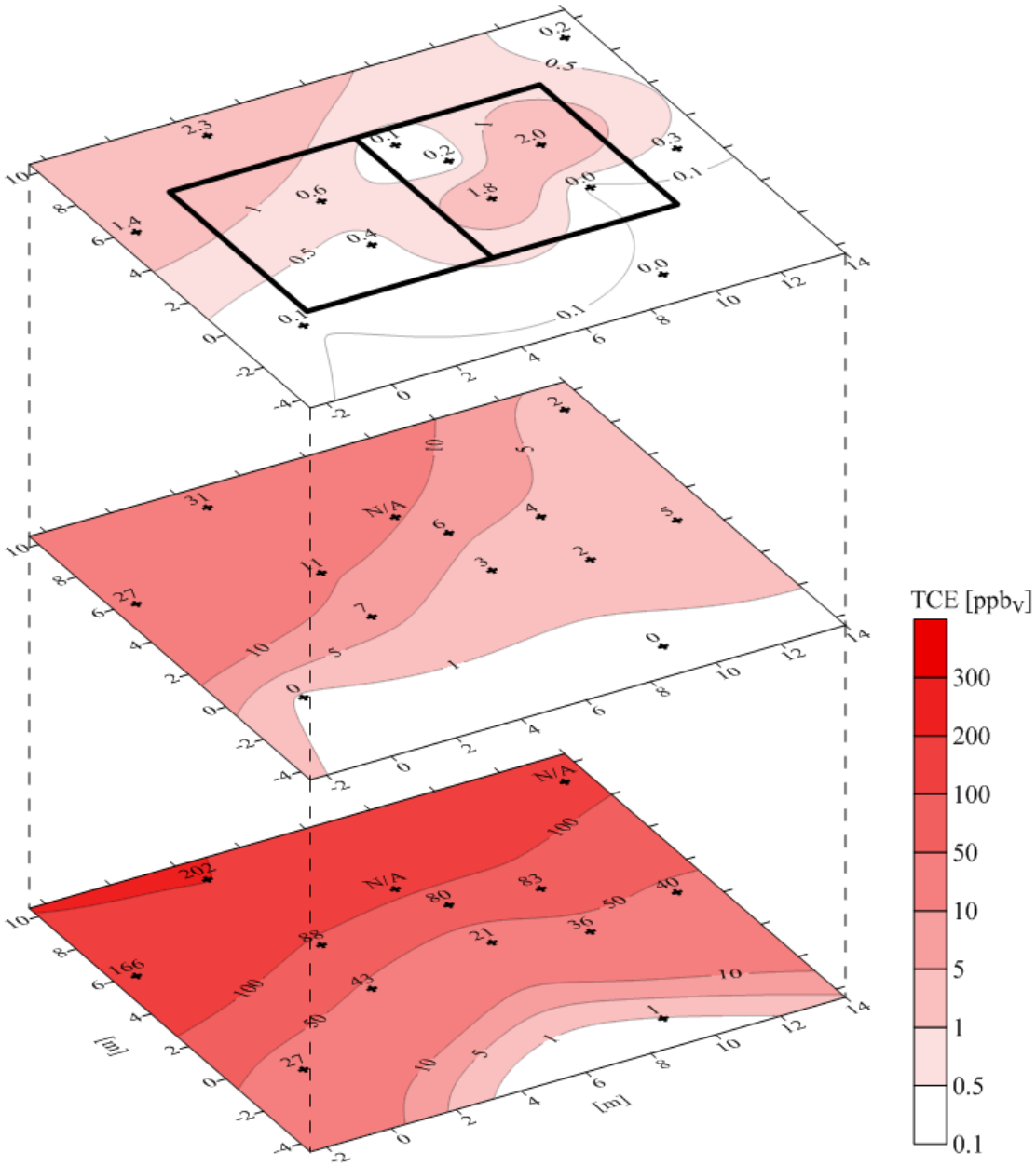

Figure A.14. Multi-depth contour plot of TCE in soil gas for samples collected and analyzed from January 11th to January 13th, 2012.

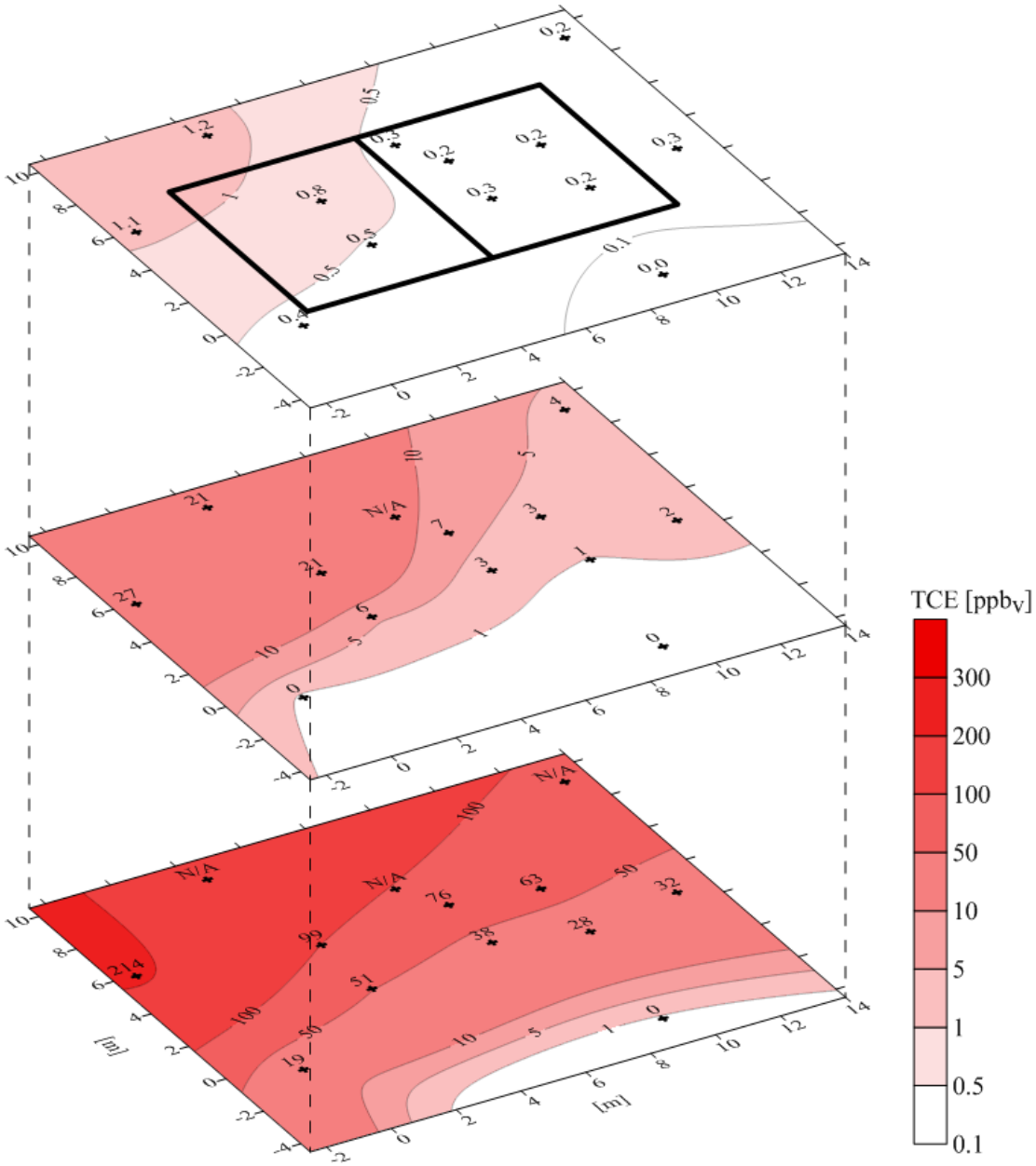

Figure A.15. Multi-depth contour plot of TCE in soil gas for samples collected and analyzed from February 16th to February 17th, 2012.

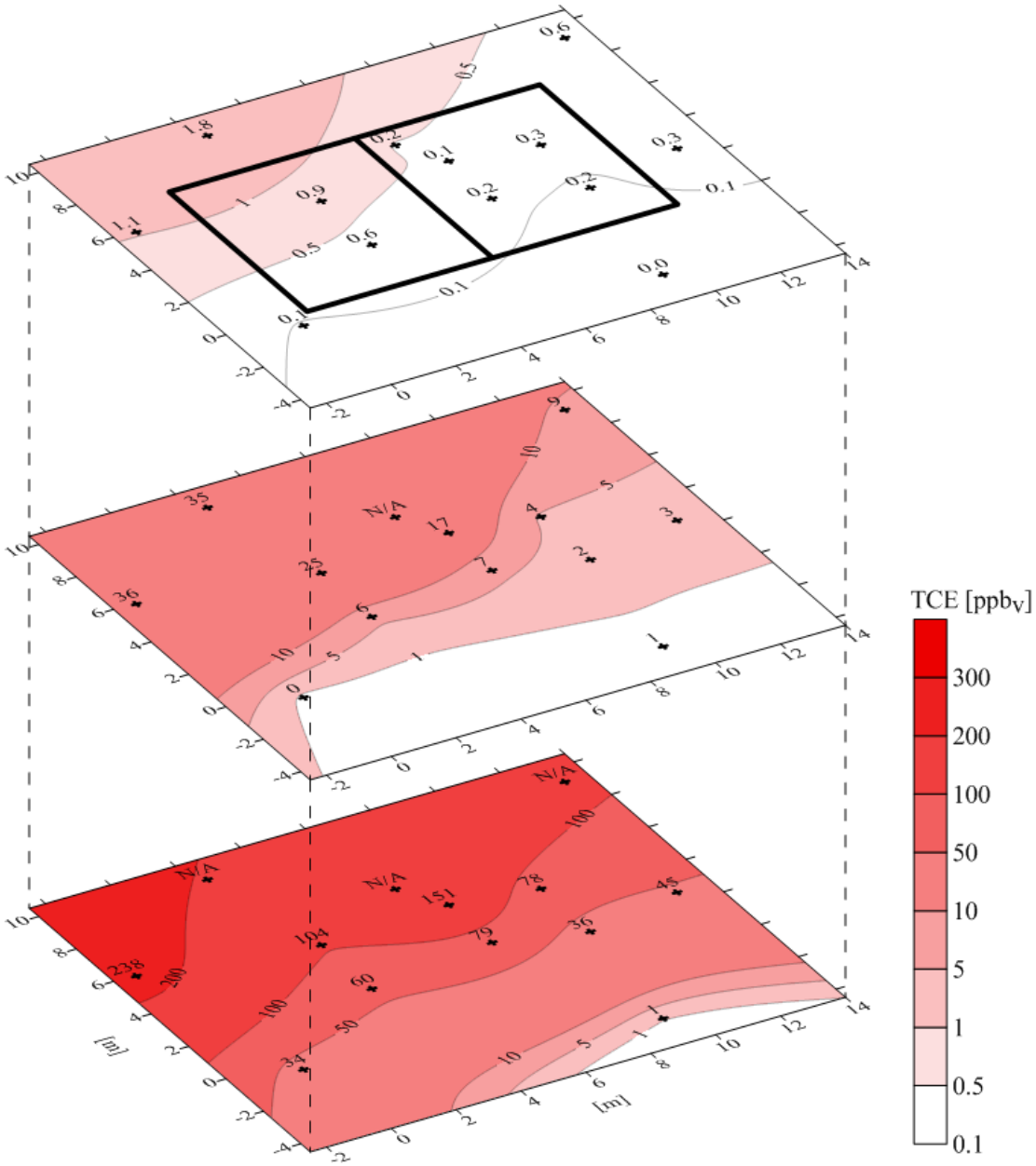

Figure A.16. Multi-depth contour plot of TCE in soil gas for samples collected and analyzed from April 30th to May 1st, 2012.

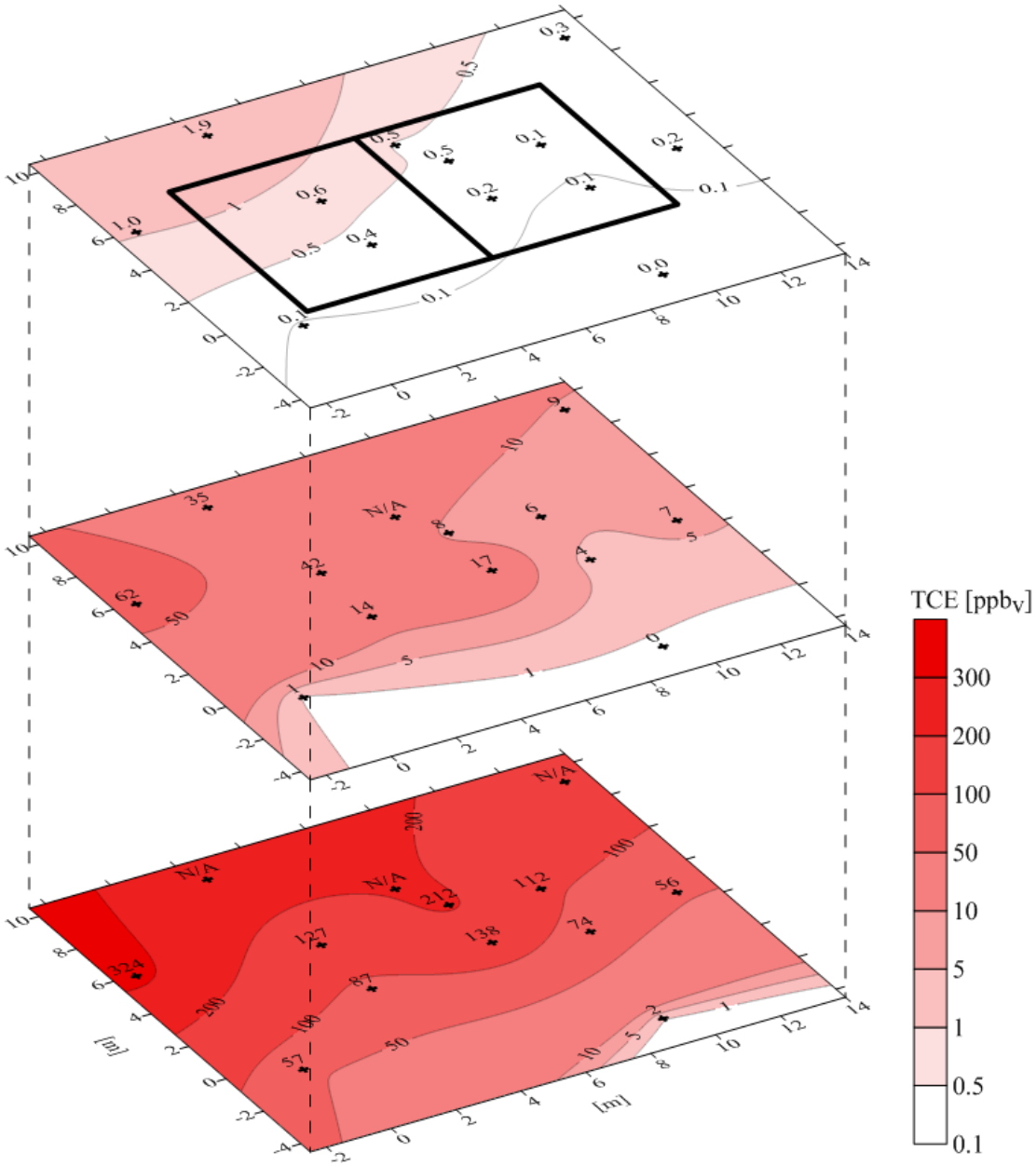

Figure A.17. Multi-depth contour plot of TCE in soil gas for samples collected and analyzed from May 27th to May 28th, 2012.

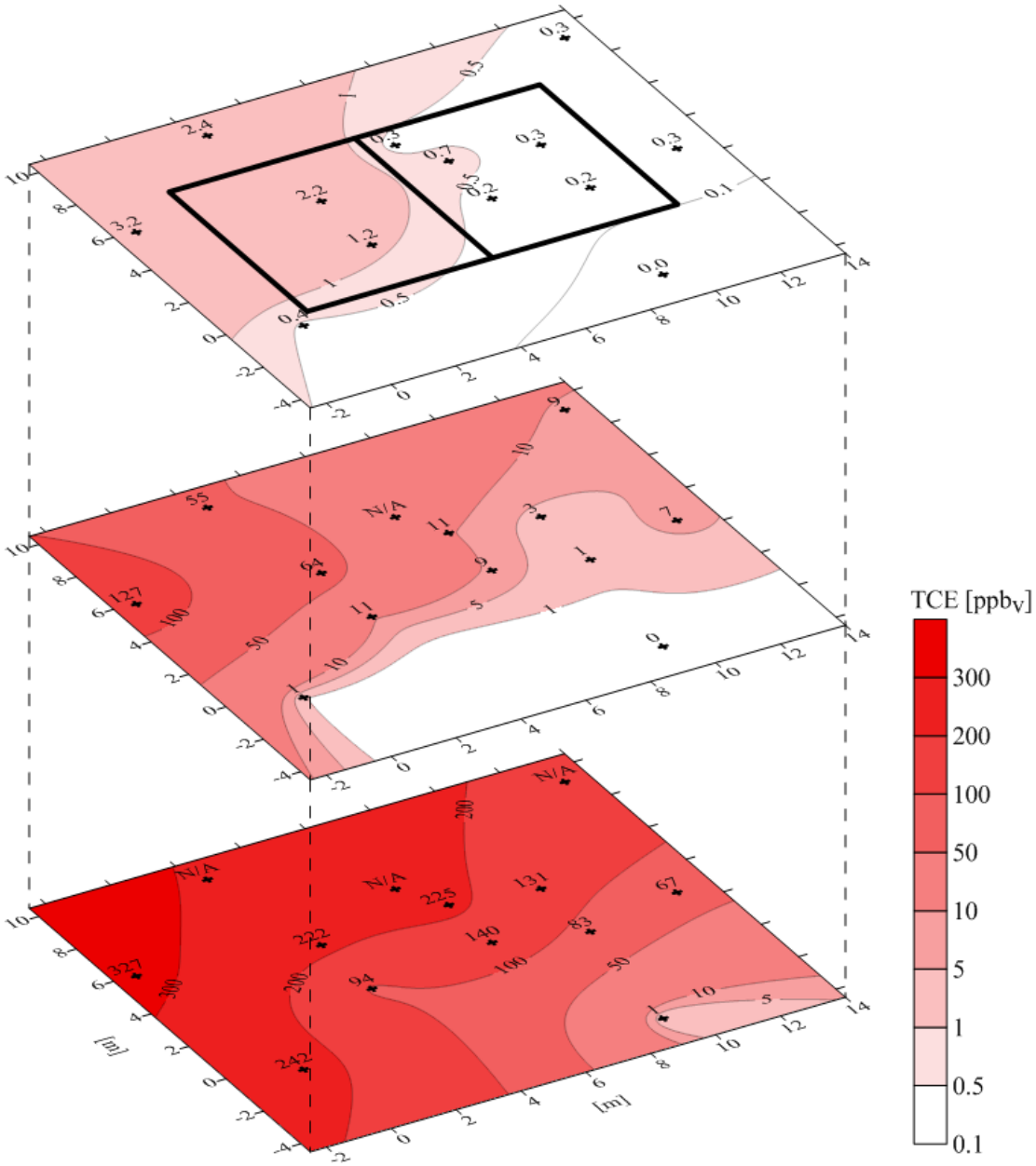

Figure A.18. Multi-depth contour plot of TCE in soil gas for samples collected and analyzed from August 20th to August 21st, 2012.

As discussed in section 3, soil gas was monitored in real-time at several sampling points during natural conditions. Figures A.18-A.22 show soil gas results from SS and 0.9 m BS sampling depths at locations 1, 2, and 6, respectively. In general, these results agree with the results shown in the soil gas concentration contour plots.

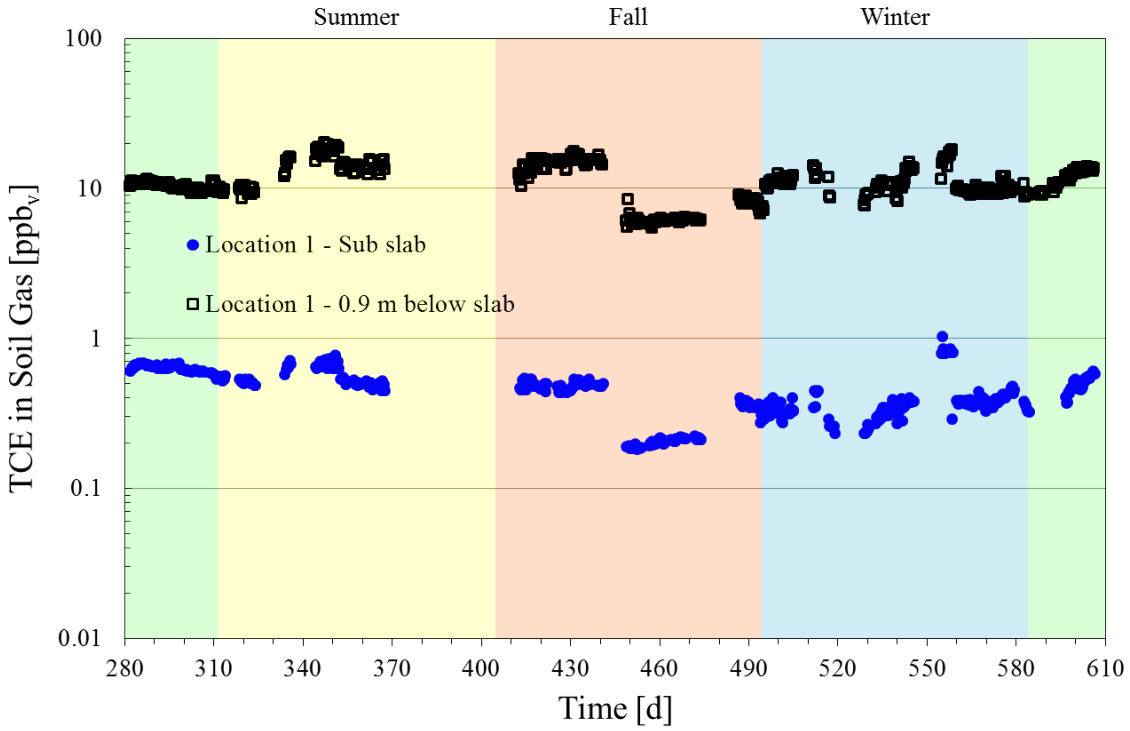

Figure A.19. TCE soil gas concentrations at sub-slab and 0.9 m below-slab depths at location 1 from May 2011 to April 2012.

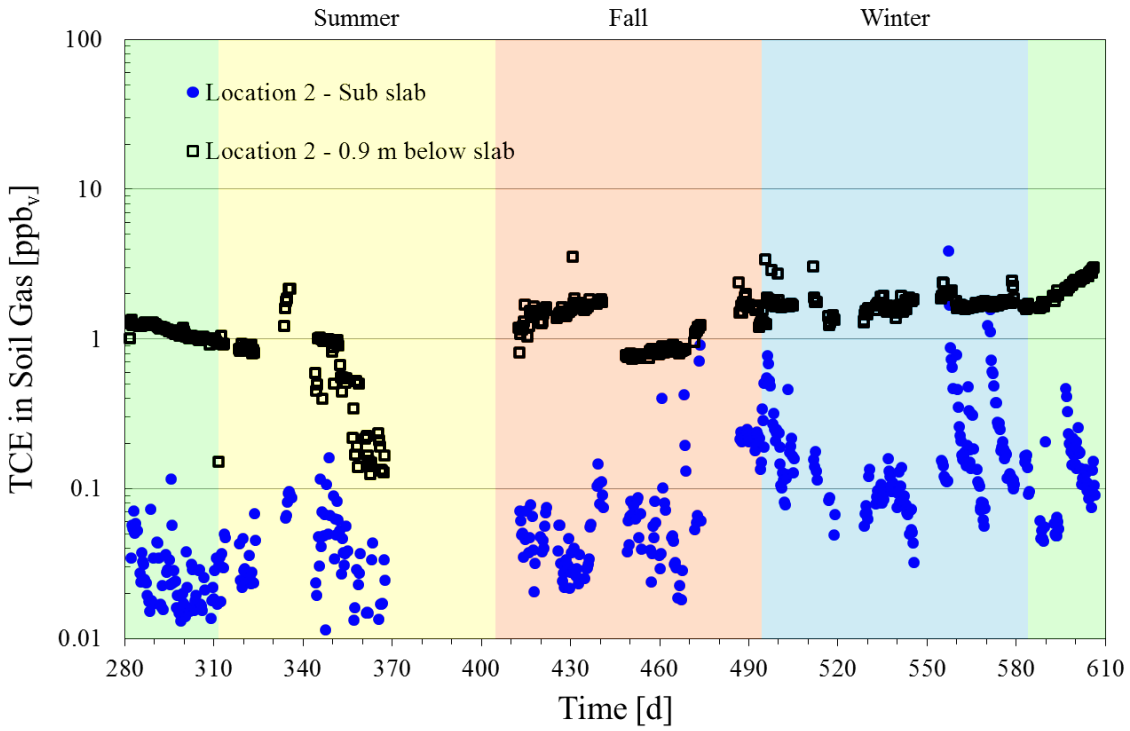

Figure A.20. TCE soil gas concentrations at sub-slab and 0.9 m below-slab depths at location 2 from May 2011 to April 2012.

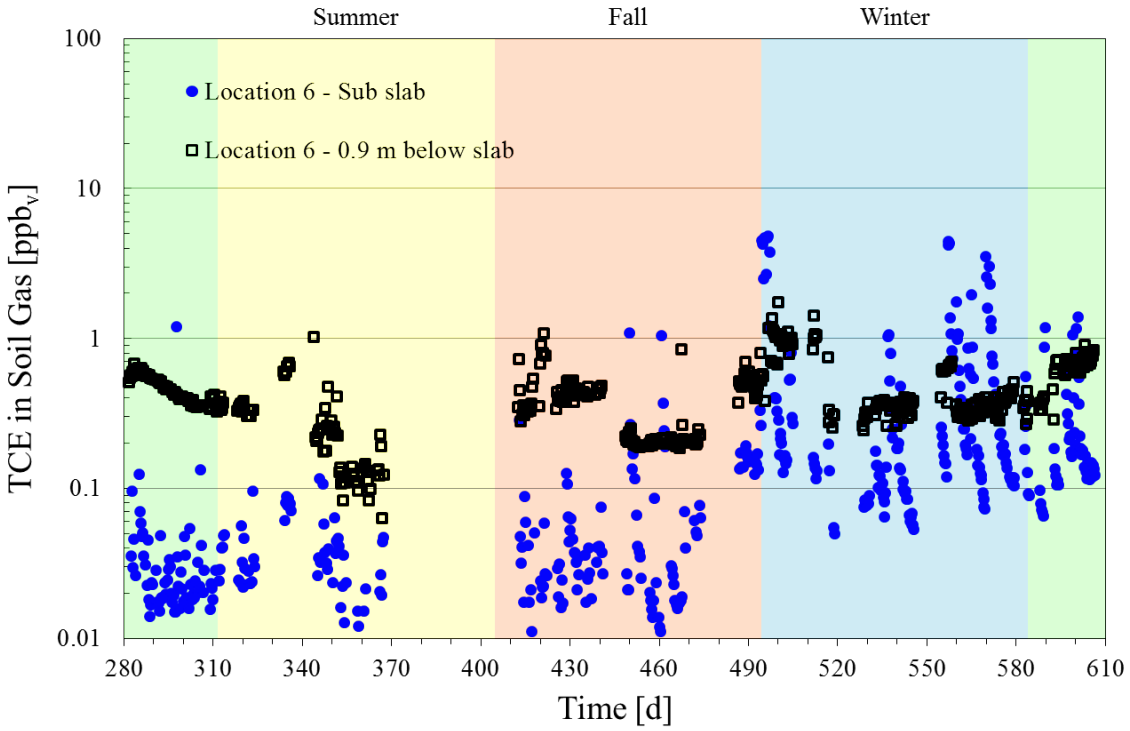

Figure A.21. TCE soil gas concentrations at sub-slab and 0.9 m below-slab depths at location 6 from May 2011 to April 2012.

Outdoor Air. Outdoor air was monitored during the majority of the study period to assess background levels CVOCs. Figure A.22 shows outdoor air TCE concentrations collected on sorbent tubes over a 4-h period and analyzed with thermal desorption and GC/MS. For comparison, the MDL for this method is shown on the plot.

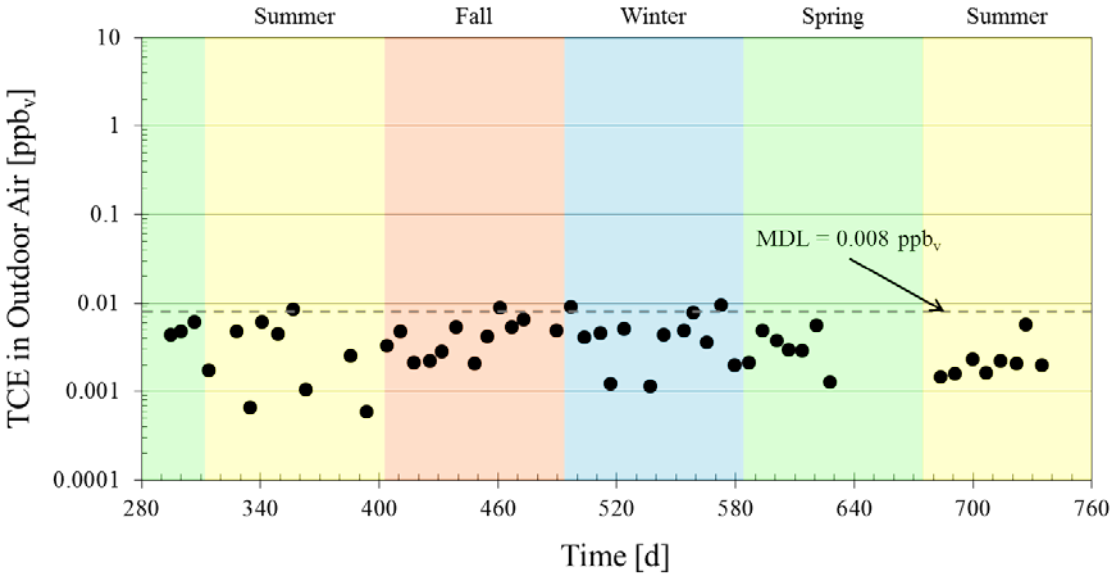

Figure A.22. Outdoor air TCE concentrations measured by sorbent tubes from May 2011 to August 2012.

A.5. Supplemental information and results from indoor source release studies

Overview. The information presented below is supplemental to the field and modeling results presented in section 4.3.

Results from indoor source studies. The field data presented below are placed on a timeline consistent with previous publications, where time (t) = 0 being 8:00 AM on 8/15/2010. A summary of study-related activities, including soil gas surveys and periods where SF_6 release was stopped, is shown in Table A.3. A timeline of the real-time monitoring performed at the study house is provided in Table A.4.

Table A.3. Summary of indoor source release study activities.

Summary of Indoor Source Study Events		
Date	Time [d]	Event Description
12/21/2010	128	SF_6 release starts
1/26/2011	164	Soil gas survey
3/1/2011	198	Soil gas survey
4/4/2011	232	Soil gas survey
5/18/2011	276	Soil gas survey
7/7/2011	326	Soil gas survey
8/18/2011	368	Soil gas survey
11/4/2011	446	Soil gas survey
12/3/2011	475	Soil gas survey
1/11/2012	514	Soil gas survey
2/16/2012	550	Soil gas survey
4/30/2012	624	Soil gas survey
5/6/2012	630	SF_6 release stops
5/27/2012	651	Soil gas survey
5/31/2012	655	SF_6 release starts
6/26/2012	681	SF_6 release stops
7/12/2012	697	SF_6 release starts
8/20/2012	736	Soil gas survey
8/21/2014	1467	SF_6 release stops

Table A.4. Timeline for real-time SF_6 monitoring during indoor source release studies.

Timeline for Real-Time Monitoring of SF_6			
Start Date	End Date	Time Elapsed [d]	Monitoring Locations
12/21/2010	4/6/2011	106	Indoor air
4/6/2011	5/12/2011	36	Indoor air, outdoor air, sub-slab soil gas (location 3), 0.9 m below-slab soil gas (location 3 and D)
5/24/2011	5/5/2012	347	Indoor air, outdoor air, standard gas, sub-slab soil gas (location 2, 3, 5, and 6)
5/5/2012	8/14/2012	101	Indoor air, outdoor air, standard gas, sub-slab soil gas (location 2, 3, 5, and 6), 0.9 m below-slab soil gas (location 2, 3, and 6)
8/14/2014	10/5/2014	52	Indoor air, outdoor air, standard gas, sub-slab soil gas (location 2, 3, and 6), 0.9 m below-slab soil gas (location 2, 3, and 6)

Long-term release of an indoor source. The long-term study of indoor source impacts to indoor air and soil gas began in December 2010 (t = 128 d) and continued through August 2012. The results from real-time monitoring of indoor air and soil gas, along with the results from synoptic multi-depth soil gas surveys, are shown below.

Figures A.24-A.27 present 24-h average SF_6 concentrations in indoor air or sub-slab soil gas during the period from $128 < t < 729$ d and includes error bars that span the daily maximum and minimum values. During this period, indoor air and sub-slab (SS) soil gas SF_6 concentrations varied by over two orders-of-magnitude and a similar seasonal trend was observed.

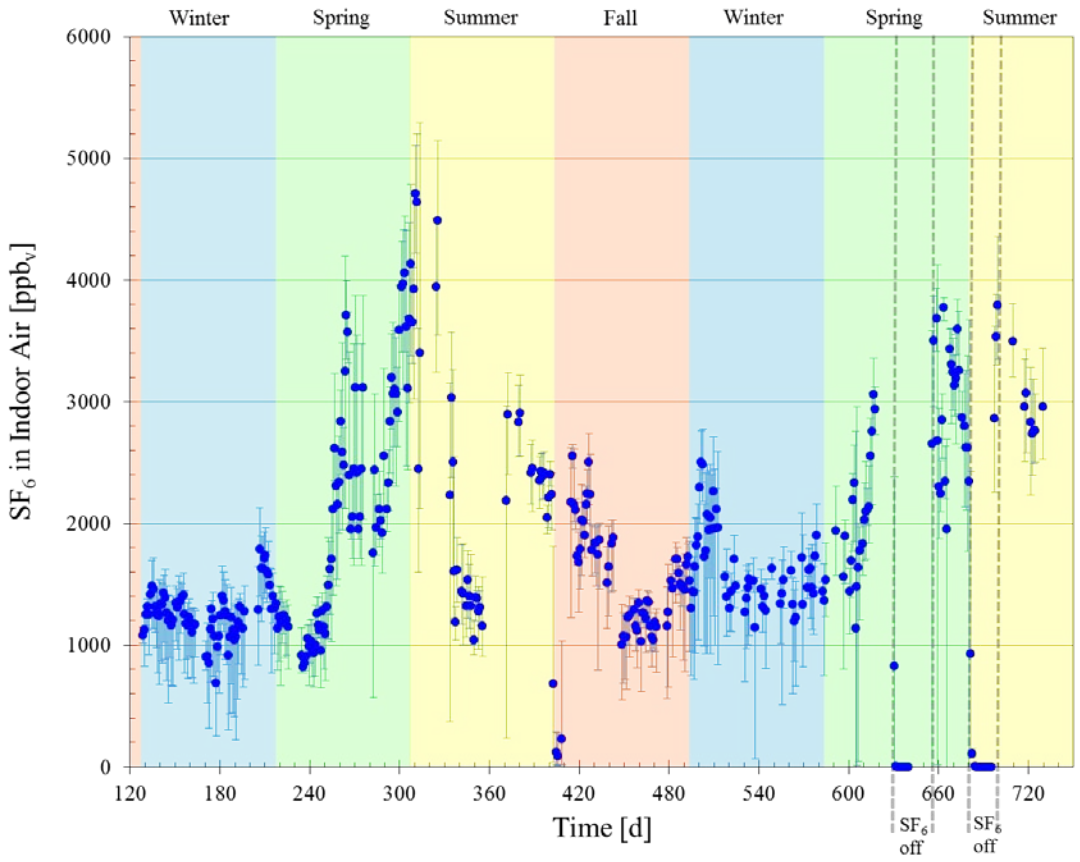

Figure A.22. 24-h averaged SF_6 concentrations in indoor air from winter 2010 through summer 2012 with error bars spanning the daily maximum and minimum values.

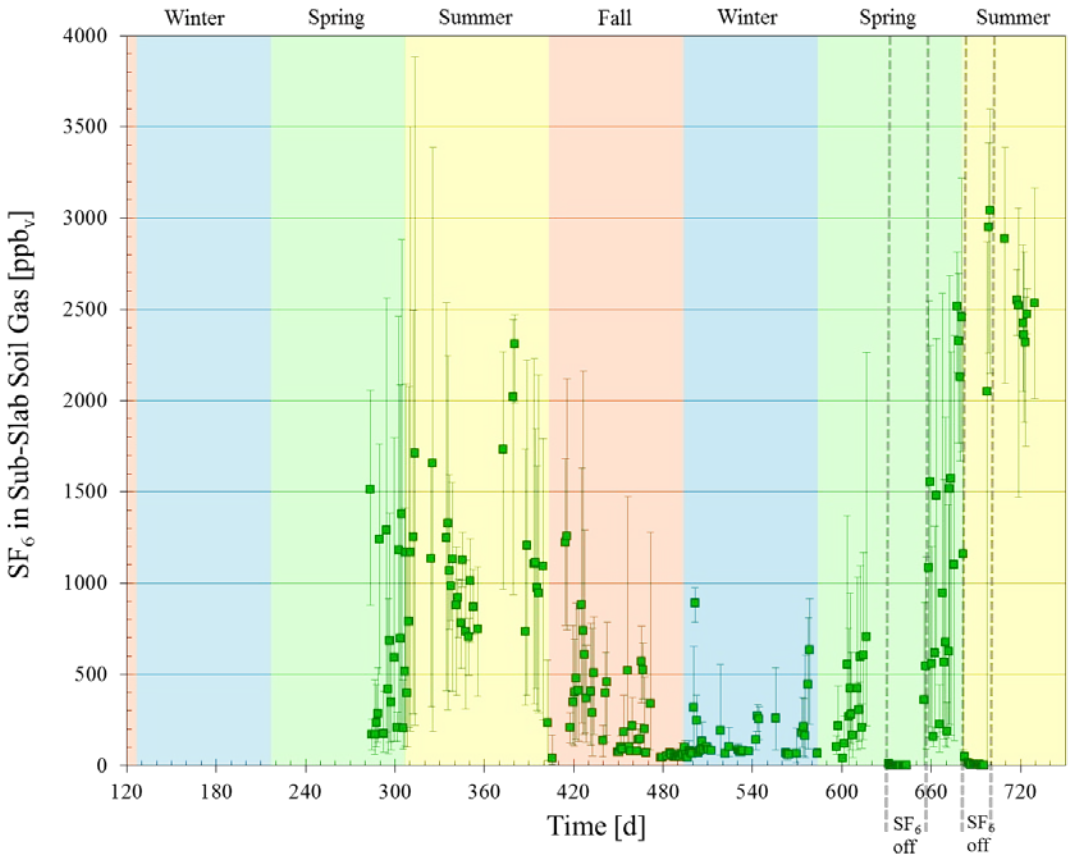

Figure A.23. 24-h averaged SF_6 concentrations sub-slab soil gas at location 2 from winter 2010 through summer 2012 with error bars spanning the daily maximum and minimum values.

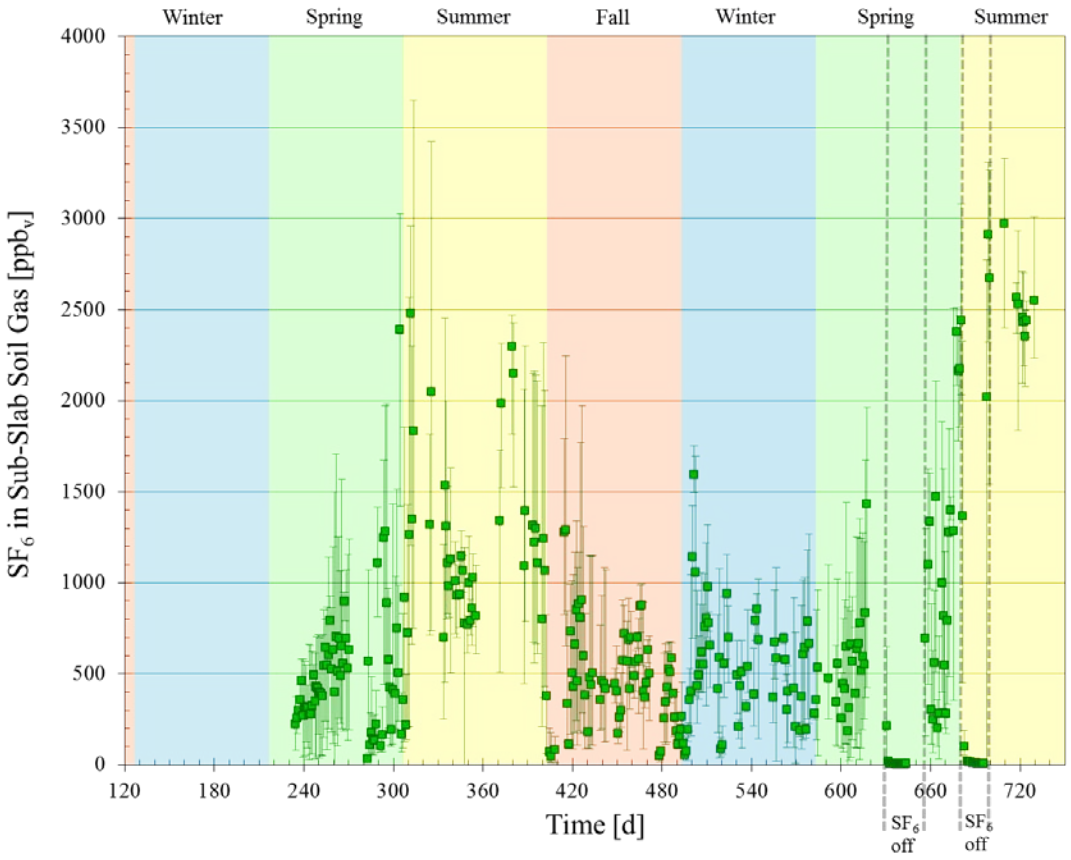

Figure A.24. 24-h averaged SF_6 concentrations sub-slab soil gas at location 3 from winter 2010 through summer 2012 with error bars spanning the daily maximum and minimum values.

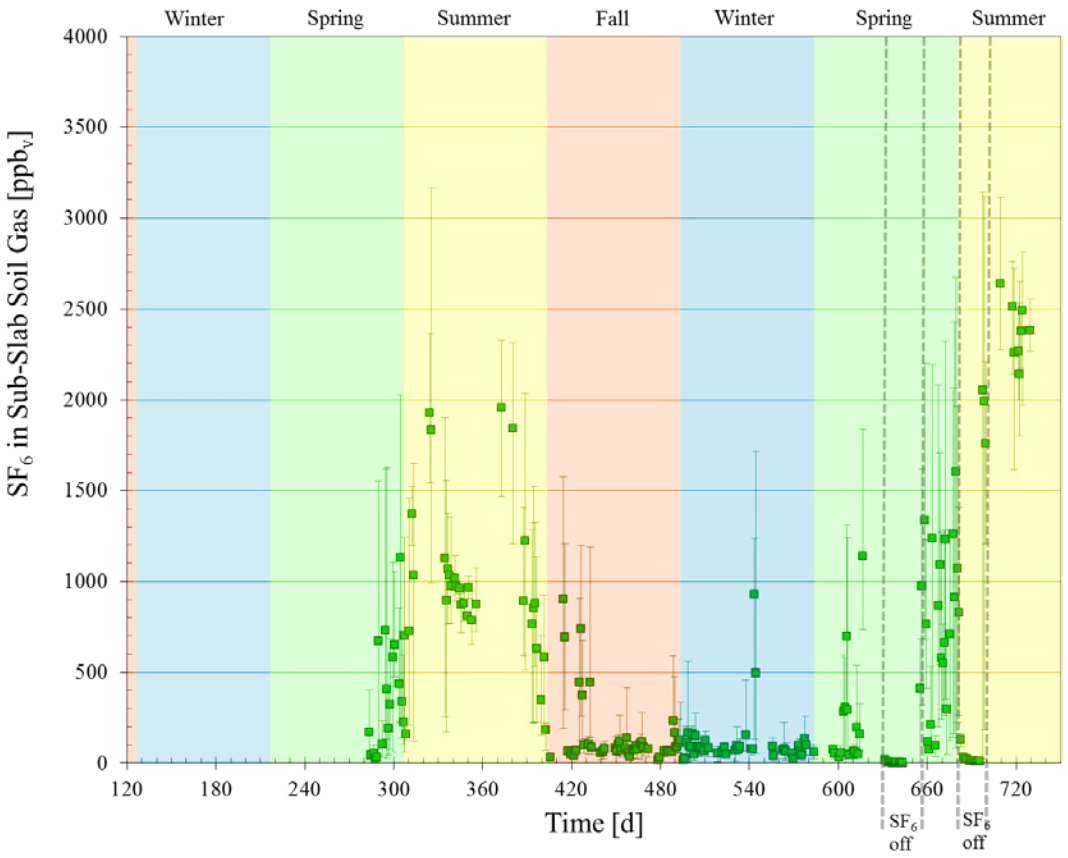

Figure A.25. 24-h averaged SF_6 concentrations sub-slab soil gas at location 5 from winter 2010 through summer 2012 with error bars spanning the daily maximum and minimum values.

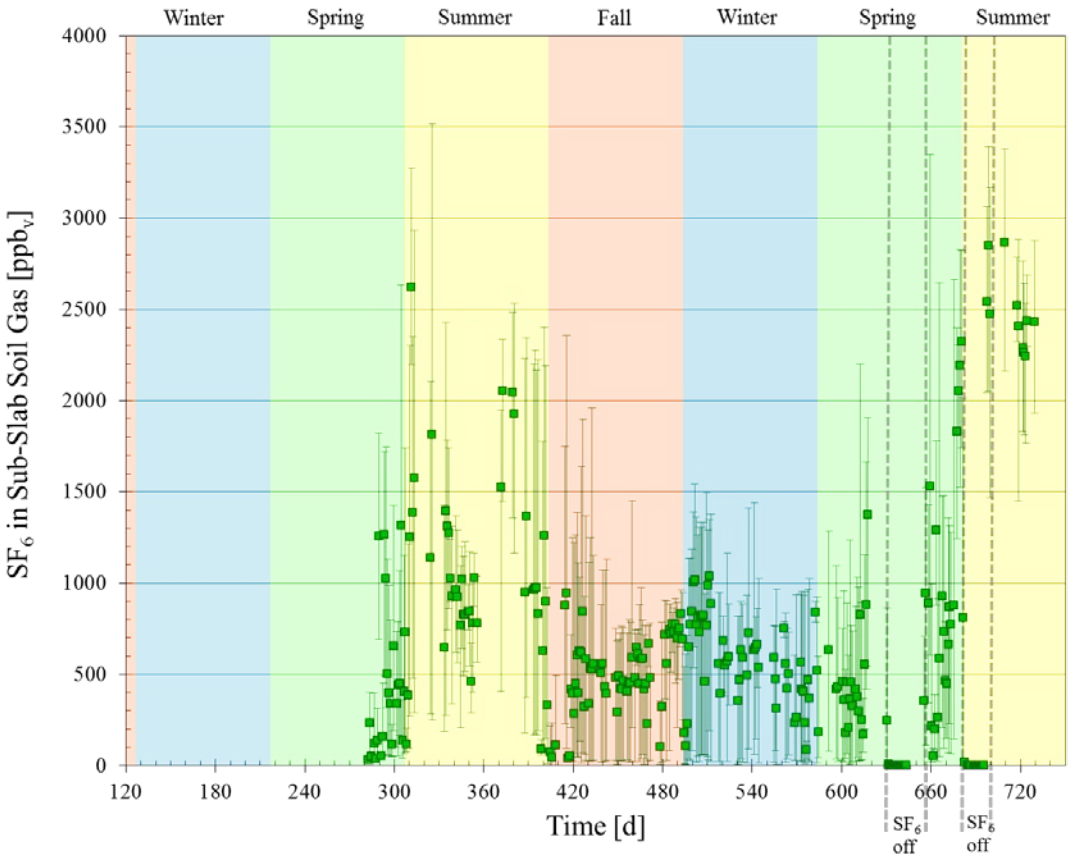

Figure A.26. 24-h averaged SF_6 concentrations sub-slab soil gas at location 6 from winter 2010 through summer 2012 with error bars spanning the daily maximum and minimum values.

Figure A.27 (BS) soil gas at location 3 from 234 < t < 271 d. In contrast to indoor air and SS soil gas, soil gas at 0.9 m BS showed less temporal variation. For the short period shown in Figure V.6, soil gas at 0.9 m BS steadily increased in concentration by approximately an order of magnitude. During this same period, SS soil gas concentration also increased but the data were more sporadic with concentrations fluctuating between indoor air and 0.9 m BS levels.

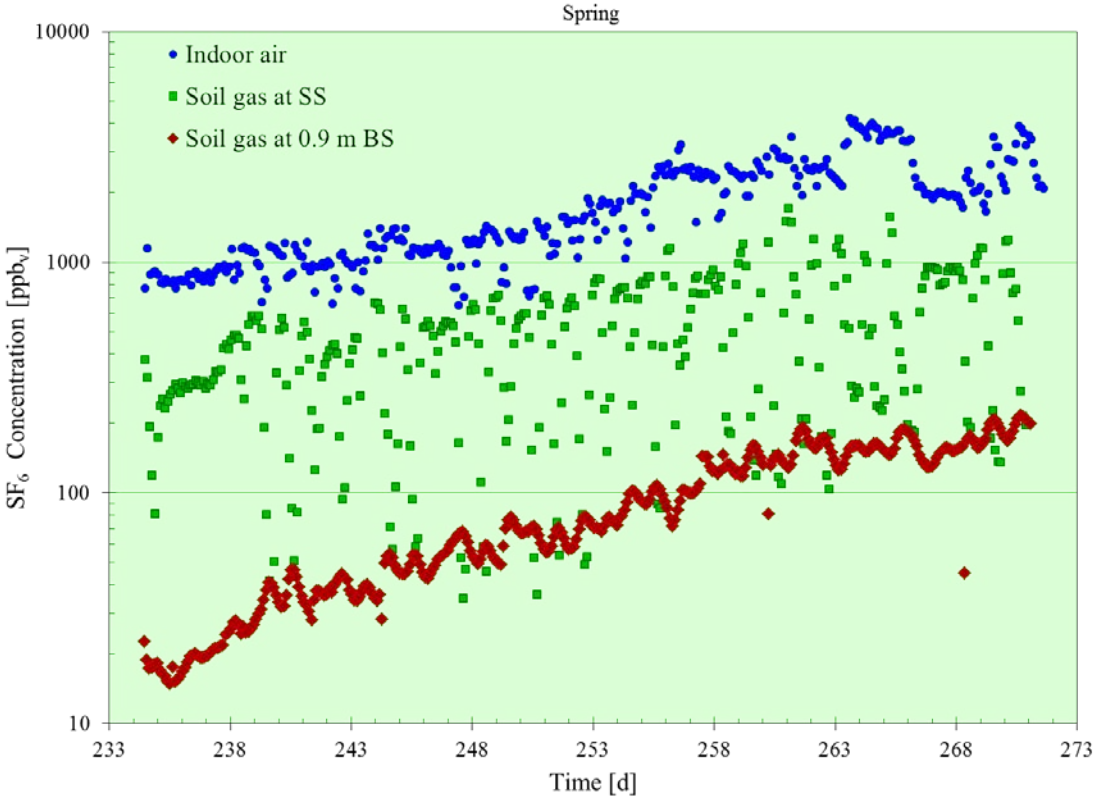

Figure A.27. Instantaneous SS soil gas, 0.9 m BS soil gas, and indoor air SF_6 concentrations at location 3 during spring 2011 for the period 232 < t < 271 d.

The results from synoptic soil gas surveys for SS, 0.9 m BS, and 1.8 m BS depths are shown in Tables A.5 –A.7, respectively. To better illustrate the distribution of SF_6 in the subsurface, the results were plotted as multi-depth contours of SF_6 concentrations in soil gas at SS, 0.9 m BS, and 1.8 m BS depths. The plots, shown in Figures A.29-A.39, were generated using Surfer 12 software (Golden Software, Golden, CO). The Kriging gridding method provided in the software was used to interpolate soil gas concentrations between monitoring points.

Table A.5. SF_6 concentrations in sub-slab depth soil gas, along with relevant statistics, for surveys performed during natural conditions.

Date of Sampling	Soil Gas Concentration [ppb_v]											
	Sampling Location (SS)											
	Garage		*Indoor*					*Backyard*		*Front yard*		
	1	*4*	*2*	*3*	*5*	*6*	*7*	*A*	*B*	*C*	*E*	*F*
3/1/2011	23	11	156	766	70	115	102	2	1	4	1	2
4/4/2011	17	7	53	388	57	185	94	1	1	4	0	1
5/18/2011	50	28	801	935	65	660	239	2	2	6	5	12
7/7/2011	803	446	1793	1657	452	561	1693	9	8	13	5	30
8/18/2011	898	549	1034	1470	760	1171	1389	13	11	31	10	19
11/4/2011	15	4	24	876	36	626	223	8	6	1	1	4
12/3/2011	10	2	50	96	21	484	7	4	13	4	1	1
1/11/2012	13	3	89	281	69	54	56	3	3	6	7	1
2/16/2012	18	5	77	564	36	28	88	9	3	8	7	8
4/30/2012	54	22	602	587	391	870	943	10	5	13	8	14
8/20/2012	2378	1316	2315	3072	1433	2849	2206	52	47	51	10	60
Mean	389	218	636	972	308	691	640	10	9	13	5	14
Median	23	11	156	766	69	561	223	8	5	6	5	8
Standard Deviation	738	414	790	842	443	801	786	14.5	13.4	15.1	3.8	17.9
Maximum	2378	1316	2315	3072	1433	2849	2206	52	47	51	10	60
Minimum	10	2	24	96	21	28	7	1	1	1	0	1

Table A.6. SF_6 concentrations in 0.9 m below-slab depth soil gas, along with relevant statistics, for surveys performed during natural conditions.

Date of Sampling	Soil Gas Concentration [ppb_v]											
	Soil Gas Location (0.9 m BS)											
	Garage		*Indoor*				*Backyard*		*Front yard*			
	1	*4*	*2*	*3*	*5*	*6*	*A*	*B*	*C*	*D*	*E*	*F*
3/1/2011	15	48	55	6	19	34	3	4	3	4	1	2
4/4/2011	10	90	67	3	30	34	1	1	3	2	1	1
5/18/2011	38	195	100	12	94	41	2	1	9	1	2	1
7/7/2011	601	1402	1194	437	1190	420	2	NS	14	15	13	13
8/18/2011	1017	1399	1149	746	1243	467	7	11	38	19	13	22
11/4/2011	18	171	92	10	188	37	7	NS	1	3	1	6
12/3/2011	8	67	18	5	39	19	4	2	4	1	0	2
1/11/2012	7	27	22	7	14	20	7	8	17	2	2	4
2/16/2012	9	81	97	6	24	44	2	3	6	3	7	3
4/30/2012	30	301	204	14	143	87	7	2	54	4	2	3
8/20/2012	1907	2767	2709	1244	2551	1137	54	41	118	38	26	49
Mean	333	595	519	226	503	213	9	8	24	8	6	10
Median	18	171	97	10	94	41	4	3	9	3	2	3
Standard Deviation	618	887	849	416	822	347	15.3	12.7	35.3	11.4	8.2	14.6
Maximum	1907	2767	2709	1244	2551	1137	54	41	118	38	26	49
Minimum	7	27	18	3	14	19	1	1	1	1	0	1

Table A.7. SF_6 concentrations in 1.8 m below-slab depth soil gas, along with relevant statistics, for surveys performed during natural conditions.

Date of Sampling	Soil Gas Concentration [ppb_v]									
	Soil Gas Location (1.8 m BS)									
	Garage		*Indoor*				*Front yard*			
	1	*4*	*2*	*3*	*5*	*6*	*C*	*D*	*E*	*F*
3/1/2011	12	24	17	6	10	7	3	3	2	1
4/4/2011	4	51	NS	1	8	7	2	1	1	NS
5/18/2011	10	62	NS	9	17	NS	2	10	3	NS
7/7/2011	154	757	NS	215	328	45	3	16	11	2
8/18/2011	630	1151	1002	596	940	130	16	22	13	8
11/4/2011	19	264	45	11	265	31	1	5	2	7
12/3/2011	16	24	7	3	21	3	1	2	2	3
1/11/2012	3	11	9	6	3	3	3	3	6	2
2/16/2012	3	23	22	3	4	2	3	4	1	2
4/30/2012	23	96	74	38	14	13	6	13	3	4
8/20/2012	1503	2600	2661	932	1967	921	135	37	27	31
Mean	216	460	480	166	325	116	16	10	6	7
Median	16	62	33	9	17	10	3	5	3	3
Standard Deviation	466	801	945	312	614	285	39.7	10.9	8.0	9.4
Maximum	1503	2600	2661	932	1967	921	135	37	27	31
Minimum	3	11	7	1	3	2	1	1	1	1

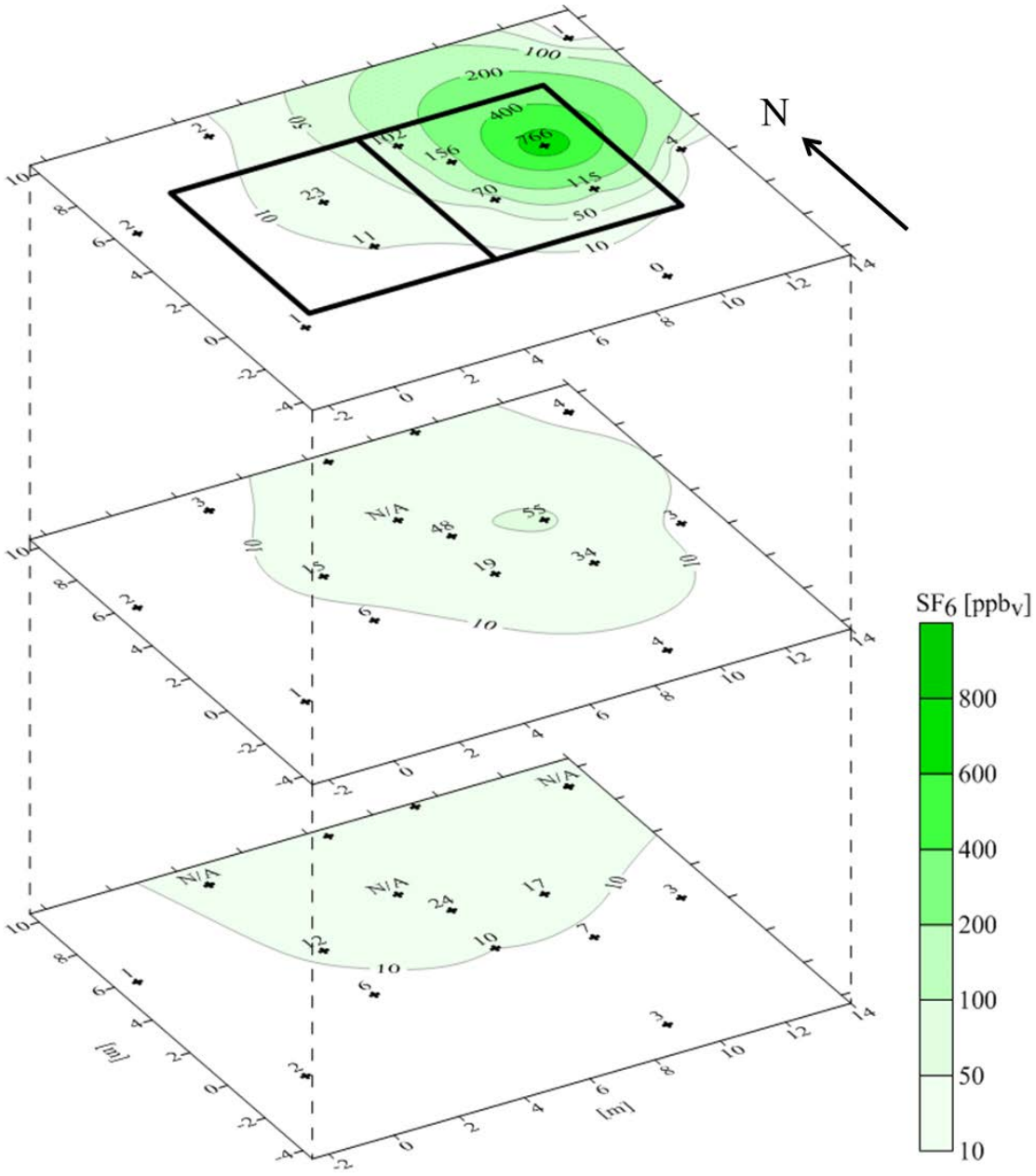

Figure A.28. Contour plots of SF_6 concentrations in soil gas at depths of SS, 0.9 BS, and 1.8 m BS from synoptic soil gas survey in March 2011.

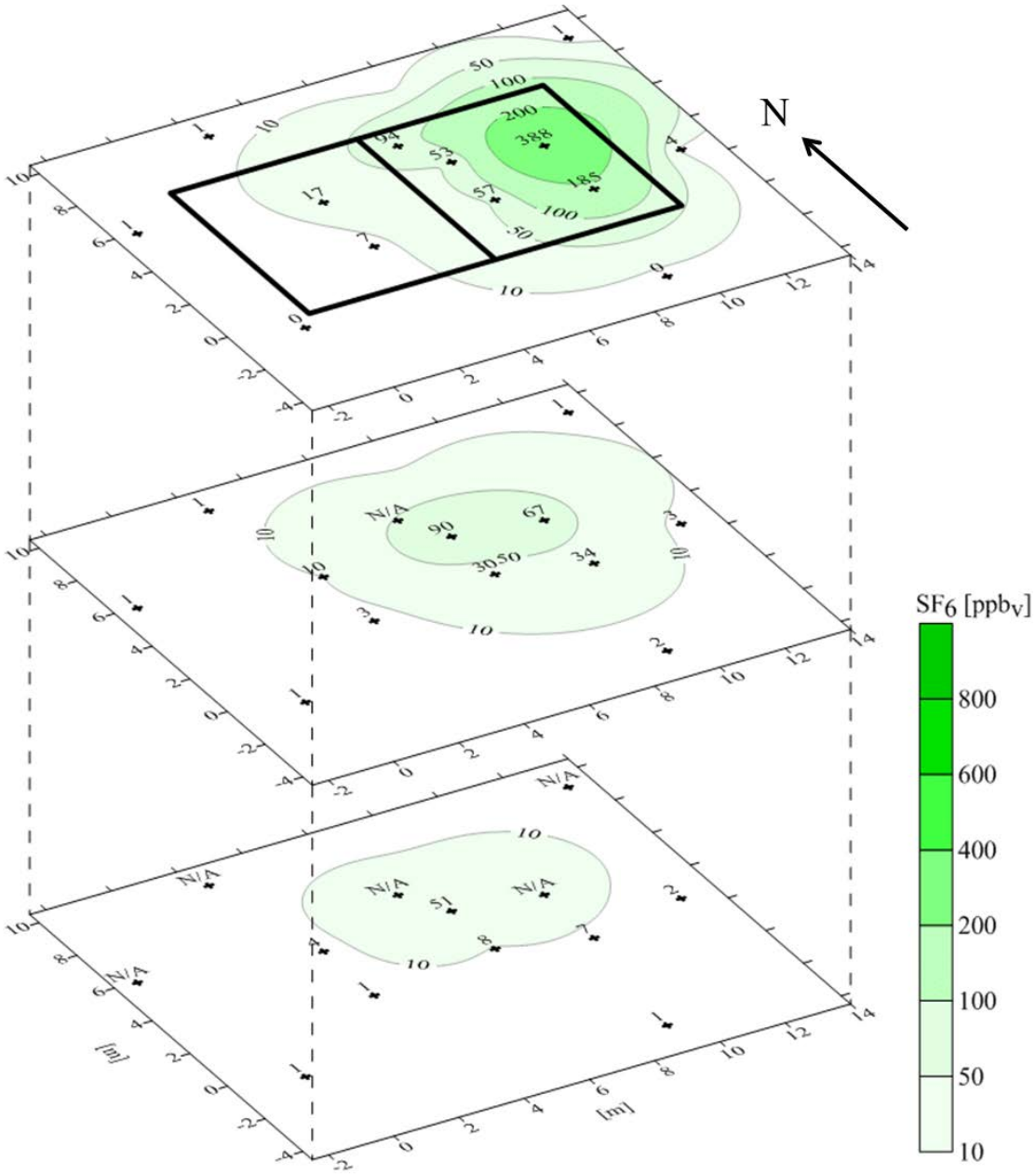

Figure A.29. Contour plots of SF_6 concentrations in soil gas at depths of SS, 0.9 BS, and 1.8 m BS from synoptic soil gas survey in April 2011.

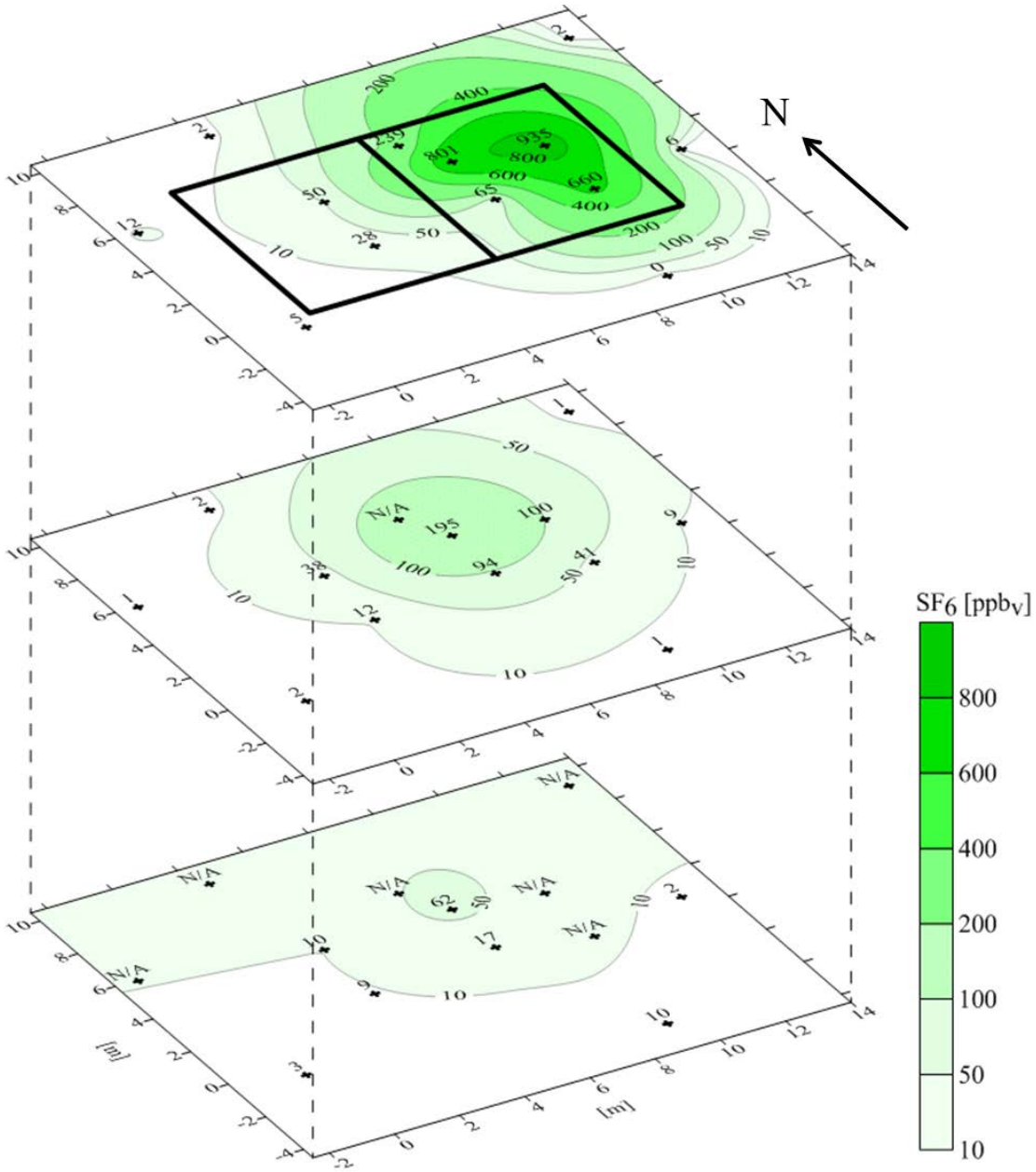

Figure A.30. Contour plots of SF_6 concentrations in soil gas at depths of SS, 0.9 BS, and 1.8 m BS from synoptic soil gas survey in May 2011.

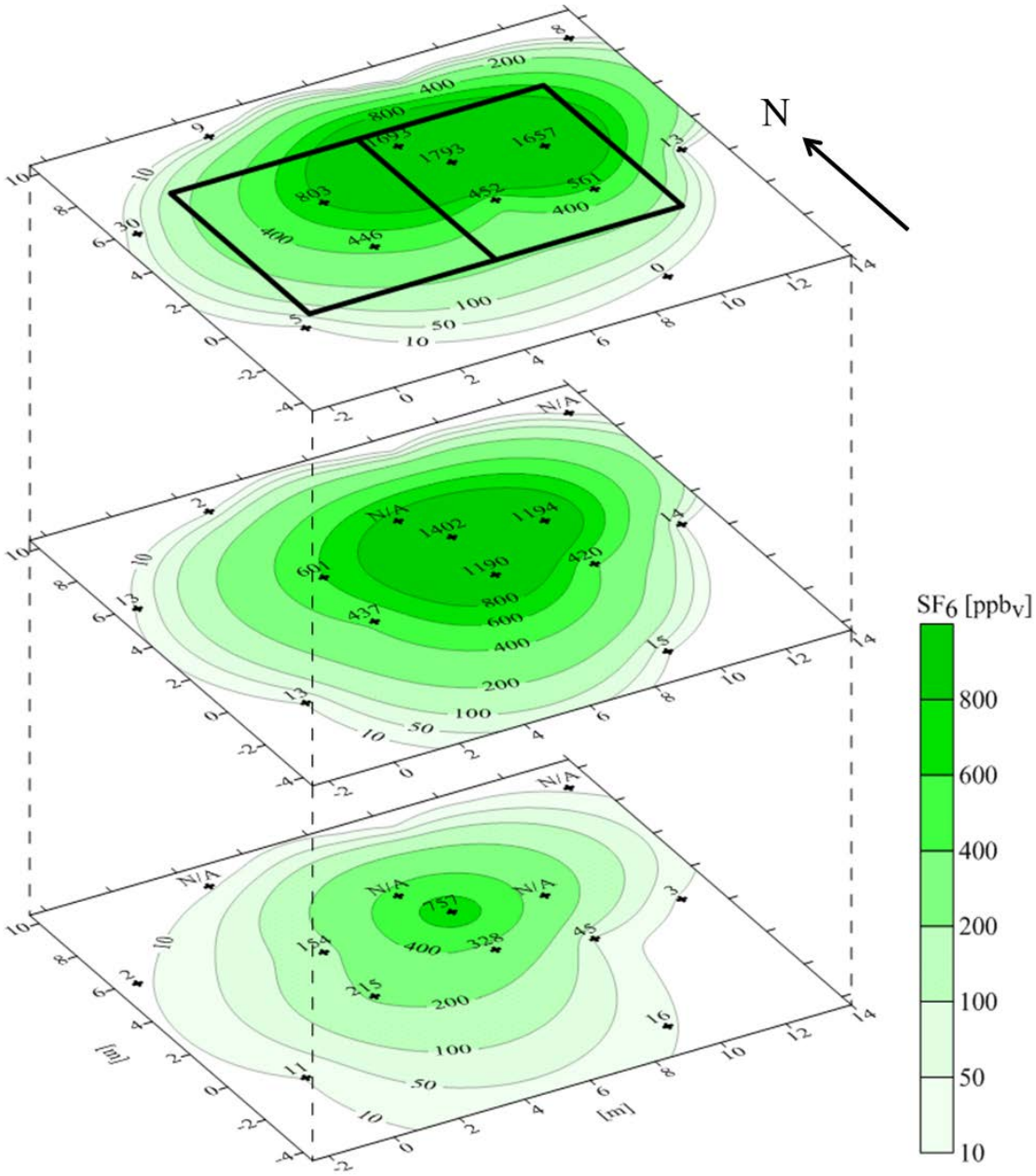

Figure A.31. Contour plots of SF_6 concentrations in soil gas at depths of SS, 0.9 BS, and 1.8 m BS from synoptic soil gas survey in July 2011.

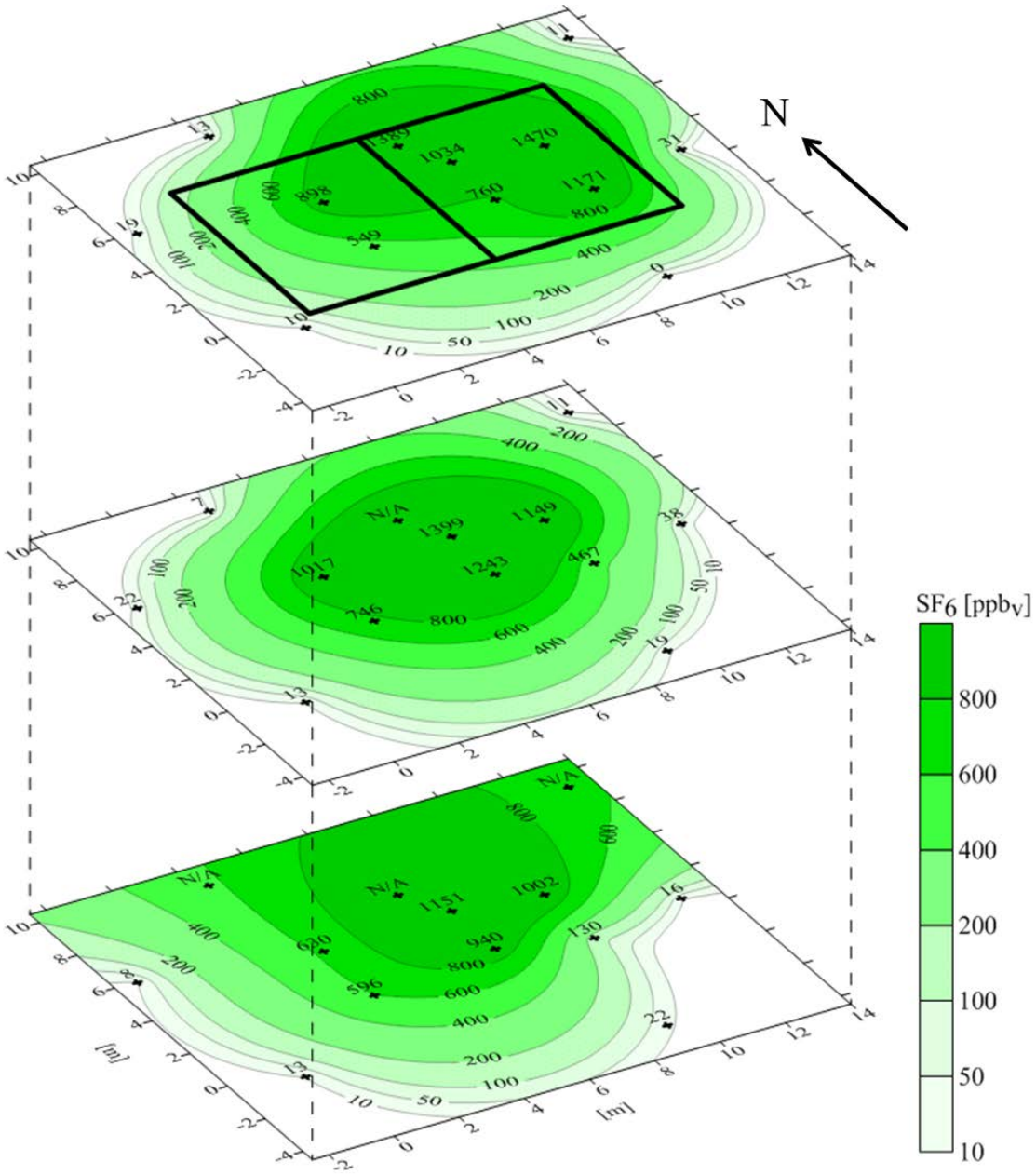

Figure A.32. Contour plots of SF_6 concentrations in soil gas at depths of SS, 0.9 BS, and 1.8 m BS from synoptic soil gas survey in August 2011.

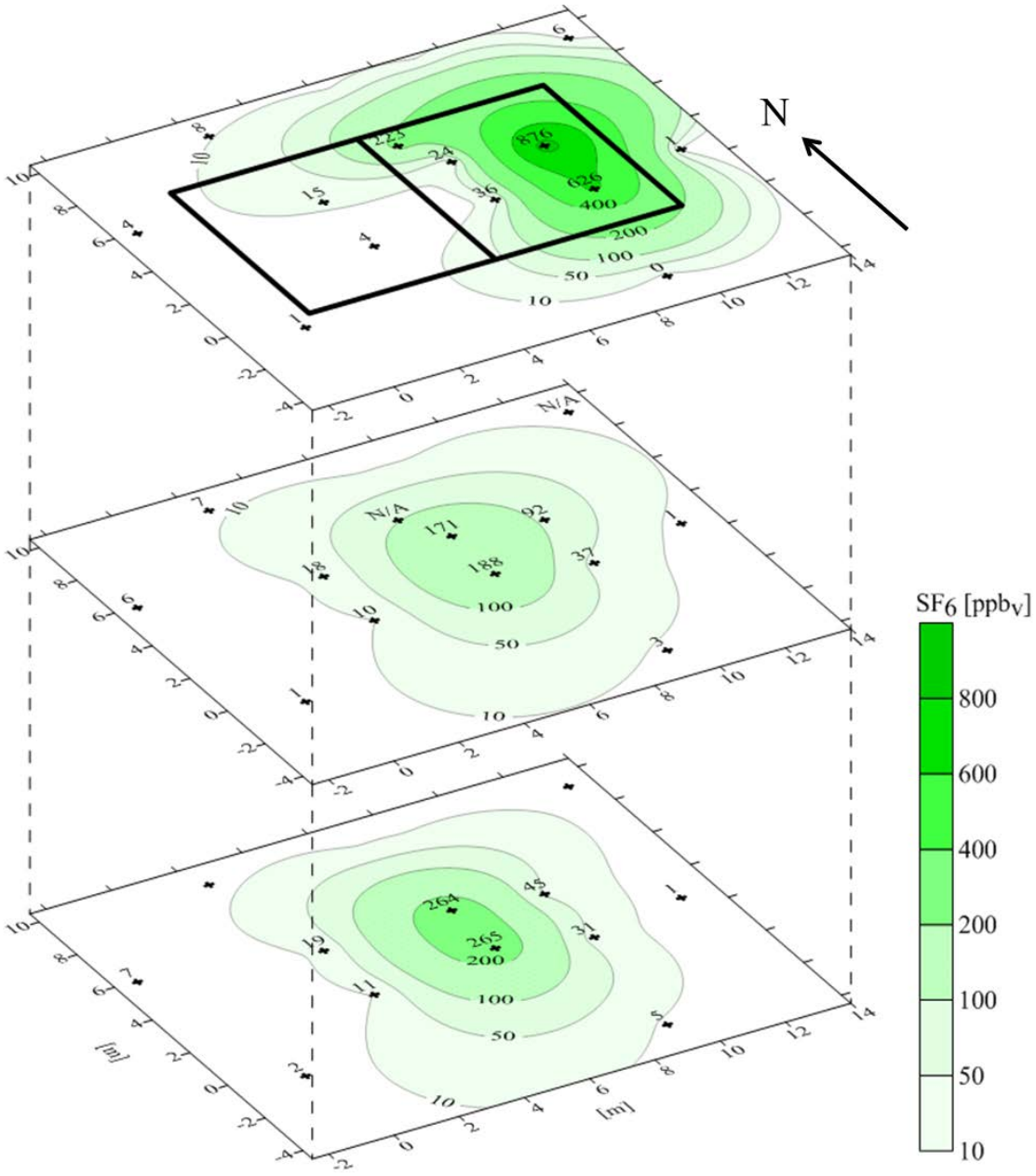

Figure A.33. Contour plots of SF_6 concentrations in soil gas at depths of SS, 0.9 BS, and 1.8 m BS from synoptic soil gas survey in November 2011.

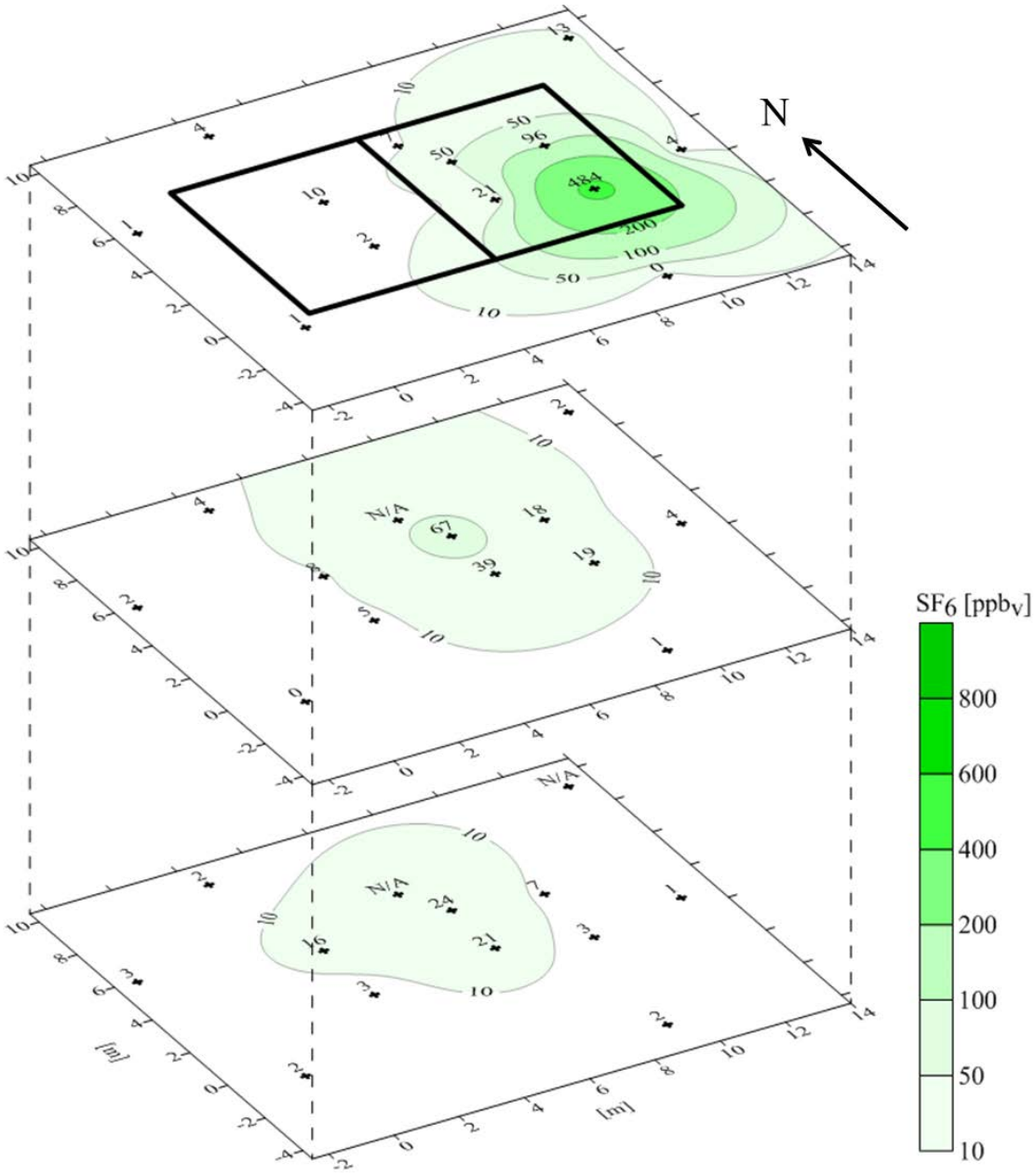

Figure A.34. Contour plots of SF_6 concentrations in soil gas at depths of SS, 0.9 BS, and 1.8 m BS from synoptic soil gas survey in December 2011.

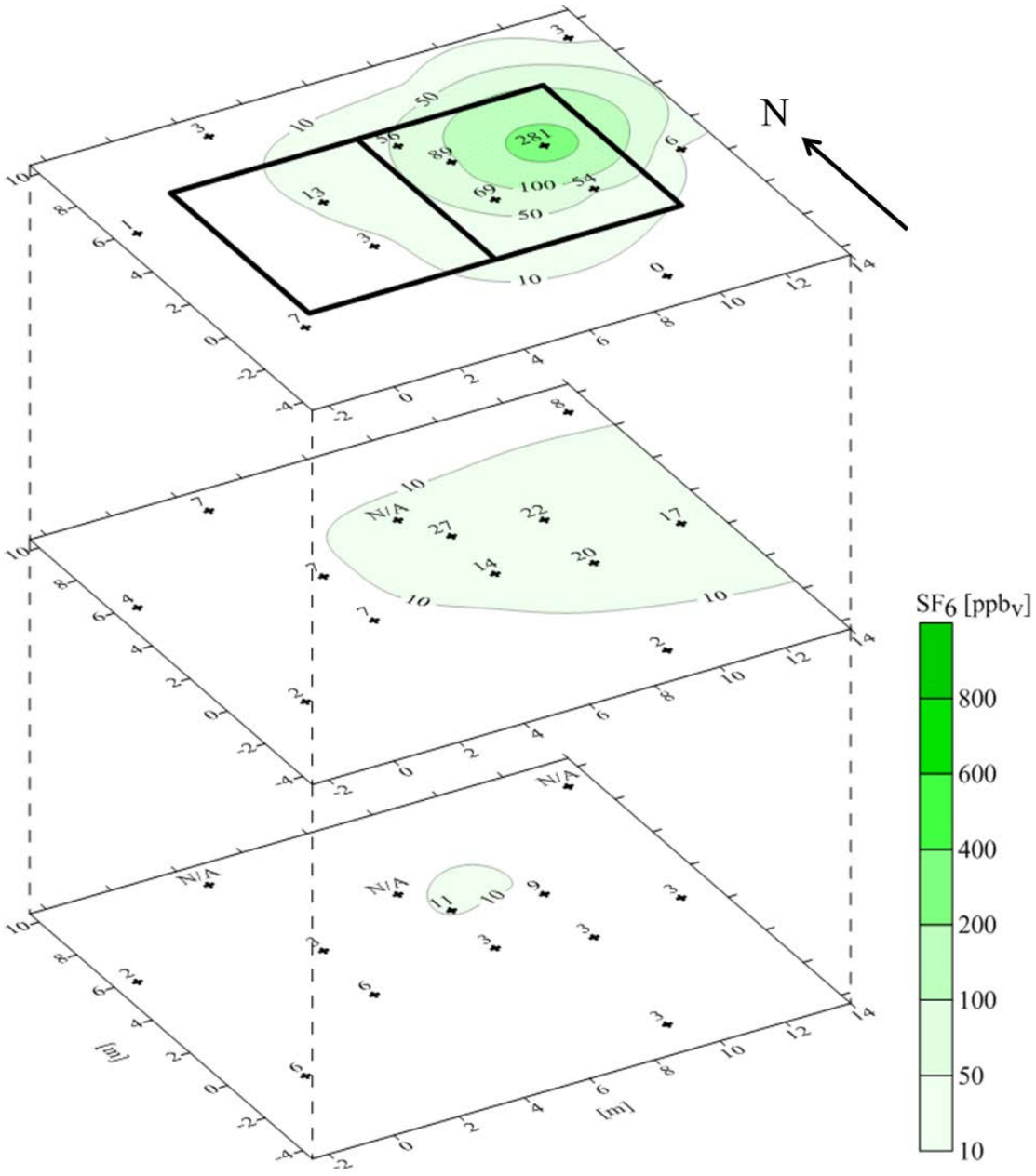

Figure A.35. Contour plots of SF_6 concentrations in soil gas at depths of SS, 0.9 BS, and 1.8 m BS from synoptic soil gas survey in January 2012.

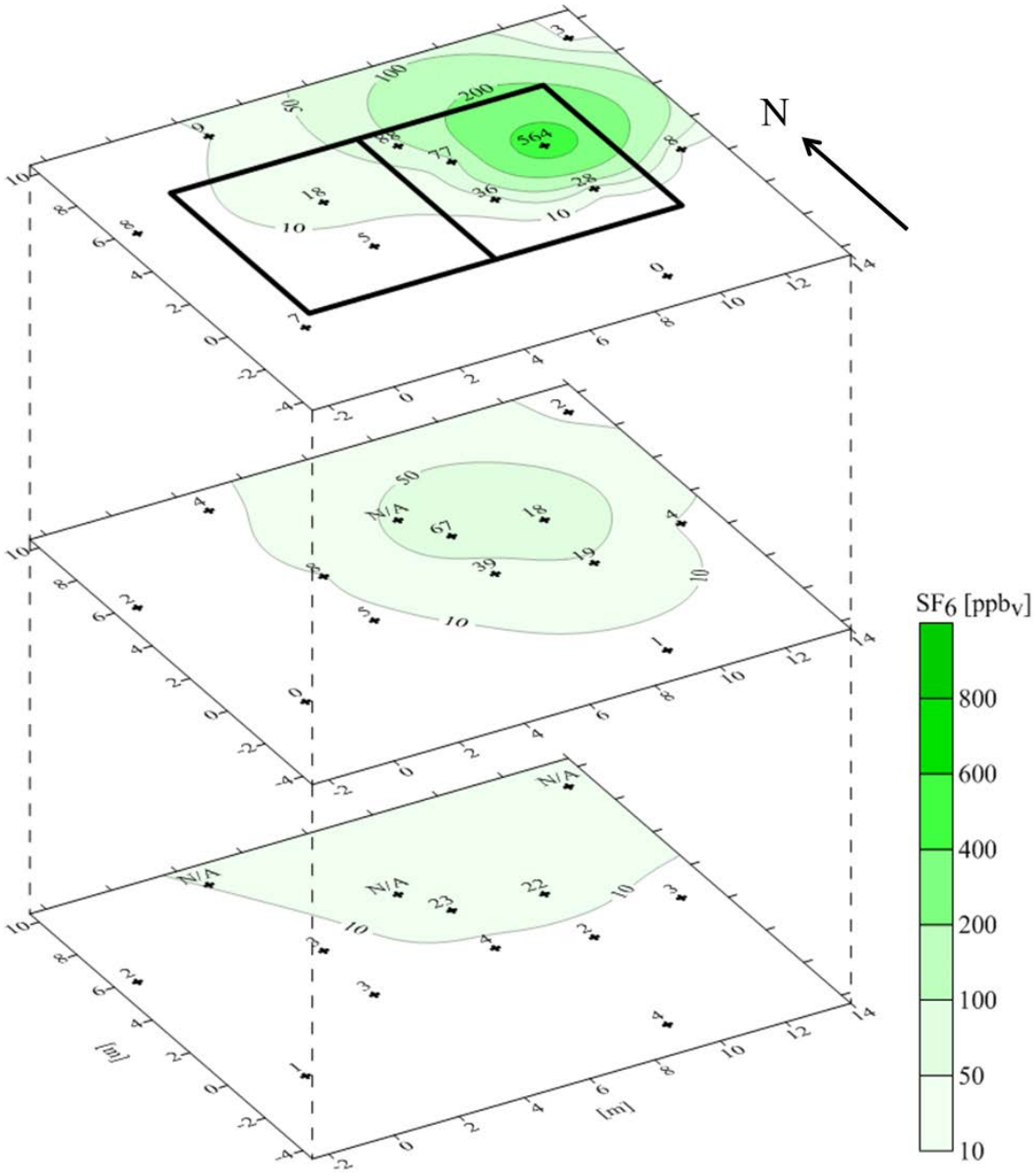

Figure A.36. Contour plots of SF_6 concentrations in soil gas at depths of SS, 0.9 BS, and 1.8 m BS from synoptic soil gas survey in February 2012.

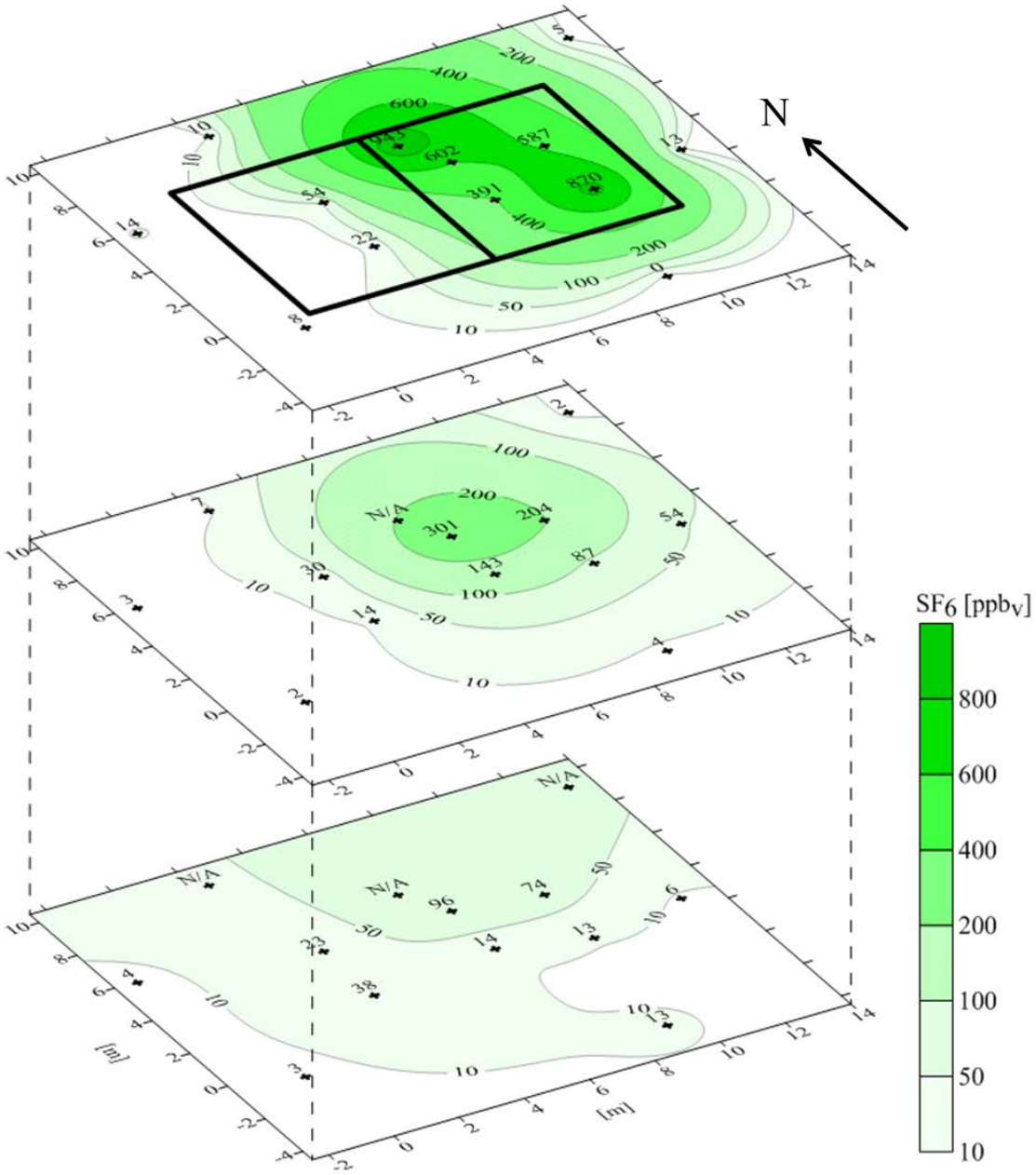

Figure A.37. Contour plots of SF_6 concentrations in soil gas at depths of SS, 0.9 BS, and 1.8 m BS from synoptic soil gas survey in April 2012.

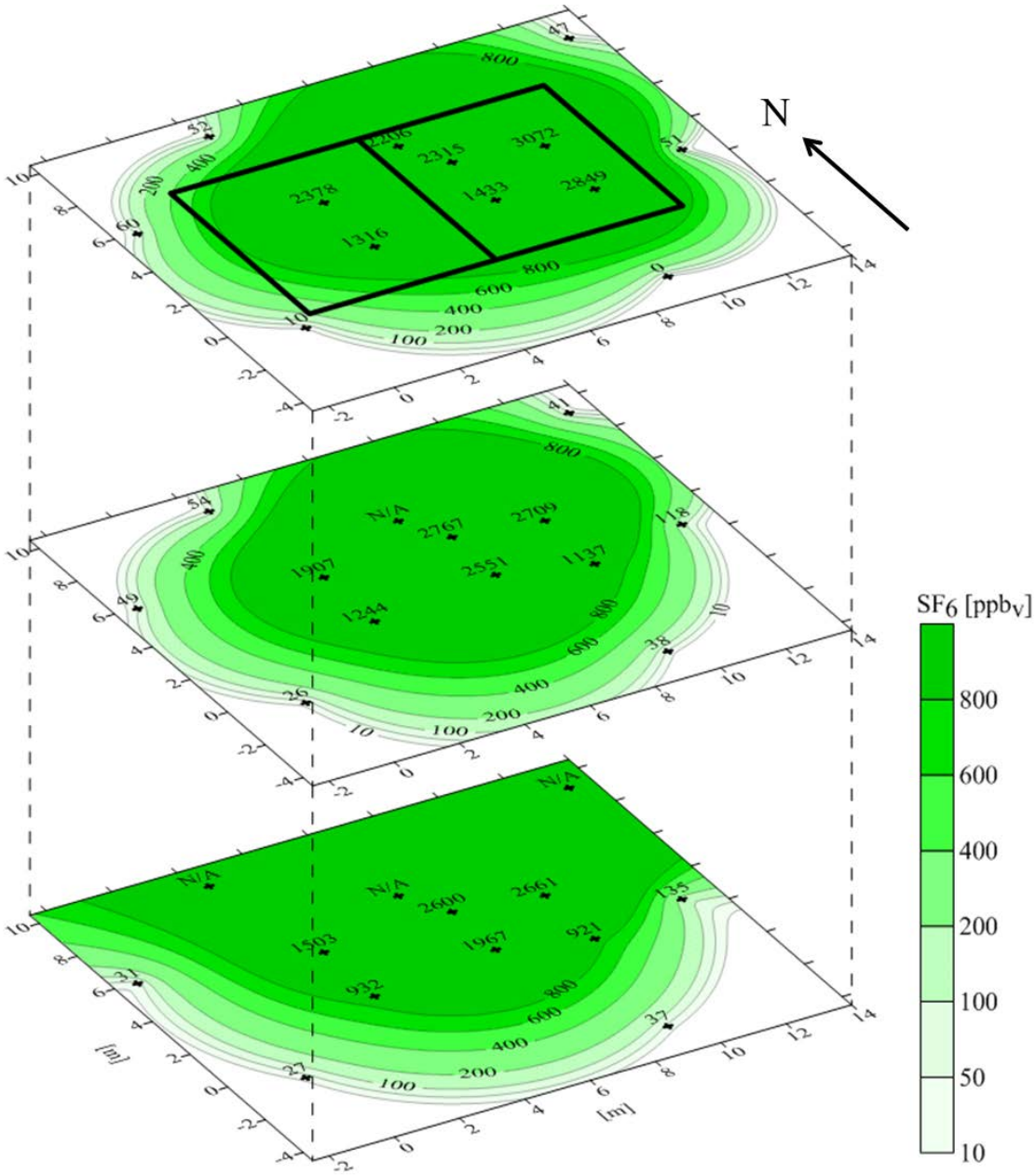

Figure A.38. Contour plots of SF_6 concentrations in soil gas at depths of SS, 0.9 BS, and 1.8 m BS from synoptic soil gas survey in August 2012.

Indoor source introduction and removal tests. Field studies to simulate the removal of indoor sources that may occur during or prior to VI site investigations occurred from 630 < t < 655 d, 655 < t < 695 d, and 1460 < t < 1512 d. The indoor air and soil gas SF_6 concentration results from these tests are shown in Figures A.40 – A.47. Due to computer and remote access issues, there are multi-day gaps of data for the first tests (630 < t < 655 d). Nonetheless, the general trend is still visible. For the second test (655 < t < 695 d), the introduction of the source was also monitored.

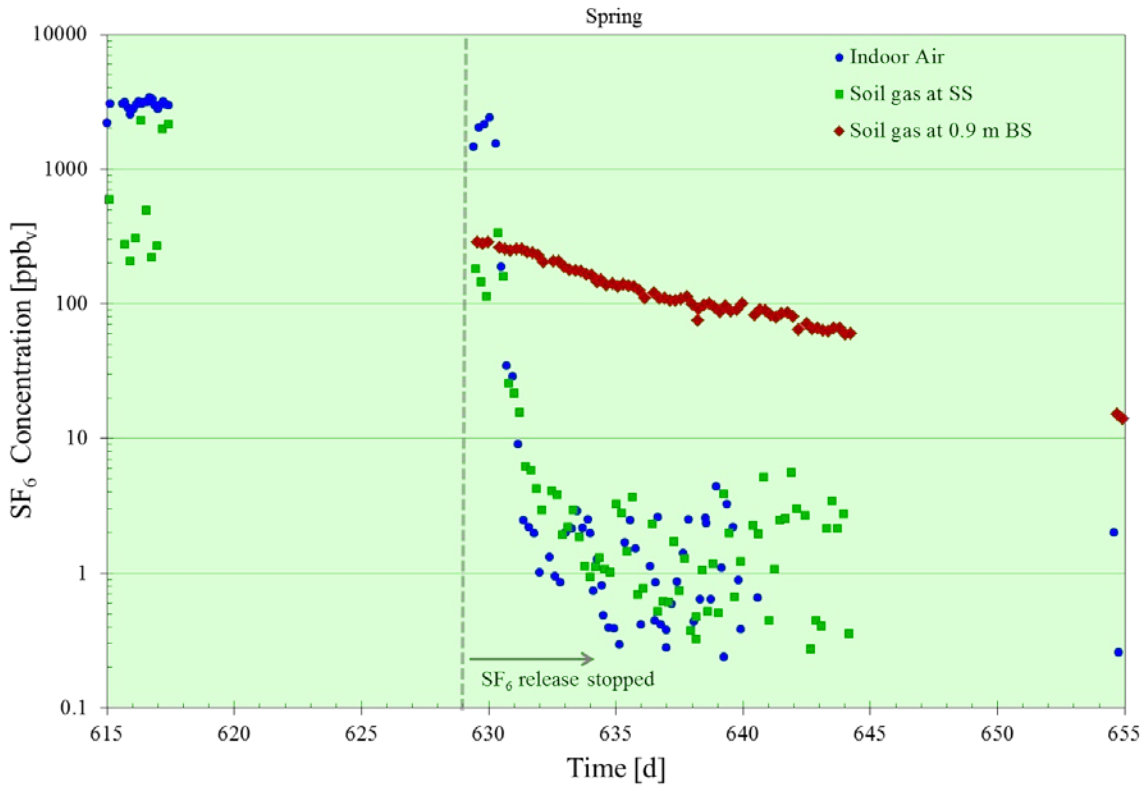

Figure A.39. Instantaneous SF_6 concentrations in indoor air and SS and 0.9 m BS soil gas at location 2 from early to late May 2012 (630 < t < 655 d) showing the results of introduction and removal of an indoor source.

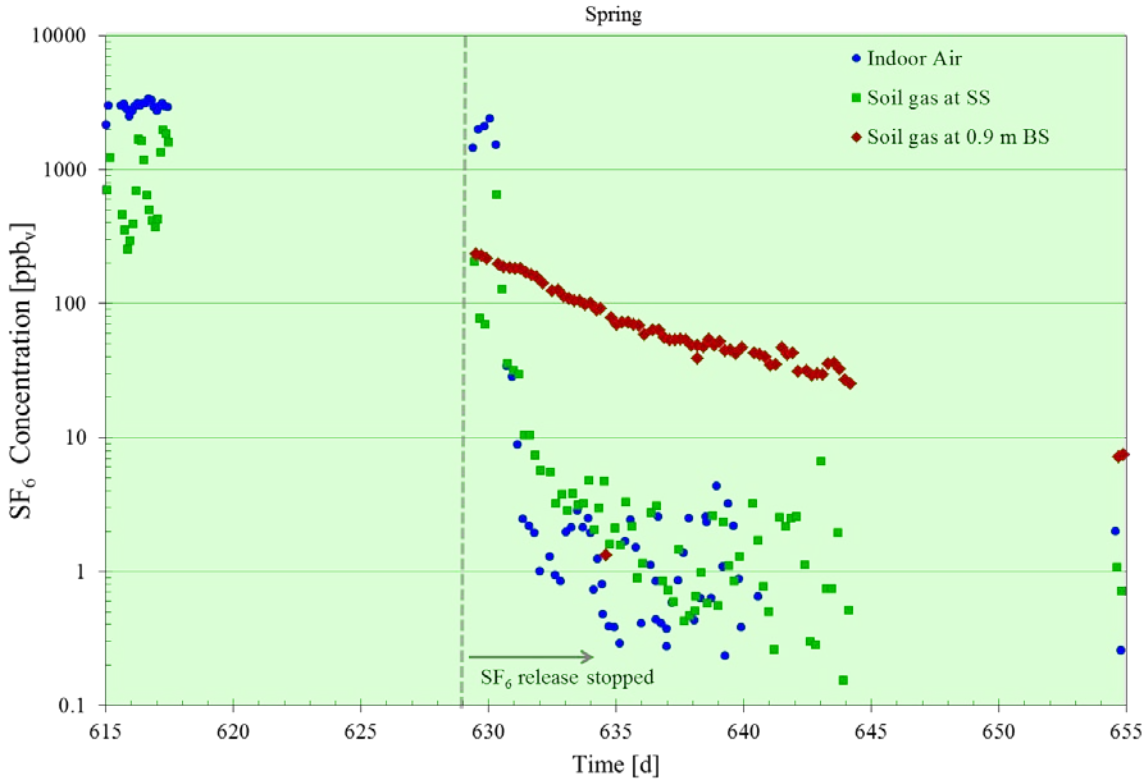

Figure A.40. Instantaneous SF_6 concentrations in indoor air and SS and 0.9 m BS soil gas at location 3 from early to late May 2012 ($630 < t < 655$ d) showing the results of introduction and removal of an indoor source.

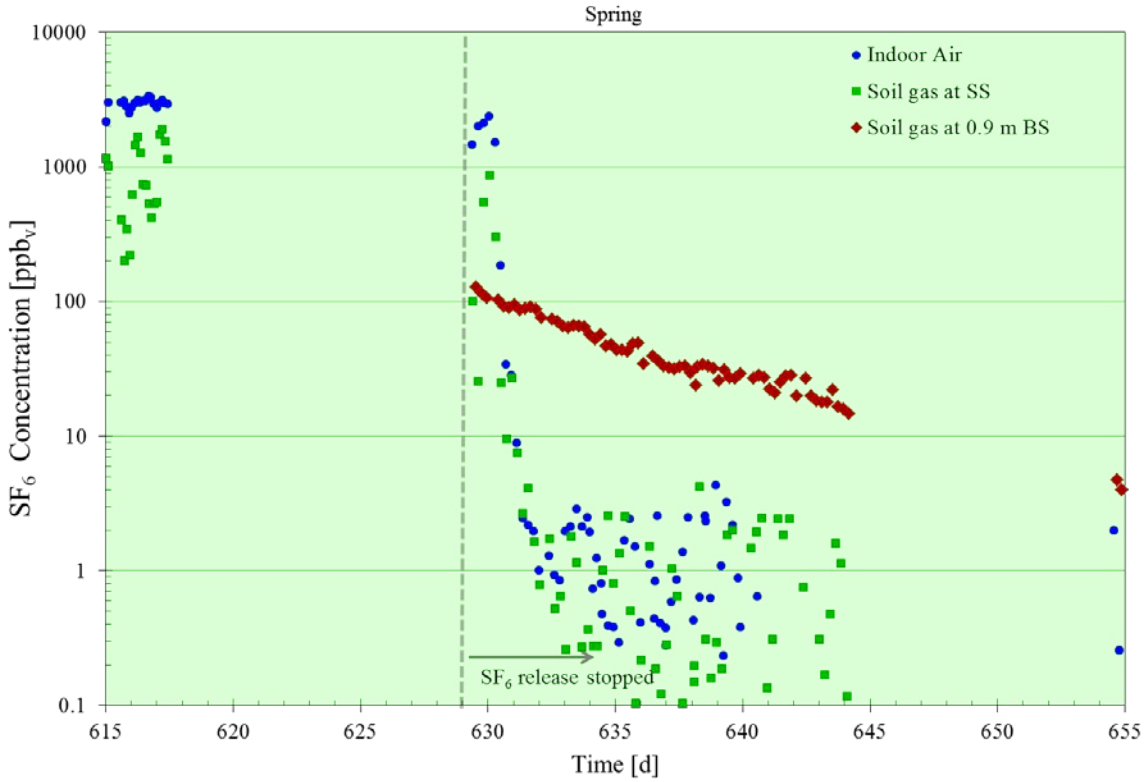

Figure A.41. Instantaneous SF_6 concentrations in indoor air and SS and 0.9 m BS soil gas at location 6 from early to late May 2012 ($630 < t < 655$ d) showing the results of introduction and removal of an indoor source.

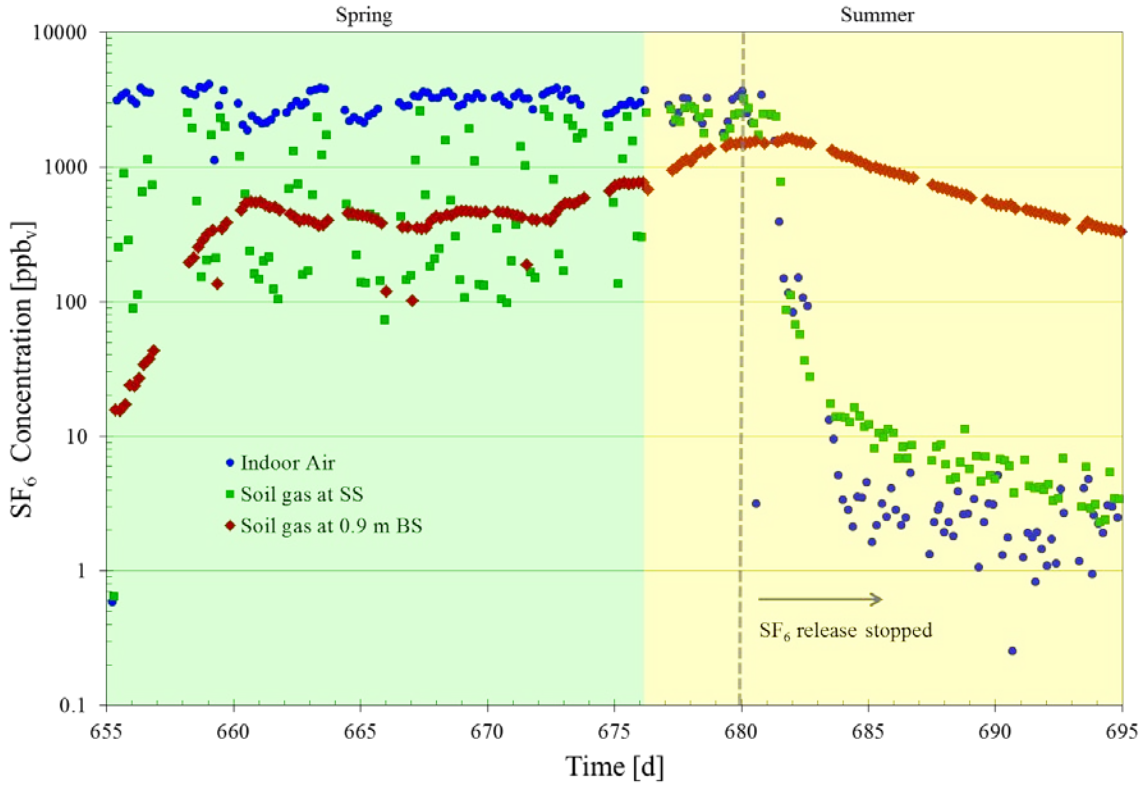

Figure A.42. Instantaneous SF_6 concentrations in indoor air and SS and 0.9 m BS soil gas at location 2 from late May to mid-July 2012 ($655 < t < 695$ d) showing the results of introduction and removal of an indoor source.

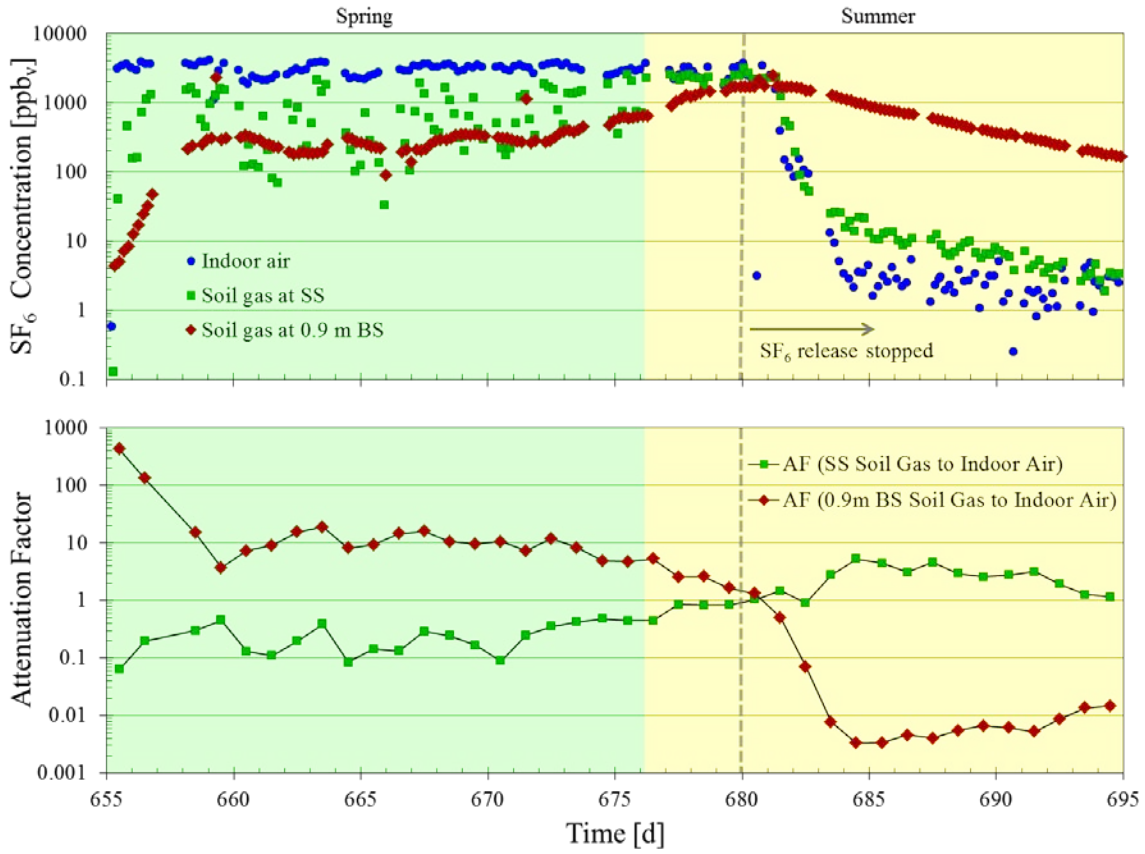

Figure A.43. Instantaneous SF_6 concentrations in indoor air and SS and 0.9 BS soil gas at location 3 from late May to mid-July 2012 ($655 < t < 695$ d) along with corresponding attenuation factors calculated from 24-h averaged indoor air and soil gas concentrations showing the results of introduction and removal of an indoor source.

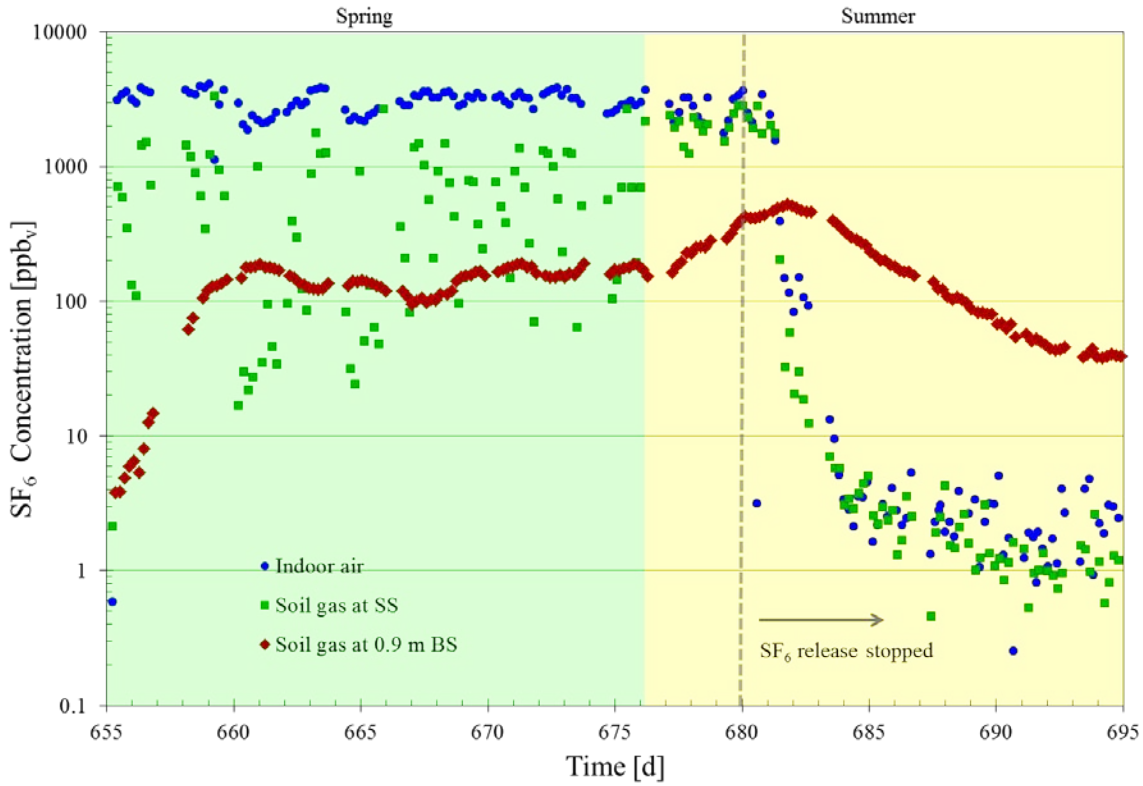

Figure A.44. Instantaneous SF_6 concentrations in indoor air and SS and 0.9 m BS soil gas at location 6 from late May to mid-July 2012 ($655 < t < 695$ d) showing the results of introduction and removal of an indoor source.

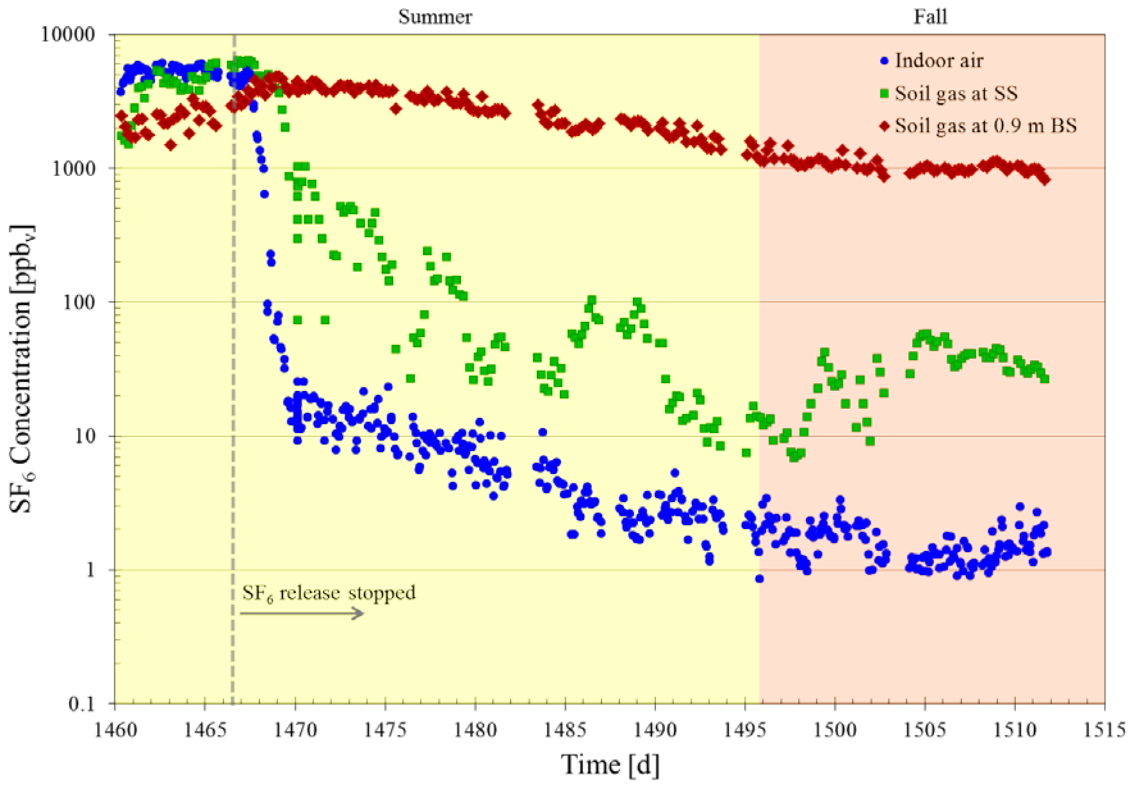

Figure A.45. Instantaneous SF_6 concentrations in indoor air and SS and 0.9 m BS soil gas at location 2 from mid-August to early October 2014 ($1460 < t < 1512$ d) showing the results of indoor source removal after modification of subsurface pathway.

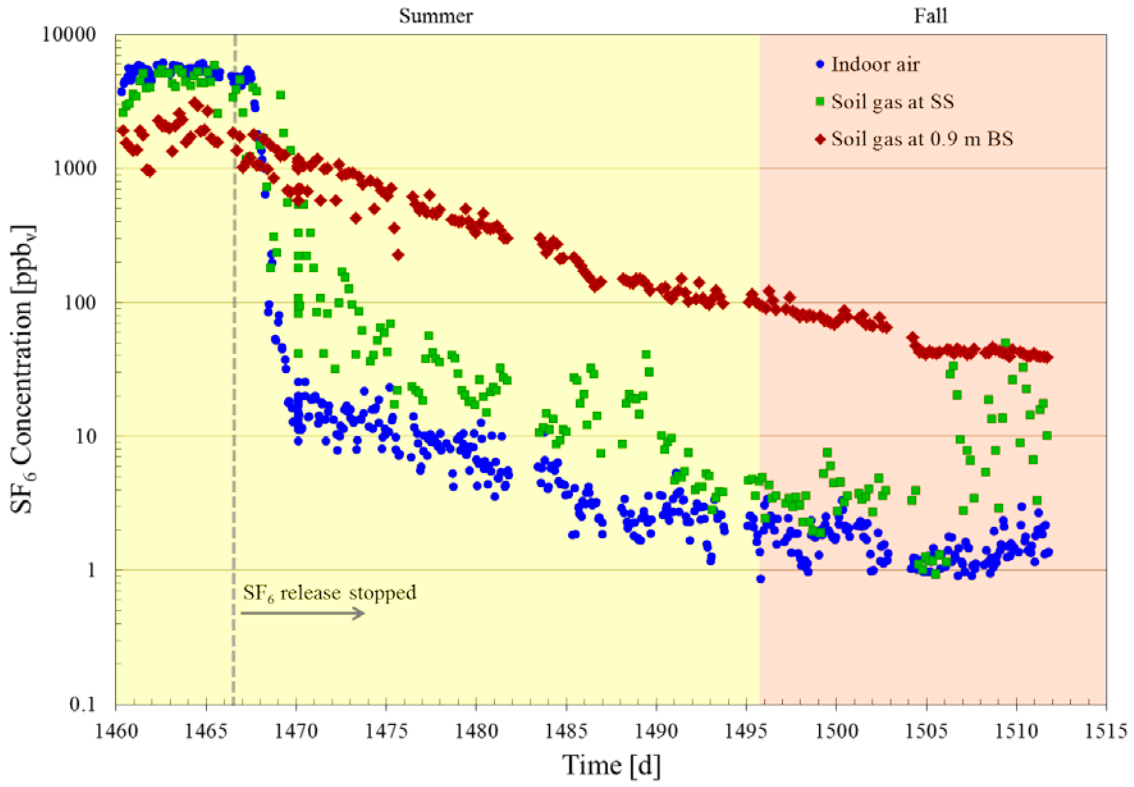

Figure A.46. Instantaneous SF_6 concentrations in indoor air and SS and 0.9 m BS soil gas at location 6 from mid-August to early October 2014 ($1460 < t < 1512$ d) showing the results of indoor source removal after modification of subsurface pathway.

Indoor source modeling studies. Modeling was performed to further explore the behavior of indoor sources in the subsurface. The modeling results were generated using a modified version of the three-dimensional, multicomponent, numerical model developed by Abreu (2005) and updated by Luo (2009). The version of the model used in these studies was modified to include the presence of an indoor source releasing to indoor air at a constant emission rate. Table A.8 provides details on the scenarios simulated. The input parameters used in generating the simulation results are provided in Table A.9.

Table A.8. Summary of indoor source removal scenarios simulated for this study.

	Creation of Subsurface Soil Gas Plume			Removal of Indoor Source	
Simulation #	Indoor source* emission rate [g/s]	Disturbance pressure ($P^{outdoor}$-P^{indoor}) [Pa]	Simulation time [h]	Disturbance pressure ($P^{outdoor}$-P^{indoor}) [Pa]	Simulation time [h]
1	4.00E-04	-2	720	-2	720
2	4.00E-04	-2	720	0	720
3	4.00E-04	-2	720	5	720
4	4.00E-04	-2	720	10	720
5	4.00E-04	0	720	0	720
6	4.00E-04	0	720	5	720
7	4.00E-04	0	720	10	720
8	4.00E-04	2	720	2	720
9	4.00E-04	2	720	5	720
10	4.00E-04	2	720	10	720

*Chemical-specific properties of sulfur hexafluoride (SF_6) were used in simulations

Table A.9. Input parameters used in generating simulations described in Table A.8.

Input Parameters used in generating indoor source simulations	
Building/foundation parameters Length: 11 m Width: 10 m Depth in soil: 1.0 m Foundation thickness: 0.15 m Enclosed space volume: 350 m^3 Air exchange rate: 0.5 h^{-1} Crack width: 0.001 m Total crack length: 32 m Crack location: perimeter **Indoor air source properties** Compound: sulfur hexafluoride (SF_6) Emission rate to indoor air: • 0.4 mg/s Molecular diffusion coefficient in air (D^a): • 6.1E-2 cm^2/s Molecular diffusion coefficient in water (D^w): • 1.2E-5 cm^2/s Henry's Law constant (H): • 170.4 m^3-water/m^3-vapor Sorption coefficient of compound to organic carbon (K_{oc}): • 13.5 g/g-oc Atmospheric concentration: negligible	**Soil Properties** Soil bulk density (ρ_b): 1700 kg/m^3 Mass fraction of organic carbon in soil (f_{oc}): 0.001 kg-oc/kg-soil Moisture-filled porosity (ϕ_w): 0.07 m^3-H_2O/m^3-soil Total soil porosity (ϕ_T): 0.35 m^3-voids/m^3-soil Soil permeability to soil gas flow (K_g): 1E-7 cm^2 Soil gas phase dynamic viscosity: 1.8E-4 g/cm/s **Soil domain dimensions (x, y, z)** • 27 m x 25 m x 3 m **Algorithm parameters** Numerical scheme: implicit (steady-state) Disturbance pressure subroutine: • Variable time step: 0.1 s – 10 h • Percent change allowed/time step: 30% Concentration subroutine: • Variable time step: 10 s – 10 h • Percent change allowed/time step: 50-80%

A.6 HYDRUS 1-D model validation

Model validation. The groundwater table fluctuation lab experiment with water recharging/depleting from the lower boundary of the tank was similar to the mathematical modeling conditions. Thus, the experimental conditions for the play sand tank were input to the simulation and then the model output results were compared with experimental results. Table A.10 summarizes model inputs for this simulation. Sorption was neglected in because the measured soil organic fraction (f_{oc}) for the play sand was very small (<0.1%).

Table A.10. Model validation simulation inputs

Experimental Conditions and Soil Properties		
Total soil profile depth	cm	180
Initial water table elevation	cm	90
Residual soil water content	cm^3-H_2O)/cm^3-soil	0.079
Saturated soil water content	cm^3-H_2O)/cm^3-soil	0.35
Parameter *a* in the van Genuchten soil water retention function	cm^{-1}	0.2
Parameter *n* in the van Genuchten soil water retention function	-	2
Saturated hydraulic conductivity	cm/h	298.8
Tortuosity parameter in the conductivity function	-	0.5
Bulk density	g-soil/cm^3-soil	1.5
Longitudinal dispersivity	cm	0.1
Algorithm parameters		
Time weighting scheme		Crank-Nicholson implicit scheme
Space weighting scheme		Galerkin formulation
Minimum time step	s	0.864
Maximum time step	hour	50
Maximum number of iterations	-	10
Water content tolerance	-	0.001
Pressure head tolerance	cm	1

The van Genuchten capillary pressure-water saturation profile parameters used were obtained by fitting simulated to measured saturation profiles as shown in Figure A.48. As mentioned in laboratory section, a concentration gradient was created by volatilization during the static water table condition preceding the water table fluctuations. A similar initial chemical profile was created in the simulation for a scenario where the water table elevation was maintained at 90 cm above the bottom boundary and groundwater contaminant concentrations were initially uniform in the saturated zone. Once this contaminant profile was generated in the model, it was used as the initial concentration input for the water table fluctuation simulations. This initial contaminant concentration profile for TCE is presented in Figure A.49.

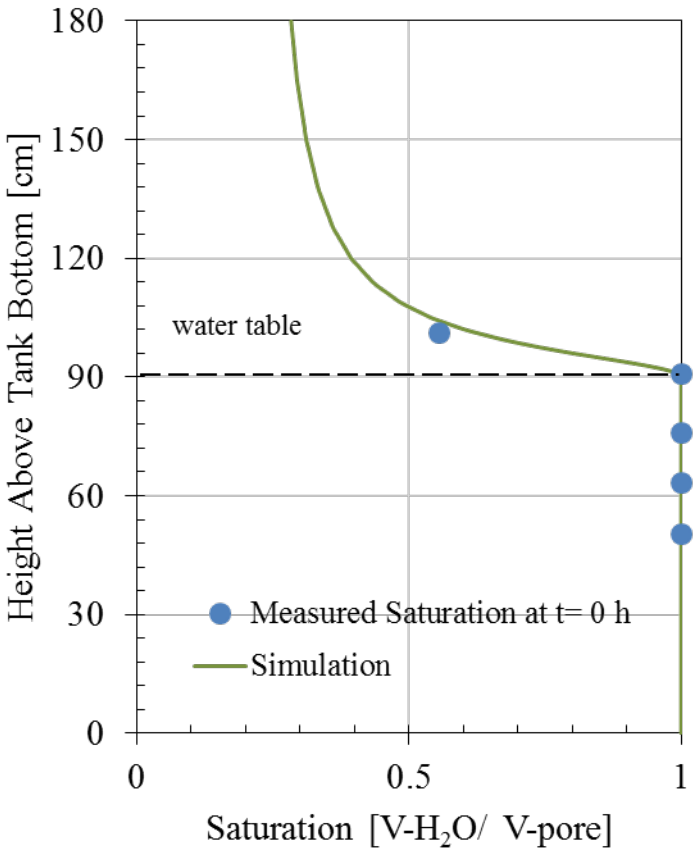

Figure A.47. Measured and simulated water saturation in play sand tank after fitting van-Genuchten parameters.

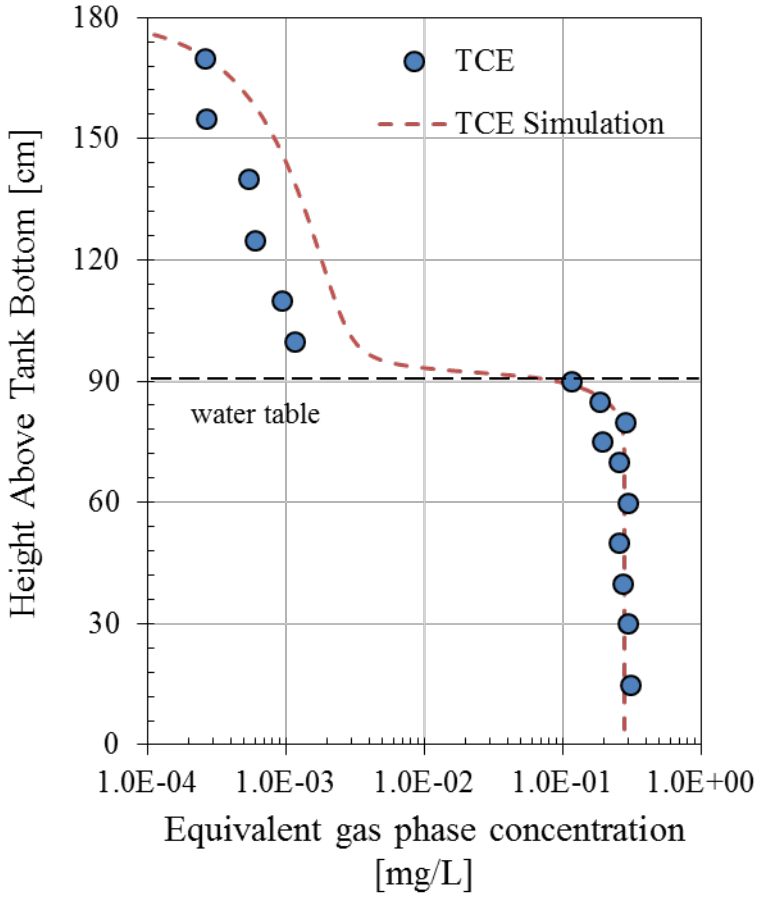

Figure A.48. Measured and simulated initial chemical profiles.

Validation simulation. Figure A.50 presents the comparison of measured vs. simulated TCE emission rates for the silica sand experiment discussed above. The results are qualitatively similar, with the emission peaks appearing at similar times in the simulation results and lab experiment data (approximately 210 h and 530 h after the beginning of the first water table fluctuation cycle). The maximum values for the first TCE emission peaks are about 2X greater than the second ones in both simulations and experiments. The normalized TCE emission values, however, were about 2X greater in the simulation results than in the measured lab results during water table fluctuations. This could be a result of the following uncertainties in model inputs:

- The fitted van Genuchten parameters may not perfectly reflect the soil saturation profiles and the fitting only occurred under static conditions. While the apparent match between measured and simulated profiles at steady state is good, the vertical resolution in soil moisture measurements is coarse and there is a significant change in moisture content immediately above the water table between the two moisture sensor locations.

- The simulation results are sensitive to the following input parameters: the saturated soil porosity, residual water content, the van Genuchten parameters defining the water flow and retention properties, and the Henry's Law Constant.

- Zero atmospheric TCE concentrations were set as an upper boundary condition in the simulation, whereas the TCE concentrations in the headspace of the experimental tank varied from less than 50 ppb_v (267 $\mu g/m^3$) to more than 250 ppb_v (1350 $\mu g/m^3$). However, this is unlikely to impact the experimental conditions because those levels are very small (nearly zero) relative to the source equivalent gas-phase TCE in the water (3×10^5 $\mu g/m^3$).

- Advective flow in the soil gas phase is not coupled in HYDRUS-1D, but does happen in the lab study. The movement of water table fills/depletes water in the soil pores, and consequently results in air movement out of and into the soil; the direction of air flow will be upward during water table rises and downward for water table drops. When the water table is moving downward, the direction of advective air flow is opposite to the diffusive flux, and this could reduce the magnitude of the emission peak. However, this is unlikely an explanation as the model results are consistently greater than the measured results, independent of water table rise or fall conditions.

Overall, HYDRUS-1D results qualitatively mimic the emission changes observed on the laboratory, with modeled emission increases being about a factor of 2X greater than the observations. This provided confidence in continuing to explore how emissions changes with time might be impacted by soil properties, chemical properties, and water table elevation patterns with time.

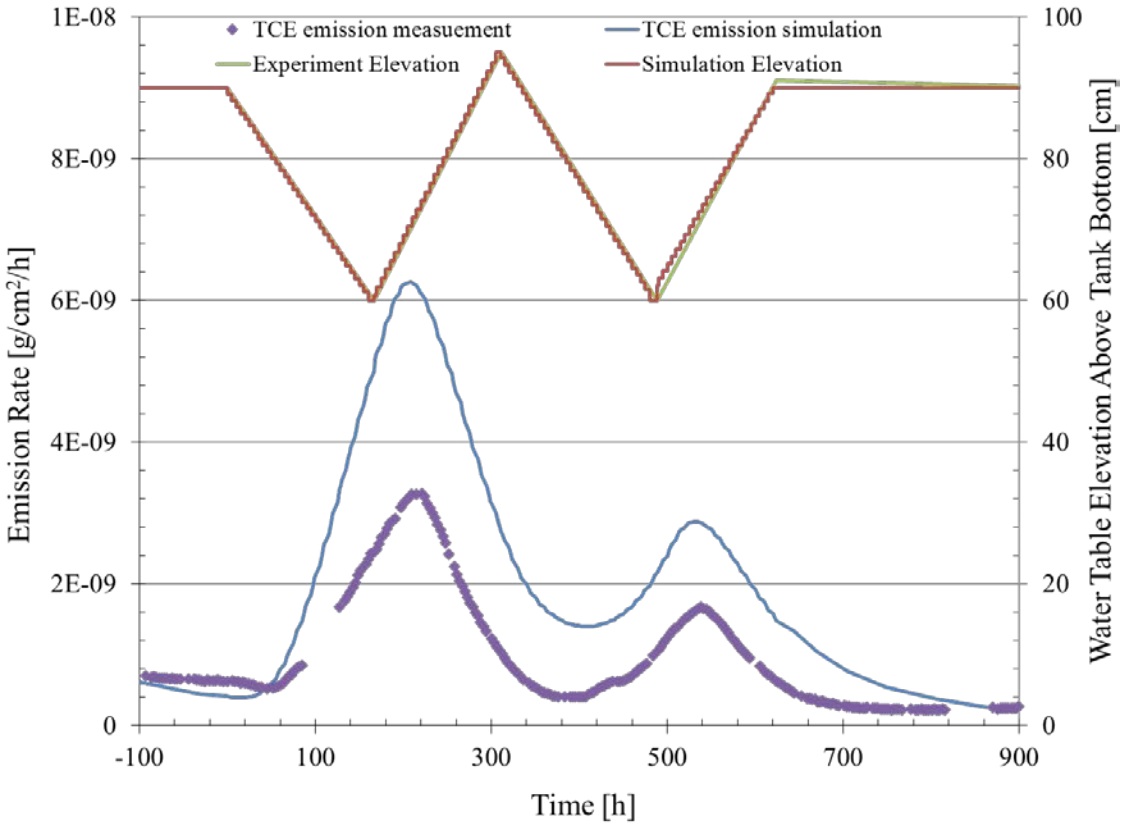

Figure A.49. Simulated vs. measured emission rate and water table elevation for the silica sand experiment presented section 4.5.6.

A.7 Differential pressure monitoring results under natural conditions

Overview. The advective flow of soil gas to indoor air is driven by a pressure gradient caused by natural environmental conditions and building operations. To gain an understanding of the direction and magnitude of the pressure gradient under natural conditions at the study site, differential pressure was monitored between sub-slab (SS) soil gas and indoor air. In addition, to gain insight into the outdoor-indoor air exchange, differential pressure was also monitored between outdoor air and indoor air.

Experimental Methods. Differential pressures between soil gas and indoor air and between outdoor air and indoor air were monitored using electronic differential pressure transducers (Model P300-0.4”-D, Pace Scientific Inc., Mooresville, NC). Data were logged every 2 minutes using a data acquisition module (Model OMB-DAQ-56, Omega Engineering Inc., Stamford, CT). The pressure transducers were re-zeroed daily using an automated valve system. The monitoring locations, including indoor and outdoor air reference points, are shown in Figure A.50. Additional information, including the calibration procedure, is provided in section 3.

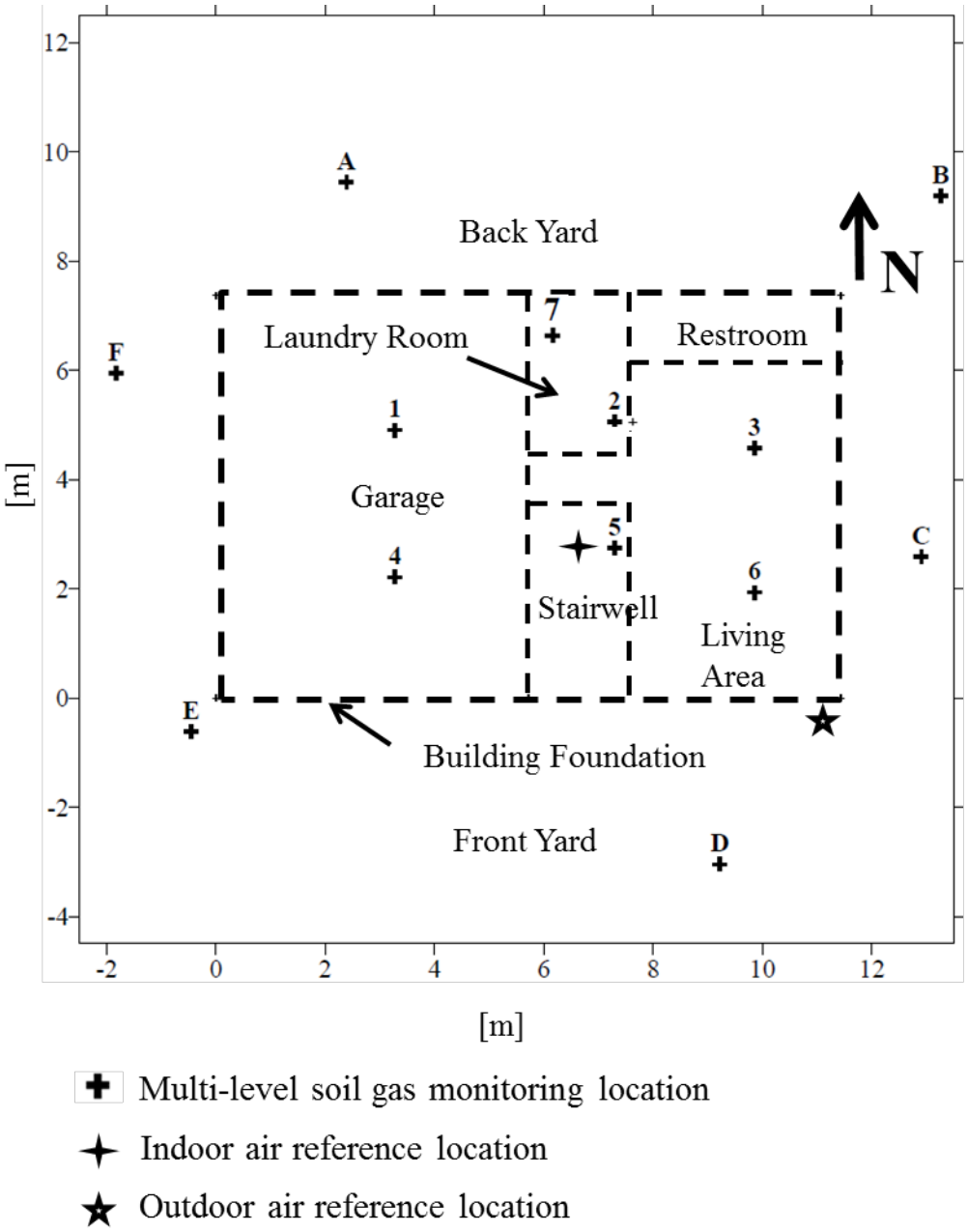

Figure A.50. Schematic of building footprint and monitoring locations.

Soil gas monitoring locations were frequently used for real-time soil gas sampling and as a consequence the data sets for several monitoring locations are limited. The results for the most complete data sets, from locations 4, 5, 7, and outdoor air (all measuring pressure differential with indoor air) are presented below. Comparisons between the results from location 5 and other monitoring locations are also presented to highlight the different behavior observed across the study site. The results from location 5 are used for the comparison due to its proximity to the center of the house and available data.

Results and Discussion. The data are placed on a timeline consistent with previous publications (Holton et al., 2013; Holton et al., 2015), where time (t) = 0 being 8:00 AM on 8/15/2010.

Figure A.51 presents 24-h average differential pressure results between outdoor air and indoor air for the time period 53 < t < 736 d. Error bars spanning the 10th and 90th percentiles of the real-time data within each 24-h period are also shown on the plots. Here, positive values are indicative of flow into the building. The 24-h average differential pressure values shown in Figure B.2 follow a slight seasonal trend, where more positive values occur in the late fall to early spring months. This trend is consistent with the seasonal trend of indoor air TCE concentrations presented and discussed by Holton et al. (2013). The 10th and 90th percentile values indicate bi-directional exchange, with positive and negative values occurring within 24-h periods.

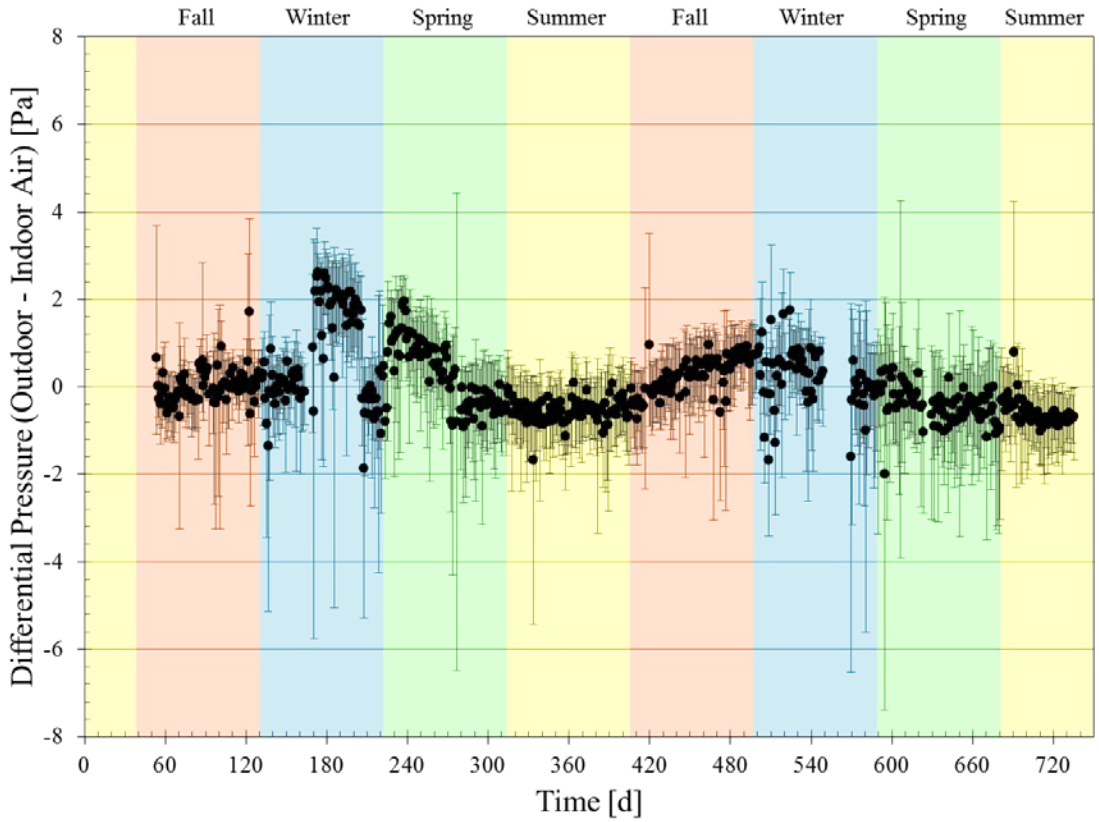

Figure A.51. 24-h average differential pressure values between outdoor air and indoor air with error bars spanning the 10th and 90th percentiles of the real-time data within each 24-h period.

Figures A.52 to A.54 show 24-h average differential pressure results between SS soil gas and indoor air at locations 4, 5, and 7, respectively for the time period 53 < t < 736 d (where data is available). Error bars spanning the 10th and 90th percentiles of the real-time data within each 24-h period are also shown on the plots. Here, positive values are indicative of advective flow from the subsurface to indoor air.

Similar to the differential pressure results between outdoor and indoor air, the results shown in Figures A.52 to A.54 demonstrate that differential pressure values between the subsurface and indoor air regularly fluctuated between positive and negative values. The variation observed at locations 4 and 5 appear to follow a similar seasonal trend as the one observed between outdoor air and indoor air, with more positive values occurring in the late fall to early spring months, however, the magnitude of variation differs with location 4 experiencing a greater number of positive days. In contrast, the results from location 7 do not follow an obvious trend. The 24-h average subsurface to indoor air differential pressures shown here are similar to observations for other residential buildings under natural conditions (McHugh et al., 2006).

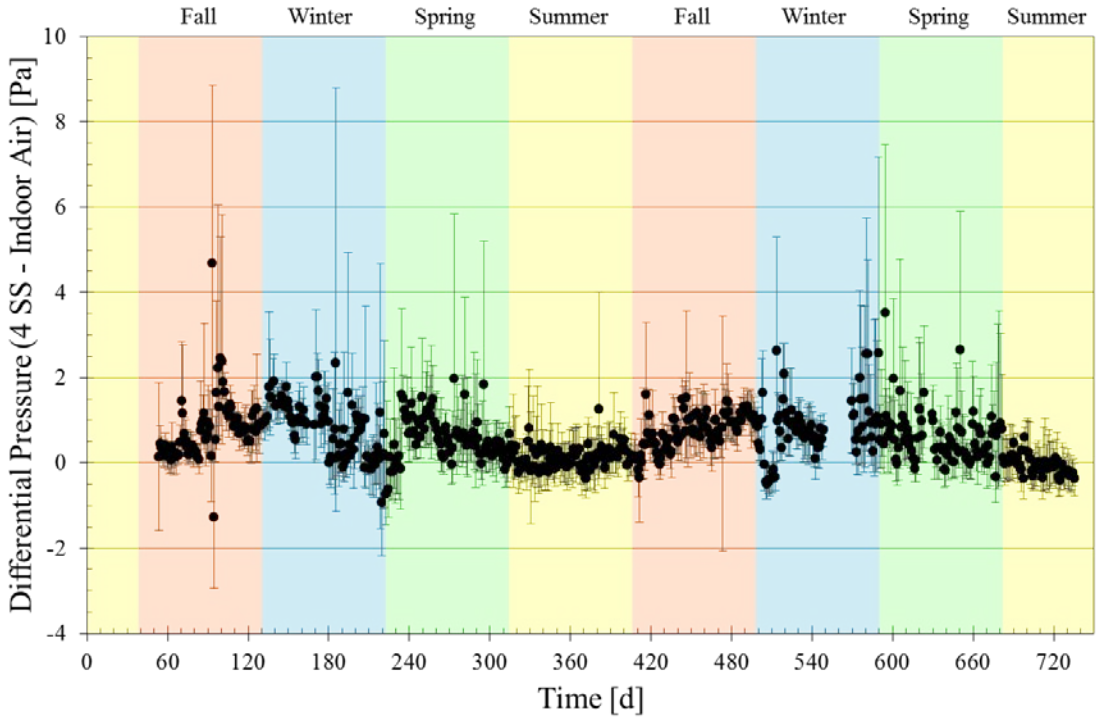

Figure A.52. 24-h average differential pressure values between sub-slab soil gas at location 4 and indoor air with error bars spanning the 90th and 10th percentile of the daily data sets.

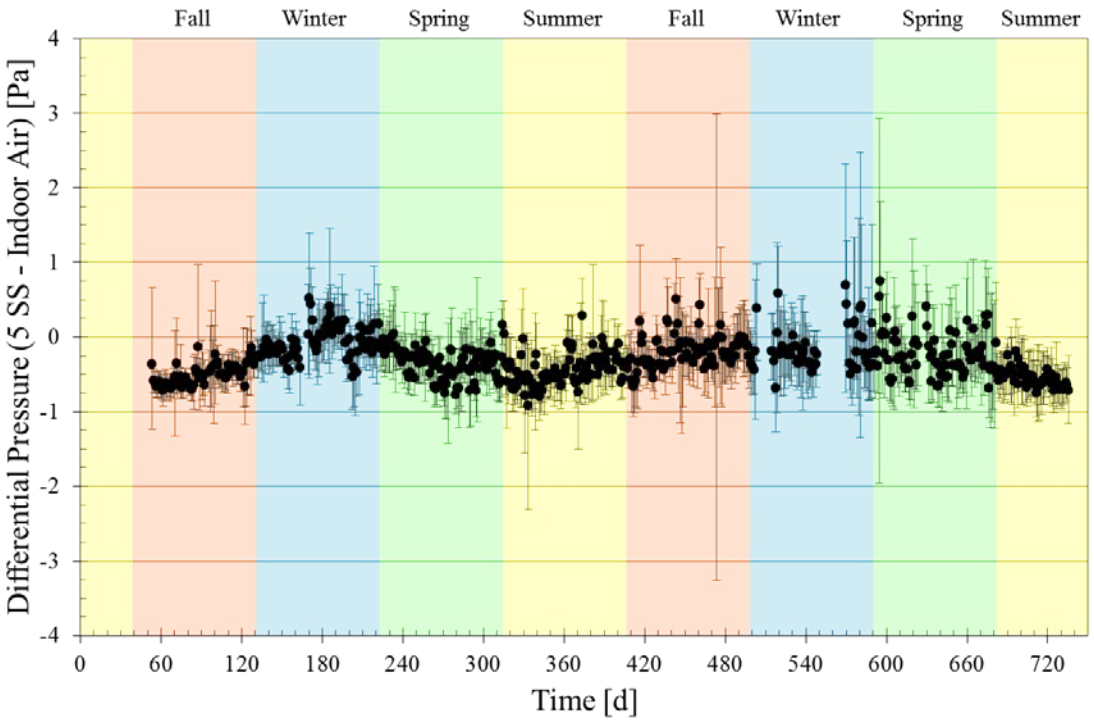

Figure A.53. 24-h average differential pressure values between sub-slab soil gas at location 5 and indoor air with error bars spanning the 90th and 10th percentile of the daily data sets.

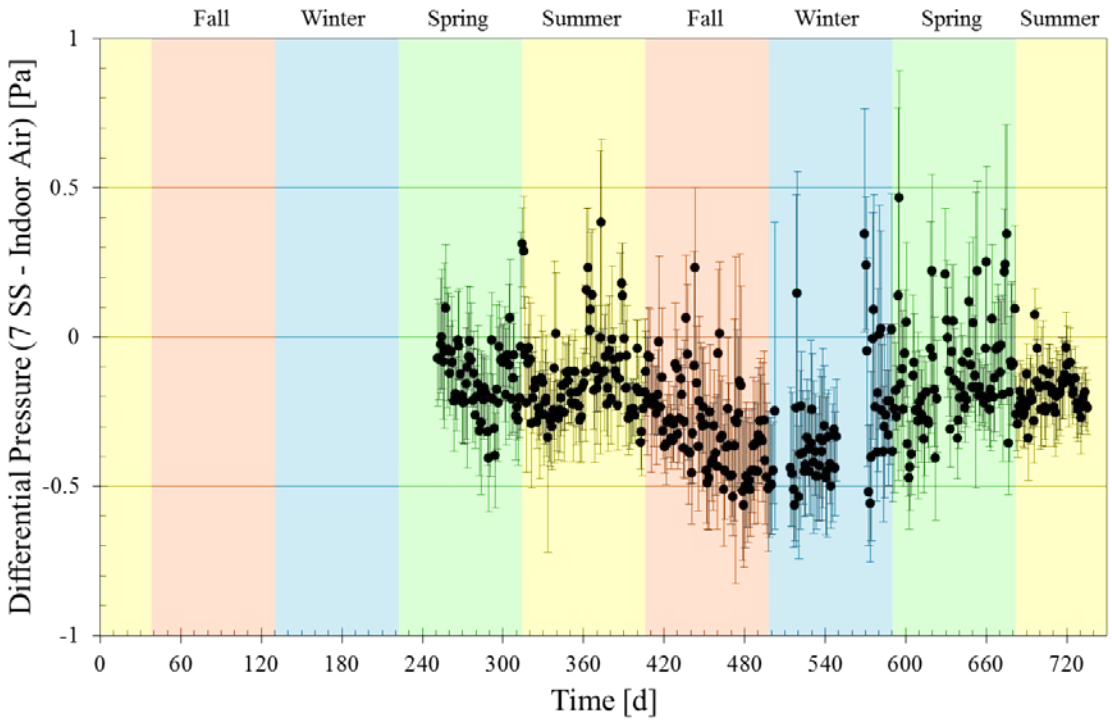

Figure A.54. 24-h average differential pressure values between sub-slab soil gas at location 7 and indoor air with error bars spanning the 90th and 10th percentile of the daily data sets.

To better understand the relationship between subsurface to indoor air differential pressure monitoring locations, time-matched 24-h average data was plotted. Figures A.55 to A.60 present time-matched comparisons of the 24-h average differential pressure results from each SS soil gas monitoring location with the results from location 5.

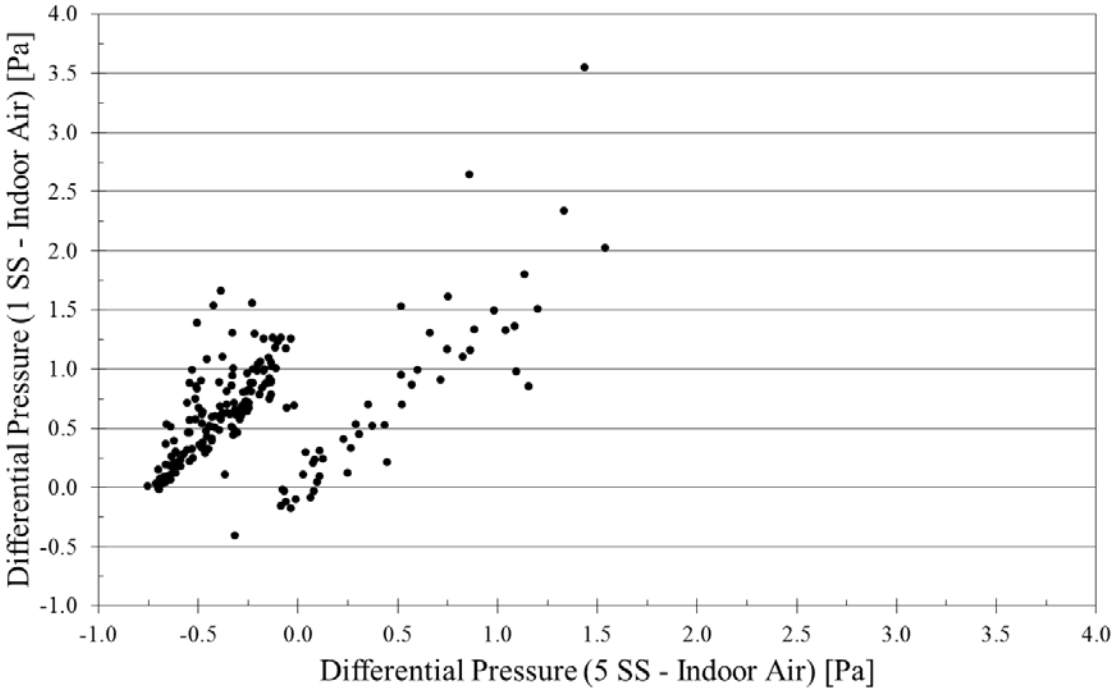

Figure A.55. Comparison of time-matched 24-h average sub-slab to indoor air differential pressure values from location 1 and location 5.

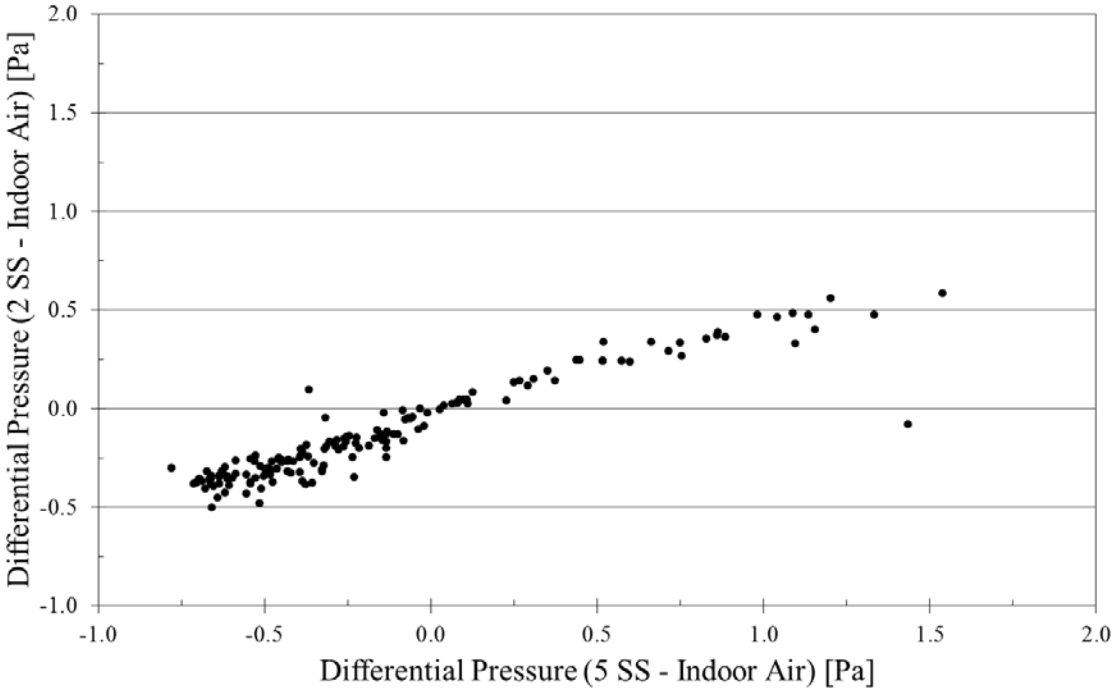

Figure A.56. Comparison of time-matched 24-h average sub-slab to indoor air differential pressure values from location 2 and location 5.

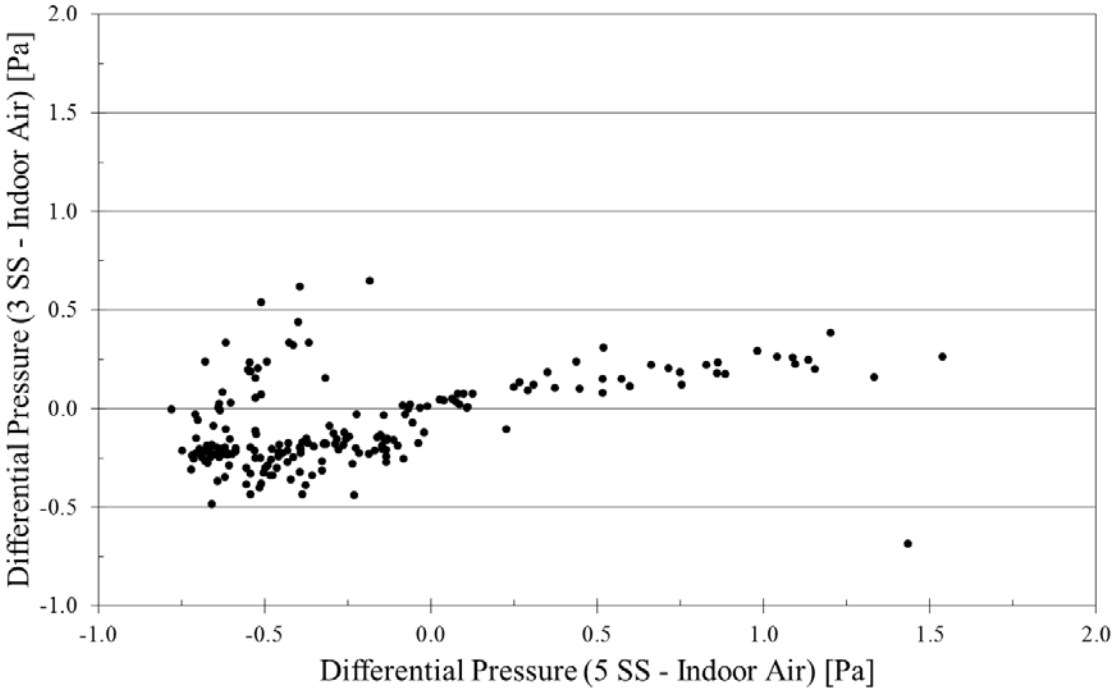

Figure A. 57. Comparison of time-matched 24-h average sub-slab to indoor air differential pressure values from location 3 and location 5.

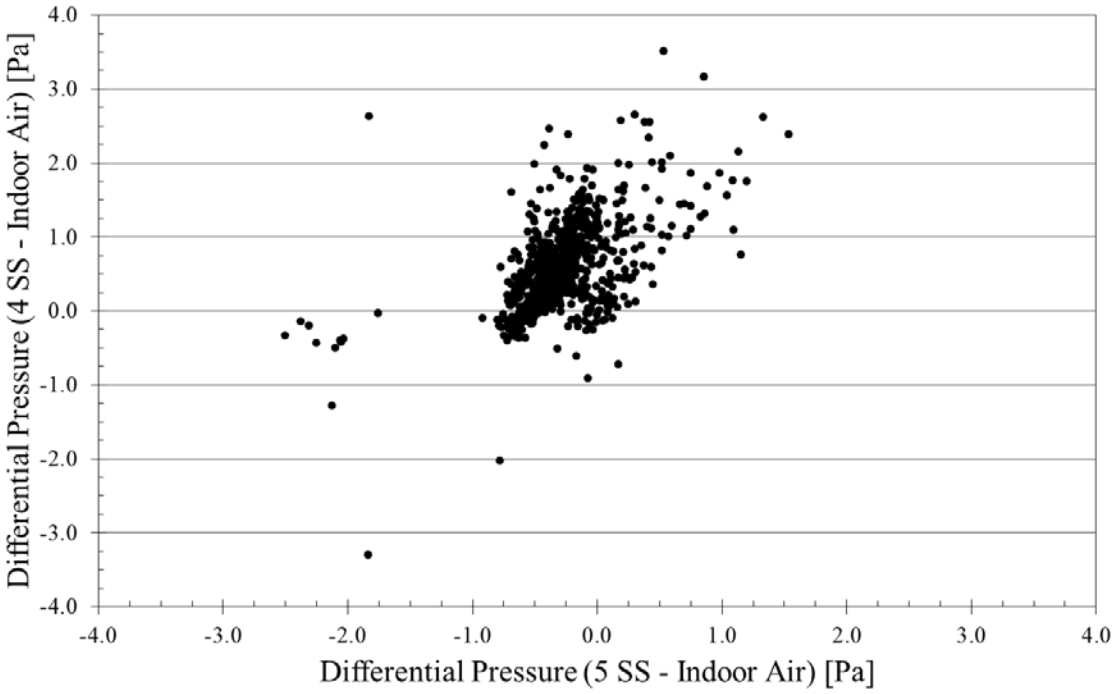

Figure A.58. Comparison of time-matched 24-h average sub-slab to indoor air differential pressure values from location 4 and location 5.

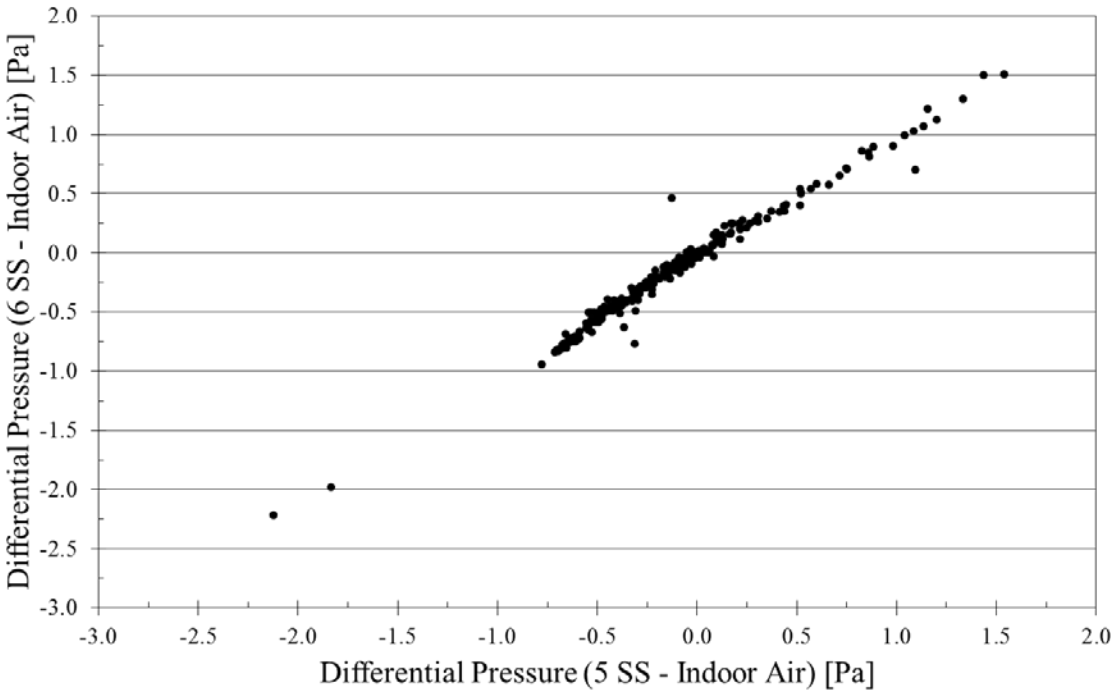

Figure A.59. Comparison of time-matched 24-h average sub-slab to indoor air differential pressure values from location 6 and location 5.

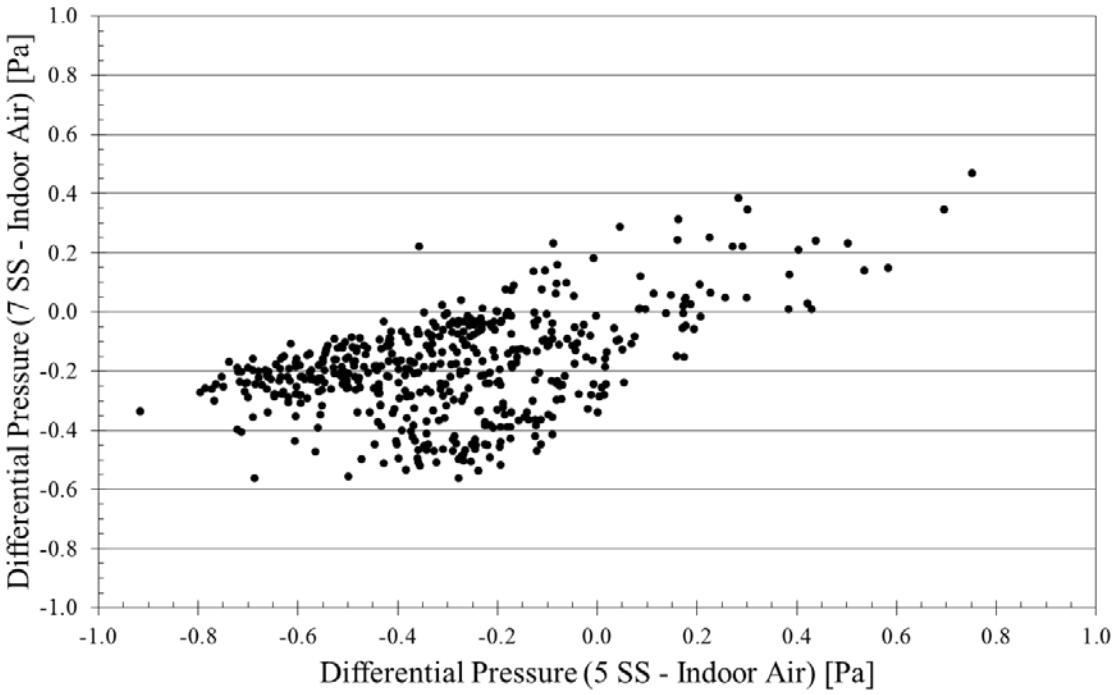

Figure A.60. Comparison of time-matched 24-h average sub-slab to indoor air differential pressure values from location 7 and location 5.

Table A.11 presents relevant statistics of the time-matched data shown in Figures A.55 to A.60 to highlight the similarities and differences observed under natural conditions. The comparisons shown in Figures A.55 to A.60 and the statistics from Table A.11 reveal that the locations within the living space (2, 3, 6, and 7) often behaved similarly to location 5, while the monitoring locations in the garage (1 and 4) often behaved differently. For example, the time-matched 24-h average differential pressure values from the garage locations were mostly positive and values from the indoor living space were often negative.

Bidirectional flow within a 24-h period, as indicated by the 10^{th} and 90^{th} percentiles of the real-time data within a 24-h period spanning positive and negative values, occurs on a similar basis for all locations with one exception. For the comparison between location 3 and location 5 (202 days of time-matched 24-h differential pressure values), location 3 had bidirectional flow for 64.4% of the 24-h periods and location 5 had 43.6%.

The differences observed between monitoring locations in the garage and living space could be due the subsurface infrastructure at the study site. A stem wall that sits between the garage and living space and extends into the sub-foundation region helps separate monitoring locations. In addition, the lateral pipe that extends from the neighborhood land drain system to below the living space may influence the subsurface dynamics beneath the living space. It's possible that both of these features played a role in the differences in differential pressures observed between the subsurface and indoor air.

Table A.11. Summary of statistics for the comparison of time-matched sub-slab soil gas differential pressure results at location 5 with other in monitoring locations within the building footprint.

Sub-slab Location	Number of Time-matched Days for Comparison	10^{th} and 90^{th} Percentile Values Span Negative and Positive Values	10^{th} and 90^{th} Percentile Values Span are Positive	10^{th} and 90^{th} Percentile Values Span are Negative	24-h Average Value is Positive	24-h Average Value is Negative
5	204	52.5%	0.5%	47.1%	20.6%	79.4%
1		52.5%	47.5%	0.0%	93.1%	6.9%
5	162	52.5%	0.6%	46.9%	25.9%	74.1%
2		56.8%	1.2%	42.0%	25.9%	74.1%
5	202	43.6%	0.5%	55.9%	20.8%	79.2%
3		64.4%	2.5%	33.2%	34.7%	65.3%
5	704	58.0%	0.3%	41.8%	17.2%	82.8%
4		55.5%	43.5%	1.0%	84.2%	15.8%
5	228	64.9%	0.4%	34.6%	32.0%	68.0%
6		64.9%	0.9%	34.2%	32.9%	67.1%
5	505	57.2%	0.2%	42.6%	11.1%	88.9%
7		42.6%	2.4%	55.0%	12.3%	87.7%

APPENDIX B: LIST OF SCIENTIFIC/TECHNICAL PUBLICATIONS

Articles in peer-reviewed journals

Holton, C.; Luo, H.; Dahlen, P.; Gorder, K. A.; Dettenmaier, E. M.; Johnson, P. C. (2013). Temporal variability of indoor air concentrations under natural conditions in a house overlying a dilute chlorinated solvent groundwater plume. *Environmental Science and Technology, 47,* 13347-13354.

Holton, C.; Guo, Y.; Luo, H.; Dahlen, P.; Gorder, K. A.; Dettenmaier, E. M.; Johnson, P. C. (2015). Long-Term Evaluation of the Controlled Pressure Method for Assessment of the Vapor Intrusion Pathway. *Environmental Science and Technology, 49,* 2091-2098.

Guo, Y., Holton, C. W., Luo, H., Dahlen, P., Gorder, K., Dettenmaier, E. M., & Johnson, P. C. (2015). Identification of Alternative Vapor Intrusion Pathways Using Controlled Pressure Testing, Soil Gas Monitoring, and Screening Model Calculations. *Environmental Science and Technology.* 49(22): 13472-13482.

Conference and symposium proceedings:

Johnson, P.C., P. Dahlen, H. Luo, C. Holton. 2011. Temporal Changes in VI Behavior: Considerations for Pathway Assessment. USEPA Workshop on Addressing Regulatory Challenges in Vapor Intrusion: A State of the Science Update Focusing on Chlorinated VOCs. AEHS 21st Annual Meeting and West Coast Conference on Soils, Sediments, Water. San Diego, CA. March.

Johnson, P.C., P. Dahlen, H. Luo, C. Holton, K. Gorder, E. Dettenmaier. 2011. Temporal Changes in VI Behavior: Considerations for Pathway Assessment. 21at Annual Training Program – National Association of Remedial Program Managers. May 16-20. Kansas City, MO.

Johnson, P.C., P. Dahlen, H. Luo, C. Holton, K. Gorder, E. Dettenmaier. 2011. Temporal Changes in VI Behavior: Considerations for Pathway Assessment. U. Washington/USEPA Superfund Research Center. June 15. Seattle, WA.

Luo, H., K. Gorder, E. Dettenmaier, P. Dahlen, P. C. Johnson. 2011. Field studies of temporal variability of sub-slab soil gas and indoor air concentrations at a house overlying a chlorinated compound impacted groundwater plume. International Symposium on Bioremediation and Sustainable Environmental Technologies. Reno, NV. June 27-30.

Johnson, P.C., H. Luo, C. Holton, Y. Guo, P. Dahlen, K. Gorder, E. Dettenmaier, 2012. Vapor Intrusion Above a Dilute CHC Plume: Lessons-Learned from Two Years of Monitoring. USEPA Workshop on Addressing Regulatory Challenges in Vapor Intrusion: A State of the Science Update Focusing on Chlorinated VOCs. AEHS 22nd Annual Meeting and West Coast Conference on Soils, Sediments, Water. San Diego, CA. March 19-22.

Luo, H., C. Holton, Y. Guo, P. C. Johnson. 2012. Field and modeling studies of indoor air source effects on subslab soil gas concentrations. The 22nd annual international Conference on Soil, Water, Energy and Air. San Diego, CA. March 19-22.

Holton, C., H. Luo, Y. Guo, K. Gorder, E. Dettenmaier, P. C. Johnson. Long-term and short-term variation of indoor air concentrations at a vapor intrusion study site. 2012. The 22nd Annual International Conference on Soil, Water, Energy and Air. San Diego, CA. March 19-22.

Holton, C., H. Luo, Y. Guo, P. Dahlen, K. Gorder, E. Dettenmaier, P. C. Johnson. Differences in Temporal Signatures in Groundwater, Soil Gas, and Indoor Air Data and Implications for Pathway Assessment. 2012. The 9th International Conference on Remediation of Chlorinated and Recalcitrant Compounds. Monterey, CA, May 21-24.

Holton, C., H. Luo, Y. Guo, P. Dahlen, K. Gorder, E. Dettenmaier, P. C. Johnson. Evaluation of Selected Environmental Factors at a Vapor Intrusion Study Site. 2013. The 23nd Annual International Conference on Soil, Water, Energy and Air. San Diego, CA. March 18-21.

Johnson, P.C., Holton, C., H. Luo, Y. Guo, P. Dahlen, K. Gorder, E. Dettenmaier. Multi-Year Monitoring of a House Over a Dilute CHC Plume: Implications for Pathway Assessment Using Indoor Air Sampling and Forced Under-Pressurization Tests. USEPA Workshop on Addressing Regulatory Challenges in Vapor Intrusion: A State of the Science Update Focusing on Chlorinated VOCs 2013. The 23nd Annual International Conference on Soil, Water, Energy and Air. San Diego, CA. March 18-21.

Johnson, P.C., Holton, C., H. Luo, Y. Guo, P. Dahlen, K. Gorder, E. Dettenmaier. Integrated Field-Scale, Lab-Scale, and Modeling Studies for Improving our Ability to Assess the Groundwater to Indoor Air Pathway at Chlorinated Solvent-Impacted Groundwater Sites. 2013. SERDP and ESTCP Vapor Intrusion Seminar and Workshop. Tempe, AZ, December 19.

Holton, C., Y. Guo, P. Dahlen, P. C. Johnson. Lessons Learned from a Multi-Year Monitoring Study at a House Above a Dilute CHC Plume. 2014. Hill Air Force Base Restoration Advisory Board Meeting. January 30.

Johnson, P.C., Holton, C., H. Luo, Y. Guo, P. Dahlen, K. Gorder, E. Dettenmaier. Lessons-Learned from Four Years of Intensive Monitoring of a House Over a Dilute Chlorinated Hydrocarbon Plume. 2014. The 24th Annual International Conference on Soil, Water, Energy and Air. San Diego, CA. March 17-20.

Holton, C., Y. Guo, P. Dahlen, H. Luo, K. Gorder., E. Dettenmaier, P. C. Johnson. Field Studies of Indoor Source Impacts on Indoor Air and Soil Gas Concentrations at a Vapor Intrusion Study Site. 2014. The 10th International Conference on Remediation of Chlorinated and Recalcitrant Compounds. Monterey, CA, May 19-22.

Johnson, P.C., Holton, C., Y. Guo, P. Dahlen, H. Luo, K. Gorder, E. Dettenmaier. Lessons Learned from Monitoring a House Overlying a Dissolved Hydrocarbon Plume Under Natural and Controlled Depressurization Conditions. 2014. SERDP & ESTCP Webinar Series. October 30.

APPENDIX C: LIST OF INDOOR SOURCES

As part of the Basewide Indoor Air Sampling Program at Hill Air Force Base, Utah, a household chemical product inventory was conducted during each sampling event. Sampling technicians reviewed chemical products stored in the home and recorded products that potentially contained contaminants of concern (COC). Records of products that may have contained COCs were stored in a household chemical product database. The data quality objective of that household chemical product inventory was to identify products in the home that could potentially affect indoor air results.

The list shown below represents the products identified as potentially containing one or more COCs during that inventory The primary method for determining the presence of a COC in a household product was a visual review of the product label during the inventory. If a COC was listed on the product label, the Material Safety Data Sheet (MSDS) may have been reviewed to support information presented on the product label. The use of a portable GC/MS may have also been used to identify, confirm or refute the presence of COCs within a product.

Please note that the product list shown was generated using the product database described above and is not definitive with regard to the presence of a COC in a product. Due to outdated or unavailable MSDS documents, potential transcription errors, or product reformulations (documented or undocumented), entries in that product database were not necessarily indicative that a product now contains (or has ever contained) a COC.

Reference:
Dettenmaier, Erik, and Gorder, Kyle. Detailed Indoor Air Characterization and Interior Source Identification by Portable GC/MS. AWMA presentation, 30 September 2010.

PRODUCT DESC	MANUFACTURER	PAR LABEL	METHOD of DETERMINATION
Fix-a-Flat	Nationwide Industries	CLME	Label
SSD Choro-Solv	The State Chemical Manufacturing Co.	CLME	Label
Clorox Cleanup	Clorox Company	CLME	GC-MS
Lysol Toilet Bowl Cleaner w/Bleach	Reckitt Benckiser	CLME	GC-MS
Brake Cleaner	Advance Auto Parts	CTCL	Label
Carbon Tetrachloride	Skaggs Drug Center	CTCL	Label
Clorox Cleanup	Clorox Company	CTCL	GC-MS
Formula 44/40	Metal Bluing Products, Inc.	CTCL	Label
Lysol Toilet Bowl Cleaner w/Bleach	Reckitt Benckiser	CTCL	GC-MS
Dorersol	Dexol Industries	DCA12	Label
Home defense fogger	Ortho	DCA12	Label
7800 Industrial Strength Craft Adhesive	Aleenes	PCE	MSDS/Label
Amarr Super Lube	Amarr Garage Door	PCE	Label
B9-Chem Dip Carb parts cleaner	Berryman	PCE	Label
Brake and Parts Cleaner	Permatex	PCE	MSDS/Label

PRODUCT DESC	MANUFACTURER	PAR LABEL	METHOD of DETERMINATION
Brake Cleaner	Advance Auto Parts	PCE	MSDS/Label
Brake Cleaner	Berryman	PCE	MSDS/Label
Brake Cleaner (Aerosol)	Berryman	PCE	MSDS/Label
Brake Cleaner	Peerless Products Company	PCE	Label
Brake Cleaner AM7_49C	GUNK/Radiator Specialty Co	PCE	MSDS/Label
Brake Cleaner AM720	GUNK/Radiator Specialty Co	PCE	MSDS/Label
Brake Parts Cleaner	NAPA	PCE	Label
Brake Parts Cleaner	Technical Chemical Company	PCE	MSDS/GC-MS
Brake Parts Cleaner	ITW Dymon	PCE	Label
Brake Parts Cleaner	Pyroil	PCE	MSDS/Label
Brake Parts Cleaner	Car Quest	PCE	MSDS/Label
Brake Parts Cleaner	Pennzoil Quaker State	PCE	MSDS/Label
Brake Parts Cleaner	Valvoline Co.	PCE	MSDS/Label
Brakleen	CRC	PCE	MSDS/Label
Brakleen (Original) white can	CRC	PCE	MSDS/Label
Break Away	AIS	PCE	MSDS/Label
CARB Compliant Seamermate Gutter Seal	Geocel Corporation	PCE	MSDS/Label
Carpet & Upholstery Spotter	Pro Link	PCE	Label
Carpet Magic Spot Lifter	Carpet Care Division	PCE	Label
Carpet Stain Remover	ScotchGard/3M	PCE	MSDS/Label
Chain Kote	Kal Gard Coating Mfg Corp	PCE	MSDS/Label
Crown Lubricating Compound	North American Professional Products	PCE	Label
Custom Silicone Watershed	Esquire	PCE	Label
Daves Flexament	Umpqua	PCE	MSDS/Label
E6000 Adhesive	Eclectic Products	PCE	MSDS/Label/GC-MS
E-6100	Eclectic Products	PCE	MSDS/Label
Electrical Parts Cleaner	CRC	PCE	MSDS/Label
Engine Degreaser	Car Quest	PCE	Label
Fast Spot Remover Spray	Sullivans USA Inc.	PCE	Label
Fel-cobond Quick Drying Adhesive	Fel Pro Chemical Products LP	PCE	GC-MS
Furniture Polish	Behold	PCE	Label
Gasket Remover	Permatex	PCE	Label
Golf Shoe Wetpruf	Kiwi Brands Inc	PCE	Label
Goop (Automotive)	Eclectic Products	PCE	Label
Graffiti Cleaner	Home Trends	PCE	Label
Gumout Professional Brake Parts Cleaner(Chlorinated)	Pennzoil Quaker State	PCE	MSDS/Label
Gun Oil	Browning	PCE	MSDS/Label
Gunk Brake Cleaner	Radiator Specialty Co.	PCE	MSDS/Label
Gunk Liquid Wrench	Radiator Specialty Co.	PCE	Label
Gunk Liquid Wrench Penetrating Oil	Radiator Specialty Co.	PCE	MSDS/Label
Handy Brake and Parts Cleaner	LYN Distributing	PCE	MSDS/Label/GC-MS
Heavy Duty Degreaser Aerosol	CRC	PCE	MSDS/Label
Heavy Duty Silicone Lubricant	Sears	PCE	Label
Home & Auto Parts Cleaner	GUNK/Radiator Specialty Co	PCE	Label
Industrial Clean Up Dry Cleaner	Sprayway Inc	PCE	MSDS/GC-MS
Jig-a-loo	Jig-a-loo	PCE	MSDS/Label
K2R Spot Lifter	American Home Foods Inc	PCE	Label

PRODUCT DESC	MANUFACTURER	PAR LABEL	METHOD of DETERMINATION
Lectra Clean® Heavy Duty Degreaser	CRC	PCE	MSDS/Label/GC-MS
Lectra Motive Auto Care	CRC	PCE	MSDS/Label
Liquid Wrench	GUNK/Radiator Specialty Co	PCE	Label
Liquid Wrench NF (non-flammable)	GUNK/Radiator Specialty Co	PCE	MSDS/Label
Liquid Wrench Super Lubricant w/Teflon	GUNK/Radiator Specialty Co	PCE	MSDS/Label/GC-MS
Misty Industrial Cleaning Solvent Aerosol	Amrep Inc	PCE	MSDS/Label
Misty Moisture Guard	Amrep Inc	PCE	MSDS/Label
Misty Penetrating Lubricant	Amrep Inc	PCE	MSDS/Label
Mopar Brake Parts Cleaner	Chrysler Motors	PCE	Label
Nissan Brake Cleaner P/N 999Mp_A3040 PCE	Nissan	PCE	Label
Non-Flammable Safety Solvent	ITW Dymon	PCE	MSDS/Label
Non-flammable Super Lubricant	GUNK/Radiator Specialty Co	PCE	MSDS/Label
Paint Stripper	JASCO Chemical Corp	PCE	Label
PEN Penetrating Oil	State Chemical Manufacturing Co.	PCE	MSDS/Label
Penetrating Oil	The State Chemical Manufacturing Co.	PCE	MSDS/Label
Powder Blast Gun Cleaner	Break Free CLP	PCE	Label
ProFlex RV Flexible Sealant	Geocel Corporation	PCE	GC-MS
Quick Cure	System Three Resins Inc	PCE	Label
Rain and Stain Potector	Champs Sports	PCE	Label
Rain Coat Silicone Treatment	Edison-Brothers Stores, Inc	PCE	Label
Safety Solvent	Brody Chemical	PCE	MSDS/Label
Santa Sno	Santa Sno	PCE	Label
Santa Sno	Changing Paradigms LLC.	PCE	Label
Seamermate Gutter Seal	Geocel Corporation	PCE	MSDS/GC-MS
Shoe Goo Adhesive	Shoe Goo	PCE	Label/GC-MS
Shoe Goo I (Not Shoe Goo II)	Eclectic Products	PCE	Label/GC-MS
Shoe Patch	Shoe Saver Brand	PCE	GC-MS
Silicone Lubricant	Nissan	PCE	Label
Silicone Spray	Toyota Motor Sales U.S.A, Inc.	PCE	Label
Silversmith Spray Polish	WJ Hagerty and Sons	PCE	MSDS/Label
Solvent Carpet Spotter	Waxie	PCE	MSDS/Label
Sport & Shoe Patch	Kiwi Brands Inc	PCE	Label
Spot and stain remover	All Solv	PCE	Label
Spray Snow	Changing Paradigms LLC.	PCE	Label/GC-MS
SSD Choro-Solv	The State Chemical Manufacturing Co.	PCE	MSDS/Label
Stain and Spot Remover	Jewel Companies, Inc.	PCE	Label
Suede Spray Cleaner & Conditioner	Kiwi Brands Inc	PCE	Label
SuperSolve	Amprep Inc.	PCE	Label
Tire Jack Inflator and Sealer	Prestone	PCE	Label
Vandal Mark Remover	Southeast Service Corp	PCE	Label
White Lithium Grease	Autozone	PCE	Label
White Lithium Grease	Permatex	PCE	MSDS/Label
White Lithium Grease	GUNK/Radiator Specialty Co	PCE	MSDS/Label
White Lithium Grease	CRC	PCE	Label

PRODUCT DESC	MANUFACTURER	PAR LABEL	METHOD of DETERMINATION
Windshield Cleaner	Temshield	PCE	Label
0-54 Safety Solvent	Macklanburg-Duncan	TCA	Label
7471 Primer T	Loctite	TCA	Label
Acrylic Sealer/Finisher	Arts & Crafts Division	TCA	Label
Action Electronic Silicone Contact Cleaner	GC Electronics	TCA	Label
All Purpose Color Spray	Cascade Sales & MFG	TCA	Label
All Purpose Lubricant	Kal Gard Coating Mfg Corp	TCA	Label
All Purpose Spray Adhesive	DURO	TCA	Label
All-Purpose Silicone Lubricant Spray	Magnolia Chemical Co, Inc.	TCA	Label
Anti-Static Spray	Crown Industrial Products Co.	TCA	MSDS/Label
Battery Cleaner & Protector	KAR Products	TCA	MSDS/Label
Battery Corrosion Preventative Spray	Custom Components, Inc	TCA	Label
Belt Dressing	Loctite	TCA	Label
Belt Dressing	Permatex	TCA	Label
Blair Satin Tole	Blair Art Products, Inc.	TCA	Label
Blast 0ff! Electric Motor Cleaner	Hobbico Duratrax	TCA	Label
Brake Cleaner	Permatex	TCA	Label
Brake Cleaner	Advance Auto Parts	TCA	Label
Brake Cleaner	Peerless Products Company	TCA	Label
Brake Cleaner AM7_49C	GUNK/Radiator Specialty Co	TCA	Label
Camp Dry 218_000 Heavy Duty Water Repellent	Kiwi Brands Inc	TCA	Label
Camp Dry silicon fabric protector	Kiwi Brands Inc	TCA	Label
Cleaning Fluid	Energine	TCA	Label
Colorado Old Tanner Water Stain Protector	Kinney	TCA	Label
Contact Cleaner & Lubricating Spray	Krylon	TCA	Label
Custom Silicone Watershed	Esquire	TCA	Label
Degreaser	CRC	TCA	Label
Doctor Spot	Certified International	TCA	Label
Dry Cleaning Solvent	Spot X	TCA	Label
Duro Contact Cement	Loctite	TCA	MSDS/Label
Electric Motor Cleaner	Berryman	TCA	Label
Energine Cleaning Fluid	Reckitt Benckiser	TCA	Label
Fabric Cleaner	Thom Mcan	TCA	Label
Fabric Guard	Fuller Brush Company	TCA	Label
Fabric Protector	Kmart	TCA	Label
Fabric Protector	ScotchGard/3M	TCA	Label
Fabric Protector	Payless	TCA	Label
Fabric Sealant	General Motors Parts Division	TCA	Label
Fel-cobond Quick Drying Adhesive	Fel Pro Chemical Products LP	TCA	GC-MS
Ferti-lome-Fruit Tree Spray	Voluntary Purchasing Groups Inc.	TCA	Label
Formula 40 Glass Cleaner Old	Sprayway Inc	TCA	Label
Garage Door Lubricant	Price's	TCA	Label
Gearshield Extra Heavy	Fiske Brothers Refining Co	TCA	MSDS/Label

PRODUCT DESC	MANUFACTURER	PAR LABEL	METHOD of DETERMINATION
Glitter Lemon Powered Siliconized Polish	Del	TCA	Label
Gun Scrubber	Birchwood Casey	TCA	Label
Gun solvent (aerosol)	Break Free CLP	TCA	Label
Hammerite Brush Cleaner & Thinner	Hunting Specialty Products Inc.	TCA	MSDS/Label
Handy Brake and Parts Cleaner	LYN Distributing	TCA	Label/GC-MS
Head cleaner	Ampex	TCA	MSDS/Label
Heavy Duty Silicone	CRC	TCA	Label
Heavy Duty Silicone	GUNK/Radiator Specialty Co	TCA	Label
HEP aerosol insect killer	B.T. Babbitt Inc.	TCA	Label
Honing Oil	KA BAR	TCA	Label
Indoor Uotdoor Carpet Adhesive	Henry	TCA	Label
K2R Spot Lifter	American Home Foods Inc	TCA	Label
Kleer Clean Degreaser	American Writing Inc. Co.	TCA	Label
Krylon Electric Motor Cleaner	Sherwin Williams	TCA	MSDS/Label
LB-1HT	Goodson Mfg. Co.	TCA	Label
Leather protector	Colorado Care Pro	TCA	Label
Lilly Miller Fruit & Berry Insect Spray	The Chas. H.Lilly Co.	TCA	Label
Liquid Gold for Wood Reg or Lemon	Scotts	TCA	Label
Liquid Gold Wood Cleaner and Preservative Aerosol	Scotts	TCA	Label
Liquid Tape	Sprayway Inc	TCA	Label
Master Carb & Choke cleaner	Master Corporation	TCA	Label
Metal Mover	Mystic	TCA	Label
Misty Antistatic Spray	Amrep Inc	TCA	Label
Misty Mizer Odor Neutralizer	Amrep Inc	TCA	Label
Mr Electric D_OS Solvent Degreaser	Franlynn Inc	TCA	Label
Non stick cookware repair	Heddy Contract Ind	TCA	Label
Oil and Paint Spot Remover	ServiceMaster Company	TCA	Label
Panel Adhesive	Henry	TCA	Label
Polish Metal	Hysan Corp.	TCA	MSDS/Label
Precise electronic solvent	Drummond American	TCA	Label/GC-MS
Preparer	Nu Life	TCA	Label
Pro Pel	Browning	TCA	Label
Raid Wasp & Hornet Killer	SC Johnson and Son Inc	TCA	Label
Rapid Tap	Relton Chemicals	TCA	MSDS/Label
Release Agent	Ren Plastics	TCA	Label
REM Spot Plus	MANTEK	TCA	Label
Remove Fabric Spot Cleaner	Amway	TCA	MSDS/Label
Retouch Varnish	Grumbacher	TCA	Label
Rifle Cleaning Kit and Shotgun Cleaning Kit	Outers	TCA	Label
ScotchGard Auto-Pak	ScotchGard/3M	TCA	Label
Shoe Renew AllGuard	WOHL Shoe Co.	TCA	Label
Silicone Lubricant	GUNK/Radiator Specialty Co	TCA	Label
Silicone Spray	Super X	TCA	Label
Silicone Spray	CC Distributing	TCA	Label

PRODUCT DESC	MANUFACTURER	PAR LABEL	METHOD of DETERMINATION
Solvent for Carpet Seam Adhesive	W W Henry Co.	TCA	Label
Sport & Shoe Patch	Kiwi Brands Inc	TCA	Label
Sportland Shoe Patch	Kiwi Brands Inc	TCA	Label
Spot-X Basic Dry Cleaning Solvent	Dura-Systems, Inc.	TCA	Label
Spra-Kleen	GC Electronics	TCA	MSDS/Label
Spra-lube	GC Electronics	TCA	MSDS/Label
Spray Belt Dressing	Cling Surface Co.	TCA	MSDS/Label
Spray Mount Artist's Adhesive	AlpA1A	TCA	Label
Spray n Seal Stop leak	Cadie Products Corp	TCA	Label
Spray on coating	Plasti Dip	TCA	Label
SSD Choro-Solv	The State Chemical Manufacturing Co.	TCA	Label
Stainless cleaner	Dutch Maid	TCA	Label
Stop-Slip Belt Dressing	Quality Care	TCA	Label
Stop-Slip Belt Dressing	Radiator Specialty Co.	TCA	Label
Suede Spray Cleaner & Conditioner	Kiwi Brands Inc	TCA	Label
Super Duty Interior Adhesive	Heads Up Industries	TCA	Label
Super Spot Remover	Fuller Brush Company	TCA	Label
Techron Water Repellant	Blue Magic Products, Inc.	TCA	Label
Tetra Gun Spray Cleaner	FTI Inc	TCA	Label
Tri-Flow superior lubrication w/ teflon	Thompson & Formby Inc.	TCA	MSDS/Label
Tuner Control Lubricant	Radio Shack	TCA	Label
Universal Belt Dressing	Polytech	TCA	Label
Unknown Cleaner	Careosol	TCA	Label
Water and Soil Repellant	Second Wind	TCA	Label
Water and stain protector	Hofco	TCA	Label
Water Shed	Outers	TCA	Label
Weather Spirits Water & Stain Protector	Wal-Mart Stores Inc.	TCA	Label
Welding Contact Cement	DAP	TCA	Label
White Grease	Gold Eagle Co	TCA	Label
White Lithium Grease	Terand Ind	TCA	Label
White Lithium Grease	Nationwide Industries	TCA	MSDS/Label
Wonder Lub	Radiator Specialty Co.	TCA	Label
Water Repellent	Kenyon	TCA	Label
X-Static	Industrial Research	TCA	Label
All Purpose Lubricant	Kal Gard Coating Mfg Corp	TCE	Label
Amarr Super Lube	Amarr Garage Door	TCE	Label
Brake Cleaner	Advance Auto Parts	TCE	Label
C-60 Solvent Cleaner	Sprayway Inc	TCE	MSDS/Label
Carpet & Upholstery Spotter	Pro Link	TCE	Label
Compound Cleaner	Caterpillar, CAT	TCE	Label
Crown Anti-Vandal Spray	Aervoe Industries Incorporated	TCE	MSDS/Label
Electric Motor Cleaner	Berryman	TCE	MSDS/Label
Electrical Cleaner and Lubricating Spray	Spray On	TCE	MSDS/Label
Fast Spot Remover Spray	Sullivans USA Inc.	TCE	Label
Garage Door Lubricant	Price's	TCE	Label
Glitter Lemon Powered Siliconized Polish	Del	TCE	Label

PRODUCT DESC	MANUFACTURER	PAR LABEL	METHOD of DETERMINATION
Gun Scrubber Degreaser	Birchwood Casey	TCE	MSDS/Label/GC-MS
Gunslick Gunflush	Gunslick/Outers	TCE	MSDS/Label
Gunslick Nu_Gun	Gunslick/Outers	TCE	MSDS/Label
HDX Heavy Duty Degreaser	LPS	TCE	MSDS/Label
Heavy Duty Degreaser (TCE)	CRC	TCE	MSDS/Label
Heavy Duty Degreaser Aerosol	CRC	TCE	MSDS/Label
Heavy Duty Garage Door Lubricant	Crawford Door Sales	TCE	Label
Heavy Duty Garage Door/Operator Lube & Rust Prevent	Lodi Door	TCE	Label
Heavy-duty Garage Door/Operator Lub & Rust Prev.	National Door Industries	TCE	Label
Industrial Clean Up Dry Cleaner	Sprayway Inc	TCE	MSDS/GC-MS
Leak Ender 2000	Leak Ender 2000	TCE	Label
Lectra Clean® Heavy Duty Degreaser	CRC	TCE	Label/GC-MS
Liquid Gasket 1104	Three Bond of America	TCE	Label
Millers insect spray	Termilind Ltd	TCE	Label
Misty Industrial Cleaning Solvent Aerosol	Amrep Inc	TCE	MSDS/Label
Misty Moisture Guard	Amrep Inc	TCE	MSDS/Label
Misty Penetrating Lubricant	Amrep Inc	TCE	MSDS/Label
Mr Electric D_OS Solvent Degreaser	Franlynn Inc	TCE	Label
Pepper "Capsicum" Spray	Omega Formulation	TCE	GC-MS
Picrin	R.R. Street & Co. Inc.	TCE	MSDS/Label
Rain and Stain Guard	Kinney	TCE	Label
Rain and Stain Guard	Kiwi Brands Inc	TCE	Label
Reel Boating Lubricant	Eezox	TCE	MSDS/Label
Rubber Cement	Schrader-Bridgeport Int'l, Inc.	TCE	MSDS/Label
Rusty Duck Gun Cleaner	Rusty Duck	TCE	Label
Rusty Duck Protective Gun Lubricant	Hydra-Tone Chemicals Inc.	TCE	Label
Safety Solvent	Brody Chemical	TCE	MSDS/Label
Shooter's Choice Quick Scrub III	Venco Industries	TCE	MSDS/Label
Slime Quick Spair	Accessories Marketing, Inc.	TCE	GC-MS
Solvent Carpet Spotter	Waxie	TCE	MSDS/Label
Solvent Cleaner	Claire Manufacturing Company	TCE	MSDS/Label
Solvent Degreaser	Steel Brand	TCE	MSDS/GC-MS
Spot and stain remover	All Solv	TCE	Label
Spot and stain remover	Sullivans	TCE	Label
Spray Grip	Chesterton	TCE	Label
Spray Super Shene Leather Finish	Tandy	TCE	Label
Starting Fluid	Pyroil	TCE	Label
Steel Brand Rust Busting Lubricant	SRC	TCE	Label
Super Safe Solv TF	Western Environmental Services, Inc.	TCE	MSDS/Label
Supersoln Fast Dry	Steelman	TCE	Label
SuperSolve	Amprep Inc.	TCE	MSDS/Label
Synthetic Premium Gun Care	Eezox	TCE	MSDS/Label
TCE/Ethylene Trichloride/Trichloroethylene/	Chem Pak	TCE	Label

PRODUCT DESC	MANUFACTURER	PAR LABEL	METHOD of DETERMINATION
Tetra Gun Degreaser Action Blaster	FTI Inc	TCE	MSDS/Label
Tru Oil Stock Finish (Aerosol)	Birchwood Casey	TCE	MSDS/Label
Virginia Blast-a-Coil	Virginia KMP Corp	TCE	MSDS/Label
Weld On 3	IPS	TCE	MSDS/Label
Windshield Cleaner	Temshield	TCE	Label
Zep 45 Penetrating Lubricant	Zep	TCE	MSDS/Label/GC-MS
Plastic and Emblem Adhesive	AlpA1A	VC	Label